Politecnico di Torino
Department of Architecture and Design
Master of Sciences in Architecture for sustainability
A.a. 2023/2024
Graduation sessionDecembre 2024

Biochar in cementitious materials and 3D printing.

Supervisor:
TULLIANI JEAN MARC CHRISTIAN (DISAT)
Correlator:
COPPOLA BARTOLOMEO (DISAT)

Students:
GONZÁLEZ ESPINOSA ANDREA (s306764)
GUERRERO RIOS MELISSA (s306758)

AKNOWLEDGEMENTS

We extend the deepest gratitude to our professors for their invaluable guidance and dedication, which have shaped our learning journey. To our families, whose unconditional support and encouragement have been essential for this process, and to our friends, who stood by us with inspiration and motivation. This accomplishment reflects the collective impact of your belief in our growth and success. Thank you all.

ABSTRACT

Currently, and for many years, there has been an ongoing dialogue regarding the concept of sustainability as one of the key elements for the development of humanity and the possibility of ensuring a livable future for subsequent generations, the search for a sustainable future is undertaken with the purpose of addressing the climate crisis we are currently facing. To achieve this, it is necessary to stabilize CO2 emissions and greenhouse gases, which in recent years have had a dramatic increase, bringing with them irreversible consequences for environmental systems. The field of architecture and construction is one of the most polluting sectors, with a significant impact on environmental problems, making it essential for innovative strategies in adaptation, mitigation, and maintenance to be implemented as a means to address the crisis.

Based on this context, this thesis explores the implementation of biochar as a sustainable construction material, influenced by the principles of sustainable economics, extending the lifecycle of materials and reducing anthropogenic emissions. As a material recovered from waste in the production of biomass through the process of pyrolysis, biochar is emerging as one of the most influential supplies for an environmentally resilient future, with numerous applications. Specifically for the construction industry, biochar is applied in concrete as a replacement for cement and in cementitious composites as an aggregate and an additive for wood polypropylene composites and plasters, with the aim of reducing environmental footprints and enhancing the capacity to capture CO2 from the air.

This experimental research made a critical analysis applying a methodology of various elaboration of distinct formulations of mortar samples maintaining the change of 5% biochar to the cement content and varying the water cement ratios, additionally, 3D printing samples were made as an application of new technologies. The different samples were subjected to various mechanical tests to identify and study mechanical properties, including flexural and compressive stresses. The research seeks to extend the scope of the advantages of biochar application as a performance-oriented material, offering profitable information for future implementations and research of biochar in Cementitious materials and 3D printing.

INDEX

ACKNOWLEDGEMENTS

ABSTRACT

LIST OF FIGURES

INTRODUCTION 12

CLIMATE CHANGE 13
PLANETARY BOUNDARIES 16
SUSTAINABILITY 18
SUSTAINABILE DEVELOPMENT 24
SUSTAINABILE DEVELOPMENT IN CONSTRUCTION 29

STATE OF THE ART

CEMENT 32
TYES OF CEMENT 34
PORTLAND CEMENT 35
PRODUCTIVE CYCLE 36
PROPERTIES 39
STANDARIZATIONS AND REGULATIONS 40
EN STANDARDS 197 – 1 40
PROPERTIES 42
TESTING AND CONFORMITY CRITERIA 43
ASTM C150 SPECIFICATION 44
PROPERTIES 45
TESTING AND CONFORMITY CRITERIA 46
ENVIRONMENTAL IMPACT - EN 197-1 & ASTM C150 47
IMPACT IN THE CONSTRUCTION INDUSTRY - EN 197-1 & ASTM C150 47
CONCRETE 48
RHEOLOGY OF CONCRETE 50
CONCRETE CONSTITUENTS 51
TYPES OF CONCRETE 52

BIOCHAR
WHAT IS IT 53
PHYSICAL CHARACTERISTICS 54
CHEMICAL CHARACTERISTICS 55
HISTORY OF BIOCHAR 56
FEEDSTOCK 57
PRODUCTION 58
APPLICATION 62
BIOCHAR IN CONCRETE 62
PREVIOUS RESEARCH 63

3D PRINTING 67
TECHNOLOGY 67
RHEOLOGY IN 3D PRINTING 72
APPLICATION IN CONCRETE 72

EXPERIMENTAL ACTIVITY

RESEARCH PARADIGMA 75

MATERIALS 77
CEMENT 77
BIOCHAR 79
SUPERPLASTICIZER 82
PEG 84

METHODOLOGY 86
BIOCHAR PREPARATION 86
SAND PREPARATION 89
GRANULOMETRY 90
GRANULOMETRY ANALYSIS 92
MORTAR MIXTURE PREPARATION 93
3D PRINTING software 99
3D PRINTING process 100
TRADITIONAL CASTING SAMPLES 105
CURING PROCESS 106
MIXTURE DESIGN RESULTS 110
SOFTWARE APPLICATION 112
SAMPLE CHARACTERIZATION 118

MECHANICAL TESTS 122
THREE-POINT BENDING TEST 122
COMPRESSION TEST 126
MECHANICAL PROPERTIES TEST SAMPLE IDENTIFICATION 128
MECHANICAL TESTS RESULTS 129
BENDING TEST RESULTS 130
COMPRESSION TEST RESULTS 139

SEM OBSERVATIONS 148
SEM SAMPLE IDENTIFICATION 149
SAMPLE PREPARATION FO ANALYSIS 149
SEM OBSERVATION ANALYSIS 150
AN OVERALL VIEW 167

CONCLUSIONS 169
OBSERVATIONS AND FURTHER APPLICATION 172

ANNEXES 178

BIBLIOGRAPHY 184

TABLE OF FIGURES

Figure 1. Cumulative total anthropogenic CO2 emissions from 1870 (GtCO2).
Figure 2. Time series of different global annual change in mean temperature for the 1900–2300 period.
Figure 3. Total annual anthropogenic GHG emissions by gases 1970–2010.
Figure 4. The 2023 update to the Planetary boundaries.
Figure 5. human perspectives.
Figure 6. World Model of Standard Run.
Figure 7. Worl Model of Natural Resources.
Figure 8. Normalized root mean square deviation for each LtG output compared with the observed data, for each scenario. Closer agreement between data and model output.
Figure 9. Sustainable Development: common concerns, differing emphases.
Figure 10. Venn diagram for sustainable development.
Figure 11. The circular economy model.
Figure 12. Sustainable Development Goals.
Figure 13. Global anthropogenic CO2 emissions related to energy processes for all development sectors and specifically for industrial emissions.
Figure 14. Normalized global demand for the five key materials since 1960.
Figure 15. World Cement production in industrialized and developing countries.
Figure 16. World Cement production 2022.
Figure 17. Portland cement manufacturing process.
Figure 18. schematic outline of kiln processes.
Figure 19. Scheme of the pyrolysis process.
Figure 20. Scheme of the general concept of pyrolysis and their outputs
Figure 21. Scheme diagram of conventional pyrolysis and microwave pyrolysis.
Figure 22. Scheme of the gasification process.
Figure 23. Scheme of kiln technology.
Figure 24. Binder jetting scheme.
Figure 25. Directed Energy Deposition scheme.
Figure 26. Extrusion method used: (a) filament-based, (b) plunger-based, and (c) screw-based extrusion.
Figure 27. Material Jetting 3D printing scheme.
Figure 28. Laser powder bed fusion process scheme.
Figure 29. Sheet lamination overview.
Figure 30. Schematic diagrams of three approaches to photopolymerization processes.
Figure 31. Simply 3D Slicing Software Extrude tab parameters (3mm nozzle).
Figure 32. Simply 3D Slicing Software Layer tab parameters (3mm nozzle).
Figure 33. Simply 3D Slicing Software Additions tab parameters (3mm nozzle).
Figure 34. Simply 3D Slicing Software Infill tab parameters (3mm nozzle).
Figure 35. Simply 3D Slicing Software Speed tab parameters (3mm nozzle).
Figure 36. Simply 3D Slicing Software Other tab parameters (3mm nozzle).
Figure 37. Simply 3D Slicing Software Advanced tab parameters (3mm nozzle).
Figure 38. Simply 3D Slicing Software Extrude tab parameters (2mm nozzle).
Figure 39. Simply 3D Slicing Software Layer tab parameters (2mm nozzle).
Figure 40. Simply 3D Slicing Software Additions tab parameters (2mm nozzle).
Figure 41. Simply 3D Slicing Software Infill tab parameters (2mm nozzle).
Figure 42. Simply 3D Slicing Software Support tab parameters (2mm nozzle).
Figure 43. Simply 3D Slicing Software Temperature tab parameters (2mm nozzle).
Figure 44. Simply 3D Slicing Software Cooling tab parameters (2mm nozzle).
Figure 45. Simply 3D Slicing Software G-code tab parameters (2mm nozzle).
Figure 46. Simply 3D Slicing Software Speed tab parameters (2mm nozzle).
Figure 47. Schematic representation of the samples' approximate dimensions in mm and positioning for a three-point bending test.
Figure 48. 3D Printed 0.38_w/c 3 mm_nozzle three-point bending test comparison between standard force (N) and deformation (%).
Figure 49. 3D Printed 0.38_w/c 2 mm_nozzle three-point bending test comparison between standard force (N) and deformation (%).
Figure 50. Traditional casting 0.38_w/c three-point bending test comparison between standard force (N) and deformation (%).
Figure 51. 3D Printed 0.36_w/c 2mm_nozzle three-point bending test comparison between standard force

(N) and deformation (%).
Figure 52. 3D Traditional casting 0.36_w/c three-point bending test comparison between standard force (N) and deformation (%).
Figure 53. 3D Printed 0.40_w/c 2 mm_nozzle three-point bending test comparison between standard force (N) and deformation (%).
Figure 54. Traditional casting 0.40_w/c three-point bending test comparison between standard force (N) and deformation (%).
Figure 55. Summarized results of the flexural strength for each mixture sample.
Figure 56. 3D Printed 0.38_w/c 2 mm_nozzle compression test comparison between standard force (N) and deformation (%).
Figure 57. 3D Printed 0.38_w/c 2 mm_nozzle compression test comparison between standard force (N) and deformation (%).
Figure 58. Traditional casting 0.38_w/c compression test comparison between standard force (N) and deformation (%).
Figure 59. 3D Printed 0.36_w/c 2 mm_nozzle compression test comparison between standard force (N) and deformation (%).
Figure 60. Traditional casting 0.36_w/c compression test comparison between standard force (N) and deformation (%).
Figure 61. 3D Printed 0.40_w/c 2 mm_nozzle compression test comparison between standard force (N) and deformation (%).
Figure 62. Traditional casting 0.40_w/c compression test comparison between standard force (N) and deformation (%).
Figure 63. Summarized results obtained from the compression test.
Figure 64. The Scanning Electron Microscope (SEM) consists of two principal sections illustrated in the image: the electron column, which houses the electron source and focusing systems, and the electronics console, responsible for controlling and processing the signals.
Figure 65. Malvern Mastersizer 3000 Aero S
Figure 66. Illustration of the laser diffraction process within the Malvern Mastersizer 3000 Aeros S instrument.
Figure 67. Simply 3D Slicing Software printing model of capsule.
Figure 68. Simply 3D Slicing Software Speed tab parameters (2 mm nozzle).
Figure 69. Simply 3D Slicing Software Speed tab parameters (2 mm nozzle).
Figure 70. Simply 3D Slicing Software Speed tab parameters (2 mm nozzle).
Figure 71. Simply 3D Slicing Software Speed tab parameters (2 mm nozzle).
Figure 72. Simply 3D Slicing Software Speed tab parameters (2 mm nozzle).
Figure 73. Simply 3D Slicing Software Speed tab parameters (2 mm nozzle)
Figure74. Cumulative Granulometric Distribution of Biochar Measured by Laser Diffraction

TABLE OF TABLES

Table 1. Planetary Boundaries.
Table 2. Values and rates of change of scenario variables compared with the data at year 2000 for three scenarios.
Table 3. Major mineral constituents of Portland Cement.
Table 4. Hydration Reactions.
Table 5. Main types of cement according to EN 197-1.
Table 6. EN 197-1 cement subtypes.
Table 7. Mechanical and physical requirements given as characteristic values.
Table 8. Chemical requirements given as characteristic value.
Table 9. ASTM Types of Portland Cement.
Table 10. Standard composition requirements.
Table 11. Optional standard composition requirements.
Table 12. Standard Physical requirements.
Table 13. Optional standard Physical requirements.
Table 14. Definition of concrete.
Table 15. Typical Engineering Properties of Structural Concrete.
Table 16. The estimation done by the authors of ref. 2.27 Pg C/year with an optimistic scenario, and two additional scenarios with lower demands 1.64 Pg C/year (Beta) and 1.01 Pg C/year (Alpha) of how much organic material (in terms of carbon) could be turned into biochar each year, based on available feedstocks like crops, waste and forestry.
Table 17. Chemical requirements
Table 18. Mechanical and physical requirements
Table 19. Summary of the mortar mix design trials.
Table 20. Final Printed mortar mixture designs.
Table 21. Printed samples properties.
Table 22. Traditional casting samples properties.
Table 23. Samples curing days process.
Table 24. Sample Labels for Mechanical Testing: Classification and Reference Guide.
Table 25. 3D Printed 0.38_w/c 3 mm_nozzle three-point bending test.
Table 26. 3D Printed 0.38_w/c 2 mm_nozzle three-point bending test.
Table 27. Traditional casting 0.38_w/c three-point bending test.
Table 28. 3D Printed 0.36_w/c 2 mm_nozzle three-point bending test.
Table 29. Traditional casting 0.36_w/c three-point bending test.
Table 30. 3D Printed 0.40_w/c 2 mm_nozzle three-point bending test.
Table 31. Traditional casting 0.40_w/c three-point bending test.
Table 39. Summarized results obtained from the three-point bending test.
Table 40. 3D Printed 0.38_w/c 3 mm_nozzle compression test.
Table 41. 3D Printed 0.38_w/c 2 mm_nozzle compression test.
Table 42. Traditional cast 0.38_w/c compression test.
Table 43. 3D Printed 0.36_w/c 2 mm_nozzle compression test.
Table 44. Traditional cast 0.36_w/c compression test.
Table 45. 3D Printed 0.40_w/c 2 mm_nozzle compression test.
Table 46. Traditional cast 0.40_w/c compression test.
Table 47. Summarized results obtained from the compression test.
Table 48. Sample labels for SEM analysis: Classification and Reference Guide
Table 49. Summary chart of the SEM analysis highlighting the best-performing sample among all tested samples.

TABLE OF IMAGES

Image 1. 3D printed elements: wall segments printed in factory and completed fabricated 3D printed concrete building in Nanjing.
Image 2. 3D printed Formworks.
Image 3. Monolithic 3D printing on site
Image 4. Apis Cor's 3D-printed concrete walls for a residential house in Melbourne, FL.
Image 5. The Canal House in Amsterdam, The World's First 3D Printed Canal House
Image 6. Cement Type I 52.5 R.
Image 7. Nero Biochar.
Image 8. Mapei Dynamon SP1.
Image 9. Biochar griding in the rolling bench.
Image 10. Gf Biochar after dry grinding, seamlessly change done to the particle size.
Image 11. Biochar hydrated pre grinding crushing process.
Image 12. Fully dried biochar after 48 hours.
Image 13. Final biochar 250 µm particle size after sieving.
Image 14. Sand sieving equipment.
Image 15. Sand placed in the electrical sieve shaker in a 250 µm sieve.
Image 16. Sand and mortar were already weighed, and biochar weighting is being carried out.
Image 17. mechanical mixture of all mortar mix design constituents.
Image18. Simulation of the 3D printer extrusion with a 5mm syringe.
Image19. Mortar paste after undergoing the syringe test without success as it lacked workability.
Image 20. Sigma-Aldrich Polyethylene Glycol 10,000
Image 21. Moldability and physical behavior test results of various mortar mix designs.
Image 22. Syringe and moldability - physical behavior mortar mixture design test results.
Image 23 Syringe test physical behavior results showing the evolution and variation of the mortars workability by creating different mis design formulations.
Image 24 Moldability test physical behavior results showing the evolution and variation of the mortars workability by creating different mis design formulations.
Image 25 Simply 3D slicing software parameterized document.
Image 26. Aluminum tank filling process.
Image 27. Aluminum tank caps and pressure piston.
Image 28. tank placement setup and connection to the pressure compression and the Teflon tube.
Image 29. Extruder placement setup and connection to the aluminum tank and the 3D printer.
Image 30. Teflon tube mixture fluidity test.
Image 31. Complete extrusion system, printing trial.
Image 32. 3D printer, first printing layer problems due to nozzle blockage.
Image 33. 3D printer, first trials with a 0.45 w/c ratio.
Image 34 3D printer, sample trial with a 0.38 w/c ratio.
Image 35. 3D printer, while printing a sample last layer.
Image 36. Traditional cast mold setup.
Image 37. 24-hour hardening phase setup.
Image 38. Unmolding process of 3D printed samples
Image 39. 28-day mortar sample hydration.
Image 40. Samples drying process.
Image 41. Drying Process of all samples after currying process.
Image 42. Simply 3D Slicing Software printing model with a different printing angle application in the infill.
Image 43. Testing machine used for the flexural and compression test.
Image 44. Measurement of samples and marking referent points in preparation for the three-point bending test.
Image 25. Positioning and centering of the specimen bars on the Zwick Line Z050 testing machine.

Image 46. Sequential images (a, b, c) illustrating the procedure for test performance on the Zwick Line Z050.
Image 47. Zwick Line-Z010 testing machine with the arrangement of compression fixtures.
Image 48. Arrangement of the fractured halves of the mortar prisms from the flexural tests, prepared to begin the compression test.
Image 49. Printed samples following the three-point bending test, displaying the failure surface of (a) sample 2 with a water-to-cement ratio of 0.38, and (b) sample 3 with a water-to-cement ratio of 0.36.
Image 50. Sequential images (a, b, c) illustrating the procedure with a 3D-printed sample during the compression test on the Zwick Line Z050.
Image 51. Hitachi S4000 SEM, DISAT, Politecnico di Torino.
Image 52. SEM image of Sample 1 at 200x magnification, captured during analysis.
Image 54. SEM image of Sample 1 at 200x magnification, captured during analysis.
Image 53. SEM image of Sample 1 at 600x magnification, captured during analysis.
Image 55. SEM image of Sample 1 at 800x magnification, captured during analysis.
Image 56. SEM image of Sample 1 at 600x magnification, captured during analysis.
Image 58. SEM image of Sample 1 at 1500x magnification, captured during analysis.
Image 60. SEM image of Sample 1 at 5000x magnification, captured during analysis.
Image 57. SEM image of Sample 1 at 1000x magnification, captured during analysis.
Image 59. SEM image of Sample 1 at 200x magnification, captured during analysis.
Image 61. SEM image of Sample 1 at 30000x magnification, captured during analysis.
Image 62 SEM image of Sample 1 at 1500x magnification, captured during analysis.
Image 63. SEM image of Sample 1 at 400x magnification, captured during analysis.
Image 64 SEM image of Sample 1 at 400x magnification, captured during analysis.
Image 65. SEM image of Sample 1 at 600x magnification, captured during analysis.
Image 66. SEM image of Sample 2 at 40x magnification, captured during analysis.
Image 67. SEM image of Sample 2 at 200x magnification, captured during analysis.
Image 68. SEM image of Sample 2 at 40x magnification, captured during analysis.
Image 69. SEM image of Sample 2 at 600x magnification, captured during analysis.
Image 70. SEM image of Sample 2 at 600x magnification, captured during analysis.
Image 71. SEM image of Sample 2 at 1000x magnification, captured during analysis.
Image 72. SEM image of Sample 2 at 1000x magnification, captured during analysis.
Image 73. SEM image of Sample 2 at 2000x magnification, captured during analysis.
Image 74. SEM image of Sample 2 at 2000x magnification, captured during analysis.
Image 75. SEM image of Sample 2 at 8000x magnification, captured during analysis.
Image 76. SEM image of Sample 2 at 2000x magnification, captured during analysis.
Image 77. SEM image of Sample 2 at 4000x magnification, captured during analysis.
Image 78. SEM image of Sample 2 at 2000x magnification, captured during analysis.
Image 79. SEM image of Sample 2 at 8000x magnification, captured during analysis.
Image 80. SEM image of Sample 3 at 50x magnification, captured during analysis.
Image 81. SEM image of Sample 3 at 200x magnification, captured during analysis.
Image 82. SEM image of Sample 3 at 100x magnification, captured during analysis.
Image 83. SEM image of Sample 3 at 200x magnification, captured during analysis.
Image 84. SEM image of Sample 3 at 200x magnification, captured during analysis.
Image 85. SEM image of Sample 3 at 400x magnification, captured during analysis.
Image 86. SEM image of Sample 3 at 400x magnification, captured during analysis.
Image 87. SEM image of Sample 3 at 600x magnification, captured during analysis.
Image 88. SEM image of Sample 3 at 2000x magnification, captured during analysis.
Image 89. SEM image of Sample 3 at 2000x magnification, captured during analysis.
Image 90 SEM image of Sample 3 at 4000x magnification, captured during analysis.
Image 91. SEM image of Sample 3 at 2000x magnification, captured during analysis.
Image 92. SEM image of Sample 4 at 100x magnification, captured during analysis.
Image 93. SEM image of Sample 4 at 1000x magnification, captured during analysis.
Image 94. SEM image of Sample 4 at 200x magnification, captured during analysis.

Image 95. SEM image of Sample 4 at 2000x magnification, captured during analysis.
Image 96. SEM image of Sample 4 at 600x magnification, captured during analysis.
Image 97. SEM image of Sample 4 at 4000x magnification, captured during analysis.
Image 98. SEM image of Sample 4 at 6000x magnification, captured during analysis.
Image 99.SEM image of Sample 4 at 2000x magnification, captured during analysis.
Image 100. SEM image of Sample 4 at 1000x magnification, captured during analysis.
Image 101. SEM image of Sample 4 at 2000x magnification, captured during analysis.
Image 102. SEM image of Sample 5 at 40x magnification, captured during analysis.
Image 103. SEM image of Sample 5 at 40x magnification, captured during analysis.
Image 104. SEM image of Sample 5 at 200x magnification, captured during analysis.
Image 105.SEM image of Sample 5 at 600x magnification, captured during analysis.
Image 106. SEM image of Sample 5 at 1000x magnification, captured during analysis.
Image 107. SEM image of Sample 5 at 2000x magnification, captured during analysis.
Image 108. SEM image of Sample 5 at 600x magnification, captured during analysis.
Image 109. SEM image of Sample 5 at 4000x magnification, captured during analysis.
Image 110. SEM image of Sample 5 at 1000x magnification, captured during analysis.
Image 111. SEM image of Sample 5at 2000x magnification, captured during analysis.
Image 112. SEM image of Sample 5 at 6000x magnification, captured during analysis.
Image 113. SEM image of Sample 5 at 6000x magnification, captured during analysis.
Image 114. SEM image of Sample 6 at 40x magnification, captured during analysis.
Image 115. SEM image of Sample 6 at 40x magnification, captured during analysis.
Image 116. SEM image of Sample 6 at 100x magnification, captured during analysis.
Image 117. SEM image of Sample 6 at 400x magnification, captured during analysis.
Image 118. SEM image of Sample 6 at 1000x magnification, captured during analysis.
Image 119. SEM image of Sample 6 at 4000x magnification, captured during analysis.
Image 120. SEM image of Sample 6 at 200x magnification, captured during analysis.
Image 121. SEM image of Sample 6 at 600x magnification, captured during analysis.
Image 122. SEM image of Sample 6 at 1000x magnification, captured during analysis.
Image 123. SEM image of Sample 6 at 1000x magnification, captured during analysis.
Image 124. Introducing biochar powder particles into the conical steel cell for granulometry analysis.
Image 125. First 3D-printed capsule recently developed.
Image 126. All the capsules produced using 3D printing.
Image 127. 3D printed capsules after curing process.

INTRODUCTION

With the current climate crisis and the ongoing dialogue of need to transform towards a sustainable future, one of the most questioned and examined industries is the construction industry as it is one of the largest contributors to the current disturbing carbon and environmental footprint due to its notable resource depletion and greenhouse gases emission. This has encouraged the emergence of innovative strategies with the implementation of new construction technologies for the development of new materials and the adaptability of the most conventional materials, in the exploration to reduce their environmental impact and the undesirable alteration in environmental systems, creating the potential to mitigate the environmental impacts of traditional building practices.

Cement and concrete are known to be one of the most important materials in construction, being one of the most used and primary materials, its reliability comes from its outstanding properties, versatility, economy and performance. However, its massive production makes it one of the mayor contributors to global carbon dioxide emissions and one of the biggest challenges in the transformative process of anthropogenic development towards a sustainable and environmentally resilient one. As a response to this premise, concrete has been meticulously studied in all production stages, but also considering various modification and variations to its formulation.

Consequently, several possibilities have derived due to this exploration, biochar incorporation into cementitious materials is one of the innovative strategies to carbon emissions reduction. Obtained as a remaining product of other chemical processes, biochar is a low-cost carbon rich waste from the pyrolysis of organic biomass. Recognized for its ability to improve concrete properties, sequester carbon and reduce its weight, makes biochar a promising additive for cementitious mixture designs working towards the reduction of cements environmental footprint and adjusting the build environment towards an energy efficient and resilient future.

Simultaneously, 3D printing has been one of the lates technologies, providing advanced possibilities in design flexibility and material efficiency. With this technology the application of cementitious material becomes more precise, reducing waste production and broadening design complexity, permitting the increase in geometry difficulty, which would be hard to achieve with traditional construction methods. The combination of innovation and technology results in biochar in cementitious materials and 3D printing, creating an opportunity to study the alliance between sustainable material and cutting-edge technology.

This thesis is exploratory research integrating biochar into cementitious materials for 3D printing applications in the field of architecture and construction. Initially the potentials of biochar as a sustainable additive are going to be studied, assessing its impact on the concrete/mortar mechanical properties, such as flexion and compression, and looking for the environmental performance when structured by 3D printing technology. In this way the experimental analysis aims to contribute in the development of more sustainable construction practices that align with the growing demand for low-carbon, high-performance building materials.

CLIMATE CHANGE

Climate change has been one of the most urgent global challenges. Throughout history the world has overcome various temperature change periods where temperature either increases or decreases. Even though, changes in temperature have always taken hundreds of years, in the last 150 years, since the beginning of industrialization the oscillation in temperature has been extremely abrupt and driving the world into a climate crisis. The term climate change refers to long-term shifts in temperature, precipitation patterns, and other enduring changes that impact Earth's climate system[1].

The Intergovernmental Panel on Climate Change (IPCC) refers to climate change as "statistically significant variations in the mean state of the climate or its variability, persisting for an extended period, typically decades or longer" (Pachauri, Meyer, & Core Writing Team, 2014). With this the recognition of various environmental problems have been identified, not only limiting human wellbeing but generating irreversible consequences to the future survival of humankind and other living organisms on the planet[2]. As shown in the graph below, even though changes can be attributed to both natural processes and anthropogenic activities, evidence shows human activity is the dominant contributor to change in the chemical composition of the atmosphere, making it the primary driver of environmental problems since the mid-20th century[3].

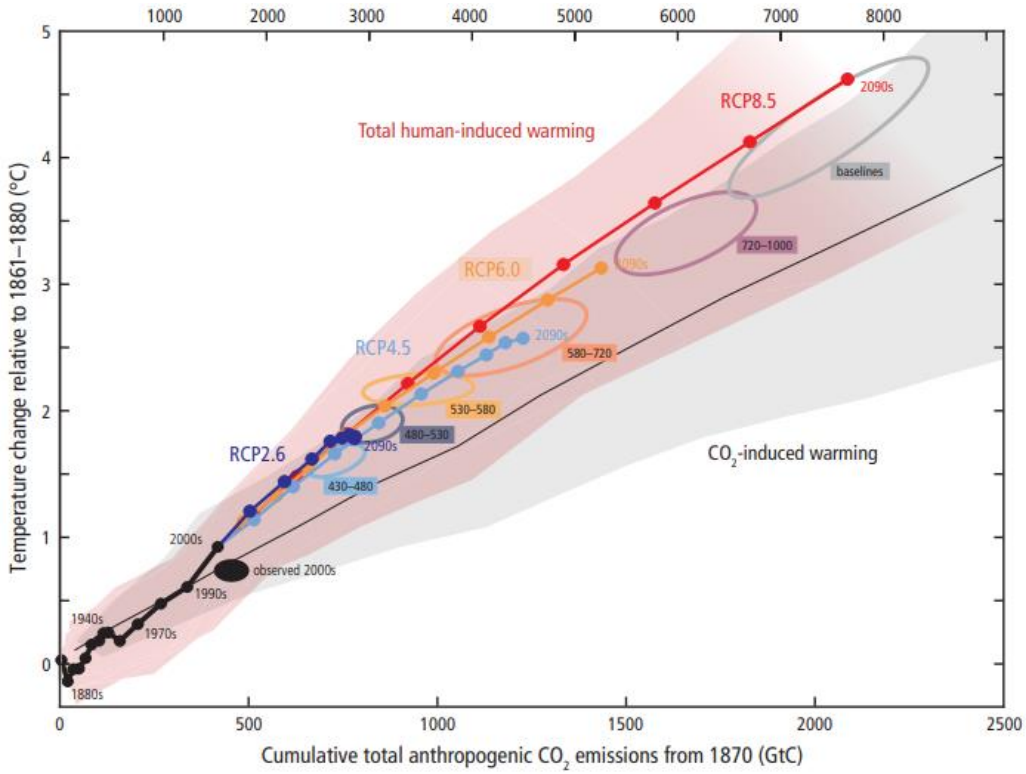

Figure 1 Cumulative total anthropogenic CO2 emissions from 1870 (GtCO2). Source: (Pachauri, Meyer, & Core Writing Team, 2014)

[1] (Hulme , 2017)
[2] (Mravcová, 2023)
[3] (IPCC, 2021)

The term "RCP" stands for Representative Concentration Pathway, a concept introduced by the Intergovernmental Panel on Climate Change (IPCC) to describe four distinct greenhouse gas concentration trajectories used for climate modeling and research. RCPs represent different scenarios of anthropogenic emissions and their resulting radiative forcing values by the year 2100, measured in watts per square meter (W/m^2) relative to pre-industrial levels. Each RCP is associated with specific socioeconomic assumptions, technological developments, and policy measures aimed at either mitigating or intensifying greenhouse gas emissions[4]. The four primary RCPs are as follows:

RCP2.6: This scenario reflects a peak in greenhouse gas emissions around 2020, followed by a significant decline, leading to a radiative forcing of 2.6 W/m^2 by 2100[5]. It assumes strong mitigation efforts, aligning with global climate goals, such as limiting global warming to below 2°C relative to pre-industrial levels[6].

RCP4.5: This pathway assumes a stabilization of radiative forcing at 4.5 W/m^2 by 2100, with emissions peaking around 2040. It incorporates moderate mitigation policies, resulting in intermediate temperature increases[7].

RCP6.0: In this scenario, emissions continue to rise until around 2080 before stabilizing, leading to a radiative forcing of 6.0 W/m^2 by 2100. It reflects the slower adoption of mitigation strategies, with a reliance on technological solutions later in the century[8].

RCP8.5: Often referred to as a "business-as-usual" scenario, RCP8.5 assumes minimal mitigation efforts, with radiative forcing reaching 8.5 W/m^2 by 2100. This pathway results in high greenhouse gas emissions and is associated with significant temperature increases, posing severe risks to ecosystems and human societies[9].

These RCPs provide a framework for understanding potential future climate outcomes based on varying levels of global action. They serve as inputs for climate models to project temperature changes, sea level rise, and other climate-related impacts, enabling policymakers to assess the consequences of different emissions trajectories and plan for adaptive and mitigative strategies[10].

To have a better understanding of the rising average global temperature phenomenon scientists and researchers have developed key indicators evidencing the negative impact of human actions on the climate system, among tis we can find global temperature increase, rising greenhouse gas concentrations, melting ice and rising sea levels, ocean acidification, extreme weather events, reduction of oceans ph, and changes in precipitation[11]. Most of these indicators have an anthropogenic origin and come either to fossil fuel combustion, deforestation and land use, or industrial processes and agriculture, integrated in the unlimited idea of growth and development in a world with limited resources. Below are some models and research studies supporting the above stated hypothesis in the concerning impacts of human actions regarding climate change.

[4] (Van Vuuren, Edmods, Kainuma, & Riahi, 2011)
[5] (IPCC, 2018)
[6] (Van Vuuren, Edmods, Kainuma, & Riahi, 2011)
[7] (Clarke, et al., 2007)
[8] (Fujino, Nair, Kaniuma, Masui, & Matsuoka, 2006)
[9] (Riahi, Shilpa, Krey, & Cho, 2011)
[10] (IPCC, 2014)
[11] (Mravcová, 2023)

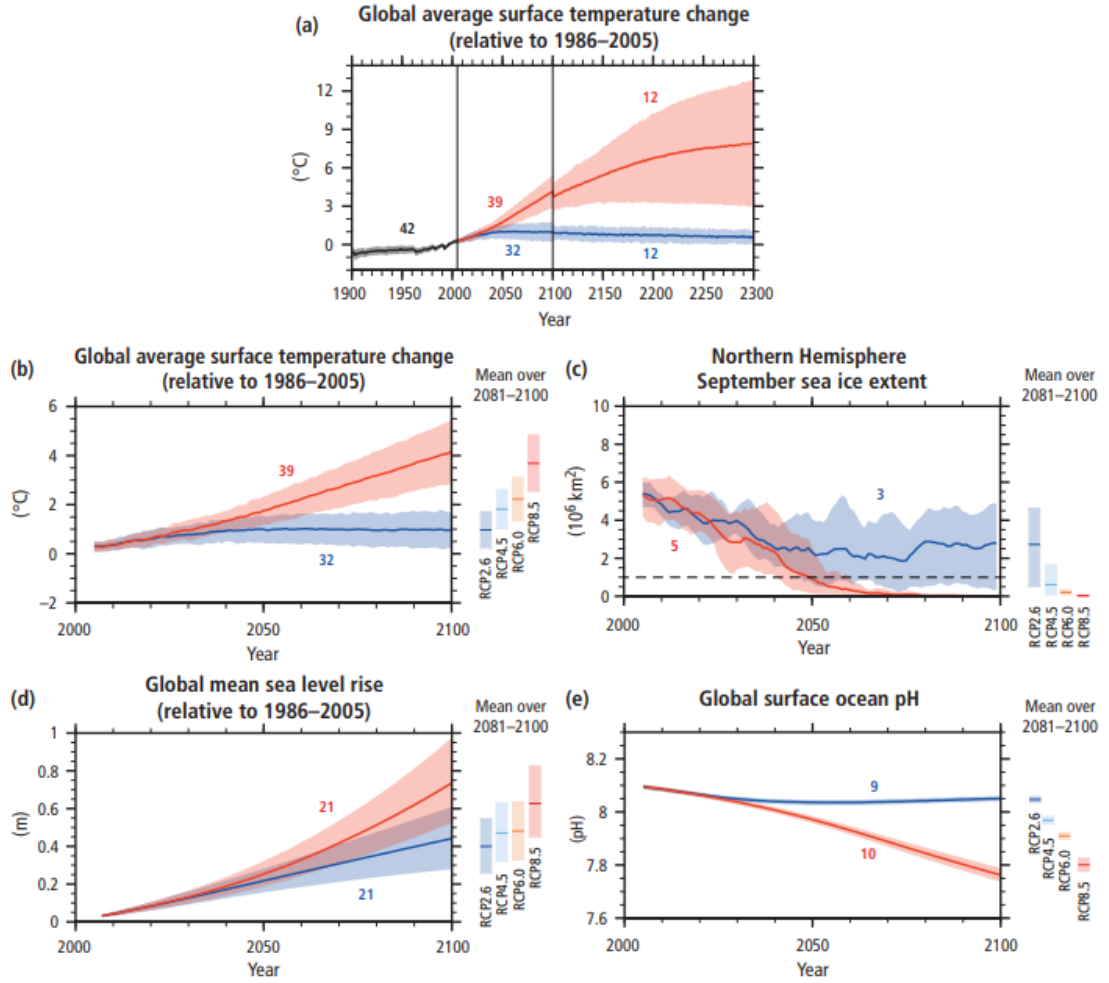

Figure 2 Time series of different global annual change in mean temperature for the 1900–2300 period.
Source: (Pachauri, Meyer, & Core Writing Team, 2014)

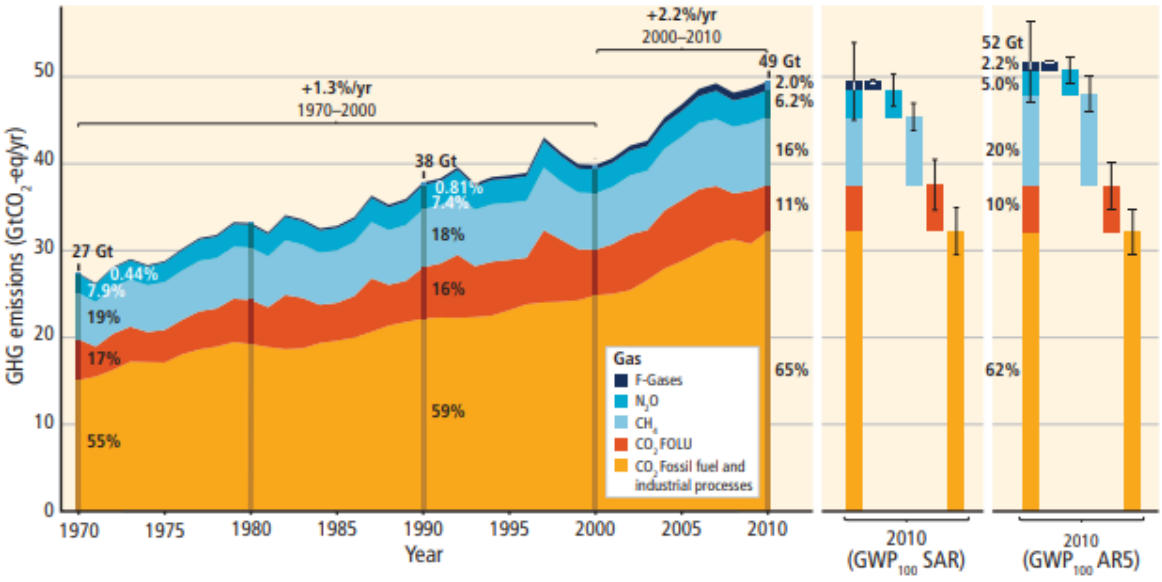

Figure 3 Total annual anthropogenic GHG emissions by gases 1970–2010.
Source: (Pachauri, Meyer, & Core Writing Team, 2014)

While climate change refers to the change in climate measurements over a long period of time, global warming refers to the increase in temperature mostly caused by atmospheric greenhouse gasses concentration increase[12]. Due to the disruptive misuse of resources and abusive production of GHG, human induced climate change is closing the gap towards threshold that could potentially cause irreversible damage to environmental systems. For this reason, after years in ongoing discussions over climate change adaptation and maintenance, according to scientists, it is imperative to control the increase in global average temperature over the following years as an increase of 2°C compared to pre-industrial could lead to catastrophic irreversible consequences (Paris Agreement, 2015). The international community therefore has created the carbon budget, the amount of carbon dioxide that can be emitted to maintain the global temperatures below that 2°C increase[13], even more, as stated in the IPCC special report: Global Warming of 1.5°C it would be preferable as an increase of 2°C is already bringing unfavorable ecological systems[14].

PLANETARY BOUNDARIES

This concept was introduced in 2009 as a new approach to global sustainability, this approach "aims to define a safe operating space for human societies to develop and thrive, based on our evolving understanding of the functioning and resilience of the Earth system"[15]. This theoretical concept highlights the pressures that anthropogenic actions have caused to the actual earth system to reach a state of abrupt changes in the environment that can no longer be excluded affecting the future of humanity.

The planetary boundaries have been identified as the limits to ensure the Earth system operates safely, seven of these boundaries can already be quantified while other two additional boundaries have not yet been identified with a boundary level. These are: climate change (CO_2 concentration in the atmosphere <350 ppm and/or a maximum change of +1 W m^2 in radiative forcing); ocean acidification (mean surface seawater saturation state with respect to aragonite >= 80% of pre-industrial levels); stratospheric ozone (<5% reduction in O3 concentration from pre-industrial level of 290 Dobson Units); biogeochemical nitrogen (N) cycle (limit industrial and agricultural fixation of N^2 to 35 Tg N yr(-1)) and phosphorus (P) cycle (annual P inflow to oceans not to exceed 10 times the natural background weathering of P); global freshwater use (<4000 km^3 yr(-1) of consumptive use of runoff resources); land system change (<15% of the ice-free land surface under cropland); and the rate at which biological diversity is lost (annual rate of <10 extinctions per million species); chemical pollution and atmospheric aerosol loading[16]. This information is graphed in the table below.

[12] (USGS, n.d.)
[13] (Levin & Tompkins, 2014)
[14] (Mann, 2024)
[15] (Rockström J., 2015)
[16] (Rockström J. S. W., 2009)

PLANETARY BOUNDARIES				
Earth-system process	Parameters	Proposed boundary	Current status	Pre-industrial value
Climate change	(i) Atmospheric carbon dioxide concentration (parts per million by volume)	350	387	280
	(ii) Change in radiative forcing (watts per metre squared)	1	1.5	0
Rate of biodiversity loss	Extinction rate (number of species per million species per year)	10	>100	0.1–1
Nitrogen cycle (part of a boundary with the phosphorus cycle)	Amount of N_2 removed from the atmosphere for human use (millions of tonnes per year)	35	121	0
Phosphorus cycle (part of a boundary with the nitrogen cycle)	Quantity of P flowing into the oceans (millions of tonnes per year)	11	8.5–9.5	~1
Stratospheric ozone depletion	Concentration of ozone (Dobson unit)	276	283	290
Ocean acidification	Global mean saturation state of aragonite in surface sea water	2.75	2.90	3.44
Global freshwater use	Consumption of freshwater by humans (km^3 per year)	4,000	2,600	415
Change in land use	Percentage of global land cover converted to cropland	15	11.7	Low
Atmospheric aerosol loading	Overall particulate concentration in the atmosphere, on a regional basis	To be determined		
Chemical pollution	For example, amount emitted to, or concentration of persistent organic pollutants, plastics, endocrine disrupters, heavy metals and nuclear waste in, the global environment, or the effects on ecosystem and functioning of Earth system thereof	To be determined		

Tale 1 Planetary Boundaries.
Source: (Rockström Johan, 2009)

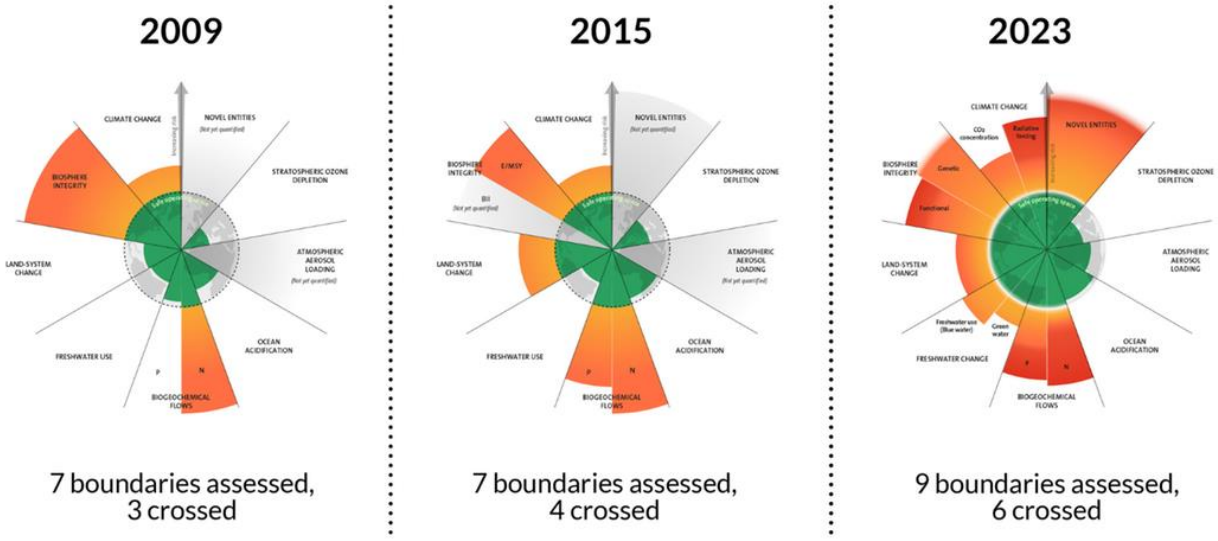

Figure 4 The 2023 update to the Planetary boundaries.
Source: (Stockhol University, 2023)

Even though "Transgressing one or more planetary boundaries may be deleterious or even catastrophic due to the risk of crossing thresholds that will trigger non-linear, abrupt environmental change within continental- to planetary-scale systems"[17], various planetary boundaries have already been transgressed. The planetary boundaries concept proposes groundwork through controlled variables towards a safe operating space that works towards a resilient[18] and Holocene[19] earth system.

SUSTAINABILITY

Sustainability was defined in 1987 by the UN (United Nations) by the Brundtland Commission as "meeting the needs of the present without compromising the ability of future generations to meet their own needs." (UN, 2012) The UN with the collaborative work of almost 140 developing countries are now seeking a sustainable future through an integrated approach concerns not only environmental consideration but also socio-economic development.

Although the concept of sustainability gained global recognition following the United Nations' formal definition, the need for a fundamental shift in the way we live and develop has been a topic of discussion for many years. An ongoing dialogue between the paradigm of perpetual growth in an environment with limitations prompted a growing awareness of the environmental, social, and economic challenges posed by unsustainable development practices. Over time, the urgency of this shift has only intensified as the negative impact of human activity on the planet has become more recognizable and gradually taken center stage in various disciplines.

It is clear the concept of sustainability is both a theoretical and political construct that has evolved over time, drawing from a diverse range of knowledge and practices. Its development has been shaped by contributions from various disciplines, as well as advocacy by international organizations. Over the past several decades, these actors have played a pivotal role in advancing the idea of sustainability, working to broaden its acceptance and integration into global policy frameworks. While the concept initially emerged from academic and activist circles, it has since gained widespread recognition as a critical guiding principle for addressing the complex challenges of environmental, social, and economic limitations, as the continuous discussion that started formerly since the 1960´s and is currently ongoing[20].

One of the first major appraising was the publication of "The Limits to Growth (LtG)" by the Club of Rome in the 1972. In 1968 The Club of Rome was created as an informal organization which purpose was to join and confront a variety of interdependent components such as economics, politics, environment and society. The interaction between these varied and diverse components will conform and study the complexity in regarding the human innovative actions confronted with the demographic and environmental limitations of the global context in which we live[21]. The limits to growth establish the challenges and preventions that humans need to face to achieve alternative patterns to assure a livable future.

[17] (Rockström J. S. W., 2009)
[18] "The climate is changing, and human activity is the primary factor in the acceleration of climate change over the past century. The ability to prepare for, recover from, and adapt to these impacts is called "climate resilience." (Center for climate and energy solutions, 2019)
[19] "Range within which Earth System processes varied in the Holocene as a scientific reference point for a desirable planetary state". (Rockström J. S. W., 2009)
[20] (Civín, 2023)
[21] (Blewitt, 2015)

The Limits to Growth was developed as a collaboration between The Club of Rome and the MIT research team with the aim to start different international debates in all societies direct the conversations as cited in the report towards the formation of ¨thoughtful men and women in all fields of endeavor to consider the need for concerted action now if we are to preserve the habitability of this planet for ourselves and our children¨[22]. One of the key issues identified by The Cub of Rome is the varying levels of human concern which arise from human perspective and the difficulty of thinking that growth has a limit. These variations in perspective are analyzed through the dimensions of space and time and are illustrated in the following figure.

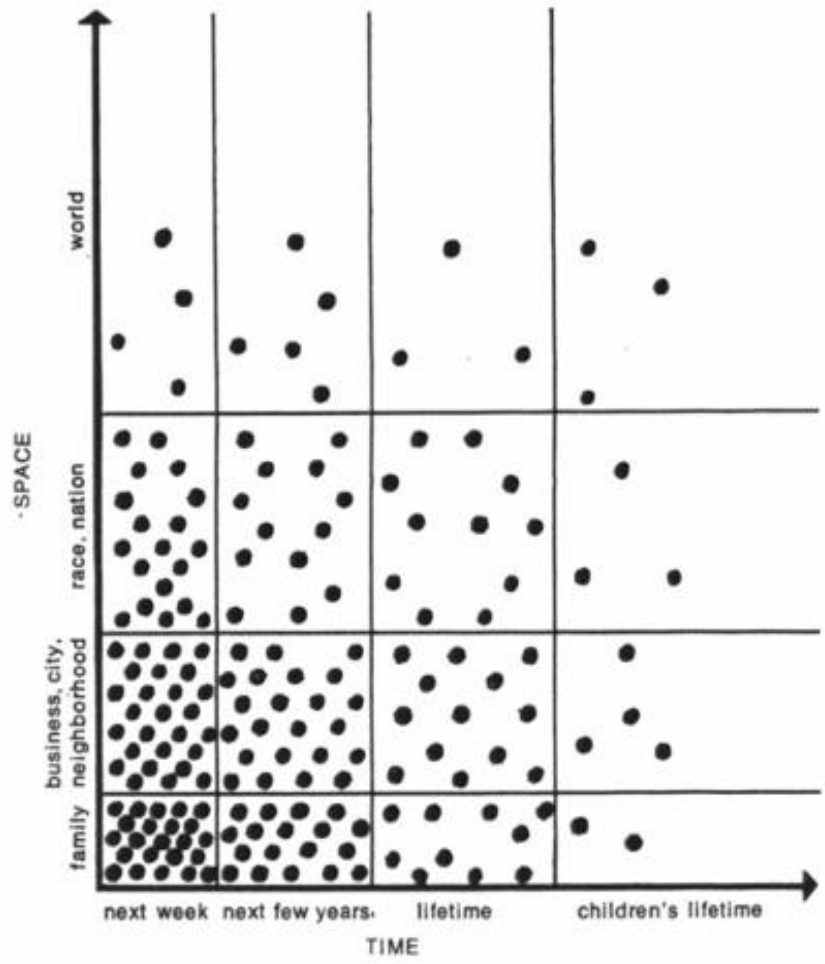

Figure 5 human perspectives.
source: (Meadows. Donella H, 1972)

The analysis concludes that "every human concern falls somewhere on the space-time graph. The majority of concerns pertain to matters affecting only family and friends, typically over a short time span. Some concerns extend further, considering issues that impact a city or nation, while only a small number of individuals possess a global perspective, encompassing both broader spatial and temporal dimensions"" (Meadows et al, 1972, p.19).

From this statement, it becomes clear that humans often overlook the long-term consequences of our current lifestyles and decision-making processes. The book emphasizes that the constant

[22] (Meadows. Donella H, 1972)

search for economic growth and consumption, without consideration for environmental limits, poses a significant threat to the sustainability of both our societies and the planet. The authors argue that the unchecked exploitation of resources, combined with growing populations, could lead to a collapse of critical ecological and social systems establishing the clean need of fundamental changes to be made.

In the light of displaying the relationships and dynamics of society to interrogate the unsuitable development towards a wellbeing for future generations[23], a model of the five major global concerns of the world was elaborated. The use of the computational modelling sicked a way to interconnect the trends of accelerated industrialization, rapid population growth, widespread malnutrition, depletion of nonrenewable resources and environmental deterioration of global economic systems and their interactions[24]. The model sought to construct a development measurement that instead of studying these trends by months or years the measurement widened into a measurement involving decades or centuries.

In this way computational modelling seeks to portray a warning, generating a better understanding of the complex world system of interdependent dynamics of exponential growth created by the different technological, economic, social and environmental factors that frame the way the world operates. By breaking down this complexity the authors illustrate the importance of current forecasts in future problems focusing on the collective relationship of different world models. Some of the world models which gave greater input and evidence of the need to reevaluate human practices and world development decisions, narrowing the path towards a state of global equilibrium and more sustainable future are the world models of standard run and natural resources.

[23] (Meadowcroft, 2024)
[24] (Civín, 2023)

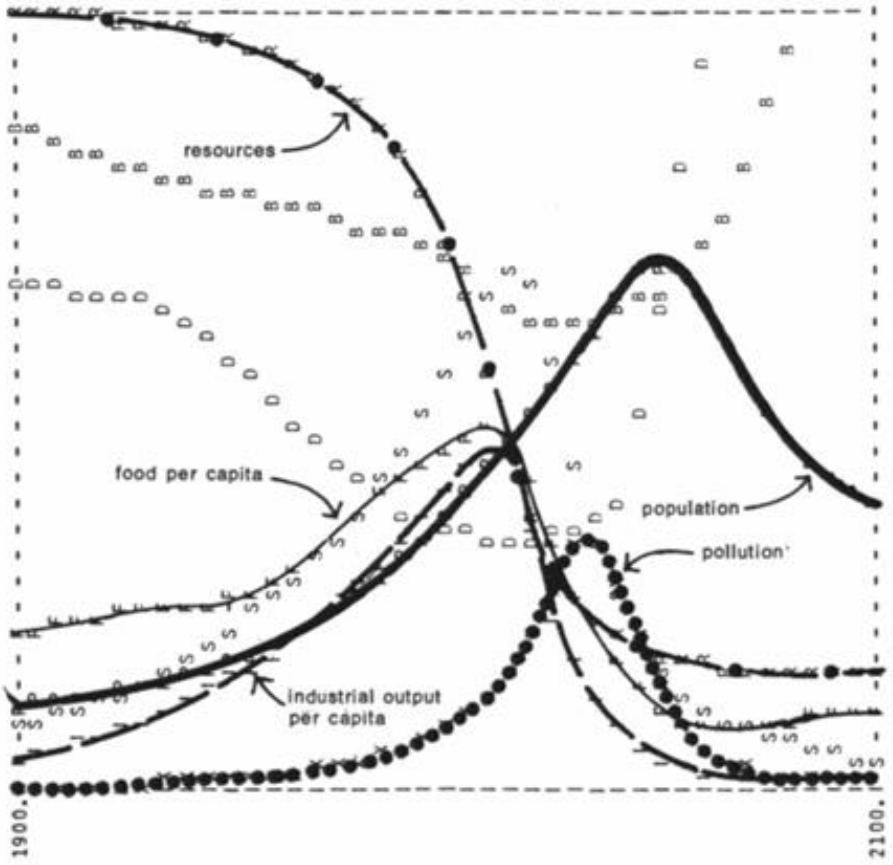

The "standard" world model run assumes no major change in the physical, economic, or social relationships that have historically governed the development of the world system. All variables plotted here follow historical values from 1900 to 1970. Food, industrial output, and population grow exponentially until the rapidly diminishing resource base forces a slowdown in industrial growth. Because of natural delays in the system, both population and pollution continue to increase for some time after the peak of industrialization. Population growth is finally halted by a rise in the death rate due to decreased food and medical services.

Figure 6 World Model of Standard Run.
Source: (Meadows. Donella H, 1972)

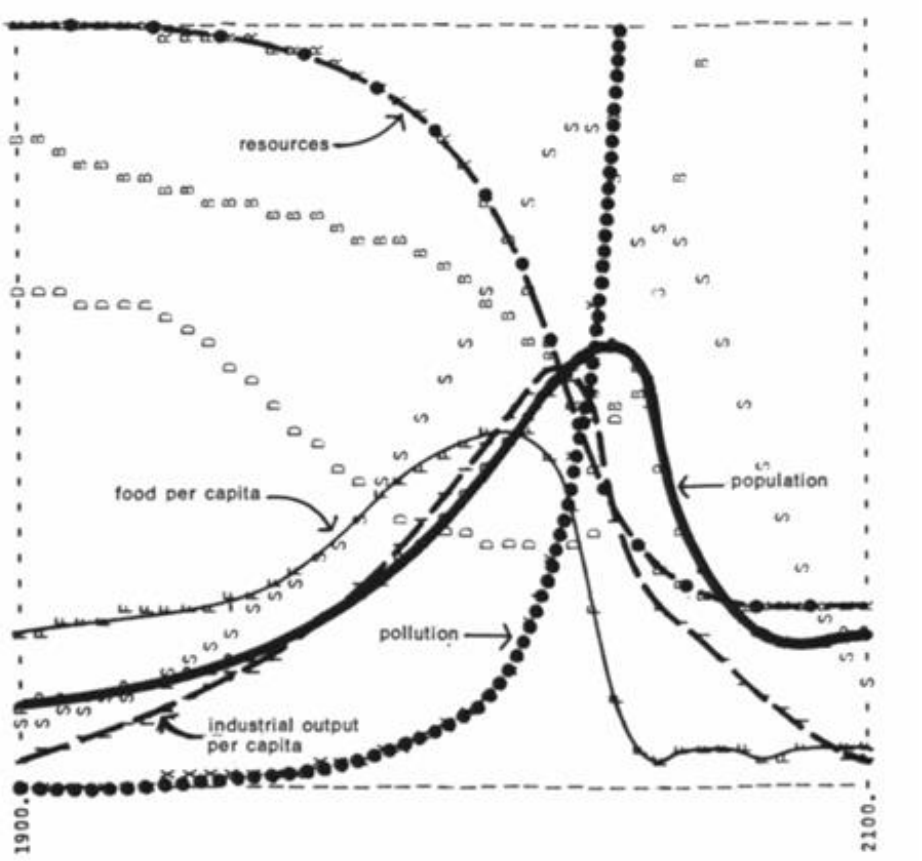

To test the model assumption about available resources, we doubled the resource reserves in 1900, keeping all other assumptions identical to those in the standard run. Now industrialization can reach a higher level since resources are not so quickly depleted. The larger industrial plant releases pollution at such a rate, however, that the environmental pollution absorption mechanisms become saturated. Pollution rises very rapidly, causing an immediate increase in the death rate and a decline in food production. At the end of the run resources are severely depleted in spite of the doubled amount initially available.

Figure 7 World Model of Natural Resources.
Source: (Meadows. Donella H, 1972)

In conclusion, *The Limits to Growth* highlight the critical need for a paradigm shift starting from the assumption that without taking care or resource availability the world economy will collapse within 50-to-100-year time[25]. "If the present growth trends in world population, industrialization, pollution, food production, and resource depletion continue unchanged, the limits to growth on this planet will be reached sometime within the next one hundred years. The most probable result will be a rather sudden and uncontrollable decline in both population and industrial capacity" (Meadows et al, 1972, p.23). This message intended to shift humanity development approaches, emphasizing the unsustainable nature of current economic and consumption patterns.

The book warns that without significant changes to the way we manage resources, population growth, and industrial output, the planet will face irreversible ecological degradation, social instability, and economic collapse. It calls for a global commitment to sustainable development, which involves reducing consumption, adopting circular economic models, and prioritizing environmental restoration. For architecture and urban planning, this means rethinking design

[25] (The Universty of Nottingham, 2012)

practices to minimize environmental impact, enhance resource efficiency, and create resilient, adaptive built environments that support both current and future generations. The model applied in Limits to Growth was verified 30 years later but some of its authors and other independent institutions such as the Commonwealth Scientific and Industrial Research Organization (CSIRO)[26] resulting in support of the previous outcomes, underscoring the urgency of integrating ecological limits into all facets of decision-making to ensure a livable and sustainable future, the result of this analysis is summarized in the following tables which present different possible scenarios depending on the future decision making[27].

Scenario	% Difference at 2000 relative to observed data	Population	Crude birth rate	Crude death rate	Non-renewable resources	Services per capita	Food per capita	Industrial output per capita	Persistent pollution
Standard run	Value	0	15	40	−25 to −5	−5 to 30	−5	5	15
	Rate of change	25	−15	70	80 to 415	25 to 470	−30	10	80
Comprehensive technology	Value	0	5	−10	0 to 30	35 to 80	100	35	−55
	Rate of change	10	0	250	−15 to −75	360 to 1970	170	65	−155
Stabilized world	Value	−25	−30	0	−10 to 20	45 to 90	25	10	−55
	Rate of change	−70	−75	130	15 to −65	20 to 450	−70	−125	−155

Percent differences are with respect to the observed data, and positive when the scenario values (or rate of change) are greater than the observed data. Entries of more than 20% in value, or greater than 50% for rates of change generally highlight discrepancies between data and model output.

Table 2 Values and rates of change of scenario variables compared with the data at year 2000 for three scenarios.
Source: (Turner, 2008)

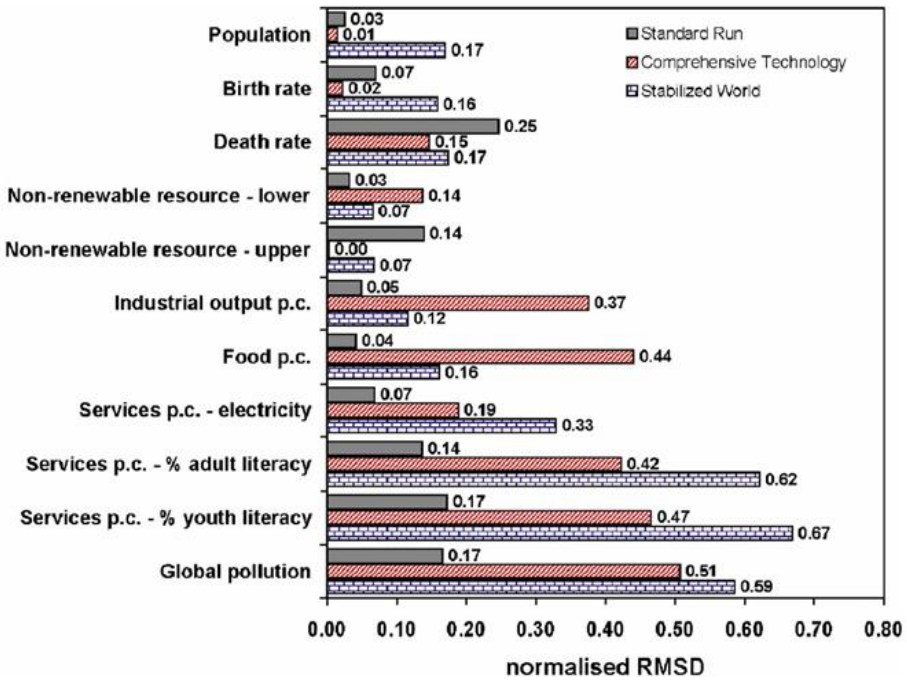

Figure 8 Normalized root mean square deviation for each LtG output compared with the observed data, for each scenario. Closer agreement between data and model output.
Source: (Turner, 2008)

Indeed, new ways of living must ensure that current development does not obstruct the future generations' well-being; it is necessary to implement sustainable practices at every level of decision-making, from the design of individual buildings to the planning of entire cities[28]. This

[26] (Meadows D.H., 2004)
[27] (Turner, 2008)
[28] (Civín, 2023)

includes adopting energy-efficient technologies, using renewable materials, and fostering designs that prioritize the health of the ecosystem and its inhabitants. As the effects of climate change intensify, it is more evident the importance of shifting towards a development model that respects ecological limits, addresses environmental justice, and supports long-term ecological and social resilience.

SUSTAINABLE DEVELOPMENT

The Stockholm Conference of 1972, entitled the United Nations Conference on the Human Environment, was one of the fundamental milestones in the history of environmental governance. Held in Stockholm, Sweden, this was the first major international conference to address the growing concerns about environmental degradation, linking human development with ecological sustainability[29]. The conference brought together 113 nations that with the help of environmental experts produced a turning point in global environmental policy "parallel processes of institution building, scientific innovation, and political engagement" (Sorlin & Paglia , 2024) in order to create shared values for a global governance. A key outcome of the conference was the adoption of the Stockholm Declaration, a series of 26 principles that set the foundation for modern environmental law and international collaboration. These principles emphasized the need for sustainable development, the right to a healthy environment, and the importance of international cooperation in addressing environmental issues[30].

Moreover, the conference highlighted the urgency of addressing issues such as climate change, ecosystemic services, pollution, resource depletion, and the protection of biodiversity, and broadened the conversation including topics such as population and poverty, which have since remained central to global environmental agendas[31]. The Stockholm Conference also led to the establishment of various conferences, action plans involving multilateral environmental cooperation, and programs such as the Conference on Environment and Development[32] or the United Nations Environment Programme[33]. The conference was not only decisive in coordinating global environmental efforts, what is more crucial is the post conference shape of institution building in government governance system[34]. While the conference did not produce legally binding agreements, it was a landmark providing the framework and groundwork for future environmental diplomacy, subsequent global agreements, including the Rio Summit (1992), Kyoto protocol (1997) and the Paris Agreement (2015), which would later build on the principles of sustainable development articulated in Stockholm.

The Rio Summit, known as the United Nations Conference on Environment and Development (UNCED) brought together representatives from 178 nations, including over 100 heads of state, international organizations, and non-governmental organizations (NGOs)[35]. By the end of the conference several official documents were developed resulting in influential agreements and declarations that continue to shape international environmental policy such as: The Rio Declaration on Environment and Development, Agenda 21, The Convention on Biological

[29] (UNESCO, 1998)
[30] (UN, 1972)
[31] (Lorenzini & Cassata, 2022)
[32] Developed in 1992, also known as the Earth Summit
[33] UNEP - Formally launched in December 1972, accumulated a mixed record in fostering global environmental cooperation. (Manulak, 2023)
[34] (Manulak, 2023)
[35] (Chasek, Downie, & Brown , 2017)

Diversity (CBD), The United Nations Framework Convention on Climate Change (UNFCCC), and The Forest Principles also leading to the creation of the commission on Sustainability Development[36].

The 2015 Paris Agreement brought together 196 Parties, including nearly every nation in the world, in a legally binding framework to address the escalating threat of climate change[37]. The Agreement marked a shift from previous climate negotiations by focusing on both mitigation and adaptation efforts, while emphasizing the importance of international cooperation commitments. The key elements on the Paris Agreement on climate change were identified as: Net Zero, limit the temperature rise to 1.5˚C; Adaptation, review countries commitment to cutting emissions, and finance, providing climate finance to developing countries[38].

The Kyoto Protocol, adopted in 1997 and enforced in 2005, is a legally binding international treaty under the United Nations Framework Convention on Climate Change (UNFCCC) that aims to reduce greenhouse gas (GHG) emissions to mitigate global warming. The protocol set mandatory emission reduction targets for 37 industrialized nations and the European Community, with an average reduction goal of 5% below 1990 levels during the first commitment period (2008–2012)[39]. In 2012, a second commitment period, known as the Doha Amendment, was established, requiring reductions of at least 18% by 2020 compared to 1990 levels[40].

[36] (UN, n.d.)
[37] (Rajamani, 2016)
[38] (UN, n.d.)
[39] (UNFCC, 2011)
[40] (UNFCC, 2013)

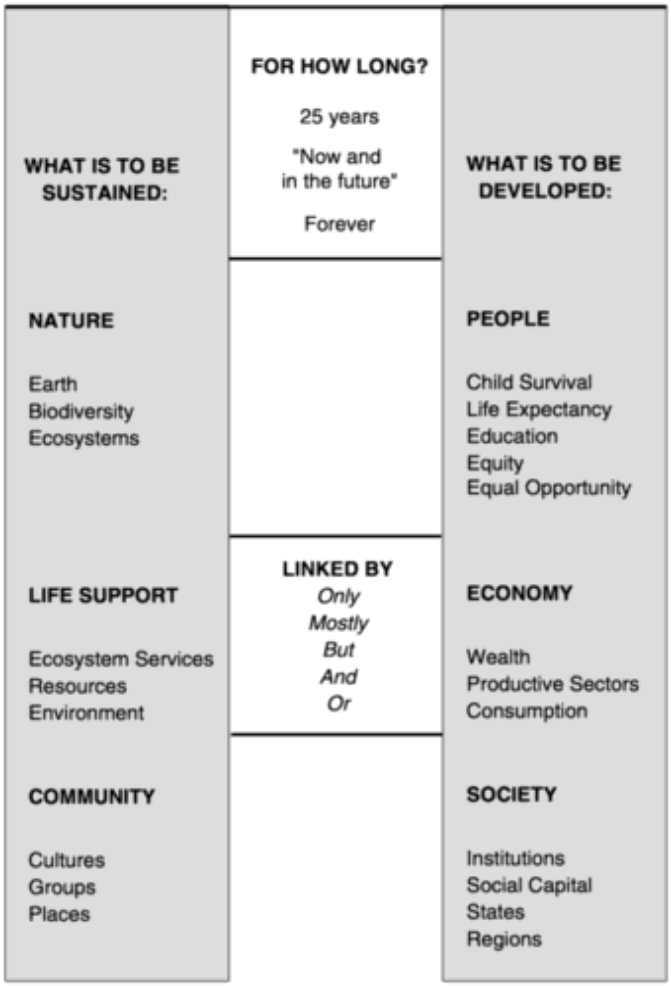

Figure 9 Sustainable Development: common concerns, differing emphases. Source: (National Academy, 1999)

Sustainable development is commonly defined as "development that meets the needs of the present without compromising the ability of future generations to meet their own needs", this definition, first articulated in the 1987 Brundtland Report - Our Common Future, was one of the fundamental elements for de development of modern sustainability discourse[41]. Sustainable development is confirmed by three pillars: environmental, economic, and social sustainability, each of which must be addressed in parallel for it to be fulfilled. These pillars are inherently interconnected, and the challenge lies in balancing these dimensions to create integrated, sustainable development pathways, achieving it requires not only mitigating environmental degradation but also promoting economic resilience and social equity[42].

[41] (World Commission on Environment and Development, 1987)
[42] (Kates , Parris, & Leiserowitz, 2005)

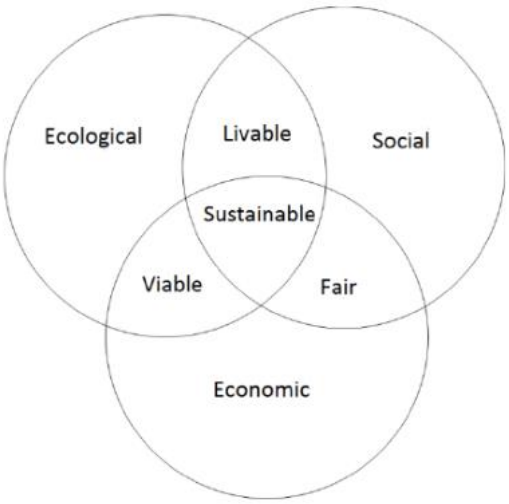

Figure 10 Venn diagram for sustainable development.
Source: (Myllyviita, 2013)

Environmental sustainability focuses on maintaining the integrity of natural systems and conserving and resources management, pollution prevent and environmental protection and restauration of future generations. This pillar is based on the concept of "planetary boundaries", introduced in 2009 by Rockstrom et al, which outline the Earth's ecological systems towards a safe operating space for humanity[43]. The boundaries provision a critical threshold of the limits beyond the Anthropocene[44] period we live on causing irreversible environmental damage may occur, including climate change, biodiversity loss, and land-system change. Thereby for Earth's life-support it is essential that human activity should stay within these boundaries with the aim of ensuring the Earth to continue working correctly. Additionally, achieving environmental sustainability requires the adoption of practices and technologies that reduce resource use and environmental degradation, including renewable energy, circular economy principle, and sustainable land use[45].

The economic dimension of sustainable development considers a change in growth concept thriving resilient, inclusive and equitable economies that settle resource depletion, this new concept of growth fosters innovation and adaptation policies promoting resource efficiency to ensure financial stability[46]. Economic resilience exposes key economic and social patterns, broadening the debate of growth addressing disparities in wealth and inequality, ensuring the presence of political economy driven by equitably distributed across societies for economic growth to be considered truly sustainable[47]. The holistic approach in global development argues that economic sustainability requires a shift from conventional economic models that prioritize growth to systems that address well-being, social equity, and the efficient use of resources[48]. A key concept in this regard is the circular economy, "model of production and consumption, which involves sharing, leasing, reusing, repairing, refurbishing and recycling existing materials and

[43] (Rockström J. S. W., 2009)
[44] "Is an unofficial unit of geologic time, used to describe the most recent period in Earth's history when human activity started to have a significant impact on the planet's climate and ecosystems" (National Geographic Society, 2023).
[45] (Geissdoerfer, Savaget, bOCKEN, & Hultink, 2017)
[46] (Oliwia, 2024)
[47] (Piketty & Goldhammer, 2014)
[48] (Sachs, 2015)

products as long as possible" (European Parliament, 2023), thereby reducing waste and extending products life cycle**.**

Figure 11 The circular economy model
Source: European Parliament Research Service

The social dimension of sustainability emphasizes justice, equity, and the improvement of human well-being, embracing social networking, and cooperation for disparities reduction and essential services to be ensured for all individuals[49]. According to Sen (1999), development should be understood not merely as economic growth but as the expansion of human capabilities where the focus is on freedom as the expansion method of societies value, depending on socioeconomical arranges and political - civil rights. Social sustainability also addresses issues such as health, education, and access to basic needs, ensuring that all individuals, particularly marginalized groups, can participate in just societies, providing equitable access to opportunities and resources[50]. This perspective is further expanded by Boström et al. (2015), who argue that social sustainability includes fostering community resilience, cultural diversity, and social cohesion. Ensuring that sustainable development initiatives address the needs of vulnerable populations is critical for achieving global social sustainability.

Governance plays one of the most important roles in facilitating sustainable development, as it involves creating the framework, policies, arrangements and institutional cooperation needed to support the integration of sustainability across all sectors. Effective governance requires collaboration among governments, businesses, and civil society creating standard quantifiable indicators to achieve common sustainability goals[51]. The implementation of sustainability policies must be supported by science and evidence of regression analyses that base decision making, testing the influence of governance participation, policy coherence, reflexivity, adaptation and

[49] (Oliwia, 2024)
[50] (enel, 2024)
[51] (Kubiszewski, et al., 2013)

democratic institutionality participation in adaptive environmental and social conditions[52]. Governance is particularly important in the context of global challenges such as climate change, where international cooperation is essential. For this reason, in 2015 The United Nations adopted the Sustainable Development Goals, representing a comprehensive framework for achieving sustainability at the global level, providing targets for governments and organizations to strive toward[53].

Figure 12 Sustainable Development Goals.
Source: (United Nations, 2015)

In conclusion, sustainable development is a complex and multiscale concept that requires the integrated consideration of environmental, economic, and social dimensions. As highlighted by Sachs (2015), achieving sustainability involves systemic change at all levels of society, from individual behavior to global governance. While there are significant challenges in the sphere of global environmental crises and socio-economic inequality, the pursuit of sustainable development becomes even more essential on account of balancing the three pillars of sustainability and ensuring a viable future for generations to come.

SUSTAINABLE DEVELOPMENT IN CONSTRUCTION

Construction and the building environment are some of the most influential elements caused by the Anthropocene, with bigger contributors to global warming, and for this same reason playing a significant role in climate change due to its substantial greenhouse gas emissions and resource-intensive practices. The building sector is responsible for a large portion of global CO_2 emissions, primarily from the production of construction materials highly relying on fossil fuels such as cement and steel[54]. Additionally, construction activities and material production, use and disposal contribute to inconceivable emissions throughput the whole material life cycle, reinforcing

[52] (Glass & Newig, 2019)
[53] (United Nations, 2015)
[54] (Oliver, 2022)

deforestation and land-use changes, creating a further reducing carbon sequestration capacity and exacerbating the greenhouse effect[55].

Beyond emissions, the construction industry is constantly exploiting the natural environment, generating substantial waste and consuming large amounts of energy and natural resources, including water and raw materials, leading to increased environmental load. To mitigate these impacts, sustainable construction policies and practices are gaining prominence, emphasizing the use of low-carbon materials, energy-efficient designs, and circular economy principles that aim to reduce resource consumption and minimize waste[56] .

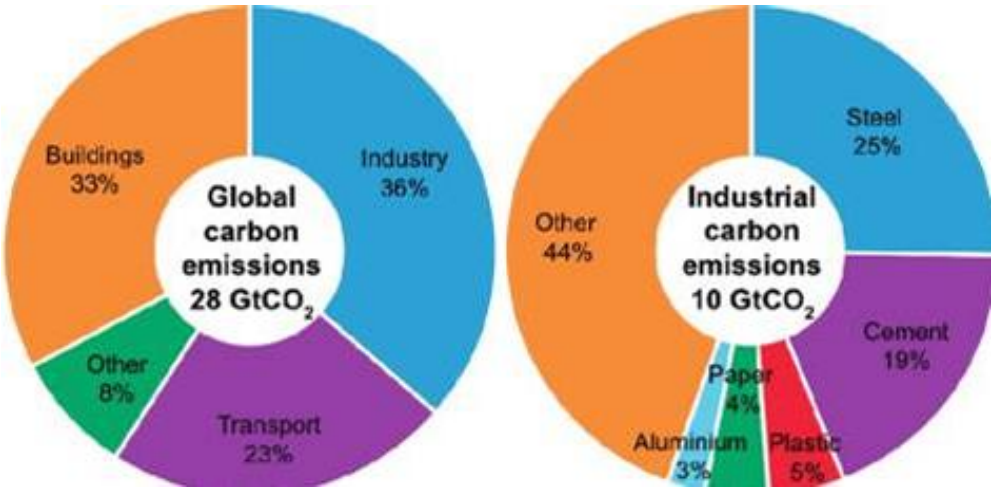

Figure 13 Global anthropogenic CO2 emissions related to energy processes for all development sectors and specifically for industrial emissions.
Source: (Allwood, Cullen, & Waught, 2010)

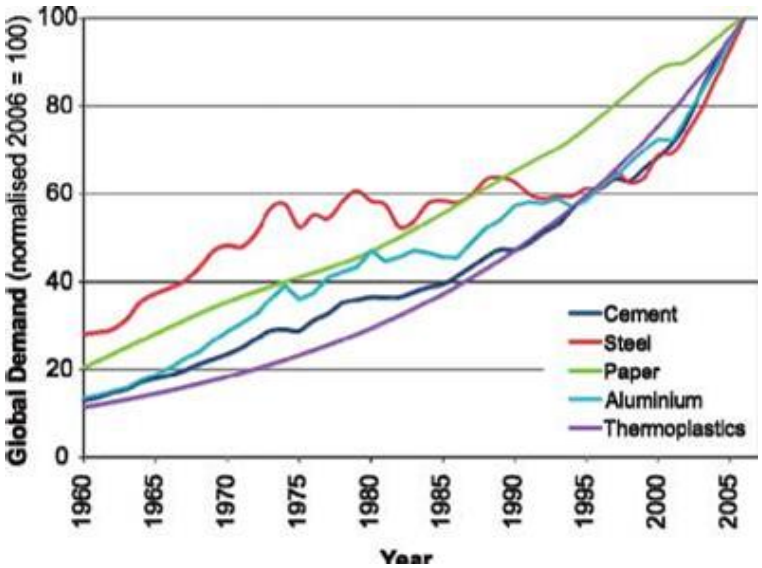

Figure 14 Normalized global demand for the five key materials since 1960.
Source: (Allwood, Cullen, & Waught, 2010)

In the hopes to adapt and mitigate the ecosystem disruption induced by activities, sustainable development has also become one of the main concepts towards achieving a net zero world. In

[55] (Hertwich, Lifset, Pauliuk, & Heeren, 2020)
[56] (Pomponi & Moncaster, 2017)

this way sustainable development in construction encompasses a broad range of considerations that span the entire lifecycle of a building, from the selection of raw materials to its end of life. One of the primary factors is to be aware of the whole life cycle of the material starting by the source of raw materials to the disposal and treatment, which includes assessing the energy consumed in their transportation and transformation[57]. According to Allwood et al. (2011), the embodied energy in construction materials plays a significant role in reducing or increasing a building's overall environmental footprint. Furthermore, the construction process must optimize energy buildings with optimized thermal performance and energy-efficient systems so that carbon emissions can be significantly reduced over time. Another essential aspect is the durability of materials and the flexibility of building design to adapt to future needs and technologies, required for the building's lifespan to be extended consequently reducing the need for cost renovations[58].

Sustainable buildings must also consider their potential for disassembly and reassembly, facilitating the reuse and recycling of materials, in line with principles of the circular economy[59]. Additionally, integrating renewable energy sources power for heating, cooling, and natural ventilation, not only decreases reliance on nonrenewable energy but also enhances the building's sustainability. Studies show that solar energy integration can significantly reduce operational energy use and improve the overall environmental impact[60] of buildings by avoiding the use of fossil fuels and lead to massive environmental problems. Achieving sustainability in construction requires a holistic approach, addressing material choices, energy efficiency, adaptability, and renewable energy integration to promote long-term environmental resilience.

[57] (Huang , et al., 2020)
[58] (Thormark , 2002)
[59] (González , Sendra, Herena, Rosquillas, & Vaz, 2021)
[60] (Hu, y otros, 2020)

CEMENT

Cement is a finely ground material primarily composed of limestone, clay, and other mineral constituents, which undergoes a high-temperature calcination process in a kiln to form clinker. This clinker is subsequently ground with a small proportion of gypsum to produce Portland cement, the most widely used type of cement[61]. Upon the addition of water to the previously explained fine powder, cement undergoes a chemical reaction known as hydration, which leads to the formation of calcium silicate hydrate and other compounds that develop strength and rigidity to the material. In this process aggregates of different origins and such as sand and gravel are additions to the mixture to produce concrete[62].

Cement is one of the most used materials throughout human history, though the first extensive construction evidence of cement implementation is found in the roman empire when lime and volcanic ash reacted with water and formed a hard mass[63], the implementation of cementitious materials started back in 2600 B.C. in the Egyptian empire with the use of calcined gypsum as part of the pyramid construction[64]. One of the first contributors in the understanding and application of cement technologies is the Roman Marcus Vitruvius, architect and engineer who captured all his knowledge and discoveries in one of the most ancient treaties ever found establishing the first principles of architecture "Ten books of Architecture".

The significance of cement for the construction sector started very early in human history, resulting in it being one of the most indispensable materials for everyday life due to its affordability, durability and mechanical properties. Nowadays cement is one of the most broadly used construction materials serving a mainstay for current infrastructure, used in almost all scopes of architecture and engineering due to its versatility and its possibility of variation in different components. Its predominancy comes from the endless possibilities that it gives us, constantly evolving, new technologies being implemented, and innovative procedures and applications constantly being, makes it the material which allowed for the development of cities and urbanization to exist worldwide.

[61] (Taylor , 1997)
[62] (Neville A. , 2011)
[63] This cementitious material would then be known as pozzlanic cement
[64] (CEMEX, 2002)

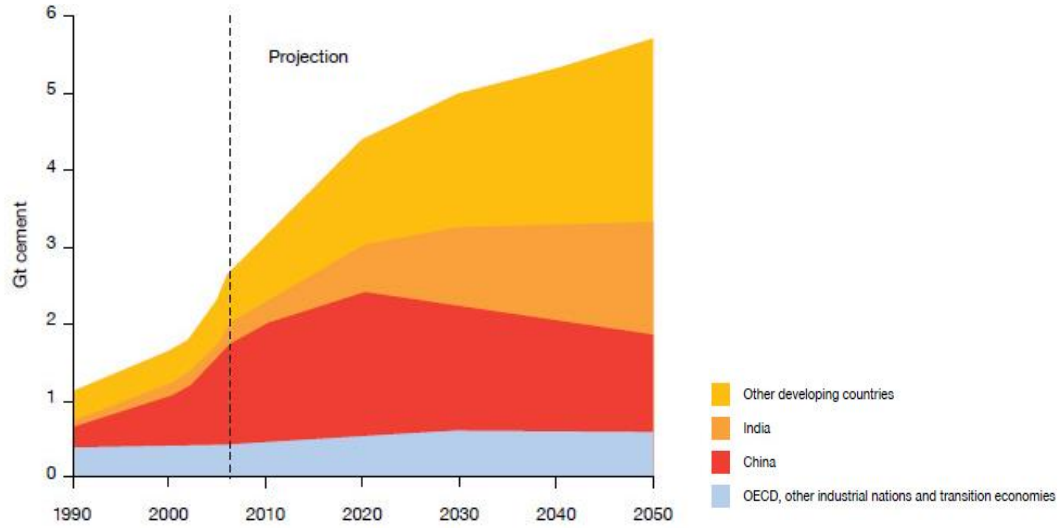

Figure 15 World Cement production in industrialized and developing countries.
Source: (Geiger, 2011)

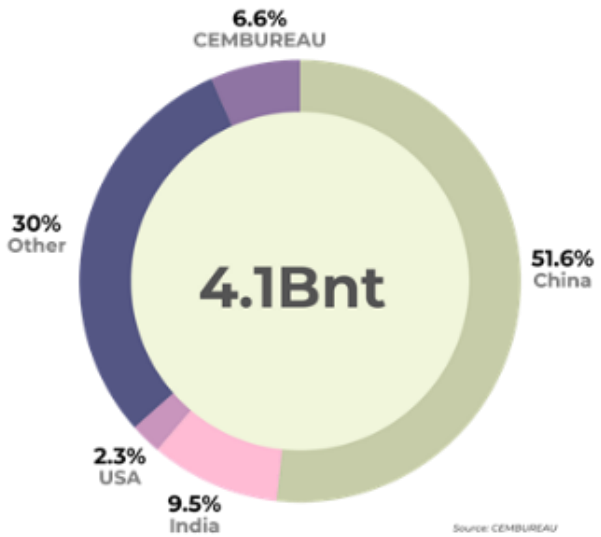

Figure 16 World Cement production 2022.
Source: (CEMBUREAU, 2022)

However, due to its feedstock and its great volume production processes it is known to be one of the bigger emitters of CO_2 in the same way, one of the major contributors to GHG emissions. Specifically, only the manufacture of Portland cement is responsible for almost 6-8% of the global GHG emissions[65] because of the calcination of limestone is one of the major inputs to carbon dioxide release as a byproduct. In the same way other GHG are released in the energy intensive heating and grinding processes of the raw material[66]. All of this has made cement production a focal point in the discussion of construction sustainability, the urgent need for alternative mitigation strategies, promoting research for alternative material implementation, carbon capture and storage technologies, and energy efficient procedures[67].

[65] (Schumacher & Juniper, 2023)
[66] (Habert, 2013)
[67] (Gupta & Chaudhary, 2020)

TYPES OF CEMENT

Cement, as the most widely used construction material worldwide, became one of the pillars needed for development in infrastructure and architecture to take place. Its versatility is evident in the wide range of types and formulations available, each designed to meet specific construction requirements and address diverse needs. The various types of cement are the result of extensive research and innovation, reflecting the evolution of architecture and engineering throughout history alongside the evolution of concrete. Over time, advancements in materials science and engineering practices have led to the refinement of cement properties, enabling the creation of specialized formulas adapting to durability, sustainability, and structural performance.

OPC - Ordinary Portland Cement is the most widely used cement in general construction, categorized into three grades (strength classes) based on the compressive strength obtained after 28 days of hydration. These grades indicate the strength in MPa achieved in standard testing conditions. This type of cement is known for its versatility, making it suitable for a wide range of applications in buildings, bridges, and pavements. As its composition is the simplest, consisting only of limestone, clay, and gypsum, it makes it easy to be produced contributing to its application in the construction industry[68].

In the early 19th century, Portland cement established itself as one of the materials that would revolutionize the construction industry. In 1824, Joseph Aspdin, an English mason, patented a method for producing a hydraulic cement by burning a mixture of limestone and clay, which he named "Portland cement" due to its resemblance to the building stones found on the Isle of Portland in England[69]. Aspdin's invention was further refined by subsequent researchers and industrialists, one of the most notable advances was the improvement in consistency and strength of the cement through advancements in kiln design technologies and when a better understanding of the chemistry behind the implementation of the raw materials used in the production process of cement was gained[70]. By the late 19th century and continuing until current dates, Portland cement is the dominant binding material used in concrete, mostly used to its improved properties such as strength and durability compared to previous material used before.

PPC - Portland Pozzolana Cement is produced by blending Ordinary Portland Cement with pozzolanic materials like fly ash or volcanic ash, with a content varying from 35-55%. These pozzolanic materials react with calcium hydroxide released during the hydration process, enhancing the durability and strength of the cement due to - lower content of Ca(OH)2 , lower content of C3A, and lower porosity[71]. It is known for its lower heat of hydration and greater resistance to aggressive chemical environments, commonly used in marine structures, dams, and sewage treatment plants, where resistance to sulphates and other chemicals exposure is critical due to the impact these chemicals can have on the structures affecting their resistance and durability.

Rapid Hardening Cement is a type of cement that sets and gains strength much faster than Portland cement. Even though it is similar in composition there is a difference found in the particle size distribution. This type of cement utilizes a finer particle size, which accelerates hydration and

[68] (Mindess, Young , & Darwin, 2003)
[69] (Nobis, n.d)
[70] (Hewlett, 1935)
[71] (Mehta & Monteiro, 2014)

strength development. Rapid Hardening Cement achieves a high early strength, making it ideal for fast-track construction projects, including pavement repairs and precast concrete elements[72].

Masonry Cement is a blend of Portland cement, including limestone, plasticizers, and other additives to improve its workability and binding strength. It is specifically designed for use in masonry applications such as brickwork, blockwork, and plastering[73].

GGBFS - Ground Granulated Blast Furnace Slag Cement, commonly known as Blast furnace Cement, is created by blending OPC with granulated blast furnace slag[74]. The inclusion of slag improves the cement's durability, reduces heat of hydration, and enhances resistance to chemicals, particularly from chlorides and sulphates[75]. Blast Furnace Cement is widely used in mass concrete applications such as foundations, marine structures, and infrastructure projects exposed to harsh environments[76]. Its lower carbon footprint compared to traditional OPC aligns with sustainable construction practices as cement with 85% of GGBS allows the saving of up to 2 GJ/ton of energy.

PORTLAND CEMENT

Portland cement is the predominant type of cement used worldwide, is the foundational cementitious component used in concrete mixtures, making it crucial for the existence of construction, civil engineering and architectural applications. The main ingredient in Portland cement is clinker, produced by calcining a blend of raw materials (most commonly limestone and clay are the ones used) and calcium aluminates, at high temperatures in a rotary kiln. This heating process causes the decomposition of calcium carbonate into calcium oxide and carbon dioxide, accompanied by a series of chemical transformations that generate calcium silicates (the primary constituents of clinker)[77]. At the end of this process, the resulting product is allowed to cool down, once cooled, the clinker is finely ground and mixed with a small proportion of gypsum to regulate the setting time, resulting in the final Portland cement product[78].

The performance characteristics of Portland cement are closely linked to its chemical composition and how fine the material resulted from the grinding process. The most crucial compounds for the strength development of the concrete in the early and long-term stages are, tricalcium silicate (C_3S) and dicalcium silicate (C_2S). During the hydration process these silicates react with water to form calcium silicate hydrates (C-S-H) and calcium hydroxide, responsible for imparting strength and durability to the concrete after it achieves its hardened state[79]. The addition of gypsum is essential to manage the rate of hydration, preventing premature setting and ensuring sufficient workability during application[80]. Properly measuring and balancing the chemical constituents of Portland cement is vital to the concrete creation, as variations to the mixture

[72] (Neville A. , 2011)
[73] (Aitcin, 1998)
[74] A byproduct of steel manufacturing, formed by rapidly cooling slag from smelted iron ore in a blast furnace, consists of at least two-thirds glassy slag by mass and exhibits hydraulic properties when properly activated.
[75] (Neville A. , 2011)
[76] (Mehta & Monteiro, 2014)
[77] (Taylor , 1997)
[78] (Neville A. , 2011)
[79] (Mehta & Monteiro, 2014)
[80] (Hewlett, 1935)

formula can impact in significant changes of the mechanical properties, including compressive strength, setting characteristics, and overall durability[81].

Despite its essential role in construction, as mentioned before the production of Portland cement has significant climate impacts that can conclude in irreversible environmental repercussions. These environmental impacts come because of the highly energy-intensive manufacturing process that relies on the combustion of fossil fuels in kilns. For this process to be carried out temperatures above 1,450°C need to be reached, leading to substantial emissions of carbon dioxide. To address these environmental challenges, there is a concerted effort that needs to be addressed by all the areas involved in construction to reduce clinker content in cement by incorporating supplementary cementitious materials (SCMs), such as fly ash, slag, and natural pozzolans. These alternatives not only decrease the carbon footprint associated with cement production but also enhance the durability and life cycle of concrete[82].

PRODUCTIVE CYCLE

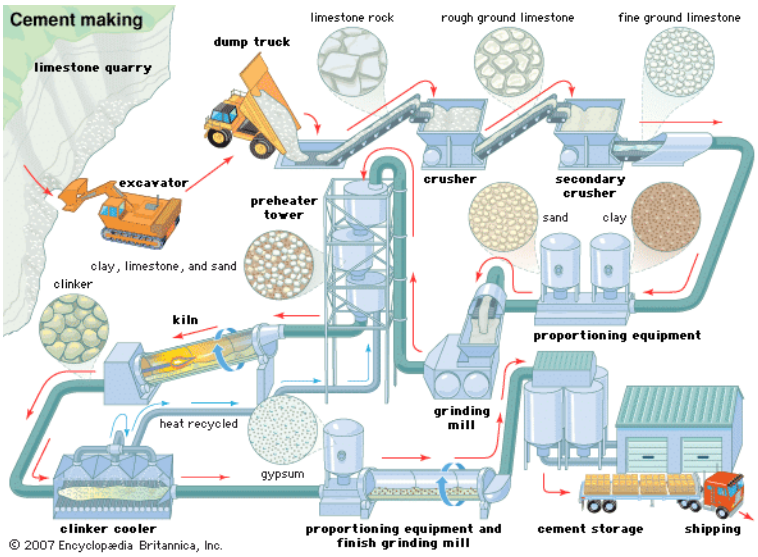

Figure 17 Portland cement manufacturing process.
Source: (Encyclopedia Britannica, 2007).

The production cycle of Portland cement is a multistage process that requires precise control over raw materials and processing conditions to ensure the desired quality of the final product. This process, even if standardized with the aim of creating lower waste and contamination, is both resource and energy intensive. The steps in the production cycle start with the extraction and preparation of raw materials, and then move on to the grinding and blending into a raw meal, clinker production in a rotary kiln, and the final grinding stage to produce cement powder[83].

The initial phase of Portland cement production involves raw materials extraction and preparation, primarily limestone and clay, which supply the necessary calcium, silica, alumina, and iron oxides required for cement formulation and manufacture[84]. These raw materials are typically mined from

[81] (Taylor , 1997)
[82] (Djettene, Dubois, Duprez, Weireld, & Thomas, 2024)
[83] (Wansbrough, 2017)
[84] (Habert, 2013)

quarries and sorted out through an arduous selection process considering their chemical compositions to ensure they meet the criteria for cement manufacturing. After the extraction process is finished, the raw materials are exposed to a crushing process to reduce their size, after which they are blended to create a homogeneous mixture. This blend, known as the raw mix, is then dried to achieve a consistent moisture content suitable for further processing[85].

The second stage involves the grinding of the raw mix to a fine powder known as the raw meal. The fineness and the mixture formula of the raw meal is critical, as it directly influences the efficiency of subsequent chemical reactions during clinker formation[86]. This process can be made in two different methods, the dry process and the wet process. In the dry process, progressively abandoned, clay and limestone are crushed, analyzed for mineral content, and mixed before being ground to a fine powder, if needed necessary minerals will be added to ensure its correct composition. In the wet process, the clay is mixed into a paste with water, then combined with crushed lime and further ground, heavy particles removed, and the resultant composition tested for proper mineral balance, with additives added as needed[87]. This finely ground material is then passed through a preheater tower and known as the pre-calciner. The preheating stage serves to partially calcine the limestone, decomposing calcium carbonate into calcium oxide and carbon dioxide, which aims to reduce the energy required in the primary kiln phase[88].

The preheated material obtained from the grinding is now ready for clinker production at the high temperature environment of the rotary kiln. The transformation process that is going to be further explained of the preheated raw meal into clinker is one of the most essential in cement manufacturing. It occurs in a rotary kiln operating at temperatures around 1,450°C[89], this high temperature energy intensive process creates a suitable environment for the creation of a series of complex chemical reactions, in which the raw materials are sintered to form nodules of clinker[90]. The production of clinkers is an energy-intensive step, largely due to the high heat required, making it the primary source of carbon dioxide emissions within the cement manufacturing cycle[91].

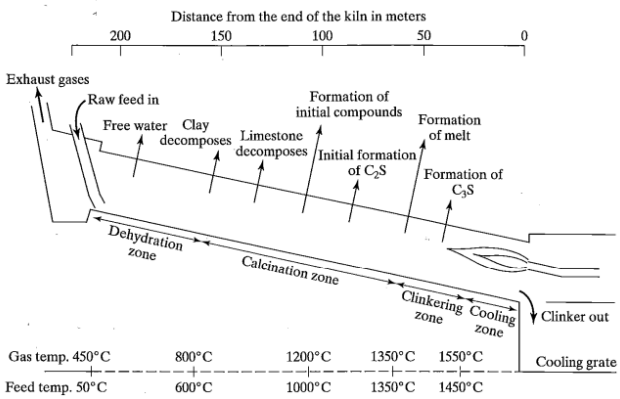

Figure 18 Schematic outline of kiln processes.
Source: (Mindess, Young , & Darwin, 2003)

[85] (Taylor , 1997)
[86] (Mehta & Monteiro, 2014)
[87] (Wansbrough, 2017)
[88] (Worell , Price, Hendriks, & Meida , 2001)
[89] (Ige, Olanrewaju, Duffy, & Obiora, 2001)
[90] (Taylor , 1997)
[91] (Griffiths, et al., 2023)

The most significant reactions involve the formation of calcium silicates (specifically, tricalcium silicate (C_3S) and dicalcium silicate (C_2S)), crucial for the cement's development of satisfactory mechanical properties[92]. From the major mineral constituents' mechanical properties and performance of the concrete can vary, C_3S (tricalcium silicate) and C_2S (dicalcium silicate) are responsible for the material strength. A higher proportion of C_3S, often accompanied by a lower percentage of C_2S (dicalcium silicate), contributes to rapid strength development, especially in the early stages, but also results in higher heat generation during the setting process. Conversely, a lower amount of C_3S and a higher concentration of C_2S causes the material to slower strength gain, extending the process over a period of 52 days instead of 28, while generating less heat. Even though C_3A affects strength contribution, it is associated with undesirable rapid heat generation and high reactivity, which can be mitigated by incorporating calcium sulfate ($CaSO_4$) into the cement. Additionally, C_3A can be converted into the more favorable C_4AF (calcium ferrite) by adding iron oxide (Fe_2O_3) prior to the heating process, considering that this conversion reduces the formation of C_3S. C_4AF enhances the cement's resistance to seawater and results in a slower reaction with reduced heat evolution[93].

Compound	Abbreviation	Chemical Formula	Weight Percent
Tricalcium silicate	C_3S	$3CaO*SiO_2$	60-70
Dicalcium silicate	C_2S	$2CaO*SiO_2$	10-20
Tricalcium aluminate	C_3A	$3CaO*Al_2O_3$	5-10
Tetra calcium aluminoferrite	C_4AF	$4CaO*Al_2O_3*Fe_2O_3$	3-8

Table 3 Major mineral constituents of Portland Cement.
Source: (Wansbrough, 2017).

Once the clinker exits the kiln, it is rapidly cooled using air to stabilize its properties and to stop any further chemical reactions. Cooling also preserves the microstructure of the clinker, essential for its reactivity. The cooled clinker is then mixed with a controlled amount of gypsum (typically around 3-5%), which regulates the setting time of the cement and prevents the rapid development of rigidity also known as flash setting [94]. This mixture is ground to a fine powder in specialized mills, the fineness of the grind significantly affects the hydration rate and, consequently, the strength development of the cement, underscoring the importance of this final step[95]. The finished cement is stored in silos before being dispatched for use in construction projects.

The hydration process of Portland cement is a multifaceted chemical process that involves a series of interactions between its components and water, ultimately forming compounds that contribute to the cement's final mechanical properties. The process undergoes a series of different reactions involving each of the previously stated chemical compounds in the composition of Portland cement, the different reaction rates result in the gradual increase in strength of the material over time.

Compound	Hydration reactions
Tricalcium silicate	Hydrates and hardens rapidly, responsible for initial set and early strength. Higher percentages of C_3S will exhibit higher early strength.

[92] (Mehta & Monteiro, 2014)
[93] (Wansbrough, 2017)
[94] (Neville A. , 2011)
[95] (Hewlett, 1935)

Dicalcium silicate	Hydrates and hardens slowly, responsible for strength increases beyond one week.
Tricalcium aluminate	Hydrates and hardens the quickest. Liberates a large amount of heat very fast, contributing to early strength. Gypsum is added to to retard C_3A hydration. Without gypsum, C_3A hydration would cause Portland cement to set almost immediately after adding water.
Tetra calcium aluminoferrite	Hydrates rapidly with almost no contribution to strength. Permits lower kiln temperatures manufacturing. Color effects are due to C_4AF.

Table 4 Hydration Reactions.
Source: (University of Washington, state DOTs, FHWA, 2024)

PROPERTIES

The physical properties of Portland cement are critical to its performance in construction. Understanding these characteristics allows the appropriate selection of cement type for each specific application. To ensure durability and structural integrity, the cement needs to be analyzed by fineness, specific gravity, consistency, setting time, soundness, compressive strength, and heat of hydration.

Fineness refers to the particle size of cement which affects the rate of hydration, strength development, and heat generation. The surface area available for hydration reactions increases in the presence of finer cement particle size, achieving faster strength gain and higher early strength, this effect is seen on the first seven days of hydration[96]. The fineness of Portland cement is typically measured using the Blaine air permeability method, with values commonly ranging between 300 to 400 m^2/kg[97].

The specific gravity of Portland cement, usually around 3.15[98], indicates its density relative to water. This property for calculating the mixed proportions of concrete, guaranteeing the correct balance of components creating the optimal specifications for workability and strength[99].

Consistency influences the workability of concrete and the hydration process, with insufficient water leading to incomplete hydration and excessive water causing segregation and reduced strength. It measures the water/cement ratio to achieve a paste of standard viscosity. It is typically determined using the Vicat apparatus, where normal consistency falls within the range of 26% to 33% of the cement's weight [100].

The setting time of cement refers to the period required for the paste to transform from its fluid state to a hardened state. The initial setting time typically ranges from 30 to 90 minutes, while the

[96] (Kosmatka, Kerkhoff, & Panarese, 2002)
[97] (Neville A. , 2011)
[98] For portland-blast-furnace-slag and portland-pozzolan the specific gravities is 2.90 (Kosmatka, Kerkhoff, & Panarese, 2002)
[99] (Mindess, Young , & Darwin, 2003)
[100] (Hewlett, 1935)

final setting time is generally within 10 hours [101]. A broad variety of tests are used to measure factors such as fineness, water content, and admixtures which can influence setting time[102].

Soundness is commonly measured by the Le Chatelier method or autoclave expansion tests. It secures the cement from undergoing significant volumetric changes after setting, the permissible expansion limit is generally set at 10 mm or less[103]. Overpassing this limit could lead to cracking or disintegration, on the other hand unsoundness is often caused by the presence of free lime or magnesia, which hydrate slowly and expand.

Compressive strength permits cement to withstand axial loads. It is measured by testing standard mortar cubes at 3, 7, and 28 days of curing. Portland cement typically achieves a compressive strength of 20 MPa at 3 days and 40 MPa at 28 days, depending on the type of cement and curing conditions[104].

The heat of hydration is the thermal energy released during the chemical reactions between cement and water. While higher heat is beneficial in cold climates, excessive heat can cause thermal cracking in massive concrete structures.

STANDARIZATIONS AND REGULATIONS

EN STANDARDS 197 – 1

The EN 197-1 standard is the European specification for cement, which defines the composition, classification, specification and conformity criteria for common cement. This standard is based on cements production and use across Europe maintain consistent quality, safety, and performance level. The objective of EN 197-1 is to standardize cement types, providing guidelines for producers and users to maintain reliability of the material used in construction applications[105]. The exploration of the EN 197-1, gives a broader understanding of cement, its implications for production, and the key properties specified within the standard.

Cement standards are looking for harmonization to assure quality and uniformity across construction materials, particularly within the European context. The EN 197-1 standard, initially published in 2000 by the European Committee for Standardization (CEN), covers various types of cements used in Europe, mainly considering different types of traditional Portland cement, composite cements, and special cements like sulfate-resistant variants[106].

EN 197-1 specifies the requirements for 27 distinct cement types, categorized into five main groups based on the clinker content and supplementary materials used. Each type of cement is further divided into subclasses based on specific composition ratios and performance requirements, reflecting variations in composition percentages, physical characteristics, and performance attributes.

[101] (Neville A. , 2011)
[102] (University of Washington, state DOTs, FHWA, 2024)
[103] (Mindess, Young , & Darwin, 2003)
[104] (Hewlett, 1935)
[105] (Dhir & Jones, 2014)
[106] (Datis Export Group, 2020)

CEM I	Portland Cement	Composed primarily of clinker, with a minor addition of gypsum.
CEM II	Portland-Composite Cement	includes up to 35% supplementary cementitious materials (SCMs) such as fly ash or limestone.
CEM III	Blast Furnace Cement	contains a significant percentage of granulated blast furnace slag (up to 95% in some types).
CEM IV	Pozzolanic Cement	includes natural pozzolans like volcanic ash or calcined clays.
CEM V	Composite Cement	mixture of clinker, slag, pozzolans, and other SCMs.

Table 5 Main types of cement according to the EN 197-1.
Source: Information adapted from the (CEN, 2011)

Main types	Notation of the 27 products (types of common cement)		Composition [percentage by mass [a]]										
			Main constituents										Minor additional constituents
			Clinker	Blast-furnace slag	Silica fume	Pozzolana		Fly ash		Burnt shale	Limestone		
						natural	natural calcined	siliceous	calca-reous				
			K	S	D [b]	P	Q	V	W	T	L	LL	
CEM I	Portland cement	CEM I	95-100	–	–	–	–	–	–	–	–	–	0 to 5
CEM II	Portland-slag cement	CEM II/A-S	80 to 94	6 to 20	–	–	–	–	–	–	–	–	0 to 5
		CEM II/B-S	65 to 79	21 to 35	–	–	–	–	–	–	–	–	0 to 5
	Portland-silica fume cement	CEM II/A-D	90 to 94	–	6 to 10	–	–	–	–	–	–	–	0 to 5
	Portland-pozzolana cement	CEM II/A-P	80 to 94	–	–	6 to 20	–	–	–	–	–	–	0 to 5
		CEM II/B-P	65 to 79	–	–	21 to 35	–	–	–	–	–	–	0 to 5
		CEM II/A-Q	80 to 94	–	–	–	6 to 20	–	–	–	–	–	0 to 5
		CEM II/B-Q	65 to 79	–	–	–	21 to 35	–	–	–	–	–	0 to 5
	Portland-fly ash cement	CEM II/A-V	80 to 94	–	–	–	–	6 to 20	–	–	–	–	0 to 5
		CEM II/B-V	65 to 79	–	–	–	–	21 to 35	–	–	–	–	0 to 5
		CEM II/A-W	80 to 94	–	–	–	–	–	6 to 20	–	–	–	0 to 5
		CEM II/B-W	65 to 79	–	–	–	–	–	21 to 35	–	–	–	0 to 5
	Portland-burnt shale cement	CEM II/A-T	80 to 94	–	–	–	–	–	–	6 to 20	–	–	0 to 5
		CEM II/B-T	65 to 79	–	–	–	–	–	–	21 to 35	–	–	0 to 5
	Portland-limestone cement	CEM II/A-L	80 to 94	–	–	–	–	–	–	–	6 to 20	–	0 to 5
		CEM II/B-L	65 to 79	–	–	–	–	–	–	–	21 to 35	–	0 to 5
		CEM II/A-LL	80 to 94	–	–	–	–	–	–	–	–	6 to 20	0 to 5
		CEM II/B-LL	65 to 79	–	–	–	–	–	–	–	–	21 to 35	0 to 5
	Portland-composite cement [c]	CEM II/A-M	80 to 94	<---------- 6 to 20 ---------->									0 to 5
		CEM II/B-M	65 to 79	<---------- 21 to 35 ---------->									0 to 5
CEM III	Blastfurnace cement	CEM III/A	35 to 64	36 to 65	–	–	–	–	–	–	–	–	0 to 5
		CEM III/B	20 to 34	66 to 80	–	–	–	–	–	–	–	–	0 to 5
		CEM III/C	5 to 19	81 to 95	–	–	–	–	–	–	–	–	0 to 5
CEM IV	Pozzolanic cement [c]	CEM IV/A	65 to 89	–	<---------- 11 to 35 ---------->					–	–	–	0 to 5
		CEM IV/B	45 to 64	–	<---------- 36 to 55 ---------->					–	–	–	0 to 5
CEM V	Composite cement [c]	CEM V/A	40 to 64	18 to 30	–	<-------- 18 to 30 ------>			–	–	–	–	0 to 5
		CEM V/B	20 to 38	31 to 50	–	<-------- 31 to 50 ------>			–	–	–	–	0 to 5

[a] The values in the table refer to the sum of the main and minor additional constituents.
[b] The proportion of silica fume is limited to 10 %.
[c] In Portland-composite cements CEM II/A-M and CEM II/B-M, in Pozzolanic cements CEM IV/A and CEM IV/B and in composite cements CEM V/A and CEM V/B the main constituents other than clinker shall be declared by designation of the cement (for example see clause 8).

Table 6 EN 197-1 cement subtypes. The name of each subcategory comes from:
CEM II / A – S
CEM (Roman number) / letter – letter
cement type / % addition – type of addition
Source: (CEN, 2011)

PROPERTIES

The EN 197-1 standard emphasizes strictly controlling the chemical composition of cement so that consistent quality and durability can be achieved. This includes setting maximum limits for

oxides such as tricalcium aluminate (C_3A), tricalcium silicate (C_3S), and dicalcium silicate (C_2S), which influence the cement's hydration behavior and long-term strength[107].

The standard presents specific guidelines for physical and mechanical properties requirements such as early strength, standard strength, initial setting time, and soundness.

Strength class	Compressive strength MPa				Initial setting time	Sound-ness (expan-sion)
	Early strength		Standard strength			
	2 days	7 days	28 days		min	mm
32,5 N	-	≥ 16,0	≥ 32,5	≤ 52,5	≥ 75	≤ 10
32,5 R	≥ 10,0	-				
42,5 N	≥ 10,0	-	≥ 42,5	≤ 62,5	≥ 60	
42,5 R	≥ 20,0	-				
52,5 N	≥ 20,0	-	≥ 52,5	-	≥ 45	
52,5 R	≥ 30,0	-				

Table 7 Mechanical and physical requirements given as characteristic values. Source: (CEN, 2011)

1	2	3	4	5
Property	Test reference	Cement type	Strength class	Requirements [a]
Loss on ignition	EN 196-2	CEM I CEM III	all	≤ 5,0 %
Insoluble residue	EN 196-2 [b]	CEM I CEM III	all	≤ 5,0 %
Sulfate content (as SO_3)	EN 196-2	CEM I CEM II [c] CEM IV CEM V	32,5 N 32,5 R 42,5 N	≤ 3,5 %
			42,5 R 52,5 N 52,5 R	≤ 4,0 %
		CEM III [d]	all	
Chloride content	EN 196-21	all [e]	all	≤ 0,10 % [f]
Pozzolanicity	EN 196-5	CEM IV	all	Satisfies the test

[a] Requirements are given as percentage by mass of the final cement.
[b] Determination of residue insoluble in hydrochloric acid and sodium carbonate.
[c] Cement type CEM II/B-T may contain up to 4,5 % sulfate for all strength classes.
[d] Cement type CEM III/C may contain up to 4,5 % sulfate.
[e] Cement type CEM III may contain more than 0,10 % chloride but in that case the maximum chloride content shall be stated on the packaging and/or the delivery note.
[f] For pre-stressing applications cements may be produced according to a lower requirement. If so, the value of 0,10 % shall be replaced by this lower value which shall be stated in the delivery note.

Table 8 Chemical requirements given as characteristic value. Source: (CEN, 2011)

TESTING AND CONFORMITY CRITERIA

The conformity criteria set forth in EN 197-1 require that all cement types undergo rigorous testing procedures to verify their compliance with the standard. The testing covers a range of factors, including chemical composition, mechanical strength, and consistency of performance[108].

[107] (Taylor , 1997)
[108] (CEN, 2011)

Cement producers are required to follow precise testing protocols, including sampling methods[109], chemical analysis[110] and Physical testing for strength, setting times, and fineness[111].

Conformity assessment is crucial for maintaining the reliability of cement materials, so that expected safety and durability standards can be met in construction. The certification process is managed by national standardization bodies, which verify that manufacturers serve the EN 197-1 guidelines.

ASTM C150 SPECIFICATION

The American Society for Testing and Materials (ASTM) is an organization that creates voluntary consensus standards on a global scale. These standards are crafted by committees comprising industry professionals, who collaborate through an open and transparent process to produce standards, test methods, specifications, guides, and best practices[112].

ASTM C150 is a recognized Standard Specification for Portland Cement regulation, setting forth the requirements for the composition, performance, and testing of Portland cement. Provides essential criteria to ensure the consistency, safety, and durability of Portland cement used in construction projects, necessary to maintain harmonized quality in concrete production[113].

Portland cement is the most used cement in the world, as it is the main ingredient in concrete, mortar, and other construction materials. The ASTM C150 standard gives guidance towards the cement industry's best practices, supporting reliable and long-lasting infrastructure. The standard Specification for Portland Cement, also known as ASTM C 150, acknowledges 8 basic types of Portland cement.

Type	Name	Purpose
I	Normal	General-purpose cement is suitable for most purposes.
IA	Normal-Air Entraining	An air-entraining modification of Type I.
II	Moderate Sulfate Resistance	Used as a precaution against moderate sulfate attack. It will usually generate less heat at a slower rate than Type I cement.
IIA	Moderate Sulfate Resistance-Air Entraining	An air-entraining modification of Type II.
III	High Early Strength	Used when high early strength is needed. It has more C3S than Type I cement and has been ground finer to provide a higher surface-to-volume ratio, both of which speed up hydration reactions. Strength gain is double that of Type I cement in the first 24 hours.
IIIA	High Early Strength-Air Entraining	An air-entraining modification of Type III.

[109] Specified in EN 196-7. (CEN, 2011)
[110] Used to determine oxide composition according to EN 196-2. (CEN, 2011)
[111]Specified in the EN 187-1. (CEN, 2011)
[112] (ASTM, 2024)
[113] (Kosmatka, Kerkhoff, & Panarese, 2002)

IV	Low Heat of Hydration	Used when hydration heat must be minimized in large volume applications such as gravity dams. Contains about half the C_3S and C3A and double the C_2S of Type I cement.
V	High Sulfate Resistance	Used as a precaution against severe sulfate action – principally where soils or groundwaters have a high sulfate content. It gains strength at a slower rate than Type I cement. High sulfate resistance is attributable to low C_3A content.

Table 9 ASTM Types of Portland Cement.
Source: (University of Washington, state DOTs, FHWA, 2024)

Each of this cement outlined types in ASTM C150 is further classified by its fineness, chemical composition, and physical properties specific to different applications, allowing engineers and builders to select the appropriate cement type based on environmental factors and performance requirements.

PROPERTIES

Chemical composition of Portland cement is strictly defined in the ASTM C150 to guarantee the materials' performance and longevity. In the same way as in the EN 197-1 standard, these standard chemical compounds include tricalcium silicate (C_3S), dicalcium silicate (C_2S), tricalcium aluminate (C_3A), and tetra calcium aluminoferrite (C_4AF), directly affecting the cements hydration rate, setting time, and long-term strength of the cement[114]. Specific requirements under ASTM C150 include chemical Composition, Physical Properties, Setting Time and Soundness.

These stringent chemical and physical criteria ensure that Portland cement produced according to ASTM C150 provides reliable performance under diverse environmental conditions.

Cement Type[A]	Applicable Test Method	I and IA	II and IIA	II(MH) and II(MH)A	III and IIIA	IV	V
Aluminum oxide (Al_2O_3), max, %	C114	...	6.0	6.0	...	...	...
Ferric oxide (Fe_2O_3), max, %	C114	...	6.0[B]	6.0[B,C]	...	6.5	...
Magnesium oxide (MgO), max, %	C114	6.0	6.0	6.0	6.0	6.0	6.0
Sulfur trioxide (SO_3),[D] max, %	C114						
When $(C_3A)^E$ is 8 % or less		3.0	3.0	3.0	3.5	2.3	2.3
When $(C_3A)^E$ is more than 8 %		3.5	[F]	[F]	4.5	[F]	[F]
Loss on ignition, max, %	C114						
When limestone is not an ingredient		3.0	3.0	3.0	3.0	2.5	3.0
When limestone is an ingredient		3.5	3.5	3.5	3.5	3.5	3.5
Insoluble residue, max, %	C114	1.5	1.5	1.5	1.5	1.5	1.5
Equivalent alkalies ($Na_2O + 0.658\ K_2O$), %	C114	[G]	[G]	[G]	[G]	[G]	[G]
Tricalcium silicate (C_3S),[E] max, %	See Annex A1	...	...	...	...	35[C]	...
Dicalcium silicate (C_2S),[E] min, %	See Annex A1	...	...	...	...	40[C]	...
Tricalcium aluminate (C_3A),[E] max, %	See Annex A1	...	8	8	15	7[C]	5[B]
Sum of $C_3S + 4.75(C_3A)$,[H] max, %	See Annex A1	...	...	100[C,I]	...	...	...
Tetracalcium aluminoferrite plus twice the tricalcium aluminate $(C_4AF + 2(C_3A))$, or solid solution $(C_4AF + C_2F)$, as applicable, max, %	See Annex A1	...	...	...	...	...	25[B]

Table 10 Standard composition requirements.
Source: (ASTM, 1940)

[114] (Neville A. , 2011)

Cement Type	Applicable Test Method	I and IA	II and IIA	II(MH) and II(MH)A	III and IIIA	IV	V	Remarks
Tricalcium aluminate (C_3A),[B] max, %	See Annex A1	...	...	...	8	...	...	For moderate sulfate resistance.
Tricalcium aluminate (C_3A),[B] max, %	See Annex A1	...	...	...	5	...	...	For high sulfate resistance.

Table 11 Optional standard composition requirements.
Source: (ASTM, 1940)

Cement Type[A]	Applicable Test Method	I	IA	II	IIA	II(MH)	II(MH)A	III	IIIA	IV	V
Air content of mortar,[B] volume %:	C185										
max		12	22	12	22	12	22	12	22	12	12
min		...	16	...	16	...	16	...	16	...	...
Fineness, specific surface, m^2/kg											
Air permeability test	C204										
min		260	260	260	260	260	260	...	...	260	260
max		...	...	...	...	430[C]	430[C]	...	...	430	...
Autoclave expansion, max, %	C151/C151M	0.80	0.80	0.80	0.80	0.80	0.80	0.80	0.80	0.80	0.80
Strength, not less than the values shown for the ages indicated as follows:[D]											
Compressive strength, MPa [psi]:	C109/C109M										
1 day		...	...	...	...	...	...	12.0 [1740]	10.0 [1450]	...	...
3 days		12.0 [1740]	10.0 [1450]	10.0 [1450]	8.0 [1160]	10.0 [1450]	8.0 [1160]	24.0 [3480]	19.0 [2760]	...	8.0 [1160]
7 days		19.0 [2760]	16.0 [2320]	17.0 [2470]	14.0 [2030]	17.0 [2470]	14.0 [2030]	...	...	7.0 [1020]	15.0 [2180]
28 days		...	...	...	...	...	...	...	...	17.0 [2470]	21.0 [3050]
Time of setting; Vicat test:[E]	C191										
Time of setting, minutes, not less than		45	45	45	45	45	45	45	45	45	45
Time of setting, minutes, not more than		375	375	375	375	375	375	375	375	375	375

iTeh Standard
(https://standards.iteh.ai)
Document Preview
ASTM C150/C150M-21

Table 12 Standard Physical requirements.
Source: (ASTM, 1940)

Cement Type	Applicable Test Method	I and II	IA and IIA	II(MH)	II(MH)A	III	IIIA	IV	V
Early stiffening, final penetration, min, %	C451	50	50	50	50	50	50	50	50
Heat of hydration:									
Isothermal Conduction Calorimetry:									
3 days, max, kJ/kg [cal/g]	C1702	...	...	335 [80][B]	335 [80][B]	...	...	200 [50][C]	...
7 days, max, kJ/kg [cal/g]		...	...	...	...	...	...	225 [55][C]	...
Strength, not less than the values shown:									
Compressive strength, MPa [psi]	C109/C109M								
28 days		28.0 [4060]	22.0 [3190]	28.0 [4060]	22.0 [3190]	...	...	...	...
Sulfate resistance,[D] 14 days, max, % expansion	C452	...[E]	...[E]	...[E]	...[E]	...	...	...	0.040
Gillmore test:	C266								
Initial set, min, not less than		60	60	60	60	60	60	60	60
Final set, min, not more than		600	600	600	600	600	600	600	600

Table 13 Optional standard Physical requirements.
Source: (ASTM, 1940)

TESTING AND CONFORMITY CRITERIA

The ASTM C150 standard requires that Portland cement develop a series of standardized tests that need to stand in a specified criterion. These tests let the cement achieve the necessary requirements for both physical and chemical properties[115], to obtain these key testing protocols

[115] (ASTM, 1940)

are needed such as Sampling methods[116], Chemical analysis[117] , Strength testing[118] Fineness assessment[119] , and Setting time evaluation[120]

Conformity with these standards is verified by independent laboratories and quality control systems implemented by cement manufacturers. The certification process provides confidence in the material's reliability, making ASTM C150 indispensable for the cement industry.

ENVIRONMENTAL IMPACT - EN 197-1 & ASTM C150

A significant aspect of the EN 197-1 standard is its encouragement of sustainable cement production. Researchers have noted the importance of EN 197-1 in setting criteria that align with environmental and durability considerations[121]. In a similar way ASTM C150 not only assures cements quality but also impacts the durability and sustainability of concrete structures with the implementation of cement based in sulfate resistance and heat of hydration, supporting the design of structures in challenging environments[122].

Both standards also prevent environmental hazards, this is evident when incorporating industrial by-products like fly ash, slag, and silica fume promote the use of supplementary cementitious materials (SCMs) to reduce the environmental footprint of cement production. The use of these materials can lower carbon dioxide emissions related with clinker production, responsible for a great portion of the cement industry total CO_2 emissions[123]. In the same way researchers state that standard detailed classification developed in the EN 197-1allows for improved predictability in the behavior of cementitious systems, especially in long-term durability assessments[124].

Although ASTM C150 does not cover blended cements, it indirectly supports sustainable practices through specifications that encourage performance-based assessment and the use of materials with lower environmental impacts[125]. In addition, the EN 197-1 standard supports the circular economy by allowing the incorporation of industrial by-products[126] like slag and fly ash, promoting the recycling of materials that would otherwise contribute to waste. As a result, EN 197-1 plays a crucial role in advancing sustainable practices within the construction sector.

IMPACT IN THE CONSTRUCTION INDUSTRY - EN 197-1 & ASTM C150

EN 197-1 implementation has influences and transformed the European construction industry. The standardization of cement types and properties has permitted improvements in trade and regulatory compliance, creating a single market for cementitious materials simplifying the production processes and supply chain for construction projects, while enhancing the durability, safety and quality of infrastructure across Europe[127]. In addition, the variety, specificity and

[116] Explained in the ASTM C183. (ASTM, 1940)
[117] Referring to the oxide content according to ASTM C114. (ASTM, 1940)
[118] Using ASTM C109 for compressive strength. (ASTM, 1940)
[119] ASTM C204 presenting Blaine air permeability. (ASTM, 1940)
[120][120] Confirmed with Vicat needle method ASTM C191. (ASTM, 1940)
[121] (Muller, 2023)
[122] (Mindess, Young , & Darwin, 2003)
[123] (Li , Dengler , & Hesse, 2023)
[124] (Taylor , 1997)
[125] (ASTM, 1940)
[126] Products that could also be a residual waste from other industrial construction processes.
[127] (Mather, 2004)

properties offered by the various types of cement outlined in EN 197-1 allows engineers and architects to select the most suitable material properties for each project, whether it involves high-strength requirements, sulfate resistance, or sustainable construction goals.

Nevertheless, ASTM C150 influences the construction industry, particularly in North America, by standardizing material specifications for Portland cement. This standardization has facilitated interstate and international trade of cement products, enabling suppliers to achieve a consistent criterion. The result is a more efficient construction sector, where design professionals can rely on the uniformity of cement quality when planning and executing projects[128], allowing versatility for cement implementation in modern construction, where materials must meet increasingly stringent demands for both performance and sustainability.

CONCRETE

We can trace "concrete" back to the Latin verb concrescere, meaning "to grow together." Appropriately, when it first entered English "concrete" could mean "connected by growth."[129]. Concrete has been fundamental to the development of modern civilization, serving as the primary material for the construction of infrastructure that supports urban and industrial growth. Its durability, versatility, and cost-effectiveness have facilitated the creation of monumental structures, which are integral to contemporary society. Concrete use has enabled the rapid expansion of cities, the improvement of transportation networks, and the advancement of technological and economic systems. In daily life, nearly every aspect of human existence is influenced by concrete, from the buildings we live in and work into the roads we travel on spaces in which we rely upon carrying out all activities. As such, concrete has become an indispensable material, supporting not only the physical framework of modern life but also the very functioning of global economies and the advancement of human civilization.

Concrete is a composite material consisting of water, cement, and aggregates, such as sand, gravel, or crushed stone. The cement, typically Portland cement, functions as the binder that holds the aggregates together, while the water reacts with the cement through a process of hydration, leading to the hardening of the mixture[130]. The creation of concrete is based on the implementation of specific proportions between cement, water, and aggregates. Maintaining the correct proportions plays a vital role in determining the material properties such as, strength, durability, and workability[131]. Furthermore, admixtures can be incorporated into the composition to modify the concrete properties, including its setting time, workability, and resistance to environmental factors[132]

Concrete	=	*Filler*	+	*Binder*
Portland cement concrete	=	Aggregate (fine and coarse)	+	Portland cement paste
Mortar	=	Fine aggregate	+	Paste
Paste	=	Cement	+	Water

[128] (Mehta & Monteiro, 2014)
[129] (Merriam Webster, n.d.)
[130] (Neville A. , 2011)
[131] (Mehta & Monteiro, 2014)
[132] (Mindess, Young , & Darwin, 2003)

Table 14 Definition of concrete.
Source: (Mindess, Young , & Darwin, 2003)

Followed by steel, concrete is the most used material in construction, gaining great importance for the development of contemporary architecture and construction, offering a range of advantages that contribute to its extensive use. Its compressive strength, durability, and adaptability to various forms and finishes make it the ideal material for a widespread implementation of structural and architectural applications, from high-rise buildings to infrastructure projects. Concrete's resistance to fire, water, and weathering ensures longevity and low maintenance, while its versatility allows for both functional and aesthetic flexibility[133]. Despite these benefits, concrete presents several limitations which have caused recent research in innovative techniques and applications to be incorporated into concrete production and manufacture. One of the biggest disadvantages of concrete utilization is the environmental impact of cement production, which by being an energy intensive procedure matter, becomes a major source of carbon dioxide emissions, remaining in a critical concern in sustainable construction[134]. Additionally, concrete exhibits limited tensile strength, ductility, strength to weight ratio and volume instability making it necessary to be reinforced with materials such as steel to address structural demands in tension[135]. Furthermore, the material's susceptibility to cracking under stress and its relatively slow curing time can pose challenges in both design and construction processes that continue to be currently studied.

Compressive strength	= 35 MPa (5000 lb/in.^{2})
Flexural strength	= 6 MPa (800 lb/in.^{2})
Tensile strength	= 3 MPa (400 lb/in.^{2})
Modulus of elasticity	= 28 GPa (4 × 10^6 lb/in.^{2})
Poisson's ratio	= 0.18
Tensile strain at failure	= 0.001
Coefficient of thermal expansion	= 10 × 10^{-6}/°C (5.5 × 10^{-6}/°F)
Ultimate shrinkage strain	= 0.05–0.1%
Density	
Normal weight	= 2300 kg/m^3 (145 lb/ft^3)
Lightweight	= 1800 kg/m^3 (110 lb/ft^3)

Table 15 Typical Engineering Properties of Structural Concrete.
Source: (Mindess, Young , & Darwin, 2003)

Mortar and concrete are fundamental components in construction, each serving specific functions and exhibiting distinct physical and mechanical properties. Concrete is the most complex and robust construction material among the two, conformed by cement paste, sand as the fine aggregate, gravel and crushed stone as the coarse aggregates, and water. The properties of concrete can be adjusted through variations in the mix design, such as alteration in the aggregate size, incorporating admixtures, or altering the water to cement ratio. These adjustments make concrete adaptable for diverse environments and physical requirements, one clear example of this is the implementation of coarse aggregates which increases the compressive strength and durability of concrete compared to mortar[136].

[133] (Mehta & Monteiro, 2014)
[134] (Mindess, Young , & Darwin, 2003)
[135][135] (Neville A. , 2011)
[136] (Aitcin, 1998)

Finally, mortar is a mixture of cement paste, sand working as the fine aggregates, and water. Sometimes, additional additives like lime or plasticizers are incorporated to improve workability or specific properties. Mortar is primarily used as an adhesive material for bonding masonry units such as bricks, blocks, or stones filling the gaps between these units, distributing loads evenly and ensuring structural stability. Compared to cement paste, mortar has enhanced workability and reduced shrinkage due to the presence of fine aggregates, which also improves its resistance to cracking[137]. The fine aggregate content in mortar also contributes to its relatively low compressive strength compared to concrete, making it more suitable for nonstructural applications.

RHEOLOGY OF CONCRETE

Rheology is the scientific study of the deformation and flow behavior of materials under applied forces, encompassing both liquids and soft solids. It examines how materials respond to stress, strain, and strain rates, providing insights into their viscosity, elasticity, and plasticity characteristics[138]. In the construction area, understanding the rheology of cementitious materials is critical, as it helps understand the complexity of the mixture in its viscous state which will influence its workability, stability, and when hardened, the mechanical properties of concrete, ensures that that the concrete will compact without segregation or excessive bleeding[139]. The key rheological parameters to consider when studying concrete are the yield stress and plastic viscosity. Yield stress represents the stress threshold required for concrete for it to start flowing, while plastic viscosity measures the resistance to flow when movement has already started[140].

The concept of workability in concrete is intrinsically tied to its rheological properties affecting the mixture ability to be placed, compacted, and finished. Traditional methods such as the slump test were used to study concrete workability, the problem with this type of test is that it provides limited information about the flow behavior of concrete. In contrast, advanced rheological tests such as rotational rheometers and portable field devices provide more accurate assessments of concrete flow characteristics, leading to better quality control[141]. Rheological measurements offer a more comprehensive analysis by quantifying both yield stress and viscosity, allowing for real-time adjustments in concrete mixtures giving a more precise understanding of how fresh concrete behaves under different conditions[142]. It is important to consider that deficient rheological control can lead to improper consolidation, increased porosity, and honeycombing, compromising concretes durability and strength[143]. Furthermore, rheological assessments help in concrete mixtures design that align with modern construction techniques, one of this is pumping and 3D printing, where consistent flow properties are essential for quality control and concrete paste workability, were concrete without blockages or segregation.

[137] (Hewlett, 1935)
[138] (Barnes, Hutton, & Walter, 1989)
[139] (Tattersall & Banfill, 1983)
[140] (Roussel, 2011)
[141] (Roussel, 2011)
[142] (Banfill, 1991)
[143] (Neville A. , 2011)

CONCRETE CONSTITUENTS

Concrete is a composite material formed by the combination of four primary constituents: cement, aggregates, water, and admixtures. Each of these components plays a distinct and essential role in ensuring that the concrete achieves the desired properties and performance. The careful selection and proportioning of these materials are crucial for optimizing the structural, mechanical, and durability characteristics of concrete.

Cement, commonly Portland cement, is the main component in concrete design mixtures, acts as the primary binding agent, initiating the hydration process when mixed with water, leading to the formation of calcium silicate hydrates (C-S-H), this imparts strength and rigidity to the hardened material[144]. Aggregates, divided into fine - sand ((ϕ<4mm) and coarse - gravel or crushed stone ((ϕ >4mm), and can be natural or artificial, serve as the main filler material as they cost less than cement. Aggregates directly influence the concrete's density, strength, and durability. These aggregates constitute the bulk of the concrete's volume, reducing shrinkage and enhancing the overall structural integrity[145]. Elements such as particle size, shape, rugosity and angularity are going to have direct impacts on the concrete's compressive strength and elastic modulus. Water is essential for the hydration of cement and the workability of the mix, with the water-to-cement ratio being a critical factor in determining the final strength and porosity of the concrete[146]. Applying the Abrams´ rule, when decreasing the water to cement ratio, the mechanical strength of concrete will increase. Additionally, admixtures such as plasticizers, accelerators, retarders, expanders, superplasticizers and air entraining agents are often incorporated to modify specific characteristics of the concrete, such as setting time, workability, and durability under various environmental conditions. These chemical admixtures allow them to work with concrete mixes with specific performance requirements, such as increased freeze-thaw resistance or enhanced compressive strength[147].

The application of these constituents in a mix design involves careful consideration of several factors, including the target compressive strength, workability, and durability under environmental conditions. One of the most important parameters in mix design is the water to cement (w/c) ratio, as it directly influences both the strength and permeability of the concrete. Normally, a lower w/c ratio enhances strength but decreases workability, requiring admixtures like superplasticizers to maintain fluidity without compromising the concrete mechanical performance[148]. The particle, size, and shape of aggregates impacts on the concrete's density, stability, and overall durability, which are key factors for long-term performance[149].

Even though, typically, the volume of a mix is about 10 to 15% cementitious material, 60 to 75% aggregate, and 15 to 20% water[150]. Entrained air in concrete mixes may also take up to 8%. Standards and guidelines such as those provided by the American Concrete Institute (ACI) and British Standards (BS EN 206) outline detailed methodologies for creating concrete mix designs suited to both local and international requirements. These standards incorporate research-backed procedures to ensure that concrete produced aligns with established safety, strength, and durability

[144] (Hewlett, 1935)
[145] (Mindess, Young , & Darwin, 2003)
[146] (Neville A. , 2011)
[147] (Kosmatka, Kerkhoff, & Panarese, 2002)
[148] (Mehta & Monteiro, 2014)
[149] (Kosmatka, Kerkhoff, & Panarese, 2002)
[150] (Caltrans, 2013)

metrics under varied conditions[151]. A well-executed cement mixture design not only enhances the mechanical and physical properties of concrete but also supports sustainable construction practices by minimizing waste and optimizing resource usage[152].

TYPES OF CONCRETE

There is a wide variety of concrete types, each designed to address specific construction needs and challenges, each type of concrete showcases unique features, making each of them suitable for diverse applications and enabling the construction industry to select materials that meet specific performance requirements for each project demands. Some of these types have origins that trace back centuries, reflecting traditional techniques and materials, while others are recent innovations developed in response to the evolving demands of modern architecture and engineering. The development and implementation of diverse concrete applications continue to create opportunities for the construction industry, allowing for new developments. Between all the types of concrete we can find:

1. HSC -High Strength Concrete
2. HPC -High Performance Concrete
3. DSP/UHPC-Densified with Small Particles/Ultra-High-Performance Concrete
4. SCC/SLC-Self Compacting Concrete/Self-Leveling Concrete
5. 3SC-3-Self Concrete: Self-compacting, Self-curing, Self-compressing
6. FCR-Fiber Reinforced Concrete
7. Gunite Shotcrete HPS-High Performance Shotcrete
8. LC-Lightweighted Concrete
9. SCLC-Self Compacting Lightweighted Concrete
10. HPLC-High Performance Lightweighted Concrete
11. RCA-Recycled Concrete Aggregates
12. PIC-Polymer Impregnated Concrete
13. SCC-Self Compensated Shrinkage

[151] (Americal Concrete Insttute (ACI), 2002)
[152] (Aitcin, 1998)

BIOCHAR

WHAT IS BIOCHAR?

UK Biochar Research Centre established a definition of biochar as "a porous, carbon-rich solid produced by the thermochemical conversion of organic materials under oxygen-limited conditions."[153]. This process, known as pyrolysis, breaks down the organic material into fine-grained, charred charcoal. Although it resembles conventional charcoal, biochar is made through a special process designed to minimize contamination and effectively store carbon. Unlike traditional combustion, where materials burn in an oxygen-rich environment and release greenhouse gases (GHGs), particularly carbon dioxide[154], pyrolysis offers a more sustainable alternative. During this process, a significant portion of carbon from the original biomass[155] is preserved in a solid form, which helps to reduce carbon emissions and facilitates carbon sequestration. This definition has been constructed intentionally to remain flexible, considering the various production methods and applications of biochar.

Biochar's most notable applications are found in agriculture, where it has been shown to enhance nutrient efficiency supplied in fertilizers, and it also improves soil and water management, both of which contribute to increased crop yields. After noticing all significant agricultural benefits, biochar is also reconsidered as an effective carbon sequester, making it an interesting material nowadays[156]. The main properties of biochar have led to its recognition as a highly versatile material with applications in various disciplines, all of which are influenced by the choice of feedstock.

The feedstock used in biochar production plays a key role in determining the properties and quality of the resulting biochar[157]. Biomass' main components are cellulose, hemicellulose and lignin. Each of them has a different composition structure, therefore reacting in a unique way

[153] (University of Edinburgh, n.d.)
[154] (Golisano Institude for Sustainability, 2021)
[155] Biomass is a renewable organic resource that can be turned into fuel. **Specificata fonte non valida.**
[156] (Lehmann & Joseph, 2024)
[157] (Sachini Supunsala , et al., 2023)

during the pyrolysis process. The lignocellulosic[158] biomass promotes the formation of biochar. A large variety of feedstocks are sourced from wood residues, biomass crops, and waste materials deriving from municipal, livestock, industrial and agricultural sectors. By using these discarded materials, biochar production not only adds value to waste, but also supports a circular economy, transforming waste into valuable resources. This process helps to reduce waste, optimize resource use, and promote sustainability by the continued cycle from production to consumption.

One of the main properties of biochar is its porosity and high carbon content[159], which together make possible the adsorption of heavy metals and organic pollutants. Its physicochemical characteristics, including a large surface area, cations exchange capacity (CEC), and electrochemical properties, enhance its ability to remove heavy metals and organic pollutants from soil and water, while also enabling energy storage. Originally recognized for its role in carbon sequestration in agricultural systems, biochar's applications have expanded into urban environments. It is nowadays used for pollutant control, waste management, and the development of construction materials and other commercial products.

Biochar is applied in roof drains and stormwater outfalls to filter bacteria and organic matter. It is also incorporated into construction materials like cement, plasters, gypsum board, plastics, and building blocks. These applications not only improve the physical properties of construction materials but also enhance their potential for carbon sequestration. As a durable carbon storage medium, biochar can reduce the demand for sand and cement[160], making construction practices more sustainable. Biochar's diverse uses, extending from agriculture to urban environments, reflect its versatility and its potential to drive environmental sustainability in a wide range of industries.

PHYSICAL CHARACTERISTICS

As previously noted, biochar is primarily characterized by its distinct physical properties. Regeneration International describes biochar as “black, highly porous, lightweight, fine-grained, and possessing a large surface area, with approximately 70 percent of its composition being carbon”[161]. The high porosity emerges from the carbon framework remaining after biomass undergoes pyrolysis, resulting in a fine-grained, porous charcoal. The size of the biochar particles varies according to the pyrolysis time, especially the size of the biomass used for its production.

Biochar’s utility is shaped by several physical properties. One such characteristic is density, commonly known as bulk density, which is determined by the mass within a given volume, depending on the raw material used for biomass. As it is discussed in the book Biochar Emerging Applications, the arrangement of graphene sheets in biochar plays a significant role: a greater number of pores leads to lower density, making biochar an excellent thermal insulator with reduced thermal conductivity. This structural configuration also enhances thermal stability, which refers to biochar's ability to resist degradation at high temperatures. When biochar is more compact and organized, it can maintain a better integrity under heat.

Another important physical property is electrical conductivity, which is determined by how carbon atoms are arranged inside biochar[162]. As biochar undergoes pyrolysis at higher

[158] Lignocellulosic materials come from natural resources, such as the stems and roots of trees, and woody plants consisting of brittle and fibrous tissues and are made up of polymers of cellulose, hemicellulose, and lignin.**Specificata fonte non valida.**
[159] (Tagliaferro, Rosso, & Giorcelli, 2020)
[160] (Tagliaferro, Rosso, & Giorcelli, 2020)
[161] (Spears, 2018)
[162] (Jindo, Mizumoto, Sawada, Sanchez-Monedero, & Sonoki, 2014)

temperatures, it forms more organized structures, allowing electrons to move freely, thereby improving conductivity. This is especially useful in applications such as energy storage and other industrial uses.

The mechanical properties of biochar, meaning to the ability to deform under stress, are closely linked to its carbon content. Generally, the higher the carbon content, the better the mechanical properties, which makes biochar suitable for use in construction materials[163].

In addition to these, porosity plays a key role in biochar's adsorption mechanisms, as mentioned in Biochar Emerging Applications, section 2.2.2. There are two important parameters that are associated with biochar porosity: the BET surface area (specific surface area of biochar) generally measures high in the presence of high microporosity with pore diameter lower than < 2nm. The pore volume measures the total space inside the biochar by considering the meso and macropores (diameter between 2 and 50nm and > 50nm, respectively). The pore size distribution, or the variation in pore sizes within biochar, directly affects its capacity to transfer mass and interact with contaminants. Fluid and biochar interactions are permitted by the macropores that act as a main access route to the micropores. Both can differ in the quality of adsorption during the pyrolysis: the process of devolatilization for lighter condensable enhances the overall pore volume. On the other hand, the presence of heavier condensable that remain in the pores reduces both the total pore volume and the specific surface area.

Considering all aspects, biochar's physical properties such as its porosity, density, thermal and electrical conductivities, mechanical strength, and adsorption capabilities; make it a highly versatile material with a broad range of potential applications across environmental, agricultural, and industrial sectors.

CHEMICAL CHARACTERISTICS

While biochar’s physical properties are essential for its functionality and wide range of applications, its chemical characteristics are just as important in shaping its performance and effectiveness. The main elements in biochar are carbon, hydrogen, and nitrogen (C, H, N), making up over 95% of its weight, along with small traces of heavy metals and inorganic minerals[164].

When considering biochar’s physical properties, it’s important to point out that characteristics like hardness and toughness are directly linked to its carbon content. As the amount of biochar increases in a mixture, it can reduce the toughness of mortar, which in turn affects its overall mechanical performance, as discussed in *Application of Biochar in Concrete*.

In terms of thermal stability, the levels of aromatization and graphitization in biochar do have an impact in boosting its resilience, thereby improving its overall performance under extreme conditions. The more graphitized the biochar, the more effective it is in enhancing adsorption. Additionally, biochar has a strong capacity to adsorb heavy metals through surface ion interactions, making it an ideal material for capturing and removing these contaminants. One mechanism at play is surface complexation, where complex structures are formed through interaction between metal ions and the surface ligands of biochar. Biochar typically carries a negative charge on its surface, allowing it to attract and adsorb positively charged compounds through electrostatic interactions. The strength of these interactions is largely influenced by the pH of the solution, which directly affects the surface charge of the biochar.

As is highlighted in the report *Application of Biochar in Concrete*, biochar with a higher density generally has a lower carbon content, allowing for higher dosages to be added to cement mortar

[163] (Tagliaferro, Rosso, & Giorcelli, 2020)
[164] (Sachini Supunsala , et al., 2023)

mixtures. This balance between biochar's chemical and physical properties makes it highly effective and sustainable material for a broad range of industrial and environmental applications.

HISTORY OF BIOCHAR

Biochar has its roots in the ancient practices of Indigenous peoples in the Brazilian Amazon. They created rich, dark soils known as Terra Preta (dark soil) in the 19th century Amazon territories were reported by Smith in the year 1879 and by Hartt in 1885. According to Sheil et al.[165], these soils were very different from poor, acidic soils around them. Nutrients were very low as also cation exchange capacity. Terra Preta was full of important nutrients like phosphorus, calcium, and potassium, making it fertile and productive.

Falcao's research in 2012 suggested that these soils were made by Indigenous peoples who added organic materials into pyrolysis, such as fishbones and biomass. They used biomass to create biochar, which helps lock nutrients into the soil. This method, known as slash-and-char, improved soil quality. Other studies also suggest controlled burning was used to clear land for farming[166]

In the 1960s, Dutch scientist Wim Sombroek revealed that Terra Preta was not a natural phenomenon, but the result of human effort. In his book Amazon Soils, he confirmed that these rich, fertile soils were created intentionally by Indigenous peoples thousands of years ago, between 3,000 to 5,000 years ago[167]. Later studies supported this view, showing that the soil's remarkable fertility was the result of careful human stewardship, not simply natural processes.

Although it was initially believed to be found only in the Amazon, there were found similar carbon-rich soils in places like Mexico, Africa, Borneo, and the United States. These soils, formed by both natural and human-caused fires, are rich in organic matter, retain moisture, and support microbial life, showing that biochar-enhanced soils have been around for over 10,000 years[168].

The main reason Terra Preta is so fertile is its high biochar content. The slash-and-char method of charring biomass, rather than burning it completely, adds carbon to the soil, which improves soil structure and helps it hold nutrients. Terra Preta fertility is due to the relevant presence of carbonaceous material, that can retain the soil nutrients in particles, and these are usually deeper than surrounding soils, sometimes up to 1-2 meters deep. Studies show that these soils could be farmed for many years without needing extra fertilizer[169]. These soils stand out for their high pH and rich concentrations of nutrients such as nitrogen (N), phosphorus (P), potassium (K), and calcium (Ca). They also contain up to 70 times more biochar than nearby soils, with carbon levels reaching up to 150 grams per kilogram, compared to just 20-30 grams per kilogram in soils without charcoal. While biochar is a major factor in the fertility of Terra Preta, other organic materials were used, such as human and animal waste, fish and animal bones, and food scraps, also helped enrich the soil with nutrients.

In the 20th century, biochar began to be used in other ways. In Japan, a type of biochar made from rice husks, called *kuntan*, was used in hydroponic farming, water purification, and gas adsorption. During World War I, biochar was used in gas masks to filter harmful gases[170]. These early uses set the stage for biochar's return and renewed significance in modern times, as it is now seen as a tool to improve soil fertility and capture carbon to fight climate change.

---

[165] (Sheil, et al., 2012)
[166] (Woods, et al., 2008)
[167] (Schmidt , et al., 2014)
[168] (Lehman, Kern, Glaser, & Woods, 2004)
[169] (Escalante Rebolledo, et al., 2016)
[170] (Meyer, 2009)

FEEDSTOCKS

Biochar varies depending on the feedstocks used, like crop residues, animal manure, and forest waste. Since these feedstocks come from waste, they help the environment by removing residues that would otherwise pollute and instead, they are transformed into a product biochar that helps restore and enrich the atmosphere. The type of feedstock also has a big impact on the nutrient content and properties of the biochar[171].

An article, published by *Nature Communications* in 2010, Woolf et al[172]. presented the "*Annual globally sustainable biomass feedstock availability*" sorted among crops, waste, and forestry, subdivided into rice, other cereals, sugar cane (crops), manure, biomass crops (waste), forestry residues, agroforestry, green/wood waste (foresty).

	Biomass available in scenario (Pg C per year)		
	Alpha	**Beta**	**Maximum sustainable technical potential**
Rice	0.22 Rice husks and 70% of paddy rice straw not used for animal feed	0.25 Rice husks and 80% of paddy rice straw not used for animal feed	0.28 Rice husks and 90% of paddy rice straw not used for animal feed
Other cereals	0.072 8% of total straw and stover (assumes 25% extraction rate of crop residues minus quantity used as animal feed)	0.13 14% of total straw and stover (35% extraction rate minus animal feed)	0.18 20% of total straw and stover (45% extraction rate minus animal feed)
Sugar cane	0.09 Waste bagasse plus 25% of field trash	0.11 Waste bagasse plus 50% of field trash	0.13 Waste bagasse plus 75% of field trash
Manures	0.10 12.5% of cattle manure plus 50% of pig and poultry manure	0.14 19% of cattle manure plus 70% of pig and poultry manure	0.19 25% of cattle manure plus 90% of pig and poultry manure
Biomass crops	0.30 50% of potential production of abandoned, degraded cropland that is not in other use	0.45 75% of potential production of abandoned, degraded cropland that is not in other use	0.60 100% of potential production of abandoned, degraded cropland that is not in other use
Forestry residues	0.14 44% of difference between reported fellings and extraction	0.14	0.14
Agroforestry	0.06 17 Mha of tropical silvopasture	0.34 85 Mha of tropical grass pasture converted to silvopasture	0.62 170 Mha of tropical grass pasture converted to silvopasture
Green/wood waste	0.029 75% of low-end estimate of yard-trimmings production and wood-milling residues	0.085 Alpha plus mid-range estimate of yard trimmings plus urban food waste, including 40% of waste sawnwood (legislation required to ensure that this fraction of waste wood is free of harmful contaminants)	0.14 Beta plus high-end estimate of global yard trimmings and food waste, including 80% of waste sawn wood
Total	1.01	1.64	2.27

Table 36 The estimation done by the authors of ref.[173]. 2.27 Pg C/yearwith an optimistic scenario, and two additional scenarios with lower demands 1.64 Pg C/year (Beta) and 1.01 Pg C/year (Alpha) of how much organic material (in terms of carbon) could be turned into biochar each year, based on available feedstocks like crops, waste and forestry.
Source: (Woolf, Amonette, Street-Perrott, Lehmann, & Joseph, 2010)

The calculation cannot be entirely precise, as the yield of biochar varies with the type of biomass used, and specific conditions during pyrolysis can significantly influence the final output.

Last publication have highlighted the most common types of feedstocks, but in the article *Suitability of Different Agricultural and Urban Organic Wastes as Feedstocks for the Production of Biochar*[174], urban wastes such as Greenwaste (GW) were introduced. This organic waste from urban areas includes a mix of grass, leaves, branches, small stems, and trimmings collected separately from gardens. It's typically shredded and chipped to make it easier to process; CellMatt (CM) is also an organic waste of urban origin produced from household, commercial and

[171] (International Biochar Initiative (IBI), 2024)
[172] (Woolf, Amonette, Street-Perrott, Lehmann, & Joseph, 2010)
[173] Pg C = petagrams of carbon, a unit used to measure large amounts of carbon. (Royal Meteorogical Society, 2024)
[174] (Lopez-Cano, et al., 2018)

industrial wastes. These wastes are sterilized to achieve the complete removal of pathogens. Finally, Municipal Press Cake (PC) is an organic waste from urban areas, obtained from anaerobic digestion[175].

Both agricultural and urban wastes are valuable as feedstocks for producing biochar through pyrolysis. However, with urban waste, it is important to perform process and evaluations with care to ensure the biochar obtained is free from harmful contaminants. Especially to guarantee that biochar will be beneficial to the environment.

PRODUCTION

Understanding the processes behind biochar production is essential to advancing its applications in sustainability. *Biochar: Emerging Applications* highlights pyrolysis, gasification, and hydrothermal processing as the primary thermochemical methods used today to convert different types of biomasses into renewable energy sources, blending traditional ecological practices with contemporary technological advancements to address modern environmental challenges.

Through the thermochemical process of pyrolysis, biomass undergoes transformation under heat and without oxygen, creating char while also yielding gases and bio-oil[176]. Reflecting cycles of renewal in nature, pyrolysis is practiced in three forms: slow, intermediate, fast and flash. Among these, slow pyrolysis is the most suitable method for biochar production.

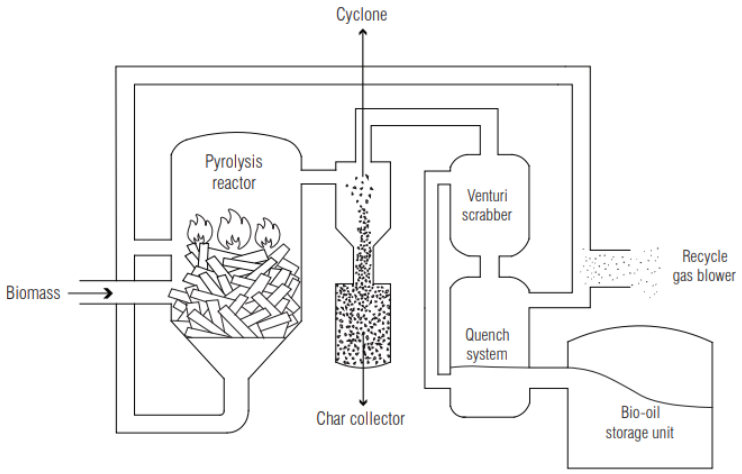

Figure 19 Scheme of the pyrolysis process.
Source: (Khaled & Erriquez, 2019/20)

Slow pyrolysis can be applied in different scales: simple and rudimental batch earth mounds to large and industrial systems. There are different classifications considering mode of operation, construction material, feedstock allowable size, portability, biomass loading mode and heating method. As outlined previously, the method that increases char yield is called slow pyrolysis or carbonization. This process is done under atmospheric pressure, with temperatures between 300°C and 550°C. The process involves slow heating rates (0.1-0.8°C/s) and long retention times (5-30 min or even 25-35 h), allowing the organic material to change gradually over several hours to days, based on the type of reactor used[177]. Slow pyrolysis increases biochar yield by allowing

[175] Anaerobic digestion is a process in which organic materials, like food waste or agricultural residues, are broken down by microorganisms in an oxygen-free environment. (American Biogas Council, s.d.)
[176] (Tagliaferro, Rosso, & Giorcelli, 2020)
[177] (Amalina, et al., 2022)

vapors to stay in the reactor longer, facilitating secondary reactions. The slow rate of heating and the moderate temperatures used in pyrolysis support the formation of biochar. The amount of biochar produced depends on the features of the material and the specifications of the pyrolysis process, as was pointed out earlier.

Intermediate pyrolysis operates between slow and fast pyrolysis, with reactions occurring at temperatures between 450°C and 550°C. It moves faster than slow pyrolysis, completing in just 10 to 30 seconds, but slower than fast pyrolysis. This method produces less charcoal than slow pyrolysis. The process leads to a variety of products: biochar, bio-oil, and gases[178].

Fast pyrolysis is a method defined by high temperatures and quick heating, reaching 10 to 1000°C per second, with very short residence times of 0.5 to 2 seconds. This process focuses on maximizing the production of bio-oil. The distribution of by-products depends on the biomass's characteristics, the heating speed, and the temperature. When bio-oil is the primary product, temperatures between 425°C and 600°C are ideal, with the heat not exceeding 650°C. However, if gas is the target, the temperature may rise to 1000°C. To achieve such intense heating, the biomass must be finely ground (typically smaller than 1 mm) allowing for better heat transfer and reducing mass and heat transfer limitations. For optimal bio-oil production, the biomass should contain no more than 10% moisture, which also allows for easier grinding and quicker heating. Flash pyrolysis works to maximize bio-oil production through the use of extremely high temperatures, rapid heating rates greater than 1000°C per second, and very brief exposure times (less than 0.5 seconds). This method creates similar products to fast pyrolysis, with temperatures ranging from 800 to 1000°C.To ensure the best results, the biomass should be finely ground to particles under 0.2 mm.

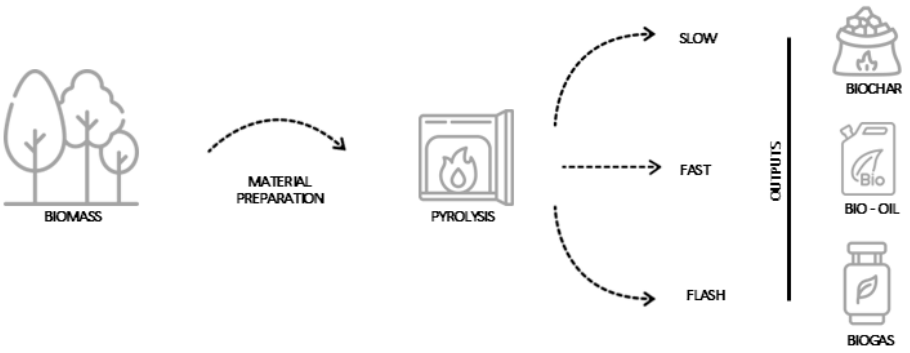

Figure 20 Scheme of the general concept of pyrolysis and their outputs
Source. (Amalina, et al., 2022)

Another type of pyrolysis, a more recent one is microwave pyrolysis. In this process microwaves penetrate the entire material at almost the same time. A uniform temperature distribution is obtained due to the heat transfer at the outer surface of the heated material and a char layer is created, and it grows to the surface direction. This means that the char and vapor products go through the same path as heat transfer. That is why the product quality is enhanced compared to the conventional heating processes.

[178] (Ge , et al., 2021)

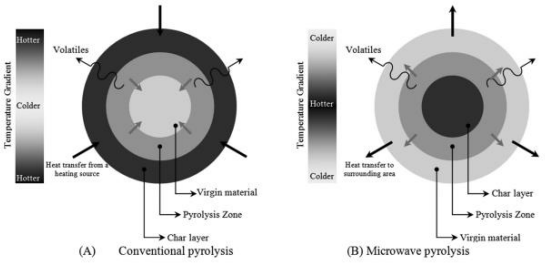

Figure 21 Scheme diagram of conventional pyrolysis and microwave pyrolysis. Source: (Tagliaferro, Rosso, & Giorcelli, 2020)

The studies made in *section 4.4* of *Biochar Emerging Applications*, have compared the conventional heating process with microwave heating process, it has been demonstrated that there is not much different between biochar yields but there are several upgrades on the process such as: lower energy consumption, better porosity (larger micropore), higher adsorption capacity, much more uniform and cleaner. In terms of the shape and size of particles there is an evident difference, and it is a better quality than the one done in microwave pyrolysis, with a higher surface area and pore volume.

Heating method is one of the most important classification criteria because it determines the energy self-sustainability of the process: allothermal carbonization or autothermal carbonization. In both cases, the pyrolysis process is performed in the full absence of oxygen, and heat is provided by an external source. In allothermal cases the combustion of pyrogases (the resulting heat) can be transferred to the reactor by directly injecting the flue gas. In the other hand, the autothermal case, heat is generated with the reactor itself by the air[179].

Building on the understanding of pyrolysis, the discussion extends to gasification and hydrothermal processing. While pyrolysis primarily focuses on maximizing char yields through controlled heating in oxygen-free environments, gasification converts biomass into syngas by heating it between 700°C and 1300°C under conditions of partial oxidation. The resulting syngas is made up of carbon monoxide (CO), hydrogen (H2), and small amounts of methane (CH4). Although it has a lower energy value, syngas can power engines, turbines, or serve as a base for chemicals like methanol. The process may or may not use catalysts, which influence the reaction temperature. Higher temperatures, longer holding times, and carefully managed water density with lower biomass amounts result in greater gas yields[180].

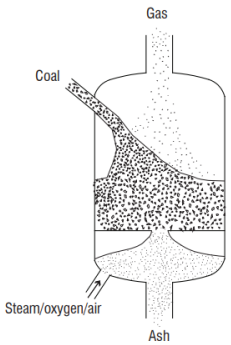

Figure 22 Scheme of the gasification process. Source: (Khaled & Erriquez, 2019/20)

[179] (Tagliaferro, Rosso, & Giorcelli, 2020)
[180] (Kee Lam, Chun Minh Loy, Yusup, & Teong Lee, 2019)

In contrast, hydrothermal carbonization uses water and pressure to convert biomass into hydrochar while preventing evaporation during heating. Unlike dry methods, it operates at lower temperatures with steady heat for the required duration. Hydrochar is removed by dewatering, leaving behind water rich in organic and inorganic compounds that must be handled carefully. Anaerobic digestion is one way to recover nutrients like phosphates from this water. In the process, water serves many roles, including transferring heat, aiding reactions, and acting as both a catalyst and a solvent[181].

Some of the technologies were proposed in *section 3.2.* of *Biochar Emerging Applications*: Kilns are simple and traditional systems for biochar production, still in use today in many places due to their low cost and straightforward operation. Logs are arranged in an earth pit, covered with soil to limit airflow, and left to slowly convert to biochar. Because kilns can be built near the harvest site, they save on transport costs. Yet, the method demands considerable effort and time. The quality and amount of biochar depend not only on the biomass but also on the material used to construct the kiln, which might be brick, concrete, or metal.

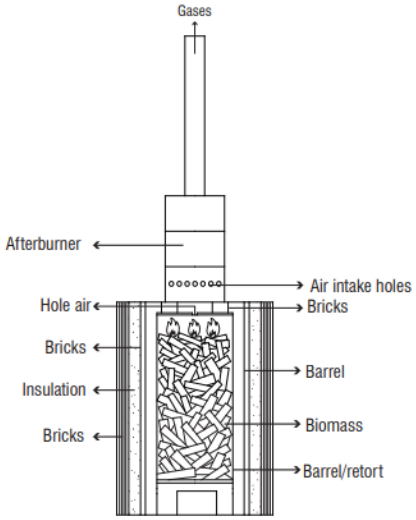

Figure 23 Scheme of kiln technology.
Source: (Khaled & Erriquez, 2019/20)

Another technique is industrial carbonization, that can be achieved with allothermal reactors, where hot vapors and gases provide heat for pyrolysis. Non-condensable gases are recycled to maintain the heating. In its simplest form, the system uses indirect heating, consisting of a closed metal container and a pipeline that carries gases to a combustion chamber. The process starts with water vapor from biomass drying, followed by pyrolysis. The generated pyrogas fuels the system, resulting in a self-sustaining process that yields more char than autothermal methods.

Not to be overlooked, converts are reactors that can carbonize small-sized biomass, like wood chips or pellets, this char is usually obtained as powder. It consists in a cylindrical shell which is inclined and rotates to allow biomass to flow down. The heat can be supplied by heating the shell from outside or inside by a hot gas flow. The main advantages are the biomass flexibility, scalability and maturity of the technology.

[181] (Amalina, et al., 2022)

APPLICATION

From the transformation of biomass through pyrolysis, biochar, along with its by-products as bio-oil and gases, reveals itself as a product of great potential. As time passes, its use has expanded, biochar helps mitigate the negative impact that biomass previously caused. Its qualities are shaped by the feedstock it comes from, the methods by which it is made, and the conditions that guide its creation. These factors shape the biochar's quality, yield, and impact[182].

From purifying air and water to producing activated carbon, biochar plays many roles. It helps in anaerobic digestion, strengthens construction materials, and supports agriculture by conditioning soil, adding to compost, and storing carbon. Biochar plays a key role in the flow of the circular economy, nurturing agriculture and horticulture. Its diverse benefits hold great promise for the sustainability of emerging bioenergy systems.

In *Biochar: Production, Applications and the Future*, the many uses of biochar are revealed. Starting in the fields of agriculture and horticulture: it supports fertilizers, strengthens the soil's ability to hold water, and helps nourish the life that lives in the soil, making nutrients more available to the crops. Biochar also works to reduce harmful metals and can bring balance to soils that are too acidic. Like compost, it can enrich the soil, but unlike compost that offers its gifts for a short time, biochar stays in the soil, continuing to offer its benefits long after it is applied.

As previously indicated, biochar stands as a protector, adsorbing all the harmful substances from the earth and waters. From switchgrass biochar, it has been used to remove the red dye from wastewater (a dye that can harm the land and creatures who rely on it). Biochar also adsorbs metals and other pollutants from soil and water. Biochar's ability to hold carbon, offers an enhanced land, purifying it in a way that sustains the earth and all living things[183].

In the construction industry, biochar has become an important component, notably in concrete mixtures. Studies in recent times have shown that adding biochar to cement yields positive outcomes, particularly in the development of fill material and paving blocks. Biochar aids the hydration process of cement, contributing to its strength.

Biochar also enhances the material's ability to capture and hold toxic substances and organic pollutants. Precisely, wood-based biochar presents a sustainable option for cement recycling, converting highly polluted waste into a useful and beneficial material. When used in construction, biochar helps buildings gather carbon dioxide, pulling it from the air and holding it in the walls, helping to mitigate the weight of greenhouse gases by as much as 25%. Likewise, clay-biochar plaster offers excellent insulation and breathability, helping to regulate humidity levels throughout both summer and winter while also preventing mold growth. With its ability to retain water and balance the pH, biochar also draws in some of the mixing water in concrete, reducing excess moisture and strengthening the foundation of the structure[184]. Biochar-concrete bricks stand out for their lightweight structure and high porosity[185]. Meanwhile, biochar in asphalt enhances its flow-induced crystallization properties, improving its performance and leading to a more durable material.

BIOCHAR IN CONCRETE

In response to the decarbonation of cement industry, the use of biochar-concrete composites has emerged as a promising solution, combining traditional knowledge with modern innovation

[182] (Kwaku Armah, et al., 2023)
[183] (Beesley, Moreno Jimenez, & Gomez Eyles, 2010)
[184] (Kwaku Armah, et al., 2023)
[185] (Khaled & Erriquez, 2019/20)

Biochar, a material used for centuries by our ancestors to enrich soil and promote growth[186] , is gaining attention in the construction industry, although its application is still in the early stages. Despite this, biochar holds great potential in advancing sustainable development. As discussed in the section on *Application*, biochar's carbon sequestration properties are key to its role in reducing greenhouse gas emissions. Its high carbon content, coupled with its porous structure and large surface area, makes it an ideal additive for enhancing concrete performance. These characteristics suggest that it is possible to reduce the cement content in concrete without compromising its strength and durability. In fact, this reduction may even improve the material's overall performance[187]. Additionally, biochar incorporation has been shown to enhance the thermal properties of concrete, improving its resistance to temperature fluctuations and increasing energy efficiency in buildings.

The thesis now shifts to a detailed review of specific research on biochar in concrete, aiming to evaluate the existing literature and highlight key developments in this field.

PREVIOUS RESEARCH

After a theoretical examination of cement, concrete, and biochar, this thesis transitions into practical research to explore the specific behaviors and relationships between these concepts. The aim is to understand how they interact in real-world applications.

The first study, entitled *Modified fracture properties of cement composites with nano/micro carbonized bagasse fibers,* investigated the use of ordinary Portland cement, a high-range water-reducing admixture, distilled water, and nano/micro carbonized bagasse particles to improve the fracture properties of the cement composites. Several experiments were conducted with different percentages of carbonized bagasse fibers as an additive, with proportions ranging from 0.025%, 0.05%, 0.08%, 0.2%, 0.5%, and 1.0% by weight of cement. The water-to-cement ratio and superplasticizer content were kept constant at 35% and 1.5% by the weight of cement, respectively[188].

The preparation process followed two steps: initially, the carbonized bagasse fibers were mixed with water using a bath sonication method. Afterward, the entire mix was combined with cement, initially merged slowly for one and a half minutes, followed by faster mixing for another two and a half minutes. The resulting formulations were poured into molds, remained in a humid environment, and left for 24 hours. After this period, the samples were demolded and immersed in water for curing over 28 days.

The tests analysis of these samples were performed using techniques such as Field Emission Scanning Electron Microscopy (FE-SEM) and a mechanical testing machine Zwick Line-Z010 under CMOD (Crack Mouth Opening Displacement), among others. All the data was digitally recorded. The test results showed an improvement in both flexural strength and fracture toughness, with the samples composed of 0.2% to 0.5% carbonized bagasse fibers exhibiting the highest resistance. Integrating the carbonized bagasse fibers effectively interrupts the crack path, creating multiple smaller cracks. Thus, this led to discontinuities and promoted crack pinning and deflection, requiring additional energy for crack propagation. This adding of bagasse fibers enhanced fracture toughness of the cement.

The next study, *Carbonized nano/microparticles for enhanced mechanical properties and electromagnetic interference shielding of cementitious materials*, examined cement composites

[186] (Woods, et al., 2008)
[187] (Sirico & Bernardi, 2021)
[188] (Arsalan Khushnood, et al., 2015)

containing carbonized nano/microparticles of peanut shells (PS) and hazelnuts shells (HS). Similar to the first research, samples were prepared with varying percentages of carbonized articles: 0.025%, 0.05%, 0.08%, 0.2%, 0.5%, and 1.0% by weight of cement. The water-to-cement ratio (0.35) and super plasticizer (1.5% by weight of cement) were maintained constant, consistent with the conditions used previously. Four samples were prepared for each composition.

The mixture preparation followed the same steps as described before: the carbonized particles were first sonicated for 15 minutes in an ultrasonic bath, then mixed with cement. The mixing process involved two minutes of slow mixing followed by two more minutes at higher speed. The paste was poured into molds, kept in a humid environment for 24 hours, and cured in water at room temperature for 28 days[189].

The test analysis remained constant with the first study, including Field Emission Scanning Electron Microscopy (FE-SEM), a mechanical testing machine ZwickLine Z010 under CMOD, and others. FE-SEM analysis revealed a well-dispersed PS and HS particles in the cement matrix, with carbon content at 87.7% for HS and 93.8% for PS.

In terms of flexural strength and fracture energy, HS samples did better than PS samples. This was likely due to HS's higher density (2.35 g/cm³) compared to PS (2.20 g/cm³). As observed in the first study, the addition of carbonized particles enhanced the material's toughness.

Shielding effectiveness was evaluated across four frequencies: mobile communications, GPS devices, microwave ovens, and radio communications. The 0.5% carbonized PS cement sample showed improvements of 353%, 214%, 122%, and 76%, respectively, compared to plain cement. The 0.5% carbonized HS cement sample indicated comparable improvements of 335%, 214%, 122%, and 76%.

Parallel to the previous study with bagasse fibers, cracks in the composition either followed weaker paths around the particles or branched into finer cracks due to the presence of obstacles. This crack branching dissipated energy and improved fracture toughness.

Overall, both PS and HS composites, like the bagasse fibers in the previous study, demonstrated increased fracture energy compared to plain cement. The addition of fine carbonized aggregates disrupted and dissipated crack energy, significantly improving both shielding effectiveness and mechanical performance.

The following study, *Crack path and fracture surface modifications in cement composites,* investigated cement composites incorporating carbonized micro particles of coconut shells. Samples were prepared with 0.05%, 0.08%, and 0.2% carbonized coconut shell particles by weight of cement. The water-to-cement ratio (0.35) and superplasticizer (1.5% by weight of cement) were maintained constant. The mixing process followed standard procedures, The samples were molded and cured for 28 days. First, flexural tests were performed, followed by compression tests to evaluate the mechanical properties.

Characterization methods included FE-SEM, mechanical testing machine ZwickLine Z010 under CMOD, and others. Mechanical testing indicated a 20% reduction in flexural strength with 0.05% carbonized coconut shell particles. CMOD results revealed the inert particles delayed crack growth and fracture, with the maximum CMOD improving by 80% to 100%, enhancing ductility and fracture energy. FE-SEM also showed that the particles forced cracks to deflect and contour, increasing energy absorption[190].

In short, adding carbonized coconut shell particles into cement composites greatly improves the fracture properties, ductility, and toughness. These analyses indicate that carbonized coconut shell

[189] (KHUSHNOOD, et al., 2016)
[190] (Ahmad , et al., 2015)

particles are a valuable additive for strengthening cementitious materials, offering a sustainable approach to improving construction materials.

This study: *Carbonaceous admixtures in cementitious building materials*, explored the integration of carbonized coconut shell and wood waste in particles of different sizes into cement composites. The materials used for the development were ordinary Portland cement, natural sand with maximum particle of 700 μm, two types of biochar commercially prepared from waste of coconut shell (COCO-BC) and mixed tropical wood wastes(W-BC). For each biochar type, two different particle size gradations: finer biochar (80 μm) and coarser biochar (250 μm)[191]. Seven formulations were tested: one control mixture without biochar and six mixtures containing biochar. The biochar dosage was fixed at 2% by weight of cement. The water-to-cement ratio was set at 0.50, and the sand-to-cement ratio at 2.50 for all mixtures.

The preparation of the mortar involved two main steps. First, the dry components (cement, sand, and biochar) were mixed for 2 minutes at 60 rpm. Then, the mixing water was gradually added over 30 seconds, followed by mixing for an additional 3 minutes at 124 rpm. Once the mixture became uniform, it was mixed at high speed (255 rpm) for 1 minute. The prepared mixtures were cast into molds and vibrated to ensure proper compaction. The sample surfaces were then covered with plastic wrap to prevent moisture loss through evaporation, maintaining conditions at 30°C and 65% relative humidity until demolding, which occurred 22–24 hours after mixing. After demolding, the samples were cured in water at 25–26°C for 3 or 7 days.

The analysis of the samples' morphology was conducted. Particle size analysis showed that coarse wood and coconut biochar (45–50 μm) were significantly reduced to 10 μm (WBC-F) and 18 μm (COCO-BC-F). Fine wood biochar (WBC-F) shares a similar particle size distribution (PSD) with cement (17 μm), improving the packing of the biochar-cement matrix. Coconut biochar (COCO-BC-F) has a slightly coarser PSD than cement but remains finer than sand grains, reducing inter-particle voids and improving matrix densification.

In terms of compressive strength, the mortars with WBC-C and CBC-C showed similar strength to the control at 7 days. This suggests that coarser biochar reveals macro-pores into the matrix, which negatively affects strength. On the other hand, for WBC-C + F, the 10% improvement observed at 7 days was not consistent enough to be statistically significant. Meanwhile, COCO-BC-C + F showed a 17–18% higher strength than COCO-BC-C, despite the different mixtures, the strength development was similar COCO-BC-F.

Adding finer biochar leads to a notable increase of strength, with increases of 12.5% and 17% observed at 7 days. While hydration occurs in the macro-pores of biochar, these pores can remain empty like air voids in the mortar, creating weak spots that are susceptible of cracking and fracture.

Using finer biochar (e.g., WBC-F or COCO-BC-F) enhances the degree of hydration by 6–12% compared to plain mortar or mortar with only coarser biochar. Mortars containing finer biochar (WBC-F-2% and COCO-BC-F-2%) show significantly higher compressive strength than the control, even though their hydration kinetics are similar. This is due to the filler effect of fine biochar: the fine particles increase surface energy, making it harder for cracks to form and spread.

A mix of coarse and fine biochar produces a similar yield stress growth rate to the control but slightly lowers overall workability. Additionally, biochar also helps with internal curing and provides a surface for hydration products to form.

[191] (Gupta, Tulliani, & Wei Kua, Carbonaceous admixtures in cementitious building materials: Effect of particle size blending on rheology, packing, early age properties and processing energy demand, 2022)

The most recent research, though not the least significant, focuses on *3D printing of ordinary Portland cement with waste wood derived biochar obtained from gasification*. This study investigated the potential of biochar, derived from wood gasification, as an additive in cement paste formulations to enhance the properties of 3D printed cementitious materials. The materials used for the developing these cement composites included ordinary Portland cement, superplasticizer, sand, kaolin, calcium carbonate, and biochar. The biochar was incorporated into the cement pastes at various proportions: 0wt%, 5wt%, 10wt%, 15wt%, and 20wt%. The process involved the use of Ordinary Portland Cement, sand sieved through a 210 μm mesh, macerated biochar sieved to the same size, kaolin (25% by weight) for improving workability and strength due to its high silica and alumina content, calcium carbonate (5% by weight) to increase alkalinity and support the hydration process, and superplasticizer (2% by weight) to improve flowability and workability of the paste.

The preparation of the cement paste followed several steps. At the beginning, as first step, the dry ingredients, including Portland cement, sand, kaolin, and calcium carbonate, were mixed. Next, water and superplasticizer were added to the mixture, and the superplasticizer maintained at 2% by weight of cement to enhance fluidity and workability. The mixture was smooth, uniform paste, ideal for 3D printing.

The following formulations were done:

- F1 (10% Biochar): Comprising 48% Portland cement, 10% sand, 25% kaolin, 5% calcium carbonate, and 10% biochar.
- F2 (10% Biochar, Most Successful Formulation): This formulation, very similar to F1 but optimized with superplasticizer, was the best formulation in terms of printability and performance. It included 48% Portland cement, 2% superplasticizer, 10% sand, 25% kaolin, 5% calcium carbonate, and 10% biochar.
- F3 (15% Biochar): A higher biochar content, but this formulation faced issues with printing and stability, causing difficulties in sample solidification.
- F4 (20% Biochar): This formulation, with the highest biochar content, had flowability issues and was excluded from further testing.

Therefore, these formulations were extruded through a nozzle in a 3D printing creating the samples for testing. The printing was considered successful for formulations F1, F2, and F3, in which F2 has shown the best performance in terms of stability and printability. Afterward, there were done twenty cylindrical samples, with a height of 25.4 mm and diameter of 19 mm, and then cured for 28 days.

The formulations were evaluated using compression tests on a Shimadzu AG100NXplus universal testing machine, along with other analyses such as scanning electron microscopy (SEM). Compressive strength tests were performed on the 3D printed samples from formulations F1, F2, and F3, with F4 excluded due to printability issues[192].

This study highlights the significant potential of using biochar, derived from wood gasification, as an additive in cement formulations for 3D printing. The F2 mix, containing 10% biochar, demonstrated good printability, along with satisfactory compressive strength (4.8 MPa) and ductility (4.6%). Promising SEM results were also observed. Incorporating biochar enhances material properties, such as surface area and thermal stability, both of which are essential for successful 3D printing applications.

Considering all that has been explored previously, this thesis focuses on exploring the practical use of biochar in 3D printing as a way to support sustainable construction. It combines insights

[192] (Vergara , Perez, & Colorado, 2023)

from both traditional practices and modern technology to explore how biochar can improve material properties and support more environmentally responsible building methods.

Looking at biochar as a material, it has a great potential on construction industry, especially by some factors such as circular economy, waste management and carbon reduction. This thesis aims to introduce biochar as an essential part of the future sustainable construction's application with the specific emphasis on 3d printing as an innovative and promising implementation.

3D PRINTING

According to Autodesk, 3D printing transforms a digital 3D computer-aided design CAD model or similar file into a physical object through an additive manufacturing process. By systematically layering material, this method builds an object with precision and depth, bringing a virtual design to life in tangible, in a three-dimensional form[193]. Additive manufacturing, widely known as 3D printing, has unlocked new possibilities in design freedom. Since the mid-1980s, it has gained popularity in industries such as biomedical, aerospace, and manufacturing for its versatility and efficiency[194].

In the construction industry, 3D printing has had a positive impact by addressing challenges such as reducing material waste, decreasing construction times, mitigating labor shortages, and breaking the limitations of conventional construction techniques[195]. The tool of 3D printing has scaled up from crafting small prototypes to producing a larger scale component, introducing complex geometric designs and cost benefit solutions.

As 3D printing continues to evolve with the applications in construction, it requires an intense understanding of the technologies that conform to the additive manufacturing. To apply 3D printing efficiently, various technological aspects must be studied

TECHNOLOGY

According to the findings in *An Overview on 3D Printing Technology: Technological, Materials, and Applications,* "the 3D printing technology has originated from the layer-by-layer fabrication technology of 3D structures directly from CAD drawing"[196]. These technologies have been classified into seven categories, as defined by ASTM Standard[197], including methods like binder jetting, directed energy deposition, material extrusion, material jetting, power bed fusion, sheet lamination, and vat photopolymerization[198].

The method of blinder jetting is based on liquid binding agent deposited on powder particles. The layers are performed repetitively to produce a solid structure, as mentioned in the research *Binder Jetting: A Review of Process, Materials, and Methods*[199]. The function of this process is essentially to bind liquid on a powder bed, which joins particles together and forms the shape defined by the CAD model. The advantage of this technique is that it does not require high temperatures, allowing the use of a wide variety of materials, which also includes sand, and the development is on high-speed production and fine resolution[200].

---

[193] **Specificata fonte non valida.**
[194] (Khan, Sanchez, & Zhou, 2020)
[195] **Specificata fonte non valida.**
[196] **Specificata fonte non valida.**
[197] **Specificata fonte non valida.**
[198] **Specificata fonte non valida.**
[199] ***Specificata fonte non valida.***
[200] **Specificata fonte non valida.**

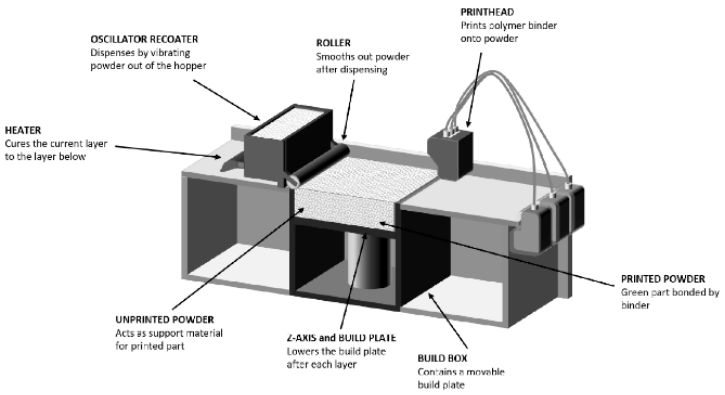

Figure 24 Binder jetting scheme.
Source: (Freeman Technology, 2019).

Another additive manufacturing method is Directed Energy Deposition (DED), which focuses on thermal energy, offers a total different approach than binder jetting, by melting materials like wire or powder, creating solid structures layer by layer, where an energy source such as laser, electron beam or plasma arc, melts the feedstock material and continuously deposits it to build geometries into structures[201]. This type of method allows the production of complex elements, with minimal waste, still contributing to both cost efficiency and sustainability[202].

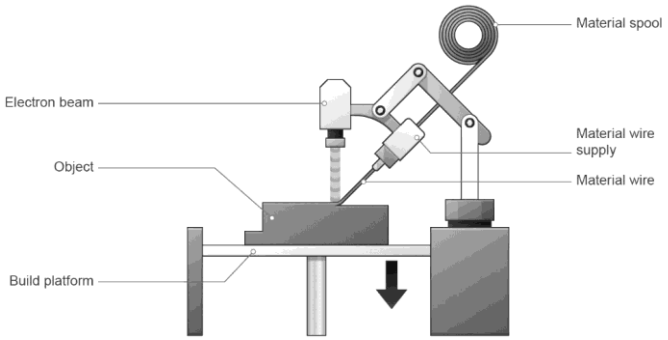

Figure 25 Directed Energy Deposition scheme.
Source: (3Ds Dassault Systemes, s.d.).

Materials Extrusion is a different technique of additive manufacturing, which is characterized by the layer-by-layer material placement through a nozzle or orifice under controlled pressure. This technology is valued for its versatility and cost effectiveness, as it can be applied for printing a wide range of materials including thermoplastics, composites, cement-based mixtures and even living cells[203]. This methodology works through extruding the material by constant pressure, in a semi-liquid condition, allowing it to cool and solidify into the final structure. This is now a large-scale implementation for construction projects[204].

[201] **Specificata fonte non valida.**
[202] **Specificata fonte non valida.**
[203] **Specificata fonte non valida.**
[204] **Specificata fonte non valida.**

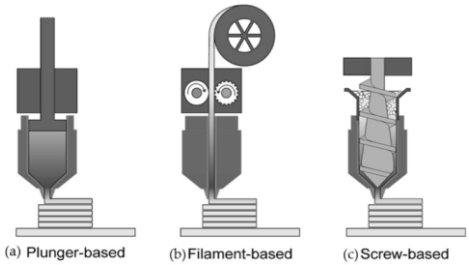

Figure 26 Extrusion method used: (a) filament-based, (b) plunger-based, and (c) screw-based extrusion.
Source: (Spina & Morfini, 2024).

Material Jetting is an additional method of 3D printing that employs the inkjet technology, similar to the traditional two-dimensional printing, by applying droplets of liquid material layer by layer, eventually creating a tangible object based on CAD model[205]. This process uses a printhead, which sprays droplets of liquid materials, such as polymers or thermoplastic materials, which are consequently cured by using UV light lamps or heat, depending on the material properties. Among its advantages, Material Jetting specializes in creating high resolution of complex geometries with fine details, making it particularly suitable for applications in aerospace, medical and automotive industries[206].

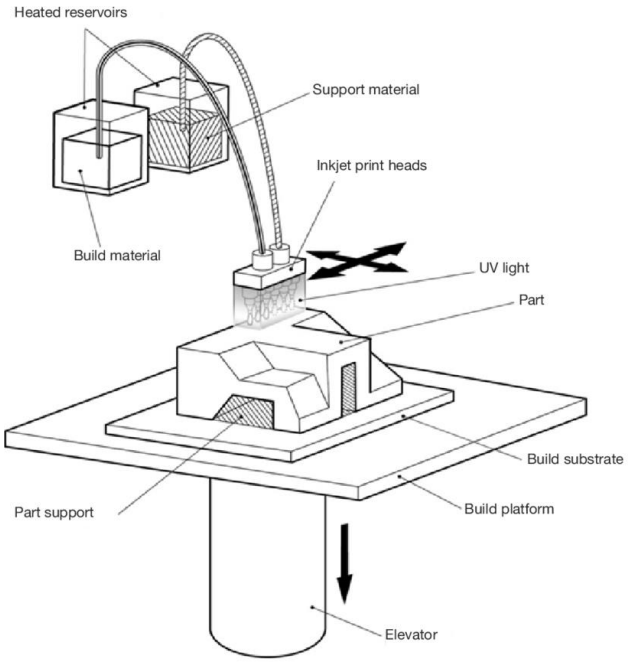

Figure 27 Material Jetting 3D printing scheme.
Source: (Otton, Hussain, Birbara, & Greil, 2017).

The next additive manufacturing technology is Powder Bed Fusion, which includes electron beam melting, selective laser sintering and selective heat sintering printing technologies. These different techniques enable enhanced productivity, and produce complex geometries with high precision, excellent mechanical properties, minimal waste and the use of different materials. All the processes share fundamental characteristics: A system that includes one or more thermal sources, usually lasers, for enabling fusion of powder particles, a method for controlling the localized fusion of powder to a specific region within each layer, and mechanisms for adding and leveling

[205] (Gibson, Rosen, & Stucker, 2015)
[206] **Specificata fonte non valida.**

the powder layers[207]. In essence, this process involves applying a thin layer of powdered material, such as metal or polymer, onto a build platform. Subsequently, heat is applied to melt or fuse the powder in predetermined regions, as specified by the design. After each layer is fused, the build platform is lowered slightly, and the procedure repeated for successive layers until the final segment is fully constructed.

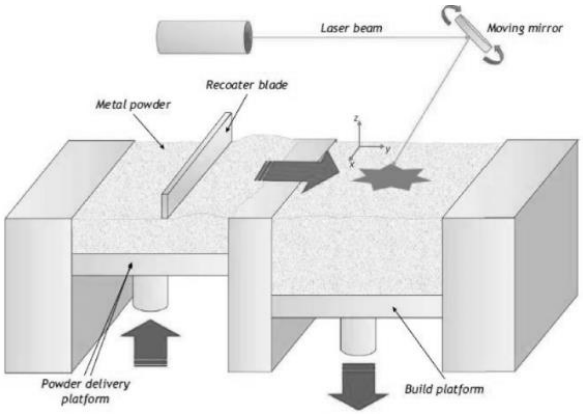

Figure 28 Laser powder bed fusion process scheme.
Source: (Cobbinah, Nzeukou, Onawale, & Matizamhuka, 2021).

Sheet lamination is an additive manufacturing technique that involves bonding material layers, which are usually composed of sheets of paper, metal or metal. In this process, each sheet is deposited onto the build platform and cutting tools such as lasers are employed to precisely cut the sheet in accordance with the design specifications. Afterwards, a bonding agent is applied, and the following layer of material is then added. This process is continuously followed until the three-dimensional object is fully formed[208]. One of the main advantages of sheet lamination is its capability to produce large and complex geometries at a cost-effective rate, making it especially favorable in applications such as tooling, prototyping, and even final product manufacturing[209].

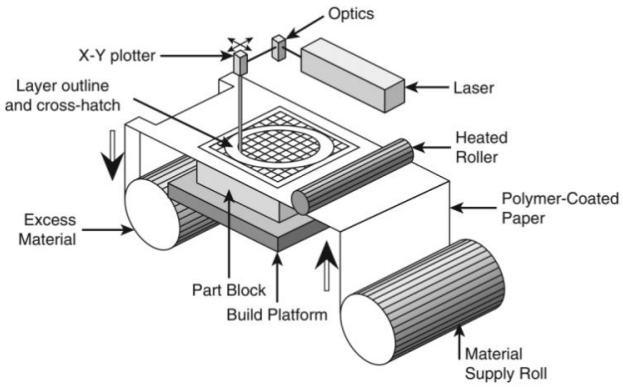

Figure 29 Sheet lamination overview.
Source: (Engineering Product Design, 2019).

The last technology is Vat Photopolymerization, which is an advanced additive manufacturing technique that employs a liquid resin cured by UV light to form solid objects layer by layer. By using ultraviolet light, this process hardens a photosensitive resin specifically, stabilizing it in precise areas by the computer-aided design model. Each layer is hardened before the next is

[207] (Gibson, Rosen, & Stucker, 2015)
[208] **Specificata fonte non valida.**
[209] **Specificata fonte non valida.**

applied, building the object incrementally and ensuring highly accurate and detailed outcomes[210]. In fact, one of the significant advantages of this technique is its ability to produce parts with extremely fine resolution, making it suitable for applications in industries requiring high-precision components, such as aerospace, medical devices, and dental manufacturing[211]. However, the process is often limited by the material's ability to fully cure and the post-processing requirements, which can be time-consuming[212].

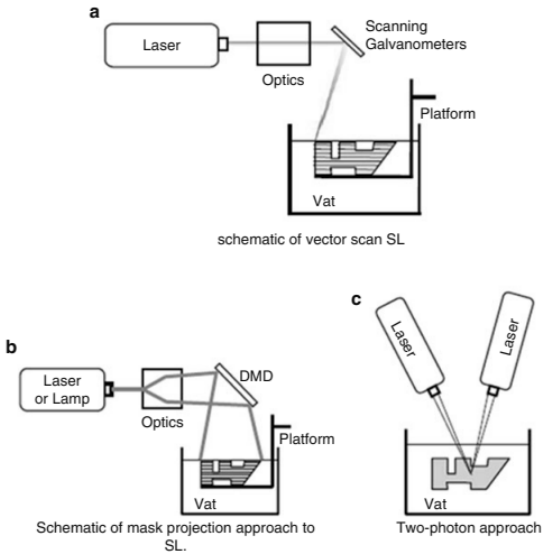

Figure 30 Schematic diagrams of three approaches to photopolymerization processes. Source: (Gibson, Rosen, & Stucker, 2015).

Given the precision and fine resolution achievable with techniques like Vat Photopolymerization, the selection of high-quality materials becomes fundamental. These materials directly influence the structural integrity, precision, and durability of the printed components. Therefore, to ensure the specifications, procedures and standards, it is necessary to control over the process.[213].

Furthermore, 3D printing technology tolerates a large variety of materials, including ceramics, metals, polymers, as well as their integration as a hybrid composition. All the different types of materials enable the versatility and the complexity of the possibles applications[214].

In the same way, in the construction sector, the development of cement-based printing inks is essential for the success of the 3D printing applications in the building sector. These inks must be balanced by the flowability, extrudability and buildability, while solidifying in time and still maintaining the structural integrity[215]. Some of the challenges that are presented in these materials include: rheological behavior, adhesion between layers and optimization of composition.

[210] **Specificata fonte non valida.**
[211] **Specificata fonte non valida.**
[212] **Specificata fonte non valida.**
[213] **Specificata fonte non valida.**
[214] **Specificata fonte non valida.**
[215] **Specificata fonte non valida.**

RHEOLOGY IN 3D PRINITNG

The importance of rheology extends beyond traditional concrete applications to modern construction techniques, including 3D printing. With the application of these new technologies, detailed rheological control is crucial for maintaining the shape stability of the first base printed layers and to ensure sufficient bonding with the successive layers. To achieve this a balance between a low yield stress to enable extrusion and high viscosity to prevent slump after deposition is required. The incorporation of supplementary cementitious materials (SCMs), such as fly ash, slag, and silica fumeamplifies the importance of rheology in concrete sustainability. The implementation of these materials starts from reducing the environmental impact of concrete, but they also introduce variability in rheological behavior that must be carefully managed as it may change the workability and viscosity of the mixture Considering this, it becomes evident that through rheological assessments, it is possible to optimize the use of SCMs, ensuring that they enhance, rather than inhibiting, the performance of the concrete mixture. Thus, rheology is essential to developing innovative and sustainable concrete technologies that meet the demands of contemporary more sustainable and resilient ways of construction.

APPLICATION IN CONCRETE

The application of 3D printing in the construction industry is changing the traditional building market, offering innovative solutions producing complex and customized structures. This technology, particularly large-scale 3D printing of concrete, has captured considerable attention due to its capacity to reduce waste, enhance precision and shorter timelines, as previously mentioned. These large technologies are typically divided into three main categories: 3D printing elements, 3D printing formworks and monolithic 3D printing applied on site, approaching into different stages and aspects of the construction process.

Image 1 3D printed elements: wall segments printed in factory and completed fabricated 3D printed concrete building in Nanjing.
Source: (Khan, Sanchez, & Zhou, 2020).

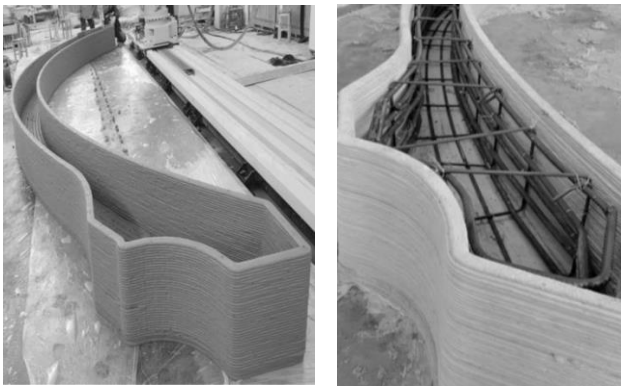

Image 2 3D printed Formworks.
Source: (Khan, Sanchez, & Zhou, 2020).

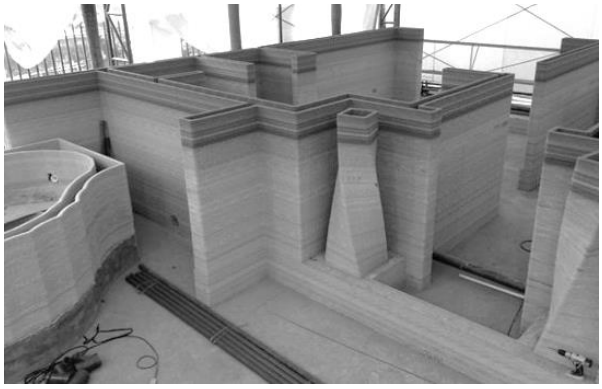

Image 3 Monolithic 3D printing on site.
Source: (Khan, Sanchez, & Zhou, 2020).

One of the most critical aspects of 3D printing in concrete is guaranteeing the structural integrity and durability of the printed concrete, which can be influenced by the printing size and the reinforcement solutions incorporated into the design[216]. As an environmentally conscious technology, 3D printing facilitates the creation of highly complex geometric structures while promoting sustainability in production processes. The capability to print with minimal waste and diverse materials aligns with efforts to reduce the carbon footprint[217]. The emergence of Building Information Modeling (BIM) enhances the application of 3D printing technology in construction[218].

Two outstanding examples of 3D printed buildings that demonstrate the potential of this technology include the Apis Cor Printed House in Melbourne, Florida and the Canal House in Amsterdam. These projects demonstrate the ability of 3D printing to create innovative, cost-effective, and environmentally sustainable housing solutions, while exploring new horizons of architectural design and construction methods.

[216] **Specificata fonte non valida.**
[217] **Specificata fonte non valida.**
[218] (Khan, Sanchez, & Zhou, 2020)

Image 4 Apis Cor's 3D-printed concrete walls for a residential house in Melbourne, FL. Soucre: (Apis Cor, a Manufacturer of Construction 3D Printing Robots, Announces Strategic Investment by D.R. Horton, 2024).

Image 5 The Canal House in Amsterdam, The World's First 3D Printed Canal House Source: (Renner, s.d.)

EXPERIMETNAL ACTIVITY

RESEARCH PARADIGMA

Throughout previous research and understanding of the main topics in the state of the art and theoretical background, it becomes evident in the urgency in the construction industry addressing climate change and developing mitigation strategies for global warming. One of the main strategies is the research of the main construction material for them to overcome variations and transformations to reduce architecture's environmental impact. Some of the main materials placed on the scope are all cement-based products such as cementitious paste, mortar, and concrete. All of them produce a high environmental footprint due to their high levels production of greenhouse gas emissions, and particularly the production of CO_2. Despite technological advancement and construction industry efforts, ranging from high-performance materials to smart building technologies, no material has been invented to meet the needs, in terms of versatility and load-bearing capacity. Consequently, cement remains the primary source for architectural and engineering development, in these ways attempt short-term strategies towards palliative and adaptive measures to mitigate the environmental impact of cement-based materials that need to be taken in reducing the negative environmental impact of cementitious materials.

Cement is one of the main sources for modern world construction, due to its characteristics, durability, versatility, and mechanical performance. However, the cement industry, accounts for approximately 6-8% of the world's anthropogenic CO_2 output as stated before. This comes from the materials calcination process during its production, and the energy intensive technology applied in the manufacturing process. Research in cementitious materials in finding a balance between achieving sustainable development needs and the essential cement reliance on the construction sector. This research aims to explore how the environmental footprint of these materials can be minimized while maintaining the high-performance parameters required for this material. One promising hypothesis is the implementation of alternative environmentally friendly materials that allow cement content reduction in concrete mixture designs.

One of the most innovative materials studied to lower carbon dioxide emissions is biochar which can partially replace cement. Biochar, a carbon-rich byproduct derived from the pyrolysis of biomass, offers the potential to sequester carbon while enhancing the sustainable value of concrete. Incorporating biochar into cementitious mixes reduces the overall cement content without compromising the essential chemical, physical, or mechanical properties. In the same way, biochar's porous structure can improve performance characteristics such as durability, water retention, and thermal insulation, making it one of the most currently studied materials for sustainable construction.

This approach not only targets the reduction of CO_2 emissions but also introduces the implementation of circular economy, where waste materials can be repurposed, extend the materials life cycle, and promote resource efficiency. By partially replacing cement with materials that have a lower carbon footprint, the construction industry can take significant steps towards minimizing its environmental impact, targeting the reducing CO_2 emissions during both the production phase and elongating concrete structures lifecycle towards a sustainable development. A critical aspect of this research is to understand if the introduction of sustainable materials, such as biochar, does not degrade the structural performance of cementitious composites, aiming for

modification in the concrete mix design to preserve the integrity, strength, and durability that concrete needs for its applications.

In addition to this, the experiment also targets the implementation of one of the most advanced technologies aligned with sustainable development in the application of 3D printing. This emerging technology permits previously unachievable, precise innovative design approaches to concrete structures production based on efficient material utilization. By minimizing material waste, the integration of 3D printing in construction brings several sustainability benefits such as: Material efficiency by reducing waste and using only the necessary and optimizing material distribution. Lowering carbon footprint allows for cement content reduction and facilitates sustainable additives integration. Innovation and optimization enhancing not only the architectural aesthetic capacity but also, optimizing structural elements by reducing the overall volume of material used. Local and on-site productions, lowering the embodied carbon of the material by avoiding transportation or prefabrication of components and implementing local components suitable for contextually adaptive practices.

Based on this understanding, this research is guided by the construction sector to achieve sustainability goals with the realities of material performance and availability. Investigating the potential of biochar and other environmentally friendly additives implementation in existing materials to make them more sustainable, integrated with 3D concrete printing implementation, the thesis aims to contribute to a more sustainable built environment. The expected outcome is to present a pathway for concrete that is compatible with the demands of climate change mitigation, enabling the construction industry to transition into a low-carbon economy.

MATERIALS

As previously stated, the experimental process required various components for the formulation of the mortar paste including cement, biochar, a superplasticizer, and polyethylene glycol (PEG). Each of these materials was meticulously selected based on their unique characterization and contribution to the overall performance of the mortar. Making it is essential to characterize and specify the significance and properties of each component to establish their roles and application.

CEMENT

Cement works as the primary binding agent in the mortar, providing strength and cohesion through the hydration process. Its chemical and physical properties are critical when determining the mechanical performance of the final mixture, that is why it is highly important the utilization of a high-quality cement which satisfies the specific requirements of fineness, setting time, and compressive strength.

The cement used in the experiment is a Buzzi Unicem Portland cement Type I 52.5 R, a high-performance cement which ensures obtaining structural integrity, optimal workability and durability. This cement is classified under the European standard EN 197-1, ensuring it meets the necessary mechanical, chemical and physical performance benchmarks.

Image 6 Cement Type I 52.5 R.
Source: (Buzzi Unicem S.r.l., n.d.)

Its primary characteristics include a high compressive strength of at least 52.5 MPa after curing for 28 days, developing rapid early strength, meeting the requirements of European Regulation 305/2011 (Construction Products Regulation, CPR) and is appropriately labeled in compliance with the regulatory framework, making it suitable for demanding construction projects that require short curing times. Buzzi Unicem Tipo I 52.5 R contains a minimum of 95% clinker and is formulated with a finely controlled particle size distribution, which enhances its reactivity and ensures fast hydration, and leaves only a 5% to secondary constituents[219]. The cement's Blaine surface area[220] optimizes to balance workability with strength, allowing for smoother applications

[219] These proportions exclude the inclusion of calcium sulfate and other additives. (Buzzi Unicem S.r.l., n.d.)
[220] Spherical Surface area found by the formula 4 *π* r^2. (CUEMATH, n.d.)

and reducing water demand, making the material highly compatible with additives like superplasticizers, which are commonly used to improve the mortar's rheology[221].

Parameter	Test method	Indicative values[222]	Characteristic limits based on the standard
Sulfates (SO_3)	UNI EN 196/2	< 3.7%	≤ 4.0%
Chlotrides (Cl -)	UNI EN 196/2	< 0.08%	≤ 0.10%
Loss to fire	UNI EN 196/2	< 5.0%	≤ 5.0%
Insoluble residue	UNI EN 196/2	< 1.0%	≤ 5.0%
Chromium VI soluble in water	UNI EN 196/10	≤ 2 ppm	≤ 2 ppm

Table 17 Chemical requirements.
Source: (Buzzi Unicem S.r.l., n.d.)

Parameter	Test method	Indicative values	Characteristic limits based on the norm
Blaine specific surface area	EN 196/6	4000-5500 cm2/g	
Setting starting time	EN 196/3	>90 min	≥ 45min
Volume stability	EN 196/3	≤10 mm	≤10 mm
Mortar consistency	UNI 7044	>70%	
Compression resistance after 2- day curing	EN 196/1	>35,0 MPa	≥ 30 MPa
Compression resistance after 28- day curing		>56,0 MPa	≥ 52.5 MPa

Table 18 Mechanical and physical requirements.
Source: (Buzzi Unicem S.r.l., n.d.)

The primary advantage of this cement is its high early strength, which accelerates the construction process and improves structural performance in early stages. Additionally, the product's superior sulfates' resistance makes it suitable for aggressive environments, such as marine or industrial settings. However, a potential limitation of Type I 52.5 R cement is its relatively higher heat of hydration, which may lead to thermal cracking in massive concrete structures. To mitigate this, careful thermal management or alternative cementitious materials might be necessary in large-scale application[223].

For more details detail refer to ANNEX 1.

[221] (Buzzi Unicem S.r.l., n.d.)
[222] The values represent the level above (or below) which it is reasonable to expect the positioning of the average values, for the parameters indicated, of the BUZZI UNICEM cements belonging to the type and class indicated in the header, calculated on an annual basis and considering internal self-monitoring data. (Buzzi Unicem S.r.l., n.d.)
[223] (Buzzi Unicem, n.d.)

BIOCHAR

Supplementary Cementitious Materials (SCMs) can be classified broadly into two categories: *natural* (e.g., volcanic ash, calcined clays) and *industrial by-products* (e.g., fly ash, silica fume, ground granulated blast-furnace slag). SCMs are soluble siliceous, aluminosiliceous, or calcium aluminosiliceous powders used as partial replacements of clinker in cements or as partial replacements of portland cement in concrete mixtures[224].

SCMs contribute to the properties of cementitious systems through hydraulic or pozzolanic activity, forming additional calcium silicate hydrates (C-S-H), which densify the matrix and reduce permeability[225]. When used independently or blended with Portland cement both fresh and hardened properties of concrete are improved, presenting a resistance improvement to sulfate attack, alkali-silica reaction (ASR), and chloride ingress while extending the service life of concrete structures ability through its refined pore structure[226].

Its incorporation is studied and applied due to its ability in improving sustainable requirements and reducing the environmental impacts of the construction industry, decreasing the clinker factor in Portland cement production, therefore lowering CO_2 emissions. The use of SCMs can result in CO_2 reductions of up to 60% when working as an environmentally approved substitute for clinker, contributing to more sustainable construction practices[227].

SCMs, as other cementitious components, are evaluated based on their physical, chemical, and mechanical requirements which establish its suitability input to cementitious materials, starting with the chemical compositions and the presence of silica (SiO_2), alumina (Al_2O_3), and calcium oxide (CaO), the percentage composition of these compounds in SCMs determining its reactivity. High silica contents undergo pozzolanic reactions, while CaO supports hydraulic reactions.

The European specification for cement EN 450-1:2012 specifies the chemical requirements for fly ash used in concrete, while EN 15167-1:2006 covers ground granulated blast-furnace slag. Both standards emphasize limits on reactive silica, free lime, and loss on ignition for cement to achieve consistent performance[228]. Moreover, The American Society for Testing and Materials Standards such as ASTM C618 presents the requirements for fly ash and natural pozzolans, ASTM C989 for slag, and ASTM C1240 for silica fume specify minimum requirements for these oxides to ensure consistent performance[229].

Particle size, specific surface area, and fineness are essential factors that significantly influence the reactivity and workability of concrete, making these the main physical requirements in SCMs materials. Finer materials, such as silica fumes[230], develop high reactivity due to their large specific surface area, concluding in faster pozzolanic reactions[231] improving strength and reducing permeability. Particle size distribution also affects water demand and rheological behavior. When finer particles are presented, the material usually increases water demand, forcing the use of admixtures to maintain workability[232]. EN 196-6 provides guidelines for determining the fineness of cement and SCMs using the Blaine air permeability method.

Pozzolanic and hydraulic reactivity in SCMs is needed to contribute to concrete strength development. Pozzolanic reactivity is characterized by the ability of the SCM to react with

[224] (Juneger, Snelling, & Bernal, 2019)
[225] (Thomas , 2013)
[226] (Neville A. , 2011)
[227] (Mehta & Monteiro, 2014)
[228] (CEN, 2011)
[229] (ASTM, 2024)
[230] As stated in EN 13263-1:2005
[231] (Mindess, Young , & Darwin, 2003)
[232] (British Standards Institution, 2013)

calcium hydroxide (CH) to form secondary calcium silicate hydrates (C-S-H), while hydraulic materials, such as slag, possess inherent cementitious properties when activated by water or calcium hydroxide. EN 196-5 outlines the pozzolanicity test, which assesses the reactivity of pozzolanic materials, ensuring compliance with performance-based criteria, also the Frattini test and strength activity index (SAI) are common methods used to assess these properties according to ASTM C311.

SCMs improve concrete resistance to aggressive environments. For instance, slag and fly ash reduce the heat of hydration, which is crucial for mass concrete applications[233]. According to BS EN 206:2013, the use of SCMs lowers the permeability of concrete, increasing resistance to chloride ingress, sulfate attack, and alkali-silica reaction, particularly relevant for marine and industrial environments, where prolonged exposure to aggressive conditions can compromise concrete integrity[234].

Despite the numerous advantages, SCMs also present certain challenges that must be addressed. Variability in the composition of by-product SCMs, such as fly ash and slag, can lead to inconsistent performance, even so, some SCMs may require longer and more controlled curing periods and environments due to their slower early strength development[235]. In this way, comprehensive quality control measures and proper mix design adjustments are essential to maximize the benefits of SCMs.

Apart SCMs, biochar, a carbon-rich material produced through the pyrolysis of organic biomass works as a sustainable admixture for the mortar mixture design. Its porous structure and high surface area contribute to improved thermal insulation, moisture regulation, and environmental sustainability while reducing the carbon footprint of the mortar. Additionally, biochar is known to improve the mortar's mechanical properties, increasing its density and reducing micro-cracking[236].

For this experiment the biochar used is produced by NERA Company, this component plays a significant role in increasing cementitious materials the sustainability and performance. Biochar is recognized for its potential to sequester atmospheric CO_2[237], reducing the carbon footprint of construction projects while simultaneously improving material properties. Its porous structure improves water retention and contributes to better curing conditions, promoting the optimal conditions for the formation of hydrated cement phases[238].

[233] (Khan & Young, 2024)
[234][234] (Pourakbar & Huat, 2016)
[235] (Gartner & Hirao, 2015)
[236] (Mishra, Danoglidis, Shah, & Gdoutos, 2024)
[237] (Lin , y otros, 2023)
[238] (Gupta, Kua, & Low, Use of biochar as carbon sequestering additive in cement mortar, 2018)

Image 7 Nero Biochar.
Source: (NERO, 2022)

NERA Biochar is obtained from pyrolyzed wood waste[239], providing a carbon content of approximately 90% because of the wood being processed at high temperatures (around 700 °C) in an oxygen-deprived environment, producing a stable and eco-friendly product. The biochar is ground to fine particles, often less than 180 µm, to maximize surface area, which enhances its integration with the cement matrix and improves mechanical properties such as compressive and flexural strength[240].

Studies have shown that incorporating biochar at low percentages maintaining a relationship of 1-5% biochar by weight of cement, can improve the compressive strength and reduce water adsorption in mortar and cement pastes[241]. However, excessive additions can compromise workability, with flow reductions of up to 20% when biochar content reaches 15%[242]. Additionally, NERA Biochar's microporous structure enhances water adsorption, promoting better internal curing and mitigating shrinkage cracking in cement-based materials[243].

Despite its benefits, challenges such as reduced workability and potential difficulty in dispersion within the cement matrix are most commonly present when implementing, additionally requiring the use of superplasticizers and polyethylene glycol as the technique to resolve the previously stated problematics. Furthermore, the specific surface area and particle size distribution are crucial parameters that influence its performance and integration[244].

For more details refer to ANNEX 2.

[239] (NERO, n.d.)
[240] (Suarez-Riera, et al., 2024)
[241] (Choi, Yun, & Lee, 2012)
[242] (Akhtar & Sarmah, 2018)
[243] (NERO, n.d.)
[244] (Suarez-Riera, et al., 2024)

SUPERPLASTICIZER

Superplasticizers, also known as high-range water reducers are chemical admixtures, designed to enhance the workability of concrete without increasing its water content. By reducing the water-to-cement (w/c) ratio, superplasticizers enable the production of high-strength, durable concrete with improved workability. They are essential in the production of self-compacting concrete (SCC), high-performance concrete (HPC), and other advanced cementitious materials[245]. According to EN 934-2:2019[246], superplasticizers reduce water content while maintaining and improving workability, thus contributing to strengthening structural performance and sustainability in construction.

For these reasons superplasticizers are critical for modern concrete applications as a technology that allows the production of concrete with low water content without compromising slump or flow is typically evaluated through standard tests such as the slump test and flow table test as stated in EN 12350-5. Reducing the w/c ratio results in enhanced compressive strength, lower permeability, and improved durability, particularly important in densely reinforced or complex-shaped structures, which are essential for long-lasting structures subjected to aggressive environments[247]. EN 934-2:2019 highlights the ability of superplasticizers as capable of reducing water content by at least 12% while maintaining a high level of workability.

Superplasticizers are categorized into different chemical families, the most used are Sulfonated Melamine Formaldehyde (SMF), Sulfonated Naphthalene Formaldehyde (SNF), and Polycarboxylate Ether (PCE). This last one is established as the most advanced one, granting superior dispersing capability and extended workability retention, also allowing for tailored molecular designs, offering enhanced control over concrete rheology and long-term stability[248].

Setting time and strength development of concrete is affected by superplasticizers as traditional sulfonate-based admixtures may slightly accelerate or retard setting, typically offering greater control over setting time without compromising early strength. This type of properties is then tested as stated in EN 480-2 specifies test methods for evaluating the setting time of concrete containing admixtures, ensuring compliance with performance criteria. Moreover, as highlighted in EN 206:2013[249] by reducing the w/c ratio, superplasticizers contribute to the production of dense, impermeable concrete, enhancing resistance to chloride ingress, sulfate attack, and freeze-thaw cycles. Additionally, superplasticizers facilitate the production of self-compacting concrete (SCC), which eliminates the need for vibration, reducing the risk of segregation and improving surface finish quality.

For the experiment the Dynamo SP1, manufactured by Mapei, a high-performance superplasticizer designed for enhancing concrete's workability and mechanical strength was used. It is particularly beneficial in applications requiring a low w/c ratio while ensuring high early and final compressive strengths. This product is primarily based on a modified acrylic polymer, making it suitable for self-compacting[250], precast concrete applications[251], and high durability structures[252]. Incorporating Dynamon SP1 into mortar paste is known to enhances flowability,

[245] (Caltrans, 2013)
[246] Defines performance requirements for concrete admixtures
[247] (Neville A. , 2011)
[248] (Flatt & Schober, 2012)
[249] The importance of admixtures in achieving durability class specifications, particularly in aggressive exposure conditions
[250] Used alongside products like Visco fluid SCC for enhanced flow without segregation risks. (Mapei, n.d.)
[251] Manufacturing prestressed beams, roofing slabs, and cladding panels. (Mapei, n.d.)
[252] Suitable for waterproof and freeze-thaw-resistant concretes, conforming to EN 206-1 exposure classifications. (Mapei, n.d.)

reduces water content, and improves the paste's durability and mechanical properties. In addition, Dynamon SP1 aids in reducing shrinkage, permeability, and the risk of segregation in concrete. This feature is particularly important for maintaining long-term performance and durability is critical[253].

Image 8 Mapei Dynamon SP1.
Source: (Mapei, n.d.)

For more details refer to ANNEX 3.

The performance of superplasticizers depends on their compatibility with different types of cement, as variations in cement composition can affect dispersion efficiency and setting time, particularly for the application of Dynamon SP1 will offer excellent water reduction and workability retention, its performance depends on proper dosage[254] and application procedures, such as adding it after other components to optimize dispersion. According to EN 197-1:2011, cements containing supplementary cementitious materials (e.g., fly ash, slag) can exhibit different interactions with superplasticizers. Another challenge presented by the application of superplasticizer is the latent potential for overdosage, which can lead to segregation, excessive bleeding, or delayed setting. Additionally, the performance of superplasticizers may vary depending on the cement composition, temperature, and mixing conditions. Therefore, careful dosage optimization and thorough compatibility testing are essential to ensure consistent performance[255].

Based on the literature, valuable insight was provided into the benefits of incorporating superplasticizers into mortar mix designs to enhance. However, during experimental trials, the interaction between the superplasticizer and biochar introduced into the mixture resulted in unexpected chemical reactions. Specifically, the presence of biochar altered the behavior of the superplasticizer, leading to segregation of the mixture and a phenomenon known as bleeding, where the mortar paste exhibited excessive separation of water from the solid components. This destabilization compromised the homogeneity of the mixture, rendering it unsuitable for practical applications and 3D printing. Consequently, the use of the superplasticizer Dynamon SP1 was no longer continued in the mortar mixture design trials, and the focus shifted to alternative admixtures , specifically polyethylene glycol.

[253] (Mapei, n.d.)
[254] 0.6-1.2 L per 100 kg of cement (Mapei, n.d.)
[255] (Mindess, Young , & Darwin, 2003)

POLYETHYLENE GLYCOL (PEG)

Polyethylene glycols (PEGs) is a water-soluble polymer commonly used in cementitious materials as a chemical admixture characterized by its chemical structure consisting of repeating ethylene oxide units, $(C_2H_4O)_n$, and its ability to be synthesized with various molecular weights[256]. PEGs consist of repeating ethylene oxide units, giving them a hydrophilic nature and a wide range of molecular weights[257]. They are known to be very versatile materials as they are presented in both liquid and solid forms which make them applicable in a wide range of different concrete formulations. PEGs are particularly beneficial in scenarios requiring internal curing, shrinkage mitigation[258], water retention agents and hydration stabilization, which are essential for high-performance and durable concrete systems for cracking, early-age shrinkage, and loss of workability, challenges presented in concrete modern technologies[259]. The effectiveness of PEG in concrete depends on several key parameters, including molecular weight, dosage, and its interaction with other cementitious components.

PEG is available in various molecular weights, ranging from low 400 g/mol, more readily soluble in water and commonly used for internal curing purposes, to high 10,000 g/mol providing longer-lasting hydration control. The choice of molecular weight significantly affects the rate of water release and the extent of hydration enhancement[260]. By retaining water within the matrix, PEG ensures continuous hydration even after the external water source is depleted mitigating autogenous and drying shrinkage. Studies have demonstrated that PEG can reduce autogenous shrinkage by 30%–50%, depending on its dosage and molecular weight[261], supported by the standard EN 12390-13, which governs the determination of shrinkage in hardened concrete, used to assess the effectiveness of PEG in reducing shrinkage.

When increasing hydration and reducing shrinkage, PEGs affect concretes mechanical properties such as compressive strength when applied at optimal dosages. PEG increases strength development by promoting hydration, however excessive dosage amounts need to be avoided as it can reduce strength because of porosity increase taking into consideration the EN 12390-3[262]. Additionally, PEG indirectly improves the long-term durability of concrete, by reducing cracking, improving resistance to chloride ingress, sulfate attack, and freeze-thaw cycles, aligning with the durability requirements specified in EN 206:2013[263].

After testing PEGs compatibility under real mix conditions with different molecular weights (600 g/mol, 4,000 g/mol, 10,000 g/mol), the implementation of the 10,000 g/mol was selected and the PEG was introduced to the mortar mixture design with a dosage of 2 grams per 10 grams of cement to improve segregation issues and maintain workability without inducing adverse chemical interactions.

[256][256] (National Center for Biotechnology Information, 2024)
[257] Ranging from a few hundred to several thousand Daltons (Mehta & Monteiro, 2014)
[258] Working as a shrinkage-reducing admixtures (SRAs)
[259] (Neville A. , 2011)
[260] (Bilek, Kalina, & Novotny, 208)
[261] (Just, Wyrzykowski, Bajare, & Lura, 2015)
[262] Gives the requirements for compressive strength testing in concrete.
[263] Standard for exposure classes relevant to marine, industrial, and freeze-thaw environments.

Image 20 Sigma-Aldrich Polyethylene Glycol 10,000
Source: (Author)

The Polyethylene Glycol (PEG) 10,000, applied in the experiment is the Sigma-Aldrich company PEG under catalog number 81281-1KG, is a high-molecular-weight polymer with a molecular range of 8 500 to 11 500. Its structure includes hydroxyl groups at both ends, contributing to its hydrophilicity, flexibility, and compatibility in various applications, particularly in modifying cementitious materials.

For more details refer to ANNEX 4.

METHODOLOGY

Firstly, it is important to state that the focus of the thesis practical work was developed based on theoretical work from the investigation of current literature in the topic and previous research findings, which indicated that the mechanical properties of mortar begin to change when the proportion of biochar as a cement replacement exceeds 5%. Therefore, to ensure the reliability of the results and maintain optimal mortar performance, the biochar-cement replacement ratio for all tests was set at 5%.

The experiment was developed using a trial-and-error model, particularly effective when dealing with empirical research in engineering and materials science, where other models may not fully capture the complexity of the system, requiring a more exploratory approach where the variables interact in an unpredictable way. This model is performed in a systematic process where variables interact with each other in different combinations, observing outcomes, and refining the experimental conditions based on the results. The model is based on the constant refining of either material proportions, environmental conditions, or processing techniques, until identifying the optimal parameters that meet the experiment specific performance criteria[264]. Although it is often considered a less structured experimental model compared to others, trial-and-error remains a valuable strategy, especially in the early stages of research, where limited theoretical data is available to guide precise predictions. The flexibility of this methodology allows for real-time adjustments and the incorporation of unexpected findings [265].

BIOCHAR PREPARATION:

The experiment's initial phase involved already prepared biochar, acquired from a controlled wood pyrolysis process (Nera biochar produced in Montestrutto, Settimo Vittone (TO)), ensuring consistency in material characteristics. The objective of this stage was to reduce the particle size of the biochar, which is a critical factor influencing the mechanical behavior and integration of the biochar in cementitious mixtures.

The biochar was placed in a closed container, filling its volume with enough quantity to allow sufficient pace for movement and grinding. In addition, agate balls were added to the container, utilized as an abrasive medium to help in the grinding process. The agate balls were selected for their hardness and size, which are suitable for breaking down the biochar particles and increasing grinding efficiency. The container was then securely sealed to prevent any loss of material when positioned on the rolling bench and subjected to continuous rotation for a period of 24 hours. The bench was set to rotate at a consistent speed, optimizing the movement of both the balls and biochar within the container.

[264] (Montgomery, 2017)
[265] (Box, Hunter, & Hunter, 2005)

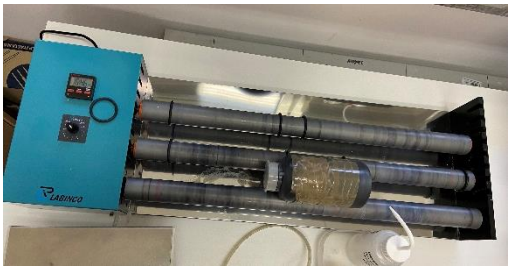

Image 9 Biochar griding in the rolling bench.
Source: (Author)

The rotation period executed a consisting grinding action with the balls moving within the confined space, creating a repetitive impact and abrasion effect on the biochar particles, trying to a reduction in their size. This method ensures a more uniform and fine particle distribution, which is essential for its role as a partial cement replacement in mortar mixtures.

Despite the long grinding process, when opening the container to check the particles size reduction obtained, no noticeable change in the particle size of the biochar was observed, indicating that the initial method was insufficient. Given the limited success, a step was introduced before subjecting the biochar to the grinding process again. This additional step aimed to improve the efficiency of the grinding while minimizing the loss of fine particles.

Image 10 Biochar after dry grinding, seamlessly change done to the particle size.
Source: (Author)

In this new process the biochar was initially placed in a mortar, and distilled water was added gradually. This water addition was crucial to reduce the dispersion of fine, pulverized particles into the air, a problem encountered when handling dry biochar. The mixture was then manually ground using An alumina pestle until the biochar transitioned from a solid to a slurry-like consistency when the distilled water and biochar were mixed, indicating a successful preliminary breakdown of particles. This pre-crush process allowed biochar breakdown facility from solid particles into a more workable form.

Image 11 Biochar hydrated pre grinding crushing process.
Source: (Author)

The slurry mixture of biochar and distilled water was then transferred into the same closed container used previously, along with the balls. This modified mixture was then subjected to a second grinding process, where the container was placed on the rolling bench and rotated for an additional 24 hours. The wet grinding approach aimed to achieve a finer and more uniform particle size.

After the 24-hour grinding period, the container was opened, and the biochar mixture was carefully transferred into a beaker placed in an oven set to a controlled temperature of 60˚C submitting the biochar into a drying process. The objective was to evaporate all water content, leaving behind only the finely ground biochar. This process lasted approximately 48 hours.

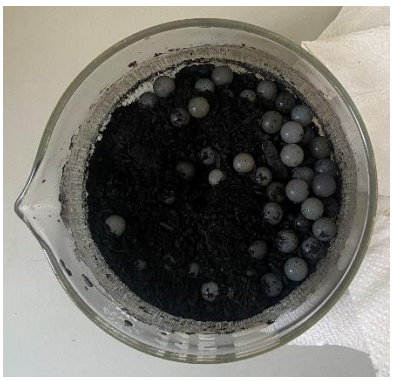

Image 12 Fully dried biochar after 48 hours.
Source: (Author)

Once fully dried, the final particle size adjustment process started with the pulverized biochar passed through a 250 µm sieve to ensure that the particle size met the criteria required for the experiment and a uniform particle distribution. The sieve with the biochar was then placed in an electrical sieve shaker and processed for 15 minutes, separating only the particles that passed though the sieve. This mechanical sieving step was critical for achieving a consistent particle size distribution that would optimize the biochar's integration into the cementitious mixtures.

Image 13 Final biochar 250 µm particle size after sieving.
Source: (Author)

The reduction of biochar particle size is a crucial step, as it directly influences its interaction with the cement matrix. Fine particles are expected to distribute more evenly throughout the mix, providing a more uniform filler effect and potentially enhancing the hydration process of the cement. This could lead to improved mechanical properties and overall performance of the biochar-cement composite. Thus, ensuring proper particle size was fundamental to the integrity of the subsequent experimental phases.

SAND PREPARATION:

Following the successful archival of biochar particles target size of 250 µm, it was necessary to follow the same process with the sand used in the experiment to ensure it also met the same size criteria. The objective of having both materials in 250 µm was to ensure consistency in particle size to achieve a homogeneous mortar mix design, crucial for reliable experimental results. Although the initial sand was already fine sand, its particle size distribution was too large to meet the specifications required for the experiment, that is why a sieving procedure needs to be done.

The fine sand was first placed in the oven to dry and ensure there was no moisture content, as humidity can affect the sieving efficiency, and introduced to the 250 µm sieve. The sieve was mounted onto an electrical sieve shaker, this sieving method provides consistent, controlled vibrations to facilitate the passage of finer particles through the mesh. The shaker's vibration frequency and amplitude also benefit optimizing sieving efficiency and time reduction required for each batch.

Image 14 Sand sieving equipment.
Source: (Author)

The electrical sieve shaker operated for 15 minutes per cycle. This duration allowed adequate time for the vibration and mechanical agitation to separate the particles in an effective way. During each cycle, the sand was shaked at a consistent speed, causing finer particles to fall through the mesh while larger particles remained on top. The material that passed through the sieve was collected and verified for particle size consistency, the left sand material that did not meet the 250 µm criterion was discarded. After each sand cycle was sieved and verified, the processed sand was collected in a sealed container to prevent contamination from dust or moisture. This process was repeated until enough sand, meeting the 250 µm specification, was accumulated to move on with the experimental mortar mixtures.

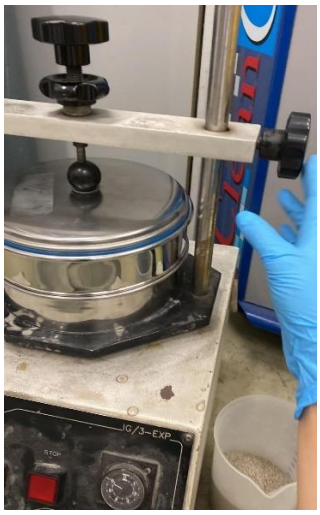

Image 15 Sand placed in the electrical sieve shaker in a 250 µm sieve.
Source: (Author)

To maintain sand quality and efficiency in the sieving, the sieve was regularly inspected for blockages at the end of each cycle. If blockages were detected, the sieving process was paused, and the sieve cleaned before resuming. One of the most significant challenges faced during the sieving process was the rapid blockage of the sieve by the sand particles that could pass though. This issue slowed down the sieving process, as it required frequent interruptions to clean the sieve.

In the interest of solving the sieve clogging problems, the sieve was regularly cleaned using an ultrasonic cleaner. The ultrasonic cleaner utilizes high frequency waves to create microscopic bubbles in a cleaning solution, removing any sand particles that had adhered to the sieve mesh. Each cleaning session took approximately 10 to 15 minutes, during which the sieve was fully immersed in the cleaning solution and subjected to ultrasonic vibrations. Once cleaned, dried completely to avoid sand humidity, and then remounted onto the sieve shaker.

Standardization of both the biochar and sand particle size assures a homogeneous mortar mixture with uniform mechanical properties such as compressive strength, tensile strength, and good durability. In the next stages of this research, the prepared biochar and sand will be used in various concrete mix designs, adhering to a 5% cement replacement ratio, to analyze its effects on the physical and mechanical properties of the composite material.

GRANULOMETRY

Biochar granulometry analysis was performed using the Malvern Mastersizer 3000 Aero S, an advanced dry powder dispersion system designed to measure particle size distributions with high

precision and reproducibility. This instrument determines particle size using laser diffraction based on the angular scattering of light as it traverses a dispersed sample. As illustrated in figure 66, the scattering of laser incident light differs based on the size of the particles, with smaller particles scattering light at larger angles and larger particles scattering light at smaller angles[266].

For dry powders like biochar, the Aero S disperser uses compressed air which accelerates the biochar particles into the system which is regulated to control the vibration of the blade, ensuring that the powder falls steadily without excessive force. The airflow then separates the powder, and the detector subsequently measures the particle sizes. Dispersion parameters like air pressure, feed rate, material's refractive index and geometry are carefully controlled to achieve the best results.

Figure 65 Malvern Mastersizer 3000 Aero S
Source: (Malvern Panalytical, 2024).

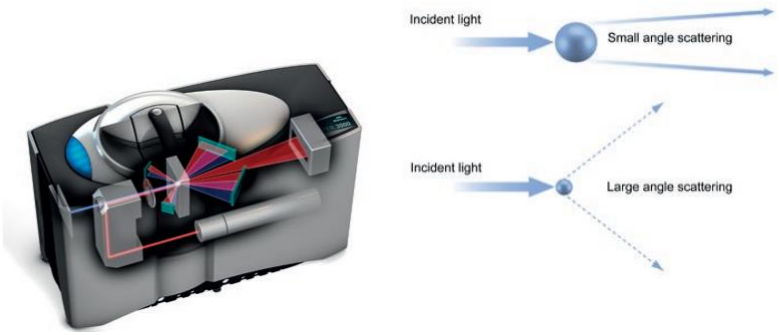

Figure 66 Illustration of the laser diffraction process within the Malvern Mastersizer 3000 Aeros S instrument
Source: (Malvern Panalytical, 2024).

The Mastersizer 3000 has a wide measuring range, from 0.01 µm to 3500 µm, and uses advanced software capable of analyzing data in real time. The system's modular design supports its versatility, allowing it to handle cohesive and fragile powders effectively. This approach avoids the use of liquid dispersants, provides accurate and economically viable assessments, and accounts for dry particle states that are important for biochar applications.

[266] (Malvern Panalytical, 2024)

Image 124 Introducing biochar powder particles into the conical steel cell for granulometry analysis
Soure: (Author).

For granulometry analysis, biochar powder particles were prepared and added to the upper part of the Malvern Mastersizer 3000 Aero S, where it is placed in a conical cell made of steel and locked by a fine mesh to prevent the passage of larger particles that could disrupt the measurement.

After loading the sample, it was fed into a vibrating conveyor belt that was designed to randomly determine the distance between the particles. This movement promoted overall mixing of the sample enabling the particles to flow into a venturi, where they were transported by a controlled suction mechanism into the area of laser diffractive measurements. In this method, patterns of scattered light from particle interaction with a laser beam were captured and analyzed to accurately measure the particle size distribution. This method achieves a high reproducibility and reliability in the granulometry characterization.

GRANOLUMETRY ANALYSIS

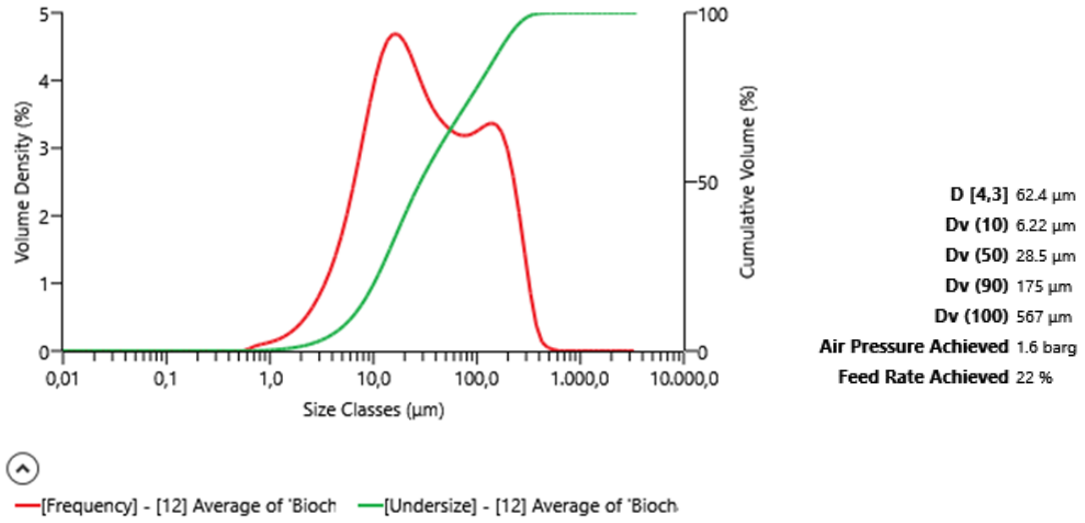

Figure74. Cumulative Granulometric Distribution of Biochar Measured by Laser Diffraction (Author).

Multiple trials were performed to acquire results with precision, upon which the final values were averaged to represent a precise particle size profile. In the first measurement we performed, the maximum particle size recorded in the measurement was 3500 μm, which is larger than expected, particularly given the 250 μm sieve used for separation. This inconsistency indicates potential issues with de-agglomeration during the measurement process. To obtain accurate results, a second measurement was taken, and the final average was based on the first four measurements, and the second 5 measurements which showed consistent and reliable results. Biochar was sieved at 250 microns, and an average of 9 different measurements was taken to obtain accurate result. The particle size span of the biochar was also wide, from 0.01 μm to around 567 μm.

Therefore, the results are presented in a single cumulative curve to represent the full range of particle sizes. Here, the cumulative distribution curve reflected information in values which correspond to the particle sizes in figure 4:

Dv (10) which corresponds to the 10% of the cumulative curve, was found to be 6.22 μm; Dv (50), the median diameter, was 28.5 μm; Dv (90), which represents the particle size below which 90% of the particles fall, was calculated at 175 μm. Dv (100), representing the diameter at which all particles are smaller, was calculated as 567 μm.

It is important to mention that the processes of the scattering of the particles are not homogeneous, nor are the particles themselves spherical, which introduces a variability into the picture, increasing also the margin of error. This variability may cause variations in the laser diffraction data. In addition, elongated particles, longer than 250 microns can pass through the apertures of the sieve and then, explain the small fraction of particles bigger than the sieve opening size. Nevertheless, the granulometry analysis still gives insight regarding the potential of the biochar to be utilized as a matrix material within the cement. The main objective is to enhance the flowability and workability of the mixture by achieving an equivalent particle size distribution among the dry components. This uniformity facilitates the processing, allowing smooth incorporation into the final product.

MORTAR MIXTURE PREPARATION:

When sieving of biochar and sand to 250 μm was achieved, the development of the mortar mixture design began. The goal of this phase was to create a mortar mix that not only met the targeted mechanical properties but also performed well firstly under conditions simulating the 3D printing process so that less material was wasted making small mixture samples in this process before making the 500g mixture needed to use the 3D printing machine.

The initial mixtures settled a starting point for the mix design from a base formula applying a traditional 3:1 sand-cement ratio. This classic ratio is widely used in mortar preparation, providing a good balance of workability and strength. Additionally, a 0.4 water-cement (w/c) ratio was used in the initial trials. This ratio aimed to maintain adequate fluidity in the mixture so that it could pass through the 3D printing equipment without compromising the structural integrity of the paste. This ratio is critical for ensuring the right consistency, hydration, and binding of the cement paste. And finally adding 5% biochar replacement level of cement as previously stated, providing a reliable basis for evaluating the mechanical and environmental performance of biochar incorporation to mortar.

Moving on to the preparation of the mortar mixture, precise and consistent repetitive steps were required to ensure that the components were fully integrated and homogeneous. This was a main factor given the experimental nature of the biochar-cement replacement and the addition of

admixtures such as superplasticizers and polyethylene glycols (PEGs). The use of a mechanical mixer was essential in achieving a high-quality and uniform mixture in order to achieve consistent distribution of biochar throughout the cement matrix[267], and more stable paste with fewer air pockets, enhancing the material's cohesion and contributing to its suitability for the extrusion process during 3D printing.

The preparation of the mortar mixture started with the precise weighing of all individual components, a critical step to accuracy and consistency in the formulation. Each material, including cement, aggregates, water, and any additional admixtures such as biochar or polyethylene glycol (PEG), was measured using calibrated equipment to minimize deviations from the target mix proportions. This meticulous process is done to maintain the integrity of the mixture, as even slight variations in component quantities can significantly affect the physical and mechanical properties of the final product. By carefully controlling the proportions of each constituent, the desired workability, strength, and durability characteristics of the cementitious composite can be reliably achieved. Moreover, this approach ensures repeatability and reproducibility in experimental trials.

Image 16 Sand and mortar were already weighed, and biochar weighting is being carried out. Source: (Author)

When all the components were correctly weighed the mixture began by mixing the dry ingredients to ensure a rigorous combination of cement, biochar and sand as the solid agents of the mixture in a mechanical mixer. This provided a consistency in material blending to achieve the desired physical and chemical interactions between the materials and allowing the cement particles to adhere uniformly to the biochar and sand, ensuring that the subsequent addition of liquid components to the mixture would not lead to clumping or uneven distribution.

After the dry components were uniformly mixed the gradual addition of the liquid components started. The water, superplasticizers (Mapei Dynamoon SP1), and PEGs (with different molecular weights: 600, and 10,000) were introduced slowly into the dry paste. This step was done maintaining the mixer running at a low speed while adding the liquid components by stages to maintain control over the paste's consistency and to prevent the formation of lumps or segregation of materials and ensuring the dry paste to moist evenly. This slow addition allowed the cement to begin its hydration process uniformly while integrating the biochar particles seamlessly.

[267] Critical for maintaining the intended mechanical properties and environmental performance of the final material

In the same way with a gradual incorporation of the superplasticizers and the PEG into the mixture, adding these admixtures in small increments to avoid over-saturation, and ensuring the full homogeneity with the other mixture components. The addition of the admixtures was slowly and in stages to monitor the paste change in viscosity and carried out over several minutes while observing the paste's consistency, ensuring that the mixture maintained a homogeneous texture without becoming overly thick or too fluid, allowed for precise adjustments in paste fluidity and viscosity, minimizing the risk of segregation or improper hydration.

Image 17. mechanical mixture of all mortar mix design constituents.
Source: (Author)

The implementation of a trial-and-error method development was essential to ensure a suitable mix design, this repetitive approach focused on optimizing the physical properties of the mortar for 3D printing. Various parameters were adjusted based on the performance of each mix after subjecting each of the previous mixtures to a manual impression test using a 5mm syringe. This test was done as a preliminary simulation of the 3D printing process, to understand the paste's behavior during the impression test, providing insights into its suitability for extrusion and the changes that needed to be made for the upcoming mixtures.

During this simulation impression tests key factors were observed which gave insight and guidelines into the variations that needed to be made. fractures in the paste such as cracking or breaking of the paste indicated inadequate cohesion or low water content. Separation of materials, segregation between sand, cement, and biochar occurred, indicated that the mix lacked sufficient binding or had an inappropriate water-cement ratio. Water drainage due to water excess runoff indicated an overly high water-cement ratio, affecting the paste's strength and stability. This trial-and-error method took place until a formula was established that met the requirements for 3D printing, demonstrating good printability as the paste was able to maintain its shape after extrusion, with minimal sagging or deformation, with a consistent texture without segregation of materials, and an adequate viscosity allowing the extrusion through a 5mm syringe without clogging.

Image18 Simulation of the 3D printer extrusion with a 5mm syringe.
Source: (Author)

Image19 Mortar paste after undergoing the syringe test without success as it lacked workability.
Source: (Author)

In addition to the syringe test which focused on mechanical and flowability assessments to simulate the 3Dprinting extrusion, during the trial-and-error phase other manual test were conducted. The physical properties of the mortar paste gave an understanding of the paste's behavior under conditions like those experiences after 3D printing. Ensuring that the mixture possessed the right rheological characteristics essential for guaranteeing the mortar's stability and structural integrity when extruded.

The moldability and physical behavior was evaluated by shaping small squares from the paste. This was done to verify if the paste exhibited plasticine[268] properties, indicating a successful paste as one that could be molded into a square without sticking to the gloves, indicating appropriate consistency and workability. Excessive stickiness would suggest too high a water content or insufficient cohesion, both undesirable for 3D printing.

[268] Malleable enough to be easily shaped by hand yet firm enough to retain its form once molded.

Image 21 Moldability and physical behavior test results of various mortar mix designs. Source: (Author)

Once molded, the small squares were left to rest for a short period to observe the paste's ability to maintain its shape and structural integrity. This square was monitored to identify if it could maintain uniformity without showing any signs of deformation, slumping or collapsing. A stable mixture would indicate that the paste possessed sufficient internal cohesion and viscosity, critical for layer adhesion during 3D printing and post extrusion performance.

This overtime test also looked for any sweating, meaning that the mortar began to exude water, indicating a poor mix balance, typically too much water or insufficient binding due to inadequate hydration. Cracking was another criterion being evaluated as any visible surface cracks that developed during this period might indicate issues with the paste's drying behavior, shrinkage potential, or insufficient cohesion between the binder (cement) and biochar, which could result in structural weaknesses during or after printing.

Image 22 Syringe and moldability - physical behavior mortar mixture design test results.
Source: (Author)

Image 23 Syringe test physical behavior results showing the evolution and variation of the mortars workability by creating different mis design formulations.
Source: (Author)

Image 23 Moldability test physical behavior results showing the evolution and variation of the mortars workability by creating different mis design formulations.
Source: (Author)

According to the behavior observed during each test, several variables were modified and adjusted in the mixed composition, including the water content, sand-cement ratio, and superplasticizers and PEGs implementation. Trials were conducted repeatedly to optimize flowability, cohesiveness, and overall performance. Providing valuable insights into how the cementitious paste would behave under real 3D printing conditions, this allowed for early identification of potential issues related to drying, shape retention, and surface quality, comprehension of structural stability in the way the paste would settle and solidify, and enhanced mixture refinement on the mixture's physical characteristics.

After numerous adjustments and trials, a suitable mixture design was identified that met the criteria for effective 3D printing. The final formula maintained the 0.95:1 sand-cement ratio and a modified water-cement ratio of 0.38 that provided optimal workability. The paste's behavior during syringe extrusion was stable, indicating a successful balance of the components. In the context of admixtures, the chemical interaction between the superplasticizers and the biochar resulted in segregation within the mixture, leading to a distinct separation between the wet and dry components. This incompatibility necessitated the exclusion of the superplasticizers from the formulation. Conversely, for the incorporation of polyethylene glycol, a PEG with a molecular weight of 10,000 was applied in the mixture, different dosages were tried with different quantities

applied in respect to cement. The final dosage was carefully controlled, with 2 grams of PEG added for every 10 grams of cement. All the above ensured optimal integration of the component into the cementitious matrix to later be printed in 3D.

3D PRINTING software

With a reliable mixture design in place, the next phase involved conducting real 3D printing trials with the implementation of the finalized mixture design prepared in larger quantities (min 500grams). The paste was loaded into the WASP 2040 printer's feed system, where it underwent a series of preliminary extrusion tests to calibrate the machine parameters, such as print speed, nozzle size, and layer height. These extrusion tests looked for the correct printing parameters evaluating the extrudability, buildability, and stability of the mixture. Extrudability focused on the mixture's ability to flow smoothly through the printer's nozzle without clogging or causing pressure fluctuations. Buildability assures the ability of printed layers to maintain structural integrity without collapsing or merging into each other, and correct layer adhesion to guarantee uniform bonding between successive layers. Finally, stability of the printed structure, assure the ability to retain the designed geometry without deformation.

The file preparation stage is crucial to ensuring the success of 3D printing experiments, especially when dealing with unconventional materials like biochar-cement composites like precision, material behavior when altering parameters such as extrusion width, nozzle diameter, and speed allowing the software to compensate for the unique behavior of the biochar-enhanced paste, which behaves differently than conventional mortar or typical 3D printing materials like PLA. Consistency is obtained by modifying the extrusion and layer height parameters.

For a correct 3D printing process to take place a precise file preparation was required to certify accurate and consistent construction of the mortar samples. This stage involved using CAD software to design the printing model, followed by the setup of Simply3D slicing software to adjust printing parameters suitable for the experimental material. The process began with the creation of a 3D model of the desired sample using AutoCAD software. A simple rectangular block with dimensions of 2x2x8cm was designed for an easy evaluation of the material's mechanical properties. After designed the model was saved in a 3D format to ensure compatibility with the 3D printing software, exporting the finalized design as an .STL[269] file.

Subsequently, the file was introduced into Simply3D slicing software utilized for setting up the 3D printing parameters. This software is widely used for its flexibility in handling various printing materials and adjusting printing specifications. Firstly, the units of measurement were confirmed to be in millimeters, ensuring that the software's scale matched the design specifications and preventing any dimensional discrepancies during printing. Once the file was imported, the next step involved a setting adjustment process configuring the settings to match the specifications of the experiment and correct parameters regarding the final formula mix design and the 3D printer that was going to be used. This required accessing the Edit Process Settings menu, where several key parameters were adjusted for the optimal performance of the mortar mixture:

Extruder Tab setting of Nozzle Diameter was adjusted according to the specific setup of the WASP2040 3D printer. This parameter is crucial because it dictates the thickness of the extruded layers, influencing both the printing resolution and the flow requirements of the paste. Extrusion

[269] A standard file format for 3D printing.

width was also set to match the nozzle size, ensuring a consistent and precise application of the mortar. This adjustment helps control the consistency of the layer adhesion and surface finish.

Modifications in the Layer Tab were made to the Primary Layer Height setting to achieve a balance between printing speed and structural fidelity, as layer height can increase resolution but requires a more stable and well-formulated paste. Another altered setting was Outline/Perimeter Shells: The number of perimeter shells was adjusted to define the wall thickness of the printed sample ensuring that the samples would have adequate structural integrity during testing.

From the Additions Tab Skirt Layers was the only changed parameter, increased to 2 layers, which helps stabilize the extrusion by priming the nozzle and ensuring a smooth flow before starting the actual print. This adjustment reduced gaps or under-extrusion in the early stages of the print.

In the Infill Tab, the alteration of the Infill Pattern, internal and external, was donde based on the specific testing requirements. A rectilinear pattern was selected for both the external and internal layers to ensure surface smoothness.

Additionally in the Speeds Tab, the Default Printing Speed was adjusted to account for the properties of the biochar-cementitious paste, which requires a slower speed than typical plastic filaments to ensure consistent extrusion without clogging or interruptions.

Finally in the Advanced Tab Extrusion Length and Printing Width were critical parameters for the stability of the printed structure. The extrusion length was carefully calibrated to ensure that the paste flow matched the intended design, preventing over- or under-extrusion. The printing width was adjusted to ensure maximum bonding strength and minimal gaps between layers.

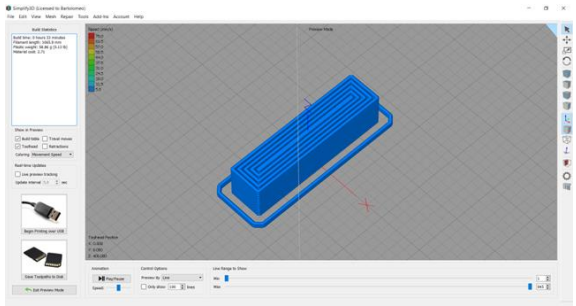

Image 25 Simply 3D slicing software parameterized document.
Source: (Author)

In this stage of the process the trial-and-error method was reintroduced into the experiment as different printing tests were made considering the internal infill patterns offset, printing speed, and nozzle size, for which different printing files were made alternating these variables. Once all parameters were configurated, the file was exported from Simplify3D in the format required by the WASP2040 3D printer.

3D PRINTING process

The preparation and execution of the 3D printing trials required detailed setup and calibration of the Delta Wasp 2040 Clay 3D printer, a machine specifically designed to handle dense and fluid materials. The following steps outline the installation, calibration, and operation procedures necessary to ensure accurate and consistent printing of the biochar-cementitious mortar samples.

The printer Installation and Extruder Setup is divided into seven different phases:

Starting with the Installation of the Extruder, from this procedure start with the printer turned off, for the extruder to be manually positioned on the printer's extrusion frame, and securely attached using two locking screws, to obtaining a correct leveling and fixation. The extruder needs to be then connected to the printer's main wiring system, ensuring a proper linkage between power and control signals.

Continuing with the preparation of the material tank, due to the small size of the samples (2x2x8 cm), the mortar mixture preparation quantity was not big enough to use the big aluminum tank that has its own structure which permits it to be clamped directly to the machine. That is why the small aluminum tank was selected to hold the mortar mixture, forcing the creation of a separate external structure to be able to support this tank conformed from a ring stand and a clamp. The tank setup began by inserting the piston into the cylinder of the aluminum tank to create an airtight chamber, that allows the insertion of pressure to the tanks to cause the extrusion of the material. The biochar-cementitious mixture was divided into manageable portions, forming small clay-like balls, which were then carefully inserted one by one into the tank, and compressed manually to remove as many air bubbles as possible, minimizing the risk of air pockets disrupting the extrusion during the printing process.

After the material was placed in the tank the following step consisted in sealing and connecting it. Once the tank was filled, the placement of the two aluminum caps needs to be secured, being very careful with the placement knowing that one cap connected the tank to the pressure manometer and a compressed air line from the compressor (placed in the side where the piston is visible), while the other linked it to the printer's extruder system (placed in the side were the mortar mixture is visible).

Image 26 Aluminum tank filling process.
Source: (Author)

Image 27 Aluminum tank caps and pressure piston.
Source: (Author)

The sealed tank is then positioned on the left side of the machine, supported by a ring stand and clamp, ensuring stability during the printing operation. Before turning on the compressor, the pressure gauge needs to be in a closed position, verifying the pressure is set at 0 bar to avoid any sudden release. Subsequently, the tank was connected to the extruder, by means of the Teflon extrusion tube, which provides a stable and flexible pipe for the paste to move from the tank to the nozzle. After the setup is correctly performed, the printer is switched on, and the basic functionality check performance is done to confirm that all components are operational and correctly placed and connected.

Image 28 tank placement setup and connection to the pressure compression and the Teflon tube
Source: (Author).

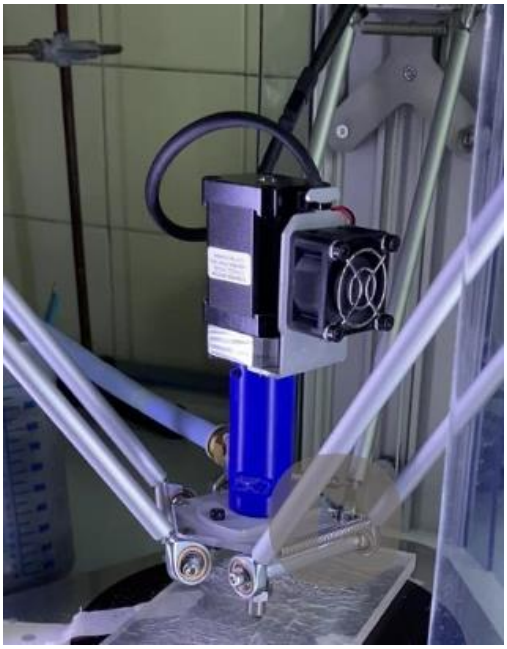

Image 29 Extruder placement setup and connection to the aluminum tank and the 3D printer.
Source: (Author)

Moving on to, the Calibration and Printing Setup process by Leveling and Setting the Z-Axis. The calibration begins by selecting the Auto Home function to position the printer's bed correctly and adjust the critical Z-value (the distance between the nozzle and the printing bed). For this to modify, the printer's knob is used to manually change the Z-value leaving a 0.5 mm gap between the nozzle tip and the bed, this precise distance is essential to maintain a proper layer adhesion and material flow. Once the correct distance is achieved, the Z-value can be saved in the printer's memory for consistent operation, remembering to repeat this process every time the height of the printing base changes.

Before printing, an initial extrusion is conducted to verify material flow, for this the Teflon tube needs to be temporarily disconnected from the extruder, starting to slowly increase the pressure from the compressor until a steady flow of the material is achieved. A recommended printing pressure varies between 4-6 bars, even though for this specific experiment a big variation in pressure for all the samples was needed.

Image 30 Teflon tube mixture fluidity test.
Source: (Author)

Once a consistent flow is verified, the tube should be reconnected to the extruder, and a second test performed with the extruder engaged, ensuring the materials correct passage through the nozzle without blockages or drainage.

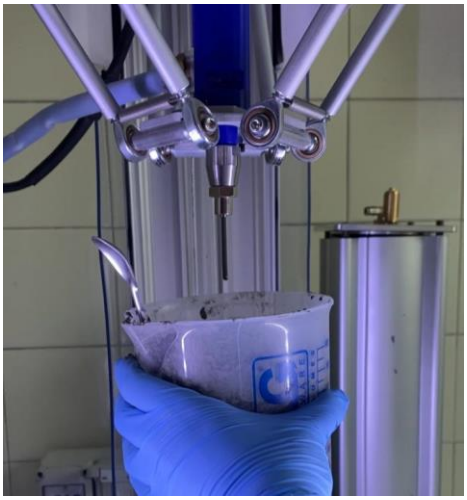

Image 31 Complete extrusion system, printing trial.
Source: (Author)

This test causes Material and Printing Test Adjustments made based on refining parameters such as the rheology, fluidity, and moldability of the mixture until the proper consistency is achieved. These refinements included modifications to the formula, nozzle size, and printing parameters. Initially for this specific experiment, a 3 mm nozzle was used, but after successful calibration, a 2 mm nozzle was adopted for a more optimal and detailed definition. Attempts with a 1.5 mm nozzle were unsuccessful due to frequent blockages, that led to no successful printed samples.

For the 3D Printing Execution process:

Preparation of the previously finalized Printing Files is involved, saved as a .gcode format, and loaded onto a SD card, inserted the SD card into the printer. This file includes all pre-determined parameters and paths necessary for printing the test samples. Select the file from the printer's interface, go to auto home, extrude, SD card and select the file, after this the printing process will begin automatically.

Once the printing starts place a close attention to the initial layer monitoring is requested, as these are crucial for guaranteeing overall structural stability. While printing issues such as layer separation, excessive extrusion, or material drainage can be monitored, real time adjustments can be made using the printer's control interface. The printer allows material flow adjustments either by increasing or decreasing the percentage of extrusion through the printer's settings, ensuring consistent layer deposition and preventing defects.

Once the printer reaches the final layer, the sample needs to be carefully removed from the print bed and set aside for curing. Each test print required precise timing and monitoring to ensure no disruptions occurred during the layering process.

For this specific experiment throughout the printing process a series of adjustments were conducted based on observations from the extrusion tests, including material composition alterations to the cement-water ratio and the PEG change were performed to optimize the paste's characteristics. Also, the printing p arameters suffered alterations until the 2 mm nozzle was standardized for reliable performance. After validating the correct printing parameters, optimizations allowed for smooth extrusion and consistent layer adhesion and achieving successful prints, three types of samples were produced with varying w/c ratios (0.38, 0.36, and 0.40) to collect comparative data on the material's performance and analyze the impact of water content on the biochar-cement mixture's physical and mechanical properties.

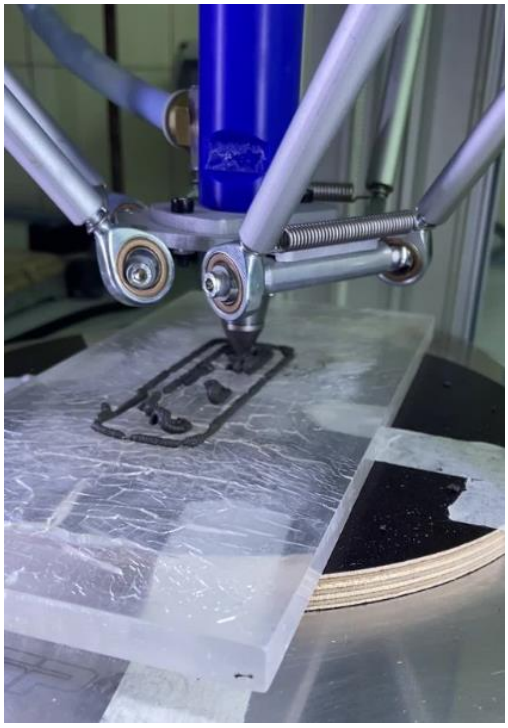

Image 32 3D printer, first printing layer problems due to nozzle blockage.
Source: (Author).

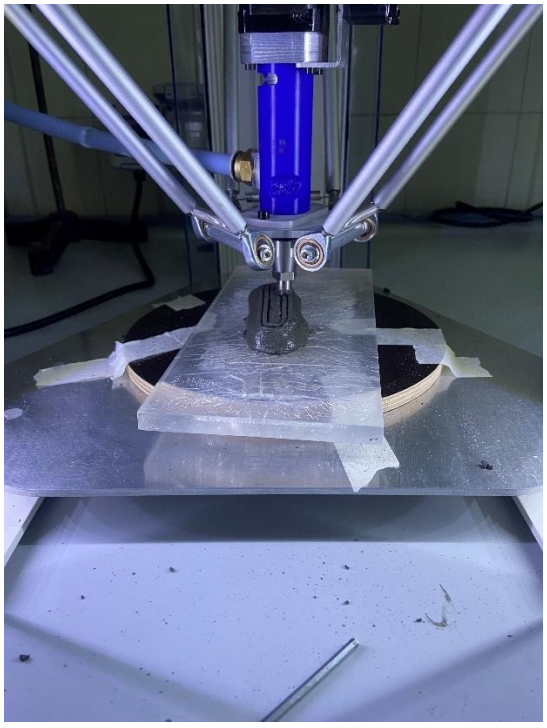

Image 33 3D printer, first trials with a 0.45 w/c ratio.
Source: (Author).

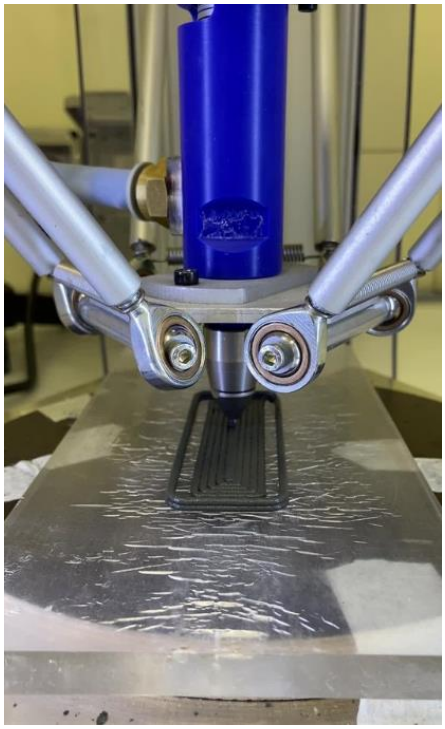

Image 34 3D printer, sample trial with a 0.38 w/c ratio.
Source: (Author).

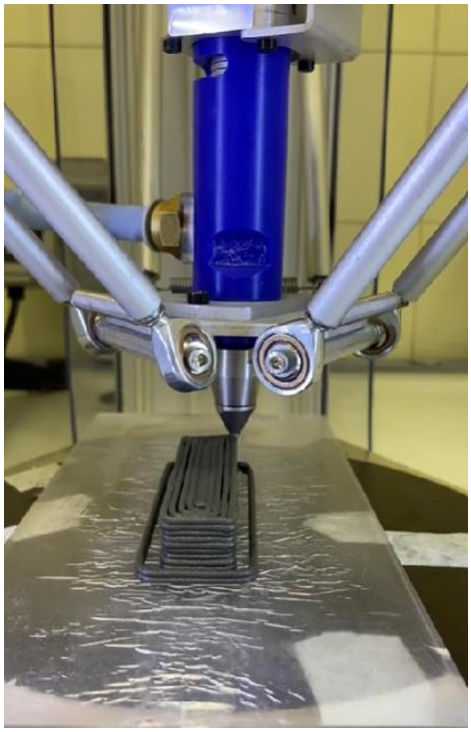

Image 35 3D printer, while printing a sample last layer.
Source: (Author).

TRADITIONAL CASTING SAMPLES

In addition to the 3D printed samples, a series of traditional cast mortar samples were made. This comparative study in this research was crucial to evaluate the impact of biochar on the performance of the mortar when using different preparation techniques like 3D printing and conventional casting. The following section describes the methodology for the preparation of the traditional cast samples.

In the preparation of traditional cast mortar samples to ensure consistency the dimensions of the cast samples were chosen to match those of the 3D-printed ones 2x2x8 cm. This allowed for direct comparison of mechanical properties and performance under identical conditions. Rectangular molds with these dimensions are implemented, made from durable plastic to facilitate easy demolding and to withstand the pressure exerted during casting. Before filling the mold with the mortar mixture, the molds need to be thoroughly cleaned and treated with a mold release agent to prevent adhesion of the mortar, ensuring clean extraction after curing. From this point the casting process starts.

Image 36 Traditional cast mold setup.
Source: (Author)

To establish a reliable comparison between the printed and traditional samples the molds are cast with the same paste used in the 3D printing. To minimize the formation of air pockets, the mortar was introduced in small increments, gently tapping the sides of the molds after each addition to release any trapped air bubbles. The filling process is done with care to ensure even compaction throughout the mold, after the mold was filled in the top surface, it was then leveled using a spatula, to be sure that all samples present a consistent height and volume.

Traditional samples were done for all three types of w/c ratios (0.38, 0.36, and 0.40).

CURING PROCESS

After casting, and 3D printing, a consistent curing process is required to be applied to both the 3D-printed and traditionally cast samples to be sure a controlled and reliable comparison of the performance of biochar-enhanced mortars can be done. Proper curing is essential in cementitious materials, as it allows for full hydration of the cement particles, leading to the development of optimal mechanical properties.

The initial curing phase starts with setting and initial hardening, when the prepared samples are ready, a 24-hour phase in a saturated humid environment is set to all the 3D-printed and traditionally cast specimens, allowing the mortar to harden sufficiently for handling and removal from the molds without disturbing the material's structural integrity.

The 3D-printed samples remain on the printer bed for the initial 24 hours. During this time, they began to set and harden, gaining strength, crucial for the initial consolidation of the layers and ensuring no premature deformation occurs. In the same way the traditionally cast samples also remained in their molds during this period. The molds were kept in a humidity controlled environment at room temperature to maintain consistent initial curing conditions.

Image 37 24-hour hardening phase setup.
Source: (Author)

Unmolding process takes careful removal from molds both for 3D printing and traditional casting. For 3D-printed samples after 24 hours, a careful detachment from the print bed needs to be done. Due to the delicate nature of the early setting mortar, a gentle removal method is necessary by lightly hydrating the samples spraying a fine proportion of water onto the sides of the sample to ease detachment. After this, using a small spatula, a pressure was carefully applied between the sample and the print bed to gradually lift the edges without causing damage. This slow and meticulous process ensured that the layers remained intact, and the sample shape was preserved.

Image 38 Unmolding process of 3D printed samples.
Source: (Author)

On the other hand, for traditional cast samples the unmolding process is much easier by removing the clamps that secured the molds, and then gently disassembling each mold, releasing the samples without applying stress to the early-stage mortar.

Once free, the samples were inspected and submerging into a 28-day curing process. This water curing procedure for both sets of samples consisted in submerged all samples in water to initiate a full curing cycle of 28 days, which is a standard curing period to assure the development of optimal strength and durability in cementitious materials.

The steps to follow for water curing are placing all samples in a controlled airtight container filled with sufficient water to completely submerge each sample, ensuring even hydration across the entire surface area. The containers demand to be kept in a controlled room temperature

environment, approximately 23°C, to avoid any fluctuations that could influence the hydration rate, to then start the post curing phase.

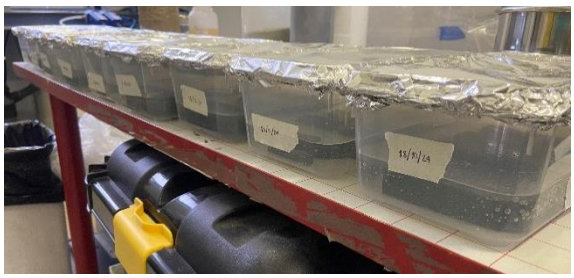

Image 39 28-day mortar sample hydration.
Source: (Author)

After the 28-day curing period, the samples start the final sample preparation for testing by removing them from the containers. 3D-printed samples: Once removed from the water, the 3D-printed samples were handled with care to avoid surface damage, considering the precision required in analyzing layer integrity. In the same way traditional cast samples are similarly taken out of the containers, with attention paid to any signs of surface swelling or cracks.

Finally, the drying process of all samples starts allowing air to dry in a controlled indoor environment after the excess water is gently wiped off the surface with a cloth, once dry, the samples were labeled and cataloged according to their fabrication method (3D-printed or traditional) and mix design parameters for identification during testing. This process ensured the correct sample development to further be mechanically tested.

Image 40 Samples drying process.
Source: (Author)

Image 41 Drying Process of all samples after currying process.
Source: (Author)

Curing was a critical phase in experimental methodology because it significantly influences the final properties of cement-based materials. Proper curing ensures that the chemical reactions within the cement matrix, particularly the hydration process, reached completion. This affects key characteristics such as compression strength, durability, and consistency.

In compressive strength an adequate curing leads to full development of the internal microstructure, crucial for bearing loads. In durability, water curing helps reduce the risk of cracking and shrinkage, making the material more resistant to environmental stress. Consistency is obtained from using the same curing methodology for both 3D-printed and traditional samples allowed for a direct and reliable comparison, isolating the effects of the fabrication method and the biochar content on the mortar's performance.

MIXTURE DESIGN RESULTS

Test	w/c ratio	s/c ratio	% biochar	Superplasticizer (g)	PEG type (g/mol)	PEG amount [270] (g)
1	0.40	3:1	5	0.20	600	-
2	0.50	3:1	5	-	600	0.08
3	0.55	3:1	5	-	600	-
4	0.75	3:1	5	0.11	600	0.29
5	0.55	2.5:1	5	0.80	600	0.29
6	0.40	1.5:1	5	0.10	600	-
7	0.40	1.5:1	5	0.15	600	0.08
8	0.45	1.5:1	5	1.50	600	-
9	0.42	1.5:1	5	1.50	600	-
10	0.45	1.5:1	5	0.12	600	0.08
11	0.47	1:1	5	0.15	600	0.29
12	0.50	1:1	5	-	600	0.70
13	0.50	1:1	5	-	600	7.00
14	0.54	1:1	5	-	600	7.00
15	0.52	0.95:1	5	-	600	7.00
16	0.48	0.94:1	5	-	600	7.00
17	0.48	0.95:1	5	-	4,000	7.00
18	0.45	0.95:1	5	-	4,000	7.00
19	0.45	0.95:1	5	-	4,000	1.50
20	0.40	0.95:1	5	-	4,000	1.50
21	0.42	0.95:1	5	-	4,000	1.50
22	0.45	0.95:1	5	-	4,000	1.50
23	0.42	0.95:1	5	-	4,000	1.50
24	0.35	0.95:1	5	-	4,000	1.50
25	0.35	0.95:1	5	-	10,000	1.50
26	0.35	0.95:1	5	-	10,000	2.00
27	0.38	0.95:1	5	-	4,000	2.00
28	0.35	0.95:1	5	-	10,000	1.75
29	0.38	0.95:1	5	-	10,000	1.75
30	0.45	0.95:1	5	-	10,000	2.00
31	0.43	0.95:1	5	-	10,000	2.00
32	0.42	0.95:1	5	-	109,000	2.00

[270] Δ g of peg for every 10 g of cement.

33	0.38	0.95:1	5	-	10,000	2.00
34	0.36	0.95:1	5	-	10,000	2.00
35	0.37	0.95:1	5	-	10,000	2.00
36	0.40	0.95:1	5	-	10,000	2.00

Table 19 Summary of the mortar mix design trials.

Table 19 above summarizes the various mortar mix design trials conducted throughout the experimental process, illustrating the chemical interactions and adjustments made based on the physical properties observed during testing. These trials were developed and refined through a systematic evaluation of the mixtures' performance, particularly after undergoing two key tests described in the Methodology section: the syringe test and the molded cube test. Each trial involved preparing a final sample weighing approximately 30 grams, allowing for consistent comparison across different formulations, and the mixture design sample to be enough to undergo both tests.

The table 19 highlights the progression of the experimental process, with specific tests marked in blue to indicate those that were selected for further testing in the 3D printing extrusion trials, also detailed in the Methodology section. For these tests, each trial involved preparing a final sample weighing approximately 250 grams so that the aluminum tank and piston could have enough material to operate correctly. These selected mixtures demonstrated sufficient stability and flow characteristics to be tested for their extrudability under 3D printing conditions. Adjustments made to the formulations were based on the observed physical properties and performance of the mixtures, including issues such as bleeding, segregation, dripping, workability, fluidity, and moisture retention.

The modifications in each trial considered the influence of additives and admixtures on the overall mixed behavior, ensuring that the mixtures achieved the necessary balance between mechanical performance and printability, highlighting the relationship between material properties and mix design, generating the need for continuous testing and adjusting so that the unique demands of innovative construction technologies such as 3D printing can be reached. This iterative process allowed for both the chemical composition and physical characteristics to be achieved, while optimizing the mortar for 3D printing applications and maintaining structural integrity and performance of the mortar.

Test	w/c ratio	s/c ratio	% biochar	PEG type (g/mol)	PEG amount [271] (g)
A	0.38	0.95:1	5	10,000	2.00
B	0.36	0.95:1	5	10,000	2.00
C	0.40	0.95:1	5	10,000	2.00

Table 20 Final Printed mortar mixture designs.

At the end of the experimental sample mixture design production, three primary mortar mix designs were obtained, showing suitable criteria for 3D printing. The implementation of variations in the three-mixture design enabled a comparative analysis of their chemical, physical, and mechanical properties generation reliability to the research results. These mix designs, as shown in the table above, were chosen to assess the impact of varying the aggregate-to-cement (w/c) ratio, as despite changes in the w/c ratio, the mixtures retained the necessary characteristics for extrusion and layer deposition. This ensured a successful printing process proceeding without interruption supported by the mixture's consistent rheological properties, granting workability and flowability, between other characteristics to achieve an effective 3D printing.

[271] Δ g of peg for every 10 g of cement.

However, attempts to alter other components of the mix design, such as the type or dosage of admixtures, resulted in significant performance issues that prevented 3D printing. When these variations were introduced, the mixtures exhibited undesirable properties, including clogging, excess moisture, stickiness, or dehydration, all of which compromised their ability to pass the extrusion tests outlined in the Methodology section. These failures demonstrated the delicate balance required between component proportions and rheological performance in 3D-printed mortar. Any deviation from this balance disrupted the extrusion process, preventing the mortar from flowing smoothly through the nozzle and adhering properly during layer deposition, findings that reinforce maintaining consistent rheological properties as crucial for achieving printability and structural integrity in additive manufacturing applications.

SOFTWARE APPLICATION

Two different G-code files were developed In Simply 3D Slicing Software for the 3D printing to take place and the mortar samples to be obtained for subsequent curing and mechanical testing. These files were specifically designed to control the 3D printer's movements and extrusion parameters, ensuring the production of consistent and uniform samples for flexural and compressive strength testing. The use of G-code allowed precise layer-by-layer deposition, ensuring that the printed samples met the geometric and dimensional requirements necessary for accurate mechanical evaluation.

Prior to printing, the software provided a digital simulation of the layer-by-layer printing process, allowing for a detailed visualization of how the printing parameters would affect the final product, offering valuable insights into potential issues, allowing identification of discrepancies or areas needing adjustment before transferring the file to the SD card for actual printing. By identifying potential problems before printing, the simulation process significantly reduced the risk of errors during the physical printing stage and minimized material waste, making 3D printing a cost-effective proactive process increasing the overall reliability of the experimental trials.

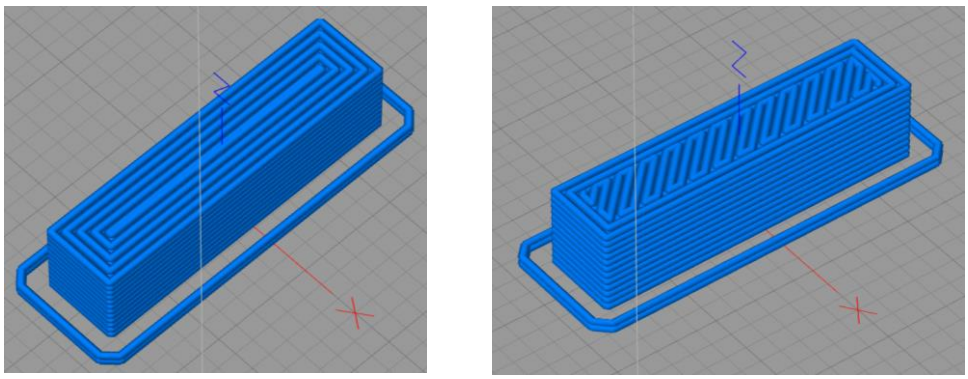

a b

Image 24 Simply 3D Slicing Software printing model with a different printing angle application in the infill.
Source: (Author)

Below are going to be presented all of the parameters measurements that were established to obtain a successful 3D printing process for both 3mm and 2mm nozzles applied.

3 mm nozzle parameters:

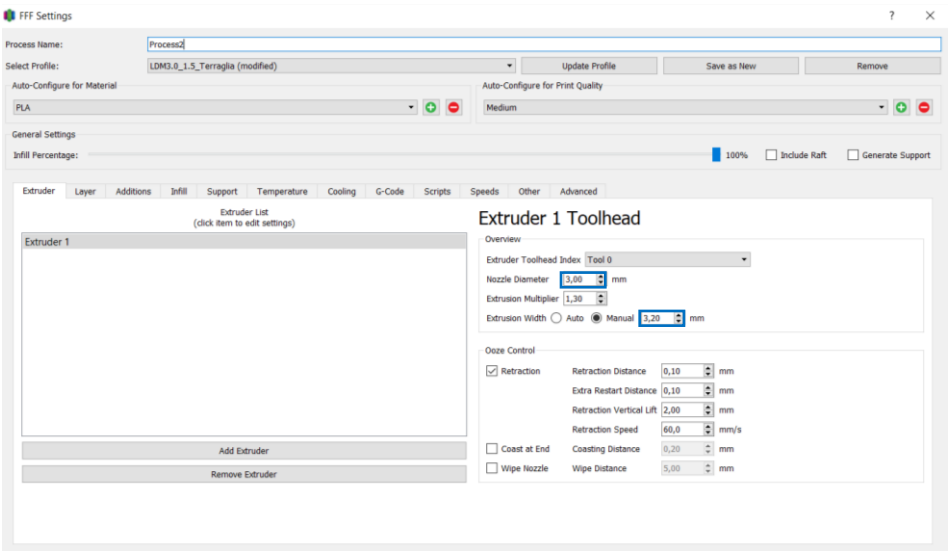

Figure 31 Simply 3D Slicing Software Extrude tab parameters (3mm nozzle).

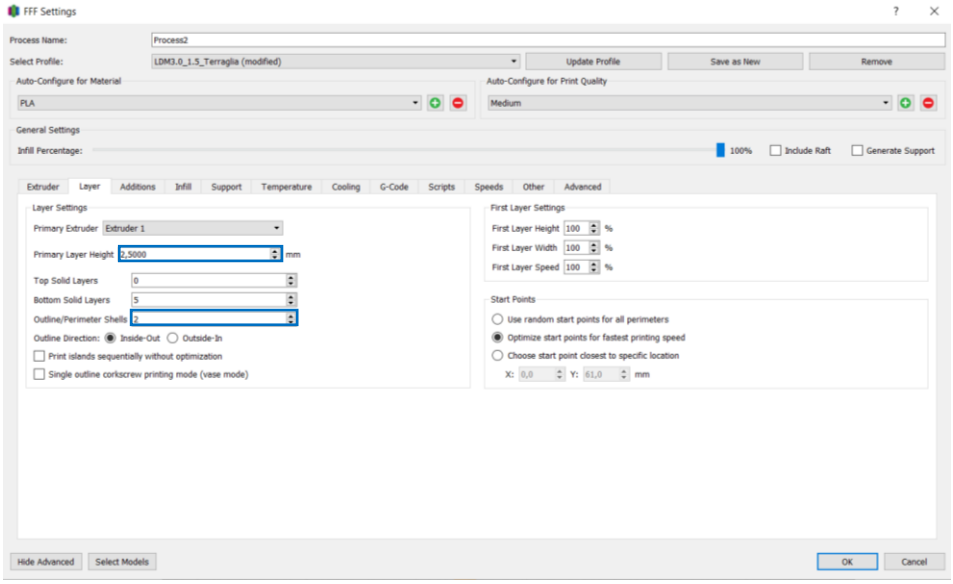

Figure 32 Simply 3D Slicing Software Layer tab parameters (3mm nozzle).

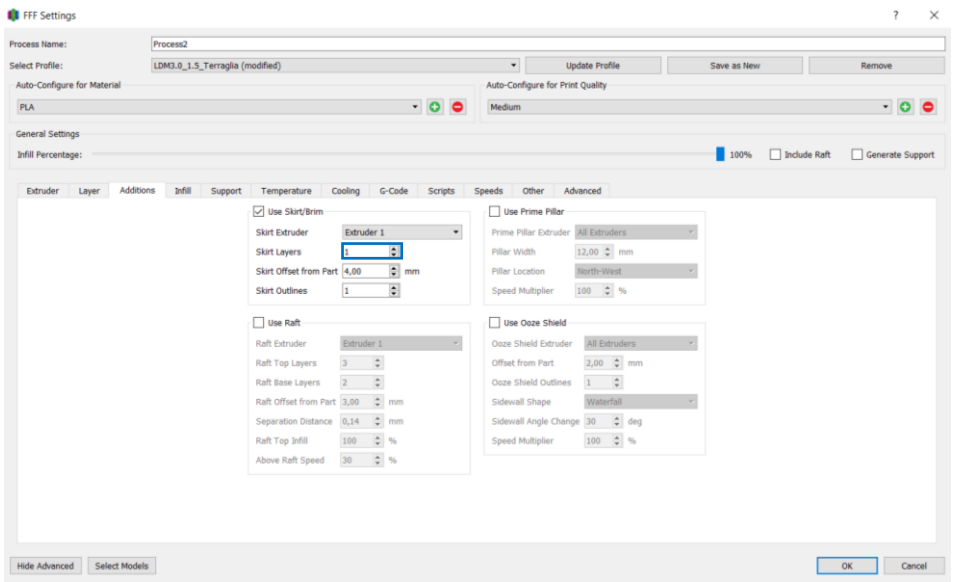

Figure 33 Simply 3D Slicing Software Additions tab parameters (3mm nozzle).

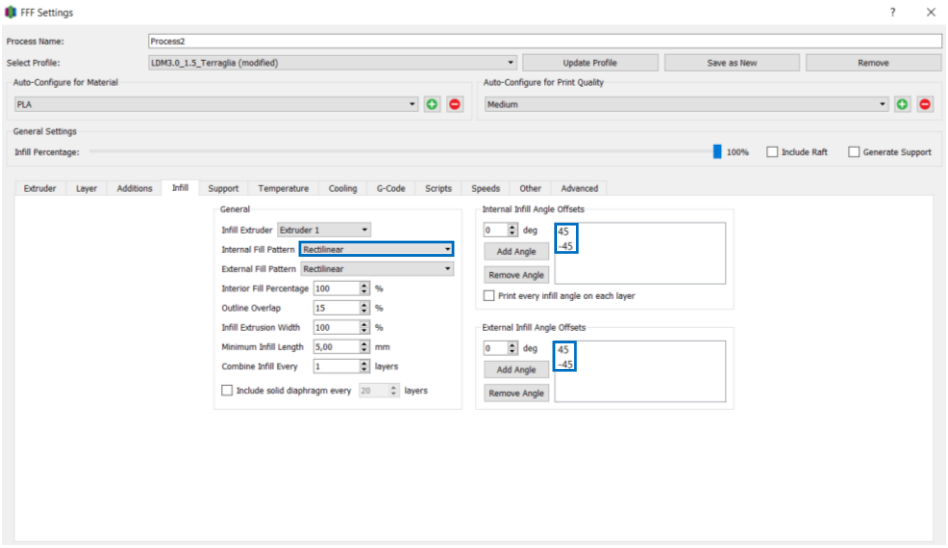

Figure 34 Simply 3D Slicing Software Infill tab parameters (3mm nozzle).

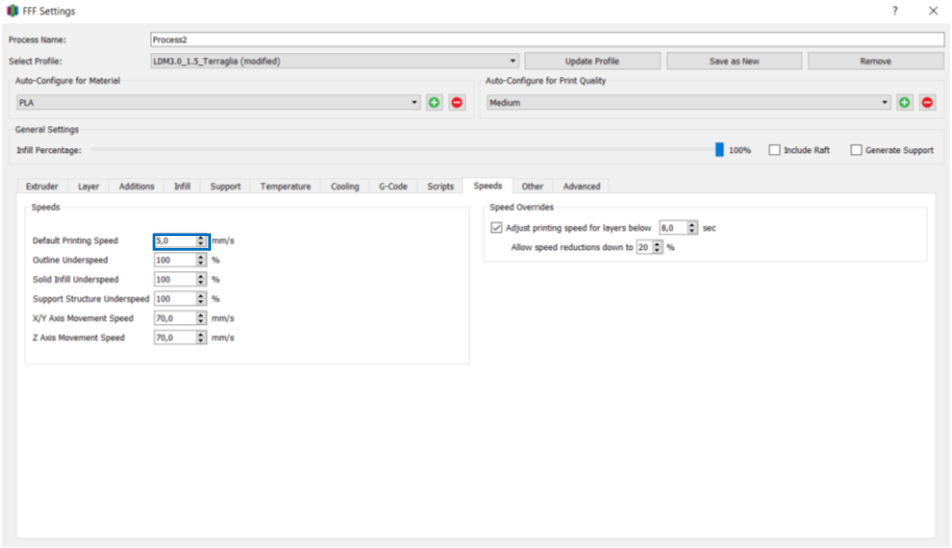

Figure 35 Simply 3D Slicing Software Speed tab parameters (3mm nozzle).

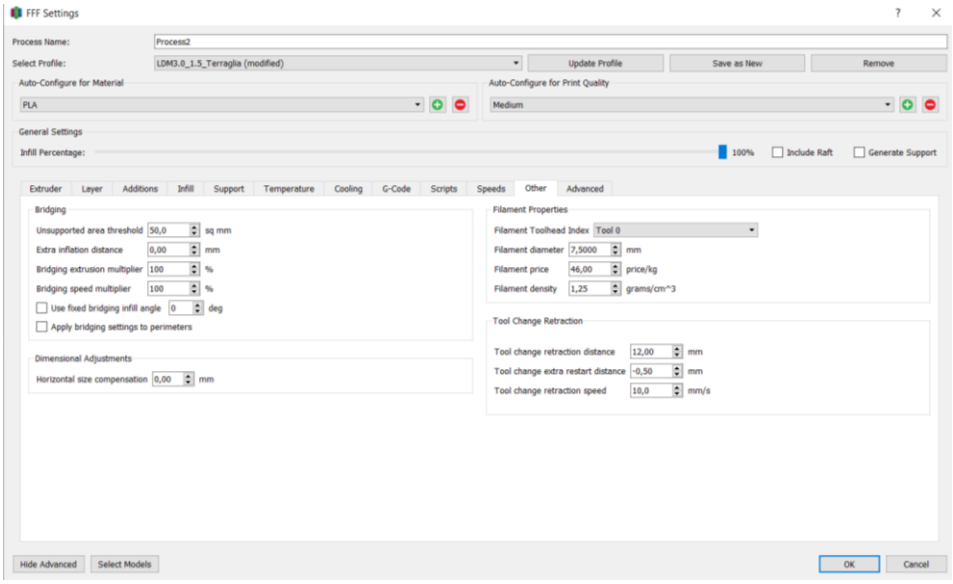

Figure 36 Simply 3D Slicing Software Other tab parameters (3mm nozzle).

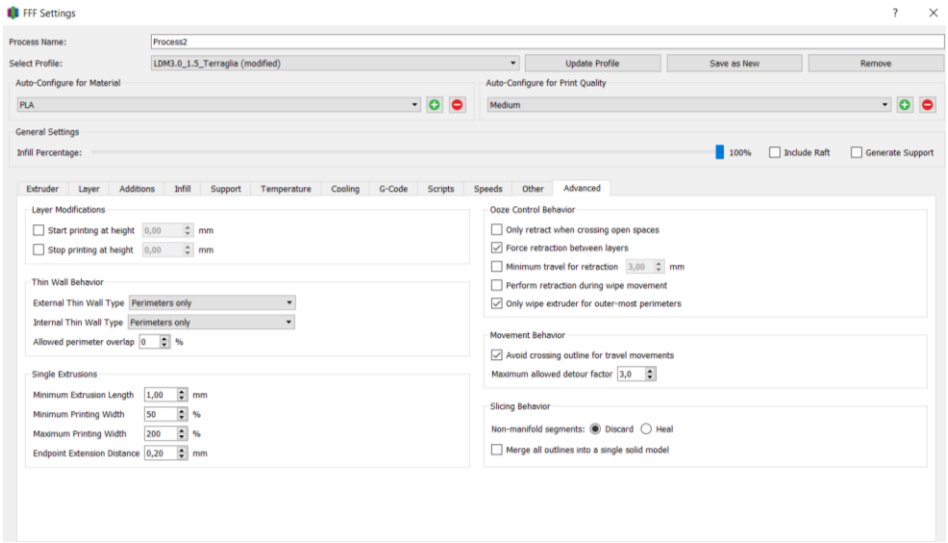

Figure 37 Simply 3D Slicing Software Advanced tab parameters (3mm nozzle).

2 mm nozzle parameters:

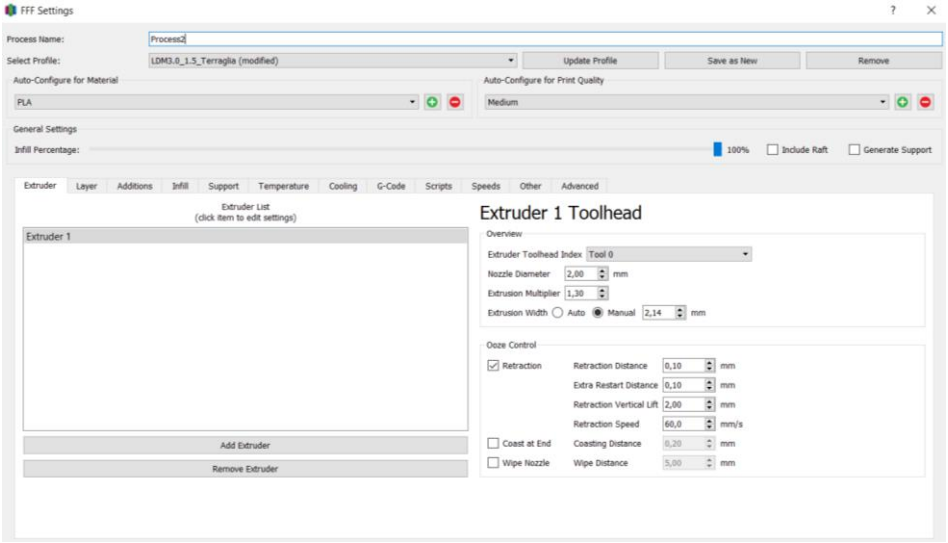

Figure 38 Simply 3D Slicing Software Extrude tab parameters (2mm nozzle).

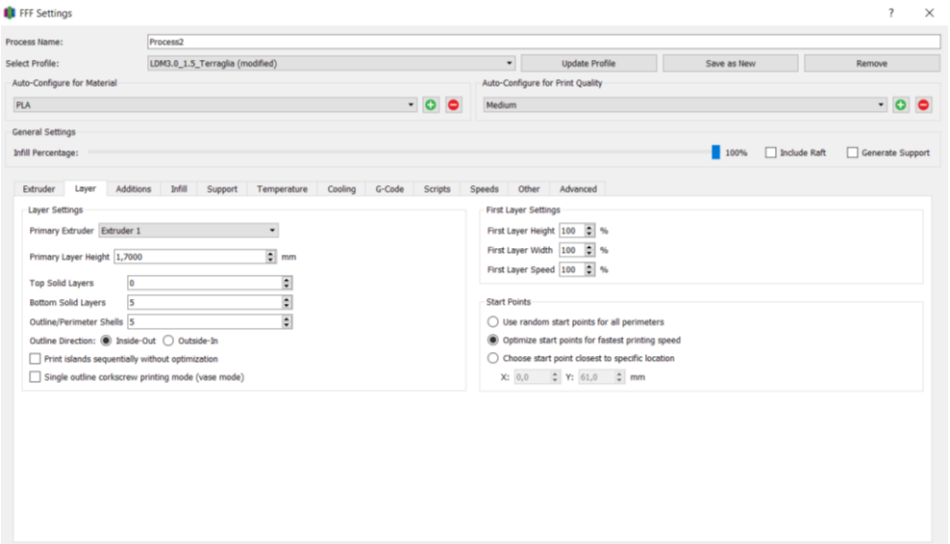

Figure 39 Simply 3D Slicing Software Layer tab parameters (2mm nozzle).

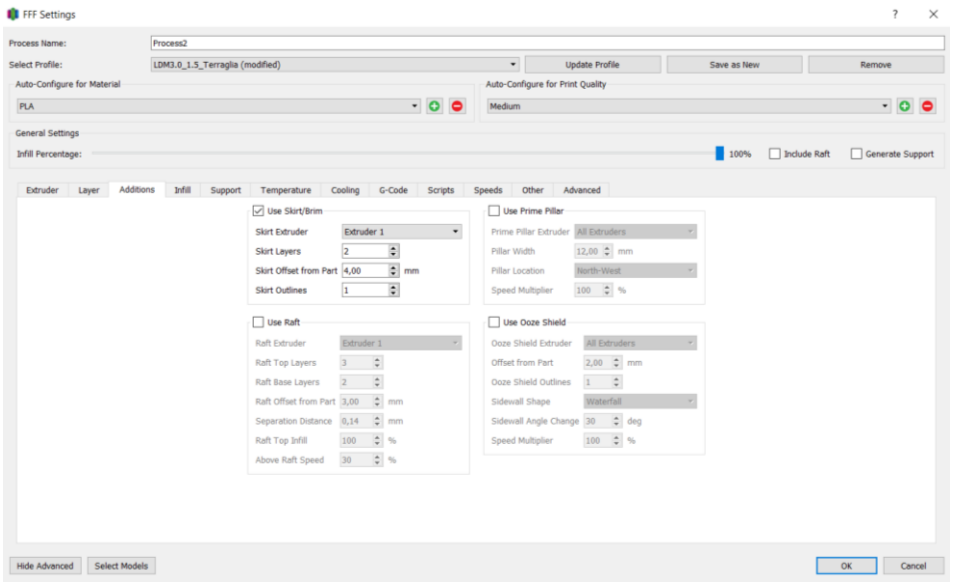

Figure 40 Simply 3D Slicing Software Additions tab parameters (2mm nozzle).

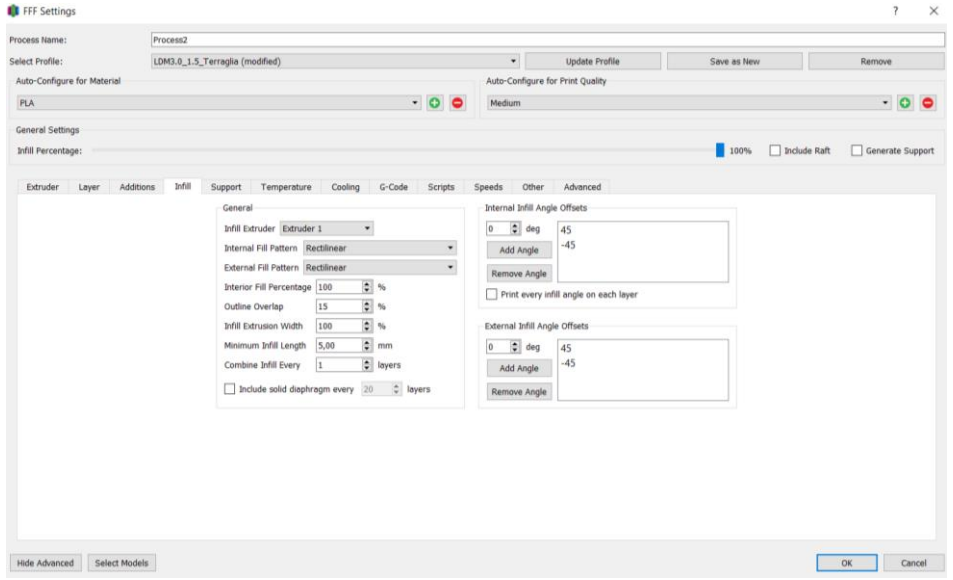

Figure 41 Simply 3D Slicing Software Infill tab parameters (2mm nozzle).

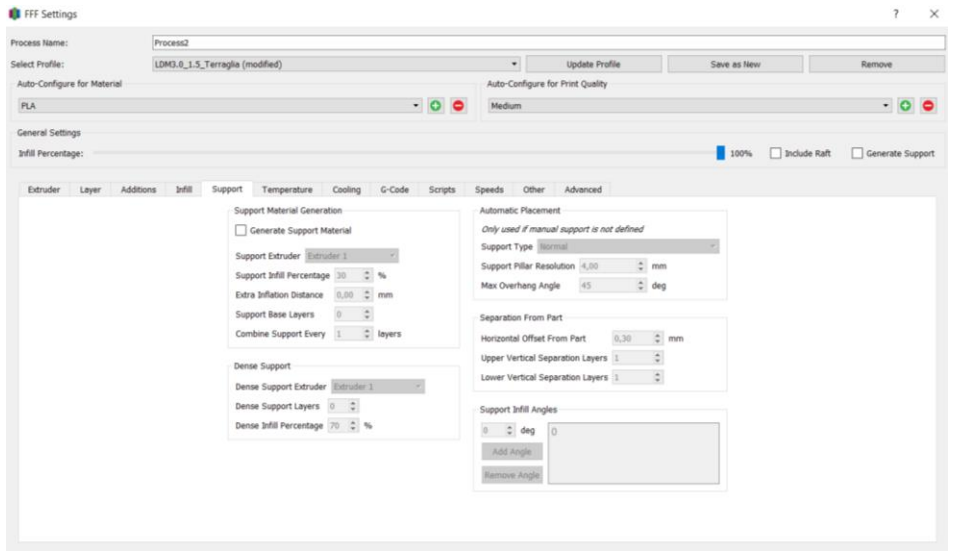

Figure 42 Simply 3D Slicing Software Support tab parameters (2mm nozzle).

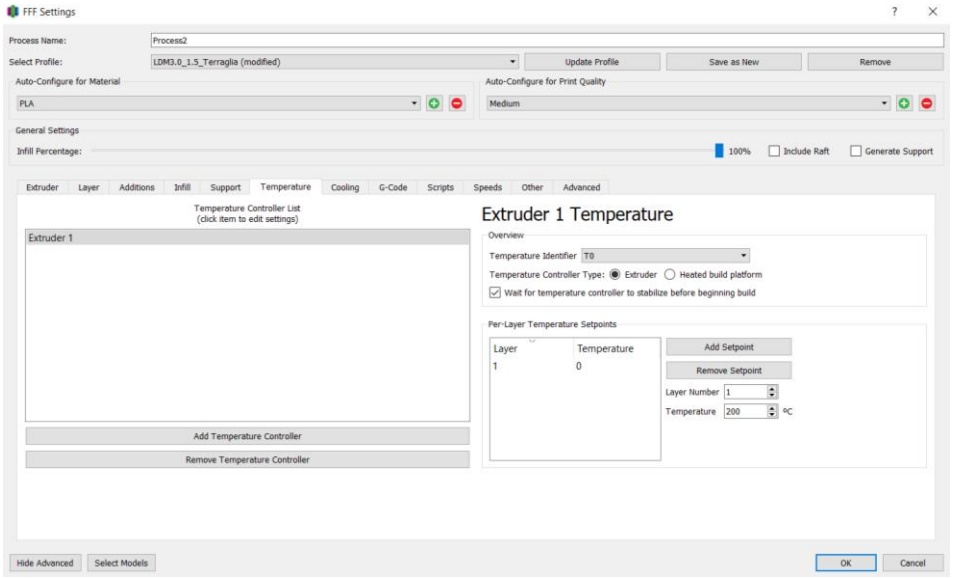

Figure 43 Simply 3D Slicing Software Temperature tab parameters (2mm nozzle).

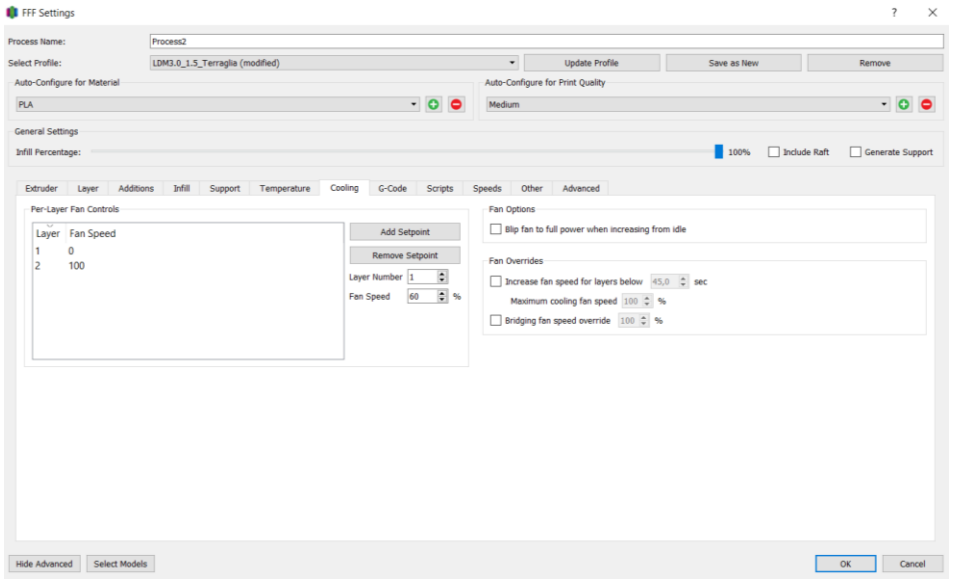

Figure 44 Simply 3D Slicing Software Cooling tab parameters (2mm nozzle).

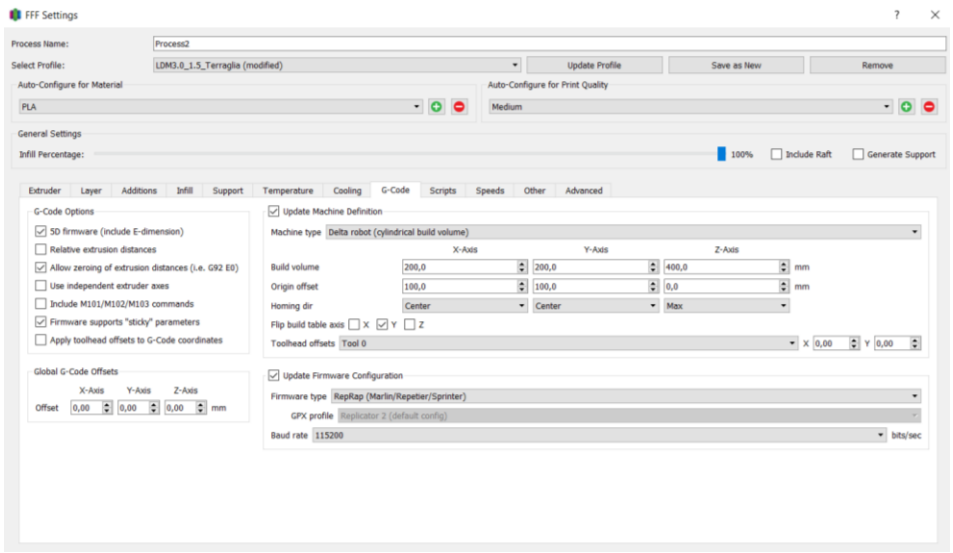

Figure 45 Simply 3D Slicing Software G-code tab parameters (2mm nozzle).

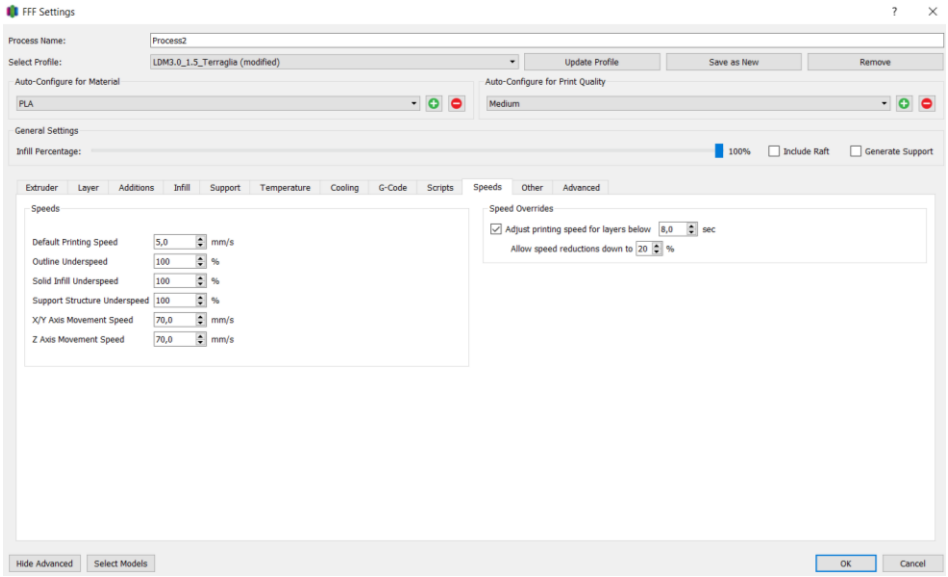

Figure 46 Simply 3D Slicing Software Speed tab parameters (2mm nozzle).

The parameters highlighted within the blue rectangular frames were identified as having the most significant impact on the printing properties and overall efficiency of the 3D printing process. These parameters were carefully analyzed and adjusted to optimize key factors such as extrusion consistency, layer adhesion, and print stability, resulting in 17 different printed samples, from which 6 samples printed using a 3 mm nozzle and 11 samples printed using a 2 mm nozzle.

SAMPLE CARACTERIZATION

In the following table, the results of these trials are meticulously documented for each sample, with its characterizations and printing parameters to ensure a comprehensive understanding of how each variable influenced the print quality and mechanical performance. Between these parameters we find the samples mix design type, extrusion pressure, printing speed, and Z-axis value relative to the printing bed. The Z-value was monitored to secure proper layer height and bond between layers, which are critical factors in maintaining structural integrity and achieving precise dimensional accuracy in the printed specimens.

This systematic approach to parameter optimization not only enhanced the efficiency of the 3D printing process but also ensured consistent output across varying nozzle sizes and mixed designs. By carefully controlling these parameters, the experiment minimized variability, allowing for a robust comparison of the samples' mechanical properties and providing valuable insights into the relationship between print settings and the structural performance of 3D-printed mortar.

Sample	Nozzle (mm)	Mix Design[272]	Pressure[273] (bar)	Printing speed (mm/s)	Z-axis value (mm)	Infill[274]
1	3	A	4.0	5	392.0	b
2	3	A	4.0	5	392.0	b
3	3	A	4.0	5	932.0	b
4	3	A	2.2	5	392.0	b
5	3	A	3.0	5	392.3	b
6	3	A	3.5	5	392.3	a
7	2	A	3.7	5	393.0	a
8	2	A	4.5	5	393.0	a
9	2	A	2.8	5	393.0	a
10	2	A	3.5	5	402.6	a
11	2	B	5.0	5	392.5	a
12	2	B	4.5	5	392.5	a
13	2	B	5.0	5	390.9	a
14	2	B	4.8	5	392.5	a
15	2	C	5.0	5	392	a
16	2	C	5.0	5	392	a
17	2	C	5.0	5	392	a

Table 21 Printed samples properties.

To ensure the generation of reliable data and enable meaningful comparisons and conclusions, traditionally cast samples were also prepared for each of the three mortar mix designs. These conventionally cast samples served as a benchmark against which the performance of the 3D-printed samples could be evaluated, providing a control group to assess any differences in mechanical, physical, and chemical properties resulting from the printing process. The results of the traditional samples will be categorized and presented in the table below, with each sample classified by its mix design type.

Sample	Mix Design[275]
18	A
19	A
20	A
21	B
22	B
23	B
24	C
25	C
26	C

Table 22 Traditional casting samples properties.

[272] Characterized in Table 19 Final Printed mortar mixture designs.

[273] Extrusion pressure exerted on the piston inside the aluminum tank

[274] Identified in Image 24 Simply 3D Slicing Software printing model with a different printing angle application in the infill.

[275] Characterized in Table 21 Final Printed mortar mixture designs.

After the samples were printed, they underwent a curing process to facilitate proper hydration and strength development prior to mechanical testing. This curing process was designed to follow a standard 28-day hydration period, which is widely recognized as the optimal timeframe for achieving the desired mechanical properties in cementitious materials[276]. Proper curing is critical for ensuring that the concrete or mortar reaches its full potential in terms of compressive and flexural strength, as it allows for the continued hydration of cement particles, reducing the risk of cracking and improving durability.

Traditionally cast samples were subjected to the same curing and testing protocols as the 3D-printed specimens, ensuring consistency in the evaluation of their flexural and compressive strength. This dual approach allows for a comprehensive understanding of the effectiveness of 3D printing as a construction technique in comparison to conventional casting, incorporating both 3D-printed and cast samples, the study was able to investigate the influence of the fabrication method on the final mechanical performance of the mortar.

Table 23 below organizes key dates related to the curing process, including the dates when each sample was printed, the initiation of curing, and the completion of the 28-day curing period. This timeline ensures that each sample receives consistent treatment, allowing for accurate and standardized comparisons of their mechanical performance. By maintaining a controlled curing environment and adhering to a strict curing schedule, the experiment aims to minimize variability and ensure that the mechanical testing results accurately reflect the influence of mix design and fabrication method on the strength and durability of the mortar samples.

Sample	Printing date	Initiation of curing	End of curing	Curing days
1	15/10/2024	17/10/2024	15/11/2024	29
2	15/10/2024	17/10/2024	15/11/2024	29
3	15/10/2024	17/10/2024	15/11/2024	29
4	17/10/2024	18/10/2024	15/11/2024	28
5	17/10/2024	18/10/2024	15/11/2024	28
6	17/10/2024	18/10/2024	15/11/2024	28
7	17/10/2024	18/10/2024	15/11/2024	28
8	17/10/2024	21/10/2024	15/11/2024	25
9	17/10/2024	21/10/2024	15/11/2024	25
10	18/10/2024	21/10/2024	15/11/2024	25
11	21/10/2024	22/10/2024	15/11/2024	25
12	21/10/2024	22/10/2024	15/11/2024	25
13	21/10/2024	22/10/2024	15/11/2024	25
14	21/10/2024	22/10/2024	15/11/2024	25
15	21/10/2024	22/10/2024	15/11/2024	25
16	21/10/2024	22/10/2024	15/11/2024	25
17	21/10/2024	22/10/2024	15/11/2024	25
18	17/10/2024	18/10/2024	15/11/2024	28
19	17/10/2024	18/10/2024	15/11/2024	28
20	17/10/2024	18/10/2024	15/11/2024	28
21	21/10/2024	22/10/2024	15/11/2024	25

[276] (Neville A. , 2011)

22	21/10/2024	22/10/2024	15/11/2024	25
23	21/10/2024	22/10/2024	15/11/2024	25
24	21/10/2024	22/10/2024	15/11/2024	25
25	21/10/2024	22/10/2024	15/11/2024	25
26	21/10/2024	22/10/2024	15/11/2024	25

Table 23 Samples curing days process.

Following the completion of the curing process, the samples were removed from the water and thoroughly dried to prepare them for the next stage of testing. A precise measurement process was then conducted, involving measuring each sample's weight and dimensions (length, width, and height). All measurements were conducted using a caliper to ensure precision. However, due to the heterogeneous nature of the samples, slight variations in dimensions were observed. To account for these inconsistencies, the width was measured at three distinct points along each sample. The average of these three measurements was then calculated and used for subsequent mechanical testing. This procedure was consistently applied to both width and length measurements to enhance the reliability of the data and ensure accurate assessment during the mechanical tests.

These measurements were essential for calculating key parameters used in the mechanical testing of the samples, specifically for flexural and compressive strength evaluations.

Sample	Weight (g)	Width (mm)	Hight (mm)	Length (mm)	Volume (m^3)	Density (g/ m^3)
1	71.44	24.13	18.40	82.65	36.70	1.95
2	73.65	20.68	25.29	82.11	42.94	1.72
3	78.35	26.63	20.07	84.70	45.27	1.72
4	52.32	19.30	20.33	79.79	31.31	1.67
5	61.02	19.35	23.06	81.37	36.31	1.68
6	75.16	21.94	22.45	81.97	40.37	1.86
7	61.94	19.91	21.42	81.00	34.54	1.79
8	69.39	24.76	19.75	81.89	40.04	1.73
9	56.06	19.70	21.60	80.74	34.36	1.63
10	71.25	23.13	19.05	83.54	36.81	1.94
11	43.39	20.45	17.35	79.79	28.31	1.53
12	90.13	28.53	21.57	84.82	52.19	1.73
13	52.33	20.52	20.70	80.52	34.27	1.53
14	52.19	19.30	20.77	80.41	32.28	1.62
15	67.66	23.74	18.98	82.43	37.14	1.82
16	68.02	19.86	22.53	83.03	37.15	1.83
17	62.08	19.25	23.56	81.23	36.84	1.69
18	78.03	23.52	20.82	80.70	39.52	1.97
19	77.71	23.95	20.72	80.23	39.82	1.95
20	78.58	23.65	20.71	80.31	44.23	1.78
21	78.59	23.59	20.94	80.49	39.76	1.98
22	78.53	24.11	20.35	80.62	39.56	1.99
23	81.33	23.79	21.31	80.83	40.98	1.95

24	79.09	23.50	20.90	80.42	39.49	2.00
25	76.79	23.69	20.56	81.13	39.52	1.94
26	79.68	23.38	21.20	80.19	39.75	2.00

Table 24 Sample measurement.

After completing the sample measuring process, the mechanical testing phase commenced, focusing on both flexural and compressive strength evaluations. Flexural testing was conducted to assess the samples' resistance to bending forces, while compressive testing evaluated their ability to withstand axial loads. The test equipment used for mechanical characterization was manufactured by MTS Systems Corporation (USA). It is a servo-hydraulic test equipment with control of load, stroke and strain. For three-points bending tests, the prisms were loaded in correspondence of the central section up to failure. The compressive tests were done on the two halves of the sample previously broken during flexural tests. These tests were designed to provide a comprehensive understanding of the structural performance and comparability of both the 3D-printed mortar and traditional cast mortar under various loading conditions.

MECHANICAL TESTS

This chapter presents a comprehensive explanation of the mechanical tests performed to characterize the mechanical properties of mortar. The investigation focuses on fundamental parameters, including flexural strength, compressive strength and fracture energy, which are essential to understand the mechanical behavior and durability of mortar as a construction material.

To achieve these goals, two well-known structural testing methods were performed: a three-point bending test and compression test. The three-point bending tests were used to measure the flexural strength and fracture energy, providing insights into the material's capacity to resist cracking and deformation under deflection loads. On the other hand, compression tests were carried out to evaluate compressive strength, an essential test of the material's performance to resist axial loads without failure. All testing procedures were performed under controlled conditions at the laboratory of Construction Risk and Durability Center at DISEG, Politecnico di Torino, guaranteeing meticulous testing protocols and reliability of the results.

THREE-POINT BENDING TEST

The three-point bending test was performed according to EN 196-1[277] (standard testing method for determining the compressive and optional flexural strength of cement mortars, as well as validating compaction equipment procedures) using a single-column displacement-controlled flexural testing machine, Zwick Line Z050.

The Zwick Line Z050 is a highly advanced testing machine commonly used in the evaluation of material mechanical properties. This universal testing machine is designed to perform a large variety of tests, including tensile, compression and flexural tests, with a certain emphasis on high-precision measurements. This machine operates with a maximum load capacity of 50 kN, making it suitable for testing small to medium sized samples. Its sophisticated control system allows for precise adjustment in load and displacement, guaranteeing reliable and stable results throughout various test procedures[278]. The machine is equipped with a set of sensors and digital interfaces, allowing real time monitoring and data gathering, which are essential for detailed analysis and

[277] **Specificata fonte non valida.**
[278] **Specificata fonte non valida.**

interpretation of the material performance. Moreover, its modular design provides flexibility, allowing users to adapt the machine's setup to suit testing needs, such as incorporating different grips or loading fixtures[279].

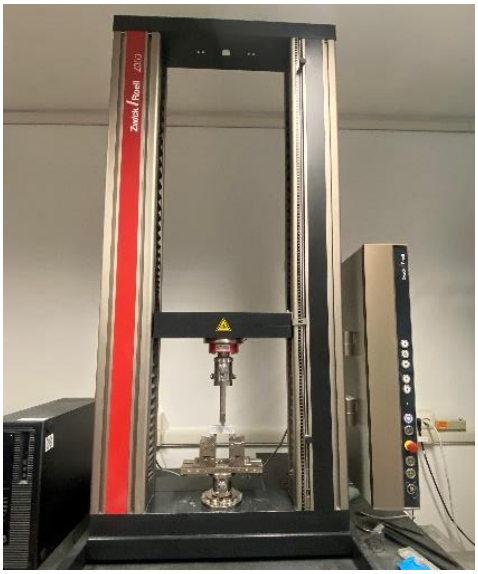

Image 43 Testing machine used for the flexural and compression test.
Source: (Author).

The Zwick Line-Z050 testing machine was used to perform the three-point bending test in this examination. Force control at a rate of 50 N/s was implemented, as suggested by the EN 196-1 standard for mortars. This method guarantees a controlled and stable application of force, aligning with the prescribed testing procedure to assess the material's behavior under progressive loading. This setup allows for precise assessment of the material's flexural performance and contributes to a reliable calculation of the modulus of rupture (MOR), which was determined using the following equation:

$$\sigma_M = \frac{1.5 \cdot F \cdot L}{A \cdot b}$$

where F represents the maximum applied force (in Newtons), L is the distance between the two support points of the sample, in this case 60 mm, A is the cross-sectional area of the sample, and b indicates the width of the sample's cross-section. The modulus of rupture, or flexural strength, is a parameter that assesses the material's resistance to bending stress, particularly in applications where materials are exposed to flexural forces. This provides an estimate of the material's ability to persist through maximum bending stress before failure, which is necessary to evaluate the structural performance and reliability of materials under load.

Before performing the three-point bending test, preparation of the mortar samples is essential to guarantee accurate and reliable results. The preparation process begins by measuring and weighing the samples to register their mass and physical dimensions, including depth, width, and length, with all values carefully recorded. Additionally, three reference points are marked on each sample to correspond precisely with the placement of the machines' supports, facilitating accurate positioning during the test.

[279] **Specificata fonte non valida.**

Image 44 Measurement of samples and marking referent points in preparation for the three-point bending test.
Source: (Author).

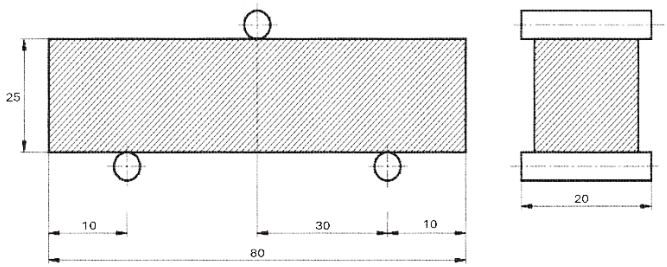

Figure 47 Schematic representation of the samples' approximate dimensions in mm and positioning for a three-point bending test.
Source: (Author)

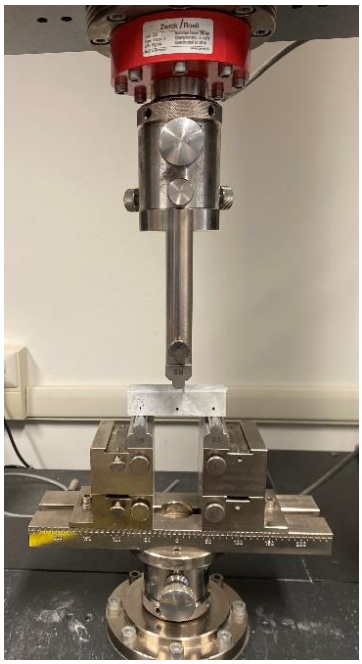

Image 45 Positioning and centering of the specimen bars on the Zwick Line Z050 testing machine.
Source: (Author).

The n-shaped supports, spaced 60 mm apart, act as the lower contact points for the sample. Given that the samples measure approximately 8 cm in length, the reference points must be aligned with

the supports, maintaining a consistent 1 cm gap between the edge of the sample and the reference points, oriented toward the center. Proper alignment also requires that the midpoint of the sample's upper surface is positioned directly below the center of the upper knife of the testing machine.

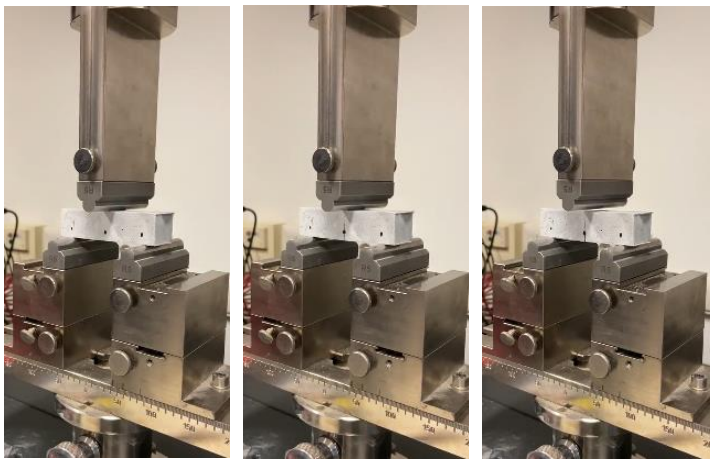

(a) (b) (c)

Image 46 Sequential images (a, b, c) illustrating the procedure for test performance on the Zwick Line Z050.
Source: (Author).

The sequence of the flexural testing process is presented in a series of images. Image 46 (a) Illustrates the precise alignment of the specimen at the onset of the test, Image 46 (b) captures the critical moment of sample failure, and Image 46 (c) depicts the fully collapsed sample following failure. Maintaining precise alignment is important for achieving uniform force distribution during testing. Any misalignment could result in uneven load application, thereby distorting the material's fracture behavior and compromising the consistency of the results.

COMPRESSION TEST

In preparation for the compression tests, the flexural testing setup of the Zwick Line Z050 machine was removed, and the necessary components were reconfigured to perform the compression test. This involved removing the bending test fixtures, installing the appropriate compression plates.

Image 47 Zwick Line-Z010 testing machine with the arrangement of compression fixtures. Source: (Author).

The compression tests were conducted in accordance with the EN 196-1[280] standard for mortars, which specifies a constant loading rate of 2400 N/s. As the study progressed, the remaining broken halves of the mortar prisms during the flexural tests were repurposed for compression testing. The samples were properly placed between the machine's steel compression plates, with the proper alignment and guaranteed uniform force distribution during loading. The Zwick Line Z050 machine was configured to apply the specified loading rate, gradually increasing the force until the sample failed. The maximum load at the point of failure was recorded, allowing the calculation of the compressive strength of the mortar.

[280] **Specificata fonte non valida.**

Image 48 Arrangement of the fractured halves of the mortar prisms from the flexural tests, prepared to begin the compression test.
Source: (Author).

a b

Image 49 Printed samples following the three-point bending test, displaying the failure surface of (a) sample 2 with a water-to-cement ratio of 0.38, and (b) sample 3 with a water-to-cement ratio of 0.36.
Source: (Author).

a b c

Image 50 Sequential images (a, b, c) illustrating the procedure with a 3D-printed sample during the compression test on the Zwick Line Z050
Source: (Author).

The sequence of the compression testing process is presented in a series of images. Image 50 (a) demonstrates the precise alignment of the specimen at the commencement of the test, Image 50 (b) captures the critical moment of specimen failure, and Image 50 (c) displays the fully collapsed specimen following failure. The precise control of the 2400 N/s loading rate was fundamental to

the reliability of the results. Throughout the test, the samples' alignment and the loading rate were maintained according to the standard, and data on the mortar's behavior under compressive stress was recorded.

To further explore the compressive strength, the two broken prisms from the three-point bending test were used for following compression tests. This methodology allowed a clear comparison of material's response to both flexural and compressive loads. The compression test aimed to quantify the maximum force the sample could withstand before rupture, a main factor that determines the material's compressive strength. The compressive strength ($\sigma_{c,max}$) was calculated using the formula:

$$\sigma_{c,max} = \frac{F_{max}}{b \cdot h}$$

Where F_{max} is the maximum force sustained by the sample before failure, and b and h represent the thickness of the sample in both, horizontal and vertical directions, respectively. Compressive strength provides an understanding of material's resistance to axial loading and its performance in real-world structural applications. The use of broken prisms from the three-point bending test allowed a more comprehensive assessment of the material's behavior under different loading modes, highlighting its mechanical properties throughout multiple testing conditions. This method aligns with established standards for compressive strength testing, validating the reliability and accuracy of the results.

MECHANICAL PROPERTIES TEST SAMPLE IDENTIFICATION

The tables below present a detailed characterization of the samples, specifying which samples were subjected to each type of mechanical test. The samples are organized and systematically renamed according to the specific test they underwent, ensuring clear identification and traceability throughout the testing process. This systematic approach allows for efficient data management and facilitates the analysis of different factors, and the correlations between mix design parameters and structural performance evaluation.

Reference Sample label	Bending test Sample label	Compression test sample label [281]	
3D Printed 0.38_w/c 3 mm_nozzle			
1	3	5	6
2	2	3	4
3	1	1	2
4	5	8	9
5	4	7	-
6	6	10	-
3D Printed 0.38_w/c 2 mm_nozzle			
7	1	1	-
8	4	5	6
9	3	4	-

[281] The spaces marked as (-) are the samples that were separated to develop further analysis if needed

10	2	2	3
Traditional casting 0.38_w/c			
18	1	1	-
19	2	2	3
20	3	4	5
3D Printed 0.36_w/c 2 mm_nozzle			
11	3	4	5
12	4	6	7
13	2	3	-
14	1	1	2
Traditional casting 0.36_w/c			
24	1	1	-
25	2	2	3
26	3	4	5
3D Printed 0.40_w/c 2 mm_nozzle			
15	3	4	5
16	2	2	3
17	1	1	-
Traditional casting 0.40_w/c			
21	1	1	2
22	2	3	4
23	3	5	-

Table 24 Sample Labels for Mechanical Testing: Classification and Reference Guide.

This table organizes the labels of samples subjected to various mechanical tests, categorizing them by their specific test type to highlight key characteristics of each sample. By referencing the assigned sample numbers, samples can be traced back to the corresponding tables above.

MECHANICAL TEST RESULTS

This section presents a detailed analysis of the mechanical test results for the mortar samples, focusing on key parameters such as flexural strength and compressive strength. The tests were conducted on both 3D-printed and traditionally cast mortar samples, allowing for a comparative evaluation of the two fabrication methods. The study incorporated varying water-to-cement (w/c) ratios, specifically between 0.36, 0.38, and 0.40, alongside the inclusion of 5% biochar, as outlined in the methodology discussed in previous chapters.

The results from the bending (flexural) and compressive tests are presented below, offering insight into the impact of different mix designs and printing methods on the structural performance of the mortar samples. This analysis provides a comprehensive understanding of the mechanical behavior and suitability of these formulations for various construction applications. It is also important to note that all samples the three point bending test were carried out using constant parameter such as: test speed (50 N/s), time save interval (0.01 s), and a pre-load (5N).

BENDING TEST RESULTS

Sample	E_{mod} (MPa)	F [282] (N)	F_{max} (N)	σ_F (MPa)	dL at F_{max} (mm)	W_o (mm)	H_o (mm)	S_o (mm²)	t_{Test} (s)
1	6.87	28.40	587.06	4.93	0.74	26.63	20.07	534.46	12.88
2	13.89	43.52	562.99	3.83	0.36	20.68	25.29	522.99	12.38
3	153.27	152.16	616.98	6.80	0.38	24.13	18.40	443.99	13.32
4	40.85	105.26	564.27	4.94	0.82	19.35	23.06	446.21	12.32
5	467.10	201.81	442.09	4.99	0.45	19.30	20.33	392.37	9.89
6	307.93	355.46	707.85	5.76	0.55	21.94	22.45	492.56	15.07
			MEAN	5.21					
			Standard deviation, σ	0.91					

Table 23 3D Printed 0.38_w/c 3mm_nozzle three-point bending test.

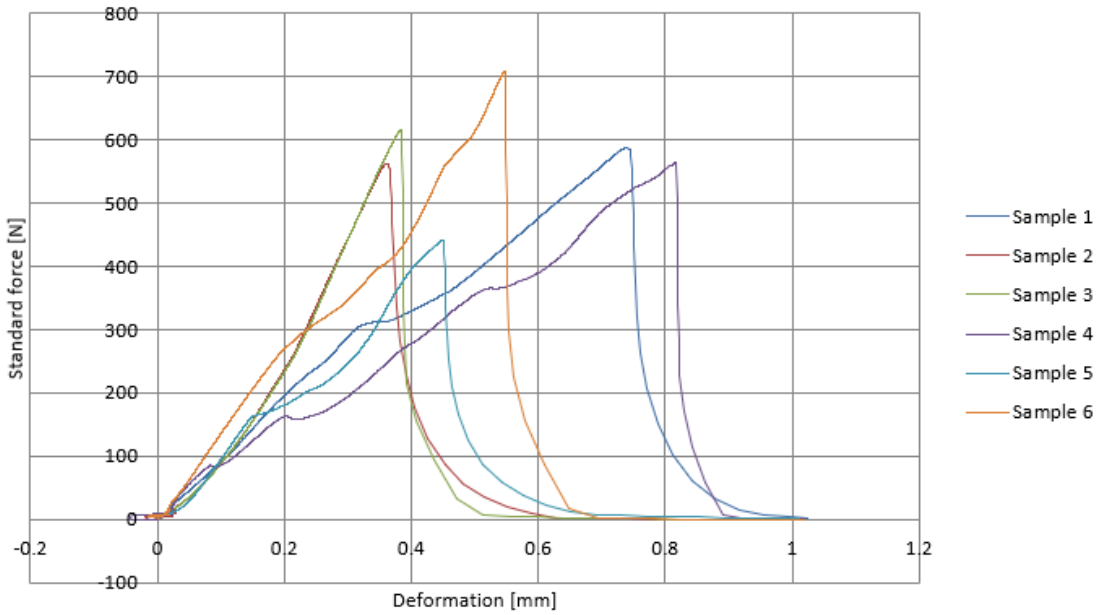

Figure 48 3D Printed 0.38_w/c 3mm_nozzle three-point bending test comparison between standard force (N) and deformation (%).

[282] at 0.2% plastic deformation

Sample	E_{mod} (MPa)	F [283] (N)	F_{max} (N)	σ_F (MPa)	dL at F_{max} (mm)	W_o (mm)	H_o (mm)	S_o (mm²)	t_{Test} (s)
1	826.44	488.73	657.56	6.45	0.22	19.91	21.42	426.47	13.92
2	578.58	477.41	600.56	6.44	0.37	23.13	19.05	440.63	12.90
3	791.61	428.25	549.18	5.38	0.25	19.70	21.60	425.52	11.94
4	353.26	508.40	627.15	5.84	0.38	24.76	19.75	489.01	13.48
				MEAN	6.03				
				Standard deviation, σ	0.46				

Table 26 3D Printed 0.38_w/c 2mm_nozzle three-point bending test.

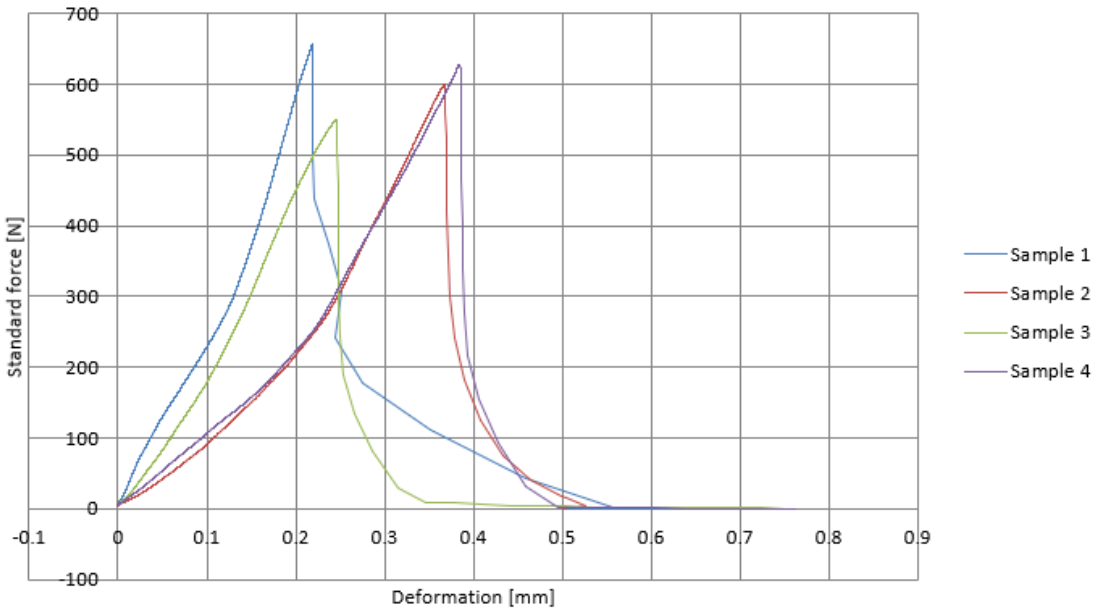

Figure 49 3D Printed 0.38_w/c 2mm_nozzle three-point bending test comparison between standard force (N) and deformation (%).

[283] at 0.2% plastic deformation

Sample	E_{mod} (MPa)	F [284] (N)	F_{max} (N)	σ_F (Mpa)	Dl at F_{max} (mm)	$W_{\circ}$ (mm)		$H_{\circ}$ (mm)	$S_{\circ}$ (mm^2)	t_{Test} (s)
1	5.55	4.14	539.97	4.77	0.22	23.52		20.82	489.69	11.44
2	91.43	80.33	575.49	5.04	0.19	23.95		20.72	496.24	15.66
3	764.39	-	462.60	4.10	0.18	23.65		20.71	489.79	9.97
			MEAN	4.64						
			Standard deviation, σ	0.39						

Table 27 Traditional casting 0.38_w/c three-point bending test.

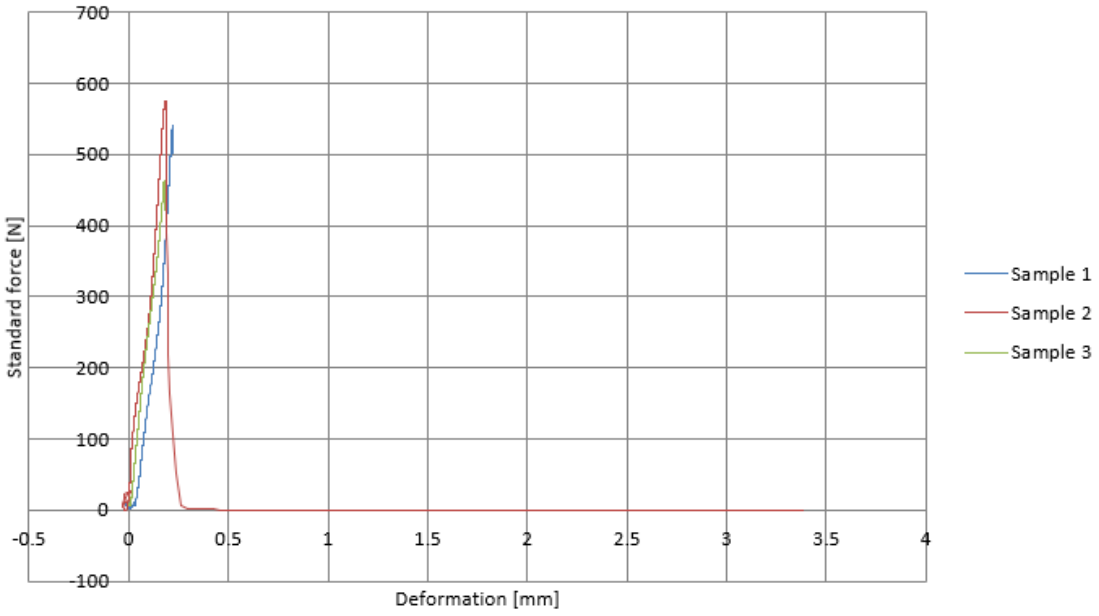

Figure 50 Traditional casting 0.38_w/c three-point bending test comparison between standard force (N) and deformation (%).

[284] at 0.2% plastic deformation

Sample	E_{mod} (MPa)	F [285] (N)	F_{max} (N)	σ_F (MPa)	dL at F_{max} (mm)	W_o (mm)	H_o (mm)	S_o (mm^2)	t_{Test} (s)
1	60.99	68.27	444.07	4.80	0.98	19.30	20.77	400.86	9.79
2	103.27	45.39	544.99	5.58	0.81	20.52	20.70	424.76	11.80
3	-	5.60	385.06	5.63	0.79	20.45	17.35	354.81	8.65
4	525.90	651.15	783.99	5.32	0.52	28.53	21.57	615.39	16.74
			MEAN	5.33					
			Standard deviation, σ	0.33					

Table 28 3D Printed 0.36_w/c 2mm_nozzle three-point bending test.

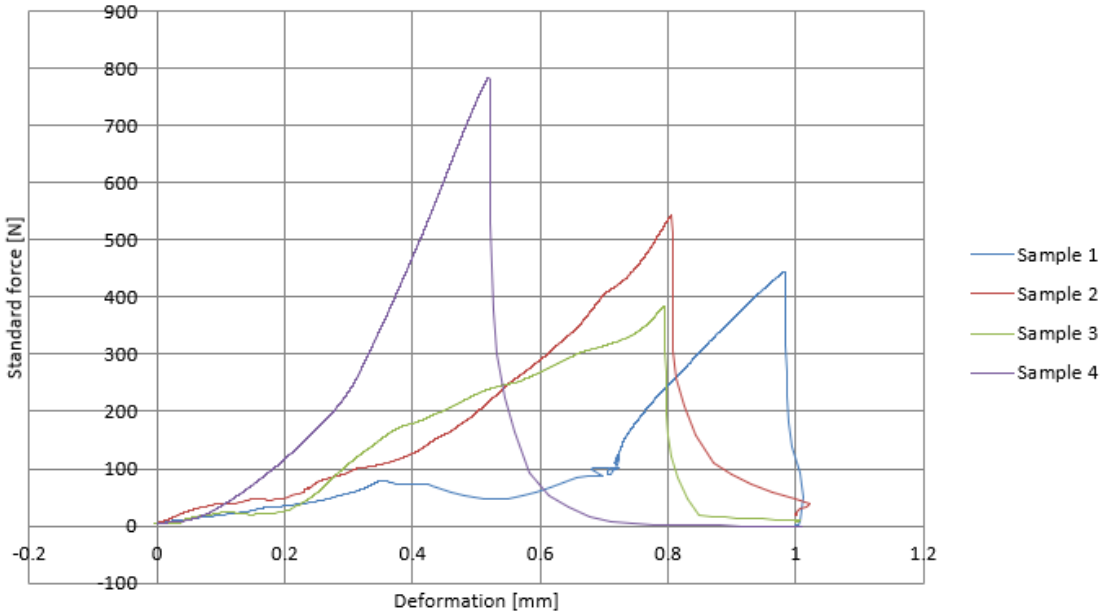

Figure 51 3D Printed 0.36_w/c 2mm_nozzle three-point bending test comparison between standard force (N) and deformation (%).

[285] at 0.2% plastic deformation

Sample	E_{mod} (MPa)	F [286] (N)	F_{max} (N)	σ_F (Mpa)	dL at F_{max} (mm)	$W_\circ$ (mm)	$H_\circ$ (mm)	$S_\circ$ (mm^2)	t_{Test} (s)
1	741.92	302.33	474.34	4.16	0.18	23.50	20.90	491.15	10.88
2	97.02	95.10	431.48	3.78	0.24	23.69	20.56	487.07	9.68
3	118.15	105.69	497.81	4.26	0.23	23.38	21.20	495.66	11.14
			MEAN	4.10					
			Standard deviation, σ	0.16					

Table 29 Traditional casting 0.36_w/c three-point bending test.

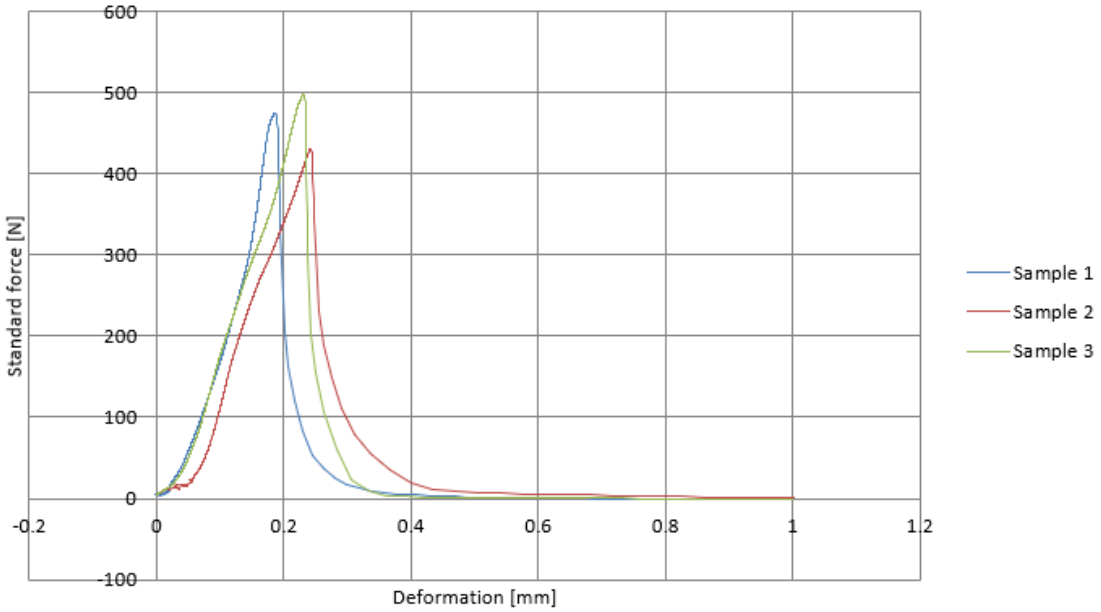

Figure 52 3D Traditional casting 0.36_w/c three-point bending test comparison between standard force (N) and deformation (%).

[286] at 0.2% plastic deformation

Sample	E_{mod} (MPa)	F [287] (N)	F_{max} (N)	σ_F (MPa)	dL at F_{max} (mm)	W_o (mm)	H_o (mm)	S_o (mm^2)	t_{Test} (s)
1	24.15	57.44	436.22	3.67	0.47	19.25	23.56	453.53	9.96
2	2.10	4.27	435.99	3.89	0.35	19.86	22.53	447.45	9.78
3	20.38	38.13	421.26	3.26	0.33	23.74	18.89	449.82	9.66
			MEAN	4.01					
			Standard deviation, σ	0.33					

Table 30 3D Printed 0.40_w/c 2mm_nozzle three-point bending test.

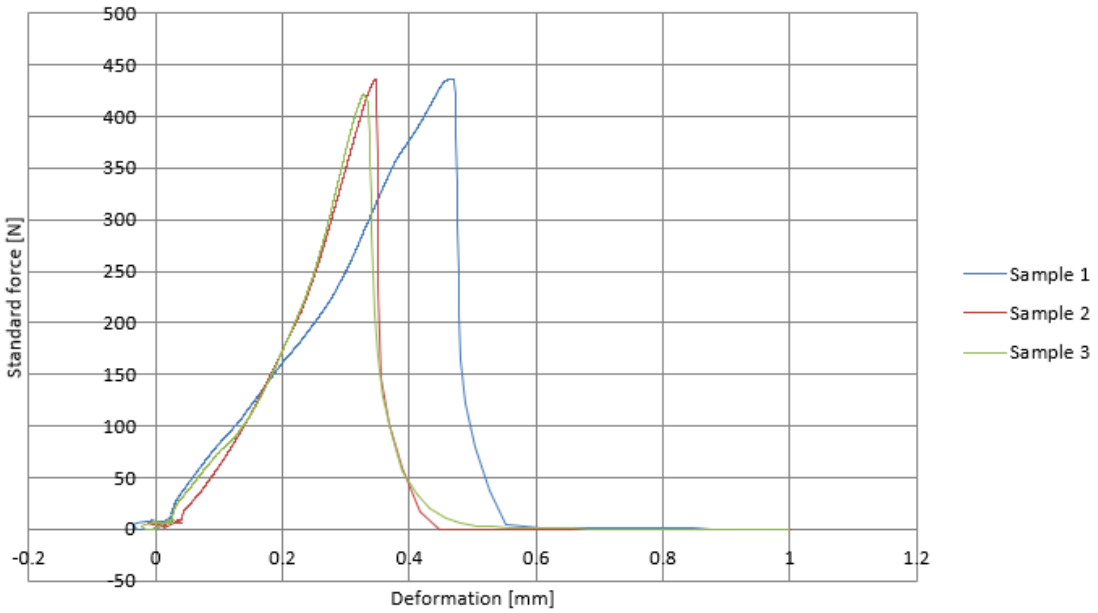

Figure 53 3D Printed 0.40_w/c 2mm_nozzle three-point bending test comparison between standard force (N) and deformation (%).

[287] at 0.2% plastic deformation

Sample	E_{mod} (MPa)	F [288] (N)	F_{max} (N)	σ_F (Mpa)	dL at F_{max} (mm)	W_o (mm)	H_o (mm)	S_o (mm^2)	t_{Test} (s)
1	-	5.52	467.61	4.07	0.35	23.59	20.94	493.97	10.36
2	112.26	10.92	444.09	4.00	0.45	24.11	20.35	490.64	9.89
3	7.55	2.78	606.93	5.06	0.24	23.79	21.31	506.96	13.30
				MEAN	4.38				
				Standard deviation, σ	0.48				

Table 31 Traditional casting 0.40_w/c three-point bending test.

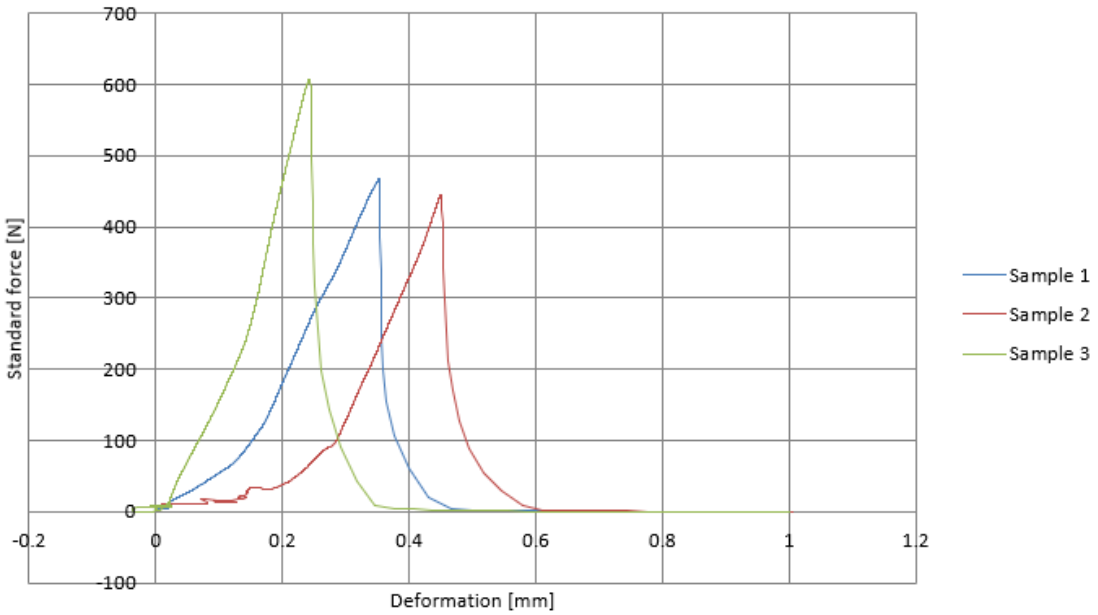

Figure 54 Traditional casting 0.40_w/c three-point bending test comparison between standard force (N) and deformation (%).

[288] at 0.2% plastic deformation

Sample Type	3D Printing 2mm nozzle		Traditional Cast	
	Mean σ_F (MPa)	Standard deviation, σ	Mean σ_F (MPa)	Standard deviation, σ
0.38_w/c	6.03	0.46	4.64	0.39
0.36_w/c	5.33	0.33	4.10	0.16
0.40_w/c	4.01	0.33	4.38	0.48
Sample Type	3D Printing 2mm nozzle		3D Printing 3mm nozzle	
	Mean σ_F (MPa)	Standard deviation, σ	Mean σ_F (MPa)	Standard deviation, σ
0.38_w/c	6.03	0.46	5.21	0.91

Table 39 Summarized results obtained from the three-point bending test.

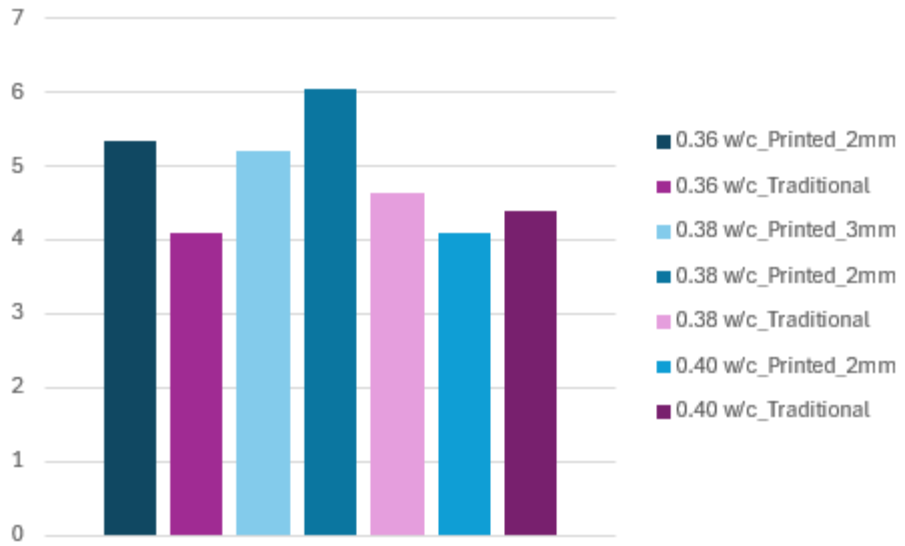

Figure 55 Summarized results of the flexural strength for each mixture sample.

The test results indicate that the flexural strength values obtained from sample tested under EN 12390-5 and ASTM C78 standards are consistent with the typical ranges found in literature. For standard-grade concrete, the flexural strength measured ranged from 3 MPa to 6 MPa using EN 12390-5, while ASTM C78 tests yielded values between 450 psi (3.1 MPa) and 700 psi (4.8 MPa) for similar concrete grades.

As the difference in testing methodologies between three-point loading and four-point loading significantly impacts the results, this specific experiment applied the method established by the EN 12390-5 to understand the flexural strength with samples of dimension of 20 mm × 20 mm × 80 mm. The four-point loading often distributes stresses more uniformly, reducing the likelihood of localized failure, which can result in slightly higher flexural strength values[289]. On the other hand, the three-point bending method concentrates stress at mid-span, making the sample more prone to tensile cracking at lower loads[290].

The flexural strength results reveal that all samples meet the minimum strength requirements established by the EN standards. However, significant differences are observed between the flexural strength values of traditionally cast and 3D-printed samples. The traditionally cast samples consistently exhibited higher tensile strength compared to the 3D-printed ones, indicating

[289] (Neville & Brooks, 2010)
[290] **Specificata fonte non valida.**

that conventional casting methods continue to provide superior structural integrity in terms of tensile performance when the workability of the material is enough for manual placing in the molds (w/c=0.4). On the contrary, for higher viscosity values of the mix, 3D printed materials showed higher mechanical properties (w/c= 0.36 & 0.38).

For 3D-printed samples, no direct correlation between thew/c ratio and tensile strength was observed. However, it could be that the w/c = 0.38 was the optimum value. Among the printed samples, those with a 0.38 w/c ratio produced using a 2 mm nozzle demonstrated the highest flexural strength, suggesting that nozzle size plays a critical role in determining the cohesion and structural stability of the printed layers, considering the size of the printed samples. Specifically, the reduction in nozzle size resulted in improved layer bonding and enhanced structural development, leading to better mechanical performance.

In contrast, the flexural strength of traditionally cast samples did not vary significantly across the different w/c ratios. Like the 3D-printed samples, there was no clear relationship between increasing the w/c ratio and a decrease in tensile strength, contrarily to initial expectations. This suggests that while the w/c ratio remains a crucial factor in mix design, its influence on flexural strength may be mitigated by the workability of the mortar.

These findings highlight the importance of nozzle size in 3D printing for improving mechanical performance and suggest that additional factors (i.e. workability), beyond w/c ratio, may govern flexural strength in both 3D-printed and traditionally cast mortars.

COMPRESSION TEST RESULTS

Sample	$W_{\circ}$ (mm)	$H_{\circ}$ (mm)	$S_{\circ}$ (mm^2)	$L_{\circ}$ (mm^2)	F_{max} (N)	t_{Test} (s)	σ_C (MPa)	dL at F_{max} (mm)
1	26.63	20.07	532.60	20.00	3804.35	2.56	7.14	4.48
2	26.63	20.07	532.60	20.00	5134.50	3.24	9.64	4.35
3	20.68	25.29	413.60	20.00	5822.98	3.71	14.08	4.37
4	20.68	25.29	413.60	20.00	5687.12	3.85	13.75	3.32
5	24.13	18.40	482.60	20.00	3278.12	2.57	6.79	4.05
6	24.13	18.40	482.60	20.00	4641.46	3.14	9.62	3.92
7	19.35	23.06	387.00	20.00	5045.29	3.42	13.04	3.83
8	19.30	20.33	386.00	20.00	1873.72	2.06	4.85	3.54
9	19.30	20.33	386.00	20.00	3268.14	2.87	8.46	3.17
10	21.94	22.45	438.8	20.00	5749.43	3.82	13.10	3.48
						MEAN	10.05	
						Standard deviation, σ	3.12	

Table 40 3D Printed 0.38_w/c 3 mm_nozzle compression test.

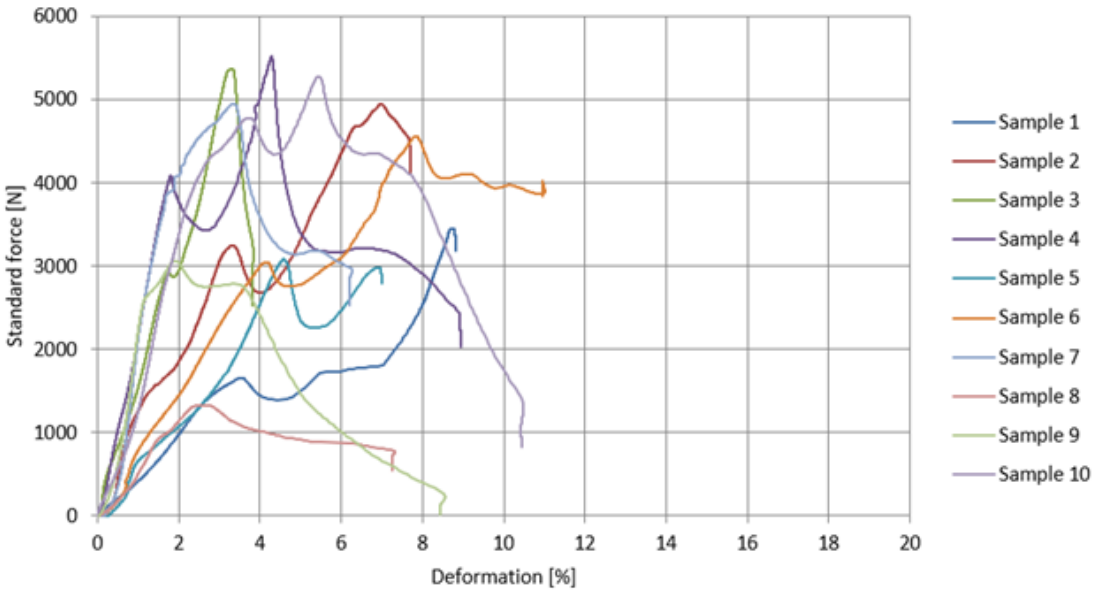

Figure 56 3D Printed 0.38_w/c 2 mm_nozzle compression test comparison between standard force (N) and deformation (%).

Sample	$W_{\circ}$ (mm)	$H_{\circ}$ (mm)	$S_{\circ}$ (mm^2)	$L_{\circ}$ (mm^2)	F_{max} (N)	t_{Test} (s)	σ_C (MPa)	dL at F_{max} (mm)
1	19.91	21.42	398.20	20.00	5811.79	3.77	14.59	3.15
2	23.13	19.05	462.60	20.00	9180.35	5.23	19.86	3.30
3	23.13	19.05	426.60	20.00	9403.24	5.29	20.33	2.95
4	19.70	21.60	394.00	20.00	4517.29	3.24	11.47	3.40
5	24.76	19.75	495.20	20.00	6573.68	4.17	13.27	3.17
6	24.76	19.75	495.20	20.00	6558.87	4.14	13.24	3.34
						MEAN	15.46	
						Standard deviation, σ	3.40	

Table 41 3D Printed 0.38_w/c 2 mm_nozzle compression test.

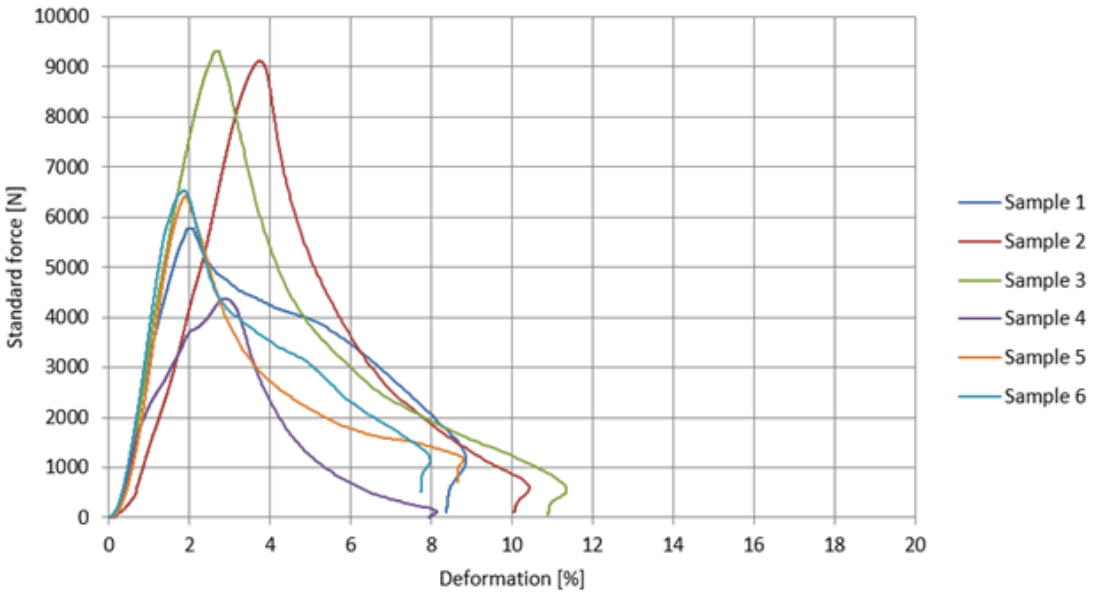

Figure 57 3D Printed 0.38_w/c 2mm_nozzle compression test comparison between standard force (N) and deformation (%).

Sample	$W_{\circ}$ (mm)	$H_{\circ}$ (mm)	$S_{\circ}$ (mm^2)	$L_{\circ}$ (mm^2)	F_{max} (N)	t_{Test} (s)	σ_C (MPa)	dL at F_{max} (mm)
1	23.52	20.82	416.40	20.00	14093.96	7.93	29.96	1.35
2	23.95	20.72	414.40	20.00	13504.99	6.93	28.19	3.43
3	23.95	20.72	414.40	20.00	13506.78	7.15	28.19	2.35
4	23.65	20.71	472.60	20.00	13905.21	7.17	29.39	3.16
5	23.65	20.71	472.60	20.00	13491.55	7.07	28.52	2.56
						MEAN	28.85	
						Standard deviation, σ	0.71	

Table 42 Traditional cast 0.38_w/c compression test.

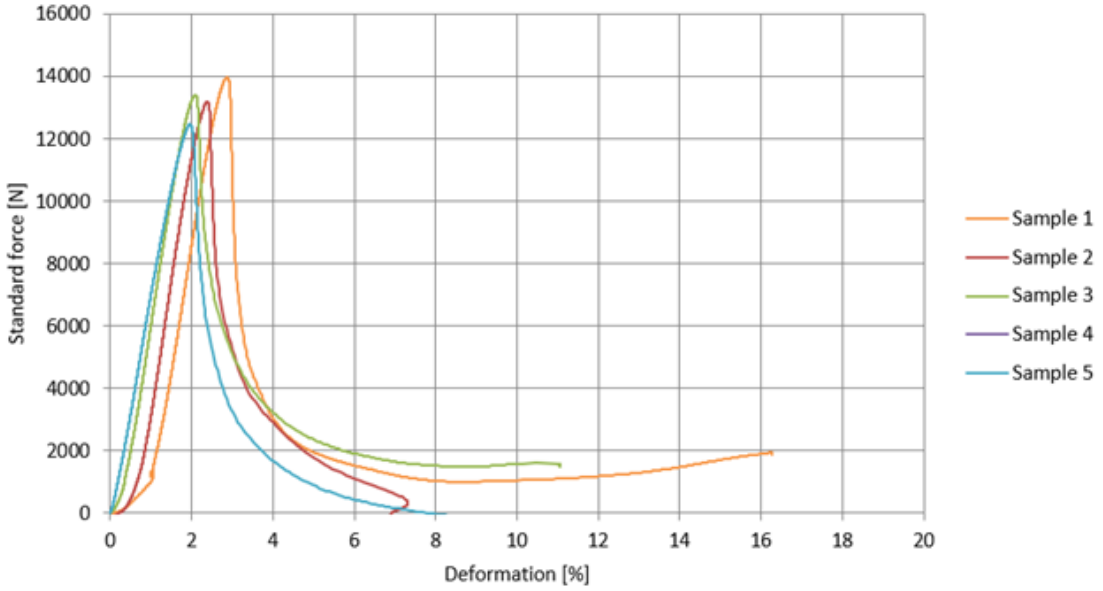

Figure 58 Traditional casting 0.38_w/c compression test comparison between standard force (N) and deformation (%).

Sample	$W_{\circ}$ (mm)	$H_{\circ}$ (mm)	$S_{\circ}$ (mm^2)	$L_{\circ}$ (mm^2)	F_{max} (N)	t_{Test} (s)	σ_C (MPa)	dL at F_{max} (mm)
1	19.30	20.77	386.00	20.00	4.99	2.72	4.99	0.41
2	19.30	20.77	386.00	20.00	5.07	2.35	5.67	3.66
3	20.52	20.70	410.40	20.00	6.18	2.36	6.18	3.87
4	20.45	17.35	409.00	20.00	6.40	-	6.40	-
5	20.45	17.35	409.00	20.00	9.98	-	9.98	-
6	28.53	21.57	570.60	20.00	9.38	3.78	9.38	3.17
7	28.53	21.557	570.60	20.00	8.82	3.49	8.82	3.17
						MEAN	7.26	
						Standard deviation, σ	1.93	

Table 43 3D Printed 0.36_w/c 2 mm_nozzle compression test.

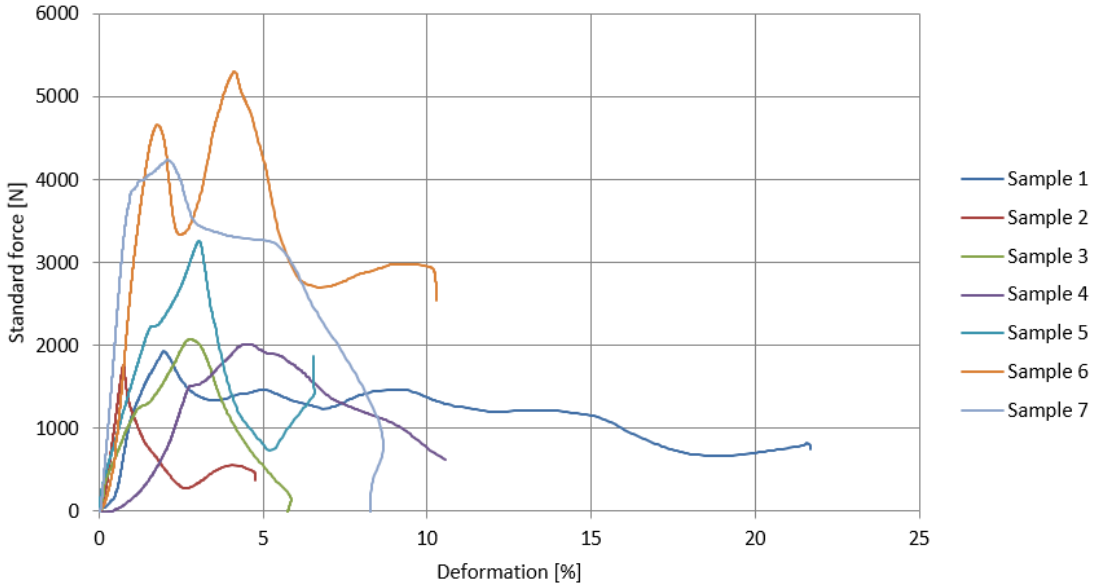

Figure 59 3D Printed 0.36_w/c 2 mm_nozzle compression test comparison between standard force (N) and deformation (%).

Sample	$W_{\circ}$ (mm)	$H_{\circ}$ (mm)	$S_{\circ}$ (mm^2)	$L_{\circ}$ (mm^2)	F_{max} (N)	t_{Test} (s)	σ_C (MPa)	dL at F_{max} (mm)
1	23.50	20.90	470.00	20.00	12725.96	6.85	27.08	27.08
2	23.69	20.56	473.80	20.00	10096.53	5.71	21.31	21.31
3	23.69	20.56	473.80	20.00	12604.01	6.64	26.60	26.60
4	23.38	21.20	467.60	20.00	13096.17	6.85	28.01	28.01
5	23.38	21.20	467.60	20.00	12834.62	6.85	27.45	27.45
						MEAN	26.09	
						Standard deviation, σ	2.43	

Table 44 Traditional casting 0.36_w/c compression test.

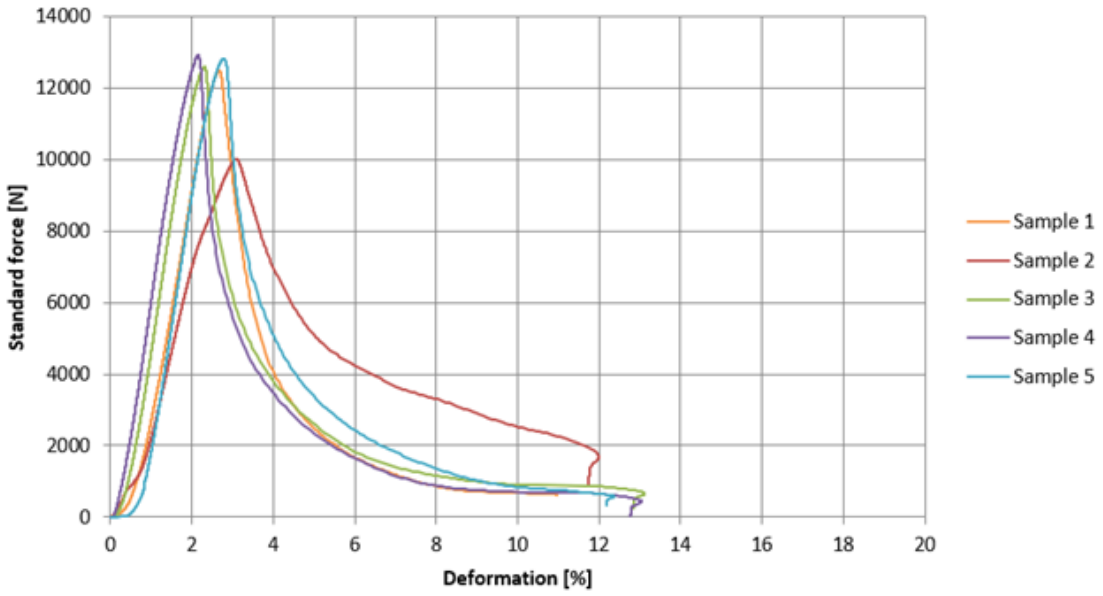

Figure 60 Traditional casting 0.36_w/c compression test comparison between standard force (N) and deformation (%).

Sample	$W_{\circ}$ (mm)	$H_{\circ}$ (mm)	$S_{\circ}$ (mm^2)	$L_{\circ}$ (mm^2)	F_{max} (N)	t_{Test} (s)	σ_C (MPa)	dL at F_{max} (mm)
1	19.25	23.56	384.60	20.00	5059.06	3.35	13.14	3.99
2	19.86	22.53	397.20	20.00	4164.92	3.06	10.49	3.69
3	19.86	22.53	397.20	20.00	4526.65	3.20	11.40	3.63
4	23.74	18.98	474.80	20.00	5976.22	3.82	12.57	3.60
5	23.74	18.98	474.80	20.00	5749.68	3.64	12.11	3.86
						MEAN	11.94	
						Standard deviation, σ	0.93	

Table 45 3D Printed 0.40_w/c 2 mm_nozzle compression test.

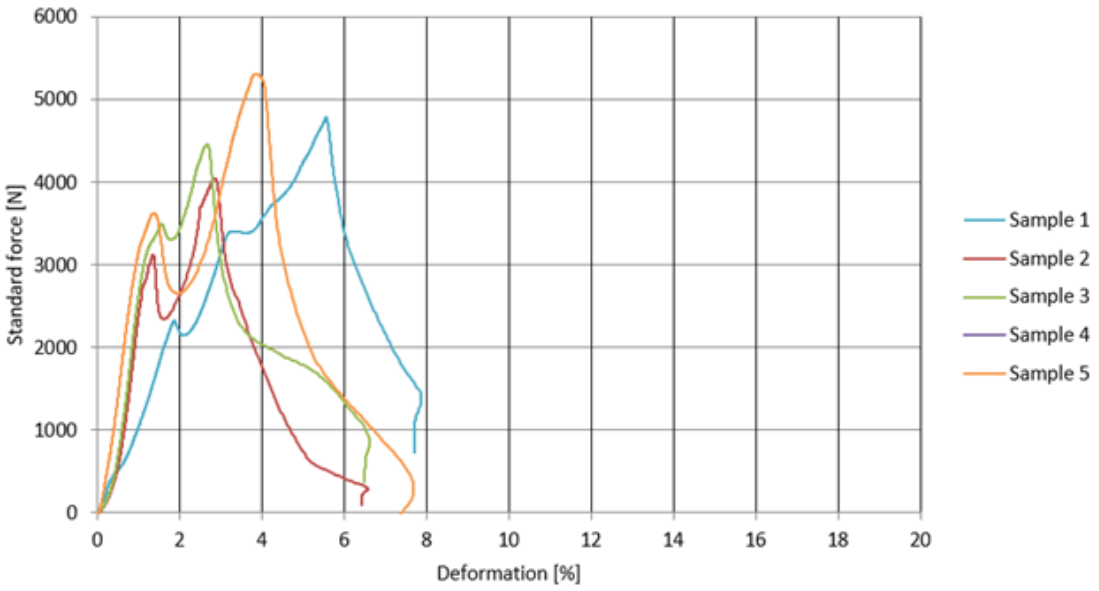

Figure 61 3D Printed 0.40_w/c 2 mm_nozzle compression test comparison between standard force (N) and deformation (%).

Sample	$W_{\circ}$ (mm)	$H_{\circ}$ (mm)	$S_{\circ}$ (mm^2)	$L_{\circ}$ (mm^2)	F_{max} (N)	t_{Test} (s)	σ_C (MPa)	dL at F_{max} (mm)
1	23.59	20.94	471.80	20.00	12504.32	6.49	26.50	3.57
2	23.59	20.94	471.80	20.00	12841.14	6.67	27.22	3.83
3	23.69	20.56	473.8	20.00	12769.23	6.58	26.95	4.29
5	23.79	21.31	475.80	20.00	13015.49	6.68	27.35	3.23
						MEAN	27.01	
						σ	0.32	

Table 46 Traditional casting 0.40_w/c compression test.

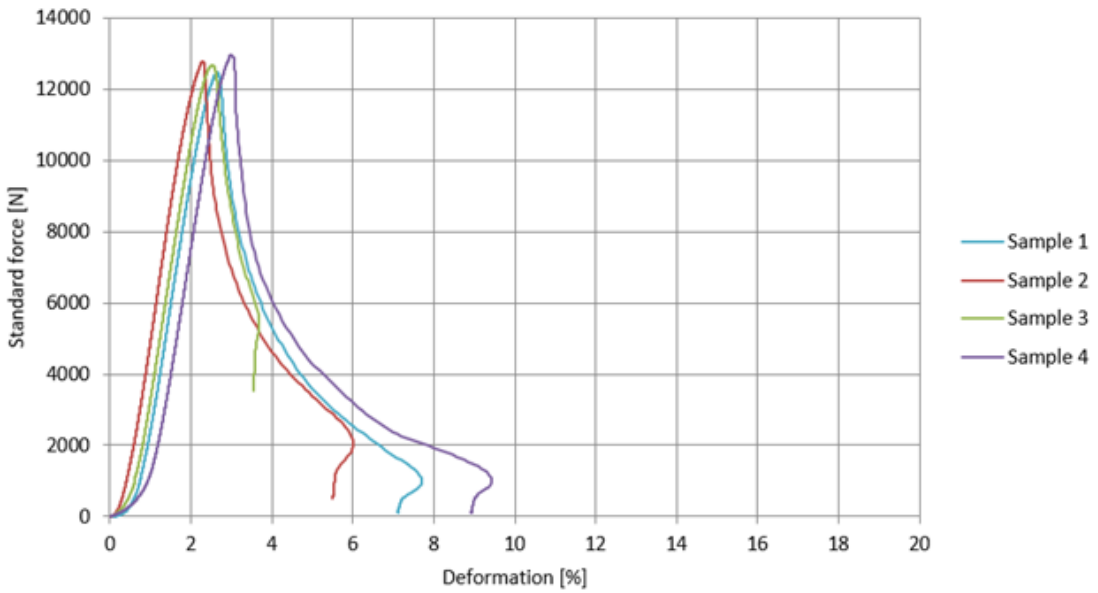

Figure 46 Traditional casting 0.40_w/c compression test comparison between standard force (N) and deformation (%).

Sample Type	3D Printing 2mm nozzle		Traditional Cast	
	Mean σ_F (MPa)	Standard deviation, σ	Mean σ_F (MPa)	Standard deviation, σ
0.38_w/c	15.46	3.12	28.85	0.71
0.36_w/c	7.26	1.93	26.09	2.43
0.40_w/c	11.94	0.93	27.01	0.32
Sample Type	3D Printing 2mm nozzle		3D Printing 3mm nozzle	
	Mean σ_F (MPa)	Standard deviation, σ	Mean σ_F (MPa)	Standard deviation, σ
0.38_w/c	15.46	3.12	10.05	0.46

Table 47 Summarized results obtained from the compression test.

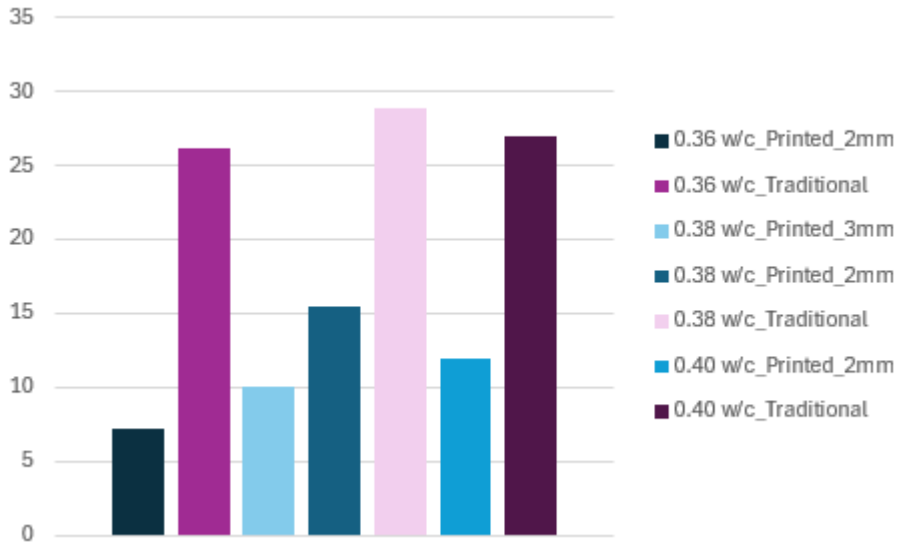

Figure 63 Summarized results obtained from the compression test.

Compressive strength is the most critical property of concrete and a key indicator of its structural performance under load. It determines the material's capacity to withstand axial loads without failure and serves as the primary basis for design specifications in concrete structures. This chapter presents the results of compressive strength tests conducted according to EN 196-1 and ASTM C39 standards, with a comparison of their testing methodologies, sample dimensions, and strength classifications.

The compressive strength results from both standards demonstrate the inherent relationship between sample shape and strength values. Concrete with a cylinder strength of 30 MPa in EN standards often exhibited a cube strength of 37 MPa due to the different failure mechanisms[291]. In the ASTM testing regime, 4,000 psi (27.6 MPa) concrete was observed to meet typical structural requirements, with strengths ranging up to 10,000 psi (69 MPa) for high-performance applications.

The results confirm that specimen shape plays a significant role in compressive strength outcomes. Cube specimens fail at higher loads compared to cylinders because the cube's uniform

[291] (Neville & Brooks, 2010)

stress distribution resists axial compression more effectively[292]. For this specifical experiment the compressive strength was calculated as stated by the European Standards.

The compressive strength results indicate that, although none of the samples fully meet the compressive strength requirements established by EN standards, the traditionally cast samples show promising performance, nearing the 30 MPa threshold. These samples demonstrated approximately double the compressive strength of their 3D-printed counterparts, highlighting the superior structural integrity achieved through conventional casting methods.

In the case of 3D-printed samples, no direct correlation was observed between the w/c ratio and compressive strength. However, as previously observed for flexural tests results, among the printed samples, the highest compressive strength was achieved with a 0.38 w/c ratio using a 2 mm nozzle, suggesting that nozzle size significantly influences the structural cohesion and strength of printed layers. Specifically, a smaller nozzle size enhances layer bonding and results in improved structural development, leading to stronger, more cohesive printed elements with less defects.

Similarly, in the traditionally cast samples, no clear relationship was found between increasing the w/c ratio and a decrease in compressive strength. Contrary to expectations, the sample with a 0.38 w/c ratio exhibited the highest compressive strength, aligning with the trend observed in the 3D-printed samples. This finding indicates that while w/c ratio remains an important factor, other variables, such as fabrication method and layer cohesion, as well as mix workability play a crucial role in determining compressive strength.

These results emphasize the potential of nozzle size reduction in 3D printing to enhance compressive performance and suggest that further optimization of mix designs and printing parameters could bridge the performance gap between 3D-printed and traditionally cast mortars. Image 49.b well illustrates the defects present in the printed samples (voids between the printed layers) that hampered the mechanical properties.

[292] (Eurpean Committee fro Standardization, 2019)

SEM OBSERVATIONS

Scanning Electron Microscopes (SEMs) are versatile tools frequently used in different sectors such as industrial, commercial, and research due to their ability to provide high resolution imaging, generally implemented for the characterization of materials, quality control and defect analysis[293]. SEMs provide a clear understanding of sample's topography, morphology, and, if equipped, chemical composition. Contrarily to a traditional optical microscope, these microscopes use electron beams instead of light to obtain a higher zoom and resolution to scan the sample's surface, enabling micro and nanoscale observations. These electrons interact with the samples, producing signals that are captured as images, which can then be used to determine information about the material's structure and properties. Versality is characterized by the integration of Energy-Dispersive X-ray Spectroscopy (EDX), Based Automated Mineralogy (SEM-AM), Backscattered Electron (BSE), among others[294] for collecting information about the chemical composition of the materials.

SEM uses a thermionic electron gun that generates electrons that are focused onto the sample surface. As the electron beam interacts with the sample, it produces both secondary and backscattered electrons which are detected to form high-resolution images[295]. In short, SEM is an essential tool for identifying various materials, offering detailed insights and revealing defects and imperfections that might alternatively go undetected[296].

While utilizing a SEM, sample preparation is a well-known preparation step to guarantee high-quality imaging. First, the sample is metallized with a thin conductive layer to prevent charging under the electron exposure. This is important for non-conductive materials, which would otherwise distort the image, as could occur in the present research with the last sample. The sample is then placed in the SEM chamber, where it is kept under vacuum conditions. Once the conditions are accurate, the electrons are directed on the sample, and images are captured. These images provide important information about the sample's surface topography and morphology, which can be analyzed for further research or quality control in industrial applications[297].

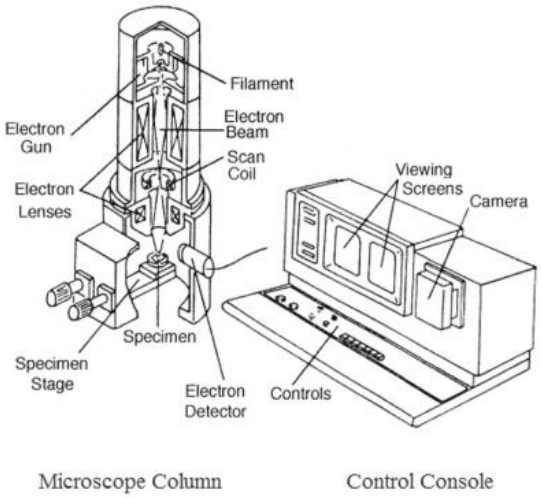

Figure 64 The Scanning Electron Microscope (SEM) consists of two principal sections illustrated in the image: the electron column, which houses the electron source and focusing systems, and the electronics console, responsible for controlling and processing the signals. Source: (Ural, 2021).

[293] **Specificata fonte non valida.**
[294] **Specificata fonte non valida.**
[295] **Specificata fonte non valida.**
[296] **Specificata fonte non valida.**
[297] (Ural, 2021)

In scientific applications, SEM is recognized for its ability to examine a large selection of samples. Sample preparation varies depending on the material type, and special care must be taken to ensure the sample's surface to be clean. Additionally, the sample must be appropriately sized to fit within the dimensions of the SEM chamber.

SEM SAMPLE IDENTIFICATION

Arriving at the Scanning Electron Microscopy (SEM) observations to examine the microstructure of the prepared materials, making it possible to observe the eventual interactions between the cementitious materials, admixtures, and additives at a microscopic level. This technique was particularly valuable for identifying potential issues related to material bonding, phase distribution, and the evidence of new chemical compound formation during the hydration process.

For this analysis, only a selected group of characteristic samples from the experimental population were analyzed. These samples were carefully chosen to represent distinctive features of the different mix designs and applied technologies, providing insights into how each formulation behaved under specific conditions, and evidence if any performance variation is occurring.

Table 48 below illustrates the relationship between the sample names used in the SEM observations and their corresponding reference sample labels. By cross-referencing these labels, it is possible to understand which specific formulations were analyzed so that a correlation between the SEM micrographs and mechanical test results can take place to evidence potential chemical interactions at the micro-level which can influence the overall durability, strength, and long-term performance of the mortars.

Type of sample	Reference sample label	SEM analysis label
Traditional casting 0.38_w/c	18	1
Traditional casting 0.40_w/c	23	2
3D Printed 0.36_w/c 2 mm_nozzle	13	3
Traditional casting 0.36_w/c	24	4
3D Printed 0.38_w/c 2 mm_nozzle	9	5
3D Printed 0.40_w/c 2 mm_nozzle	17	6

Table 48 Sample labels for SEM analysis: Classification and Reference Guide

SAMPLE PREPARATION FOR ANALYSIS

In this analysis, samples were selected from both 3D-printed and traditional cast samples to ensure a comprehensive comparative analysis. Three different water-to-cement ratios (0.36, 0.38, and 0.40) were included to observe the effect of varying hydration levels on the microstructure. Each sample was crushed into small fragments (less than 10 mm) to fit into the SEM specimen chamber and appropriately labeled. Before SEM observations, the samples were thoroughly dried in an oven at 60 °C on November 15th, and removed on the day of analysis (November 27th) to eliminate any residual moisture that could interfere with the SEM's vacuum environment during imaging. Since cementitious materials are non-conductive, all samples were coated with a thin metal layer (based on platinum) to prevent charging under the electron beam and to enhance image resolution. After metalizing the samples, they were placed in the SEM vacuum chamber to proceed with the observations.

SEM OBSERVATION ANALYSIS

Image 51 Hitachi S4000 SEM, DISAT, Politecnico di Torino.
Source: (Author).

The SEM analysis for this thesis was performed using the Hitachi S-4000 Scanning Electron Microscope (SEM) to evaluate the microstructural features of the mortar samples.

Additionally, the SEM analysis enable the identification of portlandite ($Ca(OH)_2$), a compound formed during the hydration process of Portland cement, as well as calcium carbonate ($CaCO_3$), which forms through carbonation. Carbonation occurs when portlandite in the concrete reacts with carbon dioxide (CO_2) from the air, a process that may take place during the material's lifespan[298]. Furthermore, calcium silicate hydrate (C-S-H), an important hydration product, was also identified. If hydration ceases, the formation of sufficient C-S-H is inhibited, disrupting the concrete's microstructure and allowing harmful agents to penetrate, which can lead to defects such as cracks, incomplete hydration, and surface imperfections[299]. Moreover, the SEM observations revealed another typical hydration product of Portland cement: ettringite ($3CaO.Al_2O_3.3CaSO_4.32H_2O$) which forms when tricalcium aluminate reacts with gypsum and water.

The objective of using SEM analysis was to perform a detailed examination of the microstructural integrity of materials, focusing on identifying micro-cracks, voids, and fractures within the material matrix, thereby identifying potential weaknesses. This is essential for assessing the structural integrity of concrete and other composite materials produced through various manufacturing methods, including 3D printing and traditional casting. In the case of 3D-printed materials, SEM observations can reveal issues such as incomplete bonding between layers, internal voids, or surface irregularities, all of which may compromise the material's overall strength and durability. Similarly, traditional casting methods may introduce defects, such as shrinkage cracks or voids, often resulting from improper curing or inconsistencies in the material composition[300]. By identifying these microstructural inconsistencies, SEM observations provide valuable insights into how different processing methods affect the material's performance, helping to improve manufacturing practices and increase material quality and durability.

[298] **Specificata fonte non valida.**
[299] **Specificata fonte non valida.**
[300] **Specificata fonte non valida.**

SAMPLE 1. Sample with a water-to-cement (w/c) ratio of 0.38 and produced through traditional casting methods.

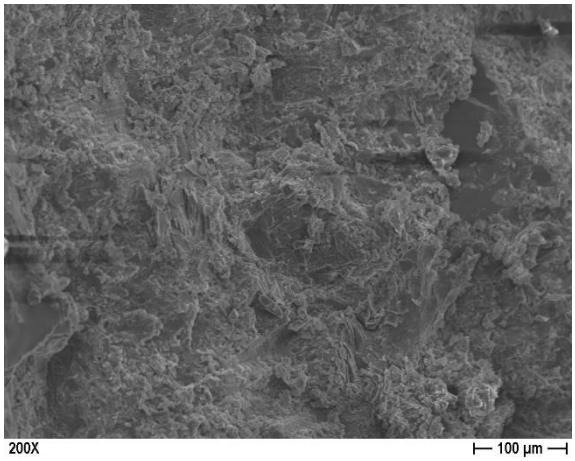

Image 52 SEM image of Sample 1 at 200x magnification, captured during analysis

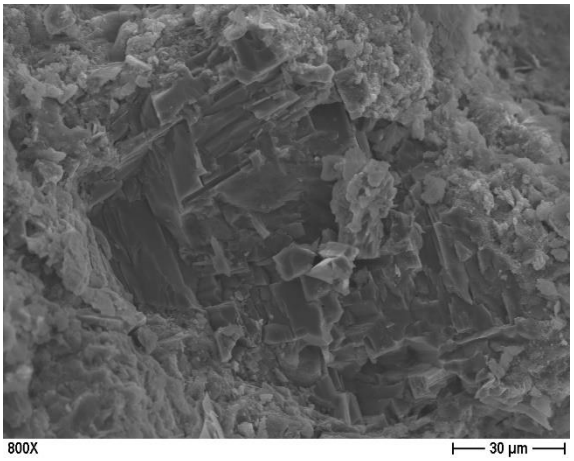

Image 55 SEM image of Sample 1 at 800x magnification, captured during analysis

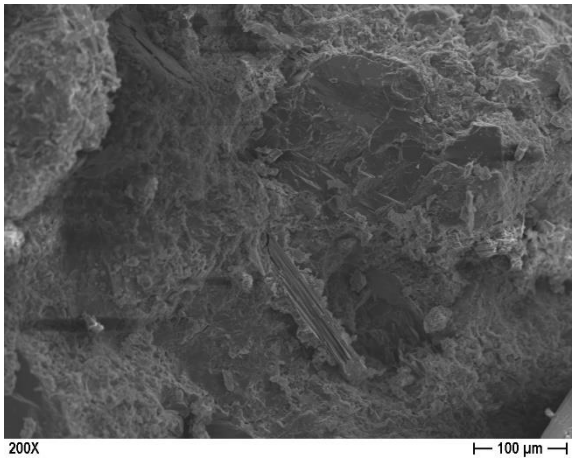

Image 54 SEM image of Sample 1 at 200x magnification, captured during analysis

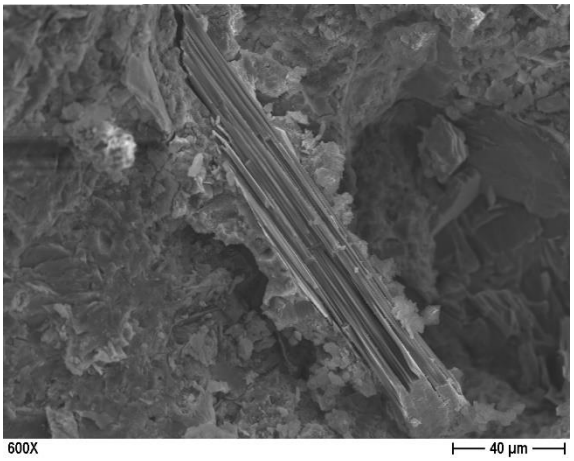

Image 56. SEM image of Sample 1 at 600x magnification, captured during analysis

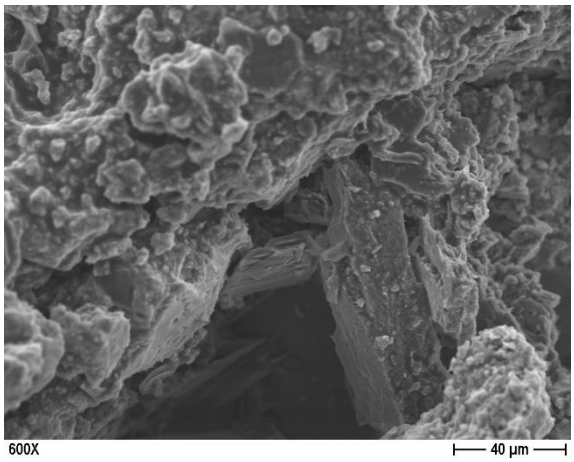

Image 53 SEM image of Sample 1 at 600x magnification, captured during analysis

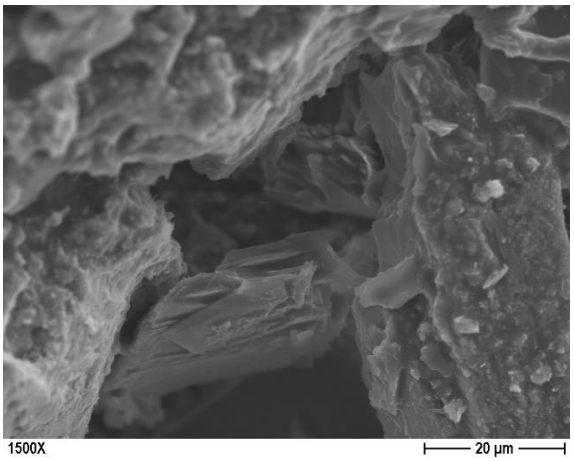

Image 58. SEM image of Sample 1 at 1500x magnification, captured during analysis

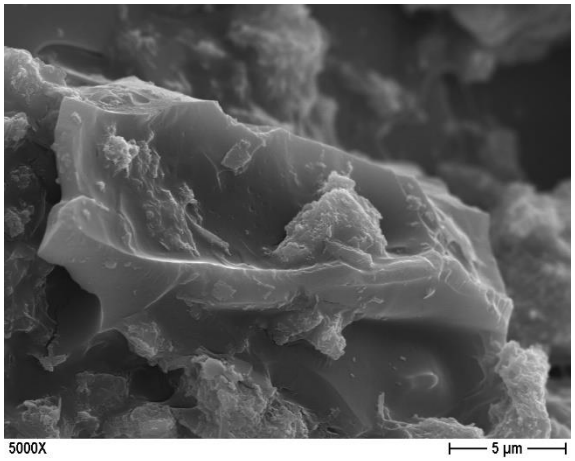

Image 60. SEM image of Sample 1 at 5000x magnification, captured during analysis

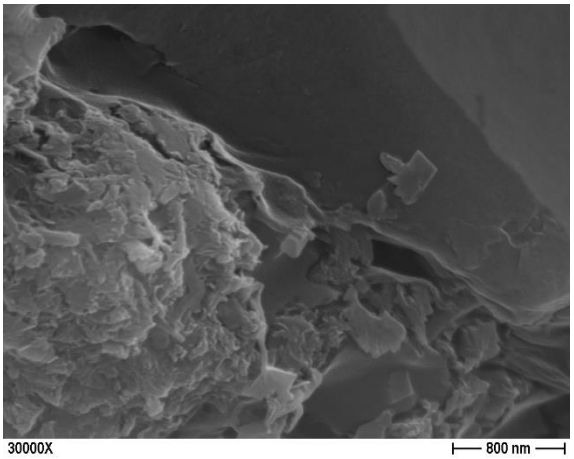

Image 61. SEM image of Sample 1 at 30000x magnification, captured during analysis

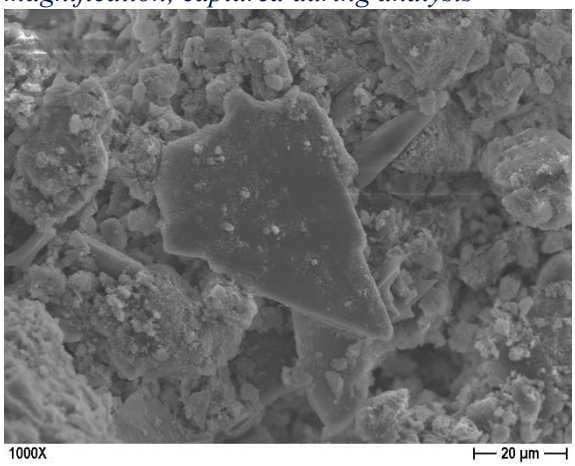

Image 57. SEM image of Sample 1 at 1000x magnification, captured during analysis

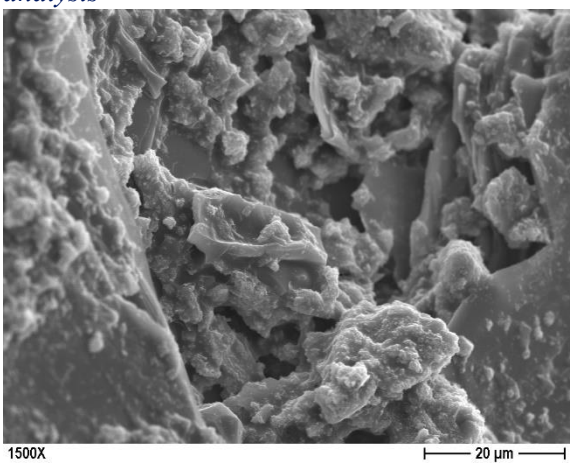

Image 62 SEM image of Sample 1 at 1500x magnification, captured during analysis

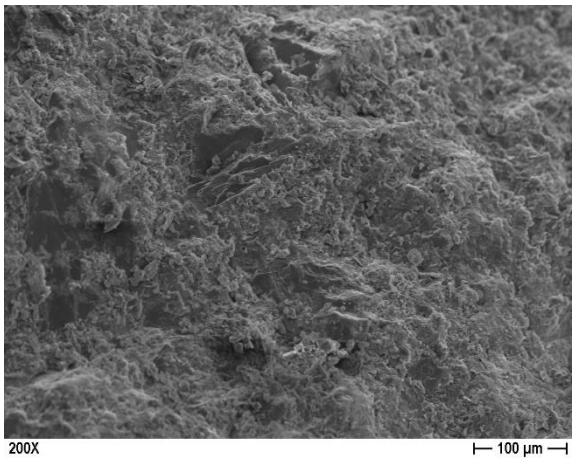

Image 59. SEM image of Sample 1 at 200x magnification, captured during analysis

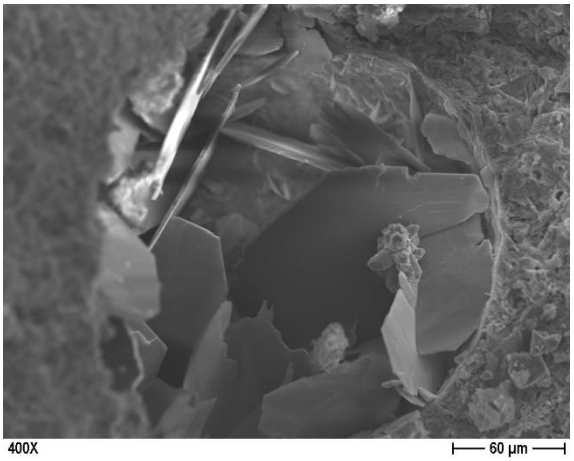

Image 63. SEM image of Sample 1 at 400x magnification, captured during analysis

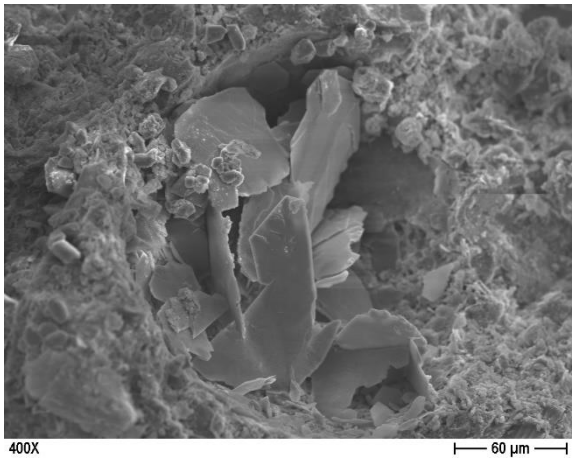

Image 64 SEM image of Sample 1 at 400x magnification, captured during analysis

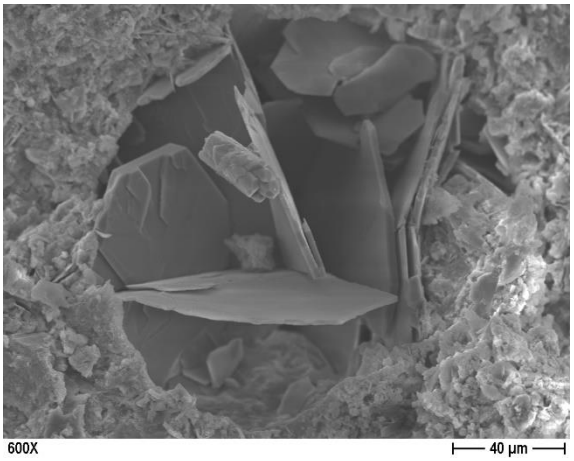

Image 65. SEM image of Sample 1 at 600x magnification, captured during analysis

The microstructural analysis of the sample, prepared with a water-to-cement (w/c) ratio of 0.38 using traditional casting methods and incorporating 5% biochar, revealed the presence of characteristic hydration products, in particular calcium silicate hydrate (C-S-H) and portlandite (hexagonal crystals in pores in images 63-65)

An element identified in images64-65, during the SEM analysis was the presence of air voids in the matrix, which interrupted the material's consistency. These voids form pathways to the access of harmful agents such as as water and carbon dioxide[301]. Moreover, the gathering of portlandite crystals near the voids indicates that these areas may act as strategic location for hydration products. However, air voids may impact negatively structural performance, as it reduces the material's resistance to mechanical stresses, potentially initiating crack formation and propagation.

Additionally, the integration of 5% biochar into the cementitious matrix presented challenges in achieving an effective binding with the cement paste. SEM imaging highlights in images 54-56 and 59,62, biochar particles, some of them poorly bound to the the cement paste (images 60)

[301] **Specificata fonte non valida.**

SAMPLE 2. Sample with a water-to-cement (w/c) ratio of 0.40 and produced through traditional casting methods.

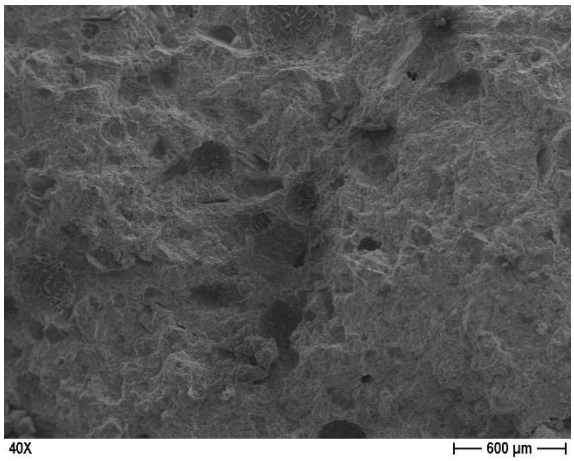

Image 66 SEM image of Sample 2 at 40x magnification, captured during analysis

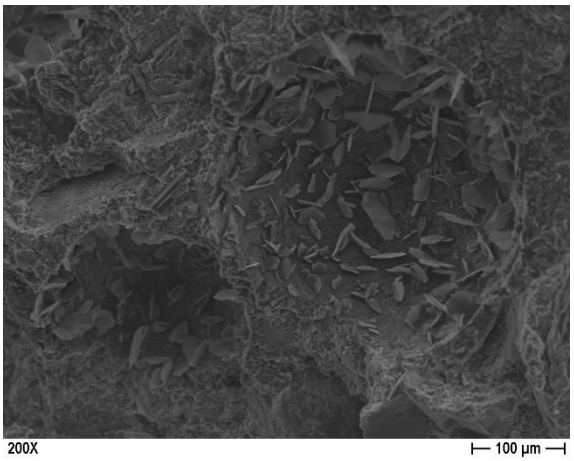

Image 67. SEM image of Sample 2 at 200x magnification, captured during analysis

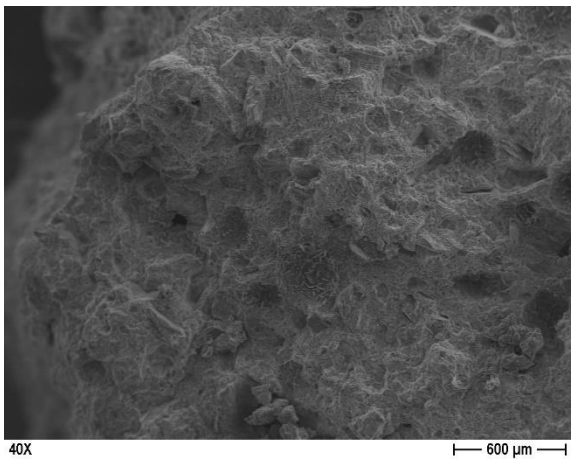

Image 68. SEM image of Sample 2 at 40x magnification, captured during analysis

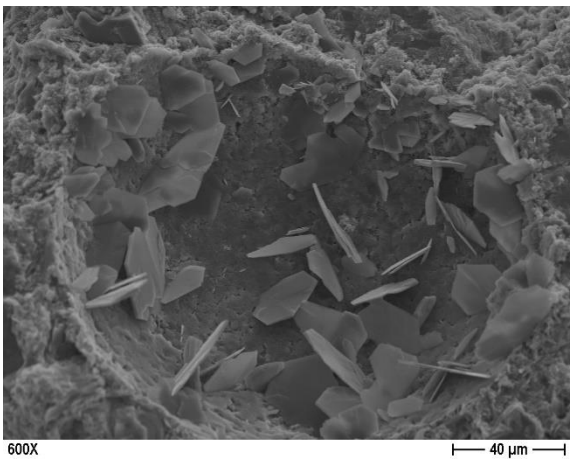

Image 69. SEM image of Sample 2 at 600x magnification, captured during analysis

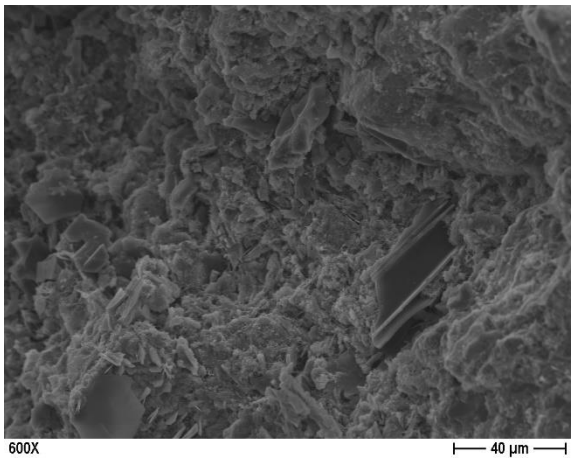

Image 70. SEM image of Sample 2 at 600x magnification, captured during analysis

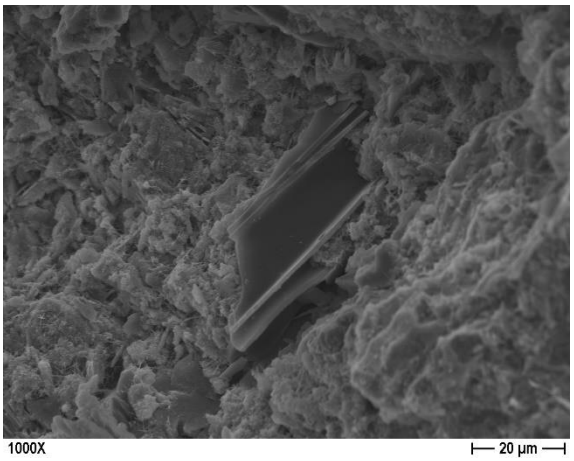

Image 71. SEM image of Sample 2 at 1000x magnification, captured during analysis

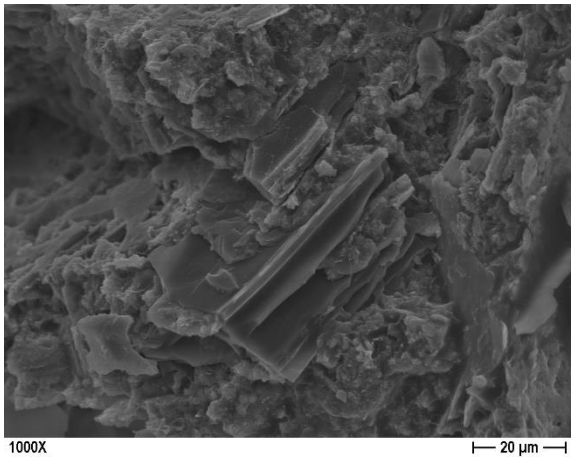

Image 72. SEM image of Sample 2 at 1000x magnification, captured during analysis

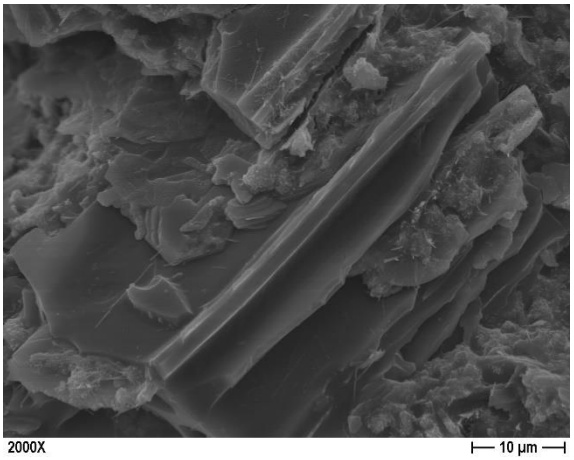

Image 73. SEM image of Sample 2 at 2000x magnification, captured during analysis

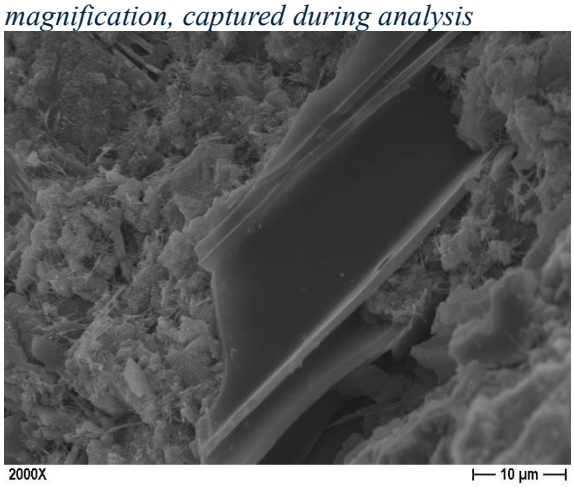

Image 74. SEM image of Sample 2 at 2000x magnification, captured during analysis

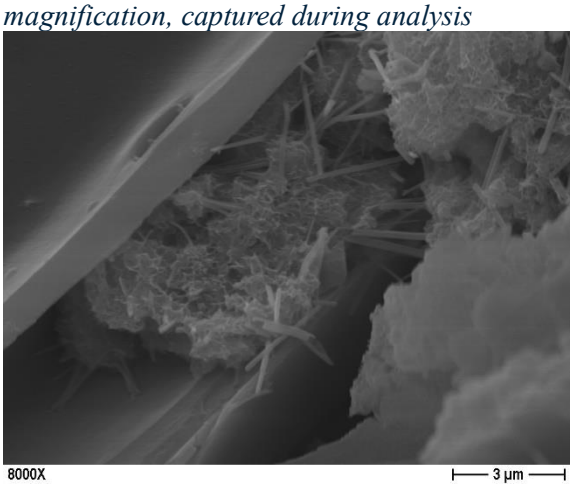

Image 75. SEM image of Sample 2 at 8000x magnification, captured during analysis

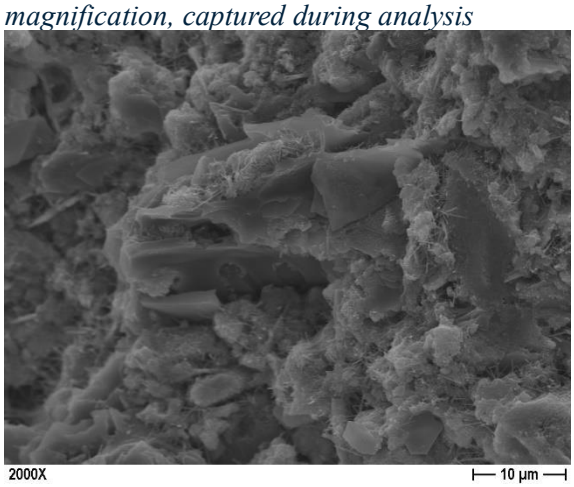

Image 76. SEM image of Sample 2 at 2000x magnification, captured during analysis

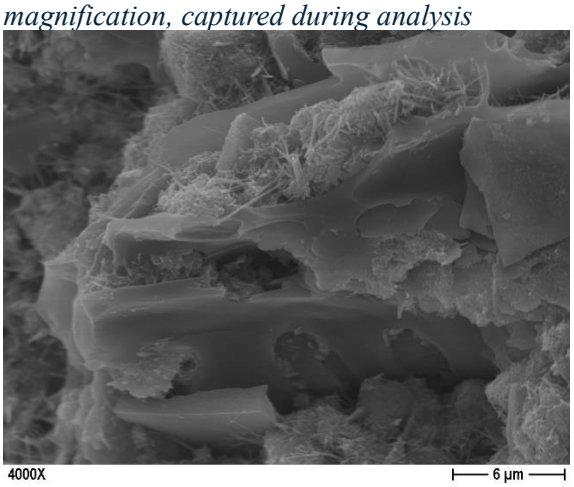

Image 77. SEM image of Sample 2 at 4000x magnification, captured during analysis

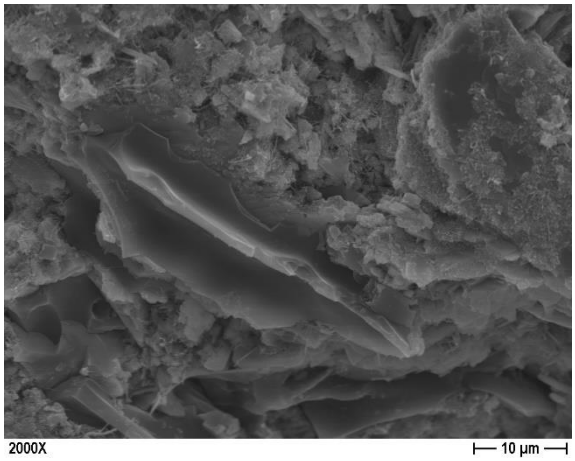

Image 78. SEM image of Sample 2 at 2000x magnification, captured during analysis

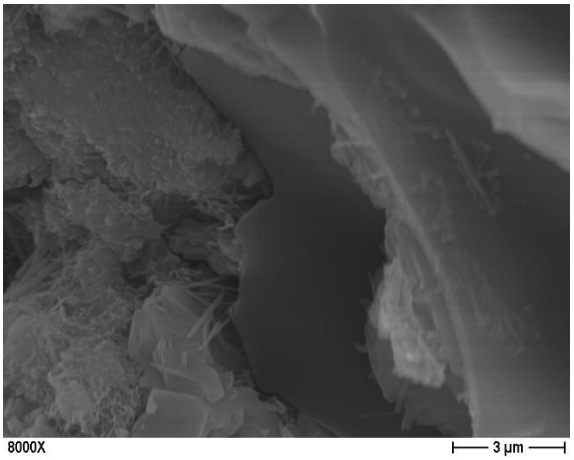

Image 79. SEM image of Sample 2 at 8000x magnification, captured during analysis

The sample, with a water-to-cement (w/c) ratio of 0.40, prepared through traditional casting methods with biochar's addition of 5%, highlights important details of the material's microstructure and compositional properties. The SEM observations highlight the presence of calcium silicate hydrate (C-S-H) in image 76-77, which is indispensable for the strength and durability of cementitious materials. In addition, portlandite ($Ca(OH)_2$) is detected in pores in images 67-69 The identification of C-S-H and portlandite confirms the expected hydration reactions in the cementitious matrix.

However, porosity as a main characteristic of biochar, was visible through their channels in images72-77. While the biochar particles are rather well dispersed throughout the matrix, they demonstrate limited adhesion to the cementitious materials. This lack of bonding is likely due to the biochar's surface characteristics, which appears incompatible with the cement's chemical composition. As a result, the biochar struggles to form a chemical bond, leading to a low seamless connection between the biochar and the cement as can be identified in image 77.

SAMPLE 3. Sample with a water-to-cement (w/c) ratio of 0.36 and produced through 3D printing (nozzle 2 mm) method.

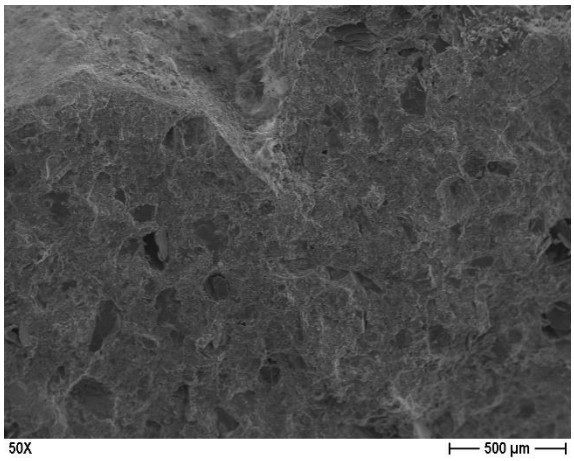

Image 80. SEM image of Sample 3 at 50x magnification, captured during analysis

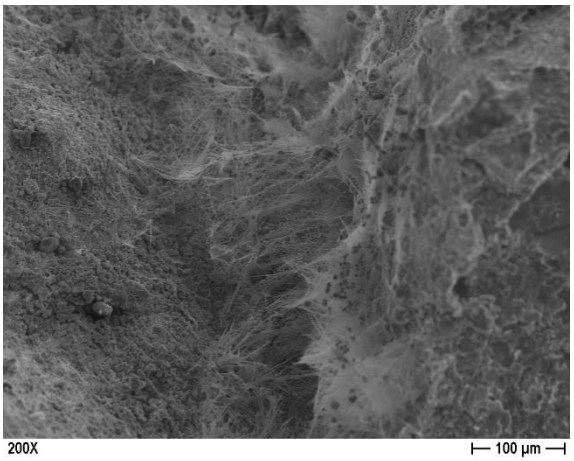

Image 81. SEM image of Sample 3 at 200x magnification, captured during analysis

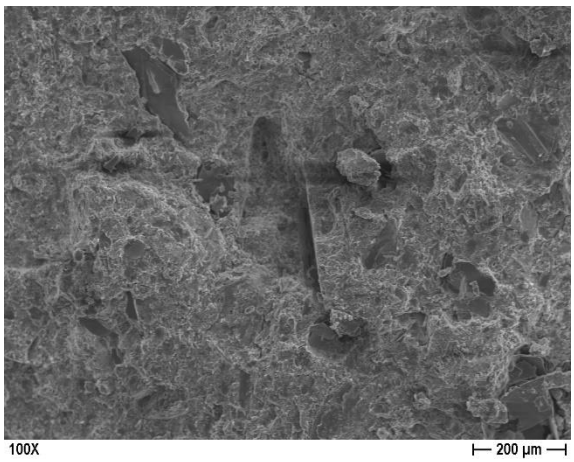

Image 82. SEM image of Sample 3 at 100x magnification, captured during analysis

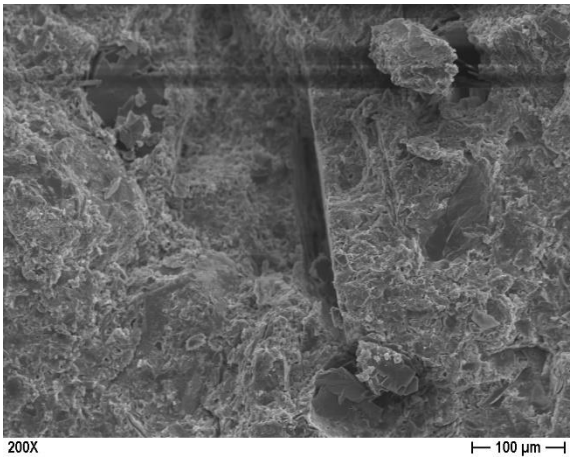

Image 83. SEM image of Sample 3 at 200x magnification, captured during analysis

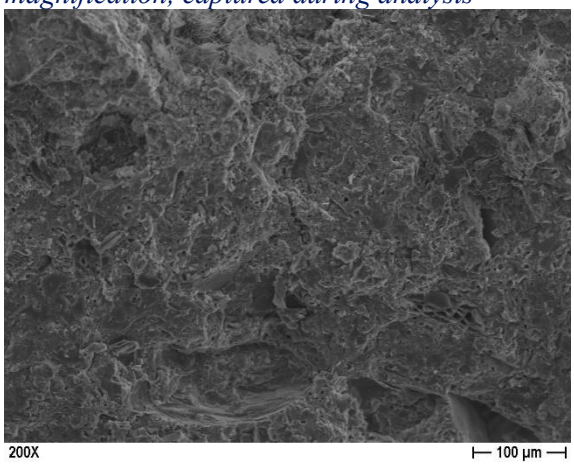

Image 84. SEM image of Sample 3 at 200x magnification, captured during analysis

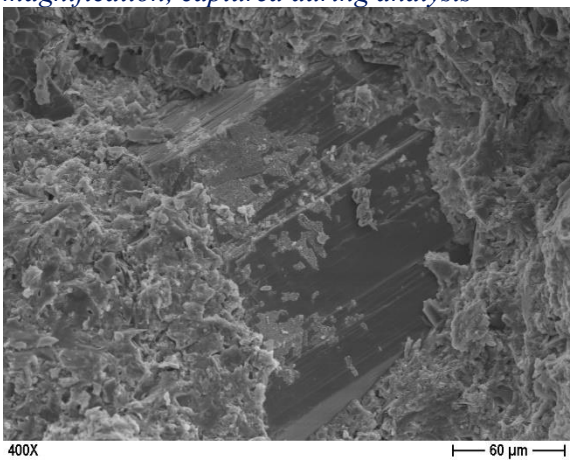

Image 85. SEM image of Sample 3 at 400x magnification, captured during analysis

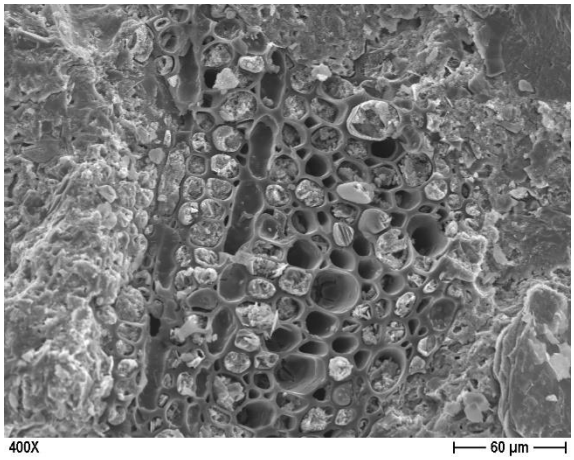

Image 86. SEM image of Sample 3 at 400x magnification, captured during analysis

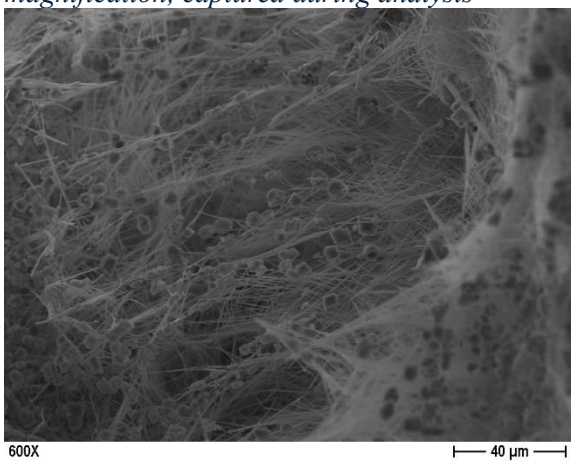

Image 87. SEM image of Sample 3 at 600x magnification, captured during analysis

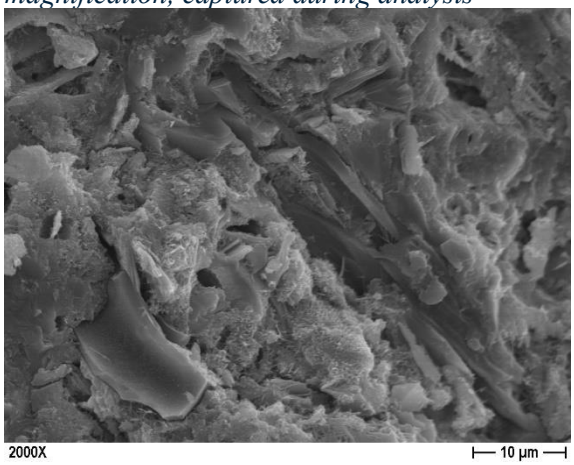

Image 89. SEM image of Sample 3 at 2000x magnification, captured during analysis

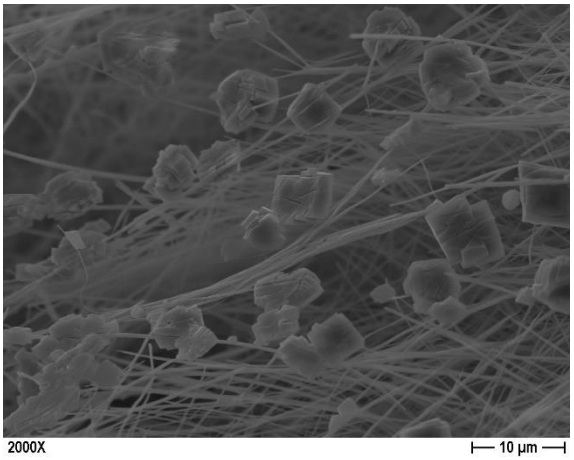

Image 88 SEM image of Sample 3 at 2000x magnification, captured during analysis

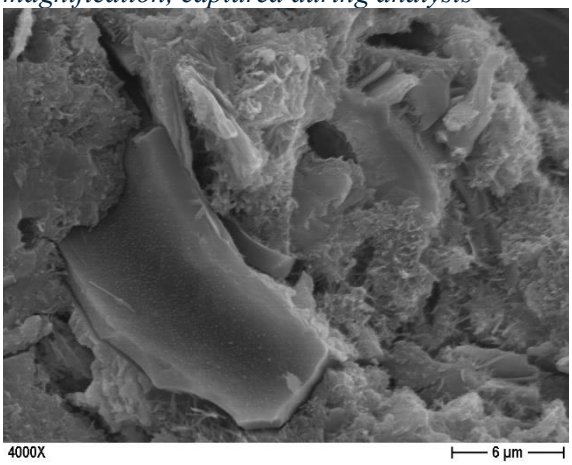

Image 90 SEM image of Sample 3 at 4000x magnification, captured during analysis

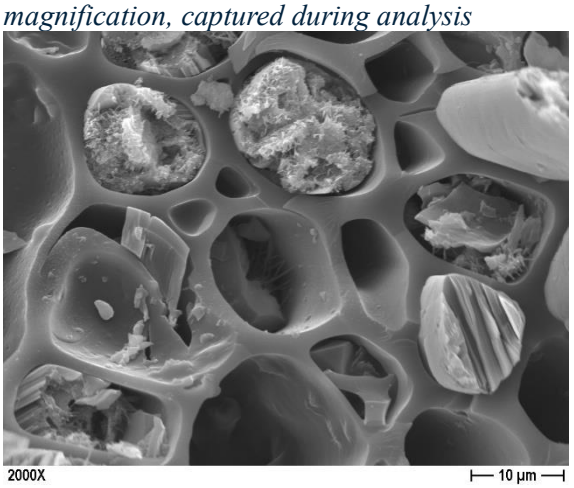

Image 91. SEM image of Sample 3 at 2000x magnification, captured during analysis

The SEM observations conducted for the 3D printed sample with a w/c ratio of 0.36 and 5% biochar incorporation reveals characteristics that are markedly different from those seen in traditional casting approaches. One such observation evidenced an apparent gap or interface between two printed layers, which was regarded as a defect in the material (images 82-83). This defect can have important implications in terms of the mechanical performance of the composite material

since the layers may not always be well-bonded in the 3D printing process, as highlighted, which represents a weak point within the material.

The results showed again the presence of portlandite ($Ca(OH)_2$) (iamges81,87,88). Portlandite crystals are converted from portlandite to calcium carbonate ($CaCO_3$) are seen in images 87 and 88. Specifically, this consists of portlandite interacting with the CO_2 present in the environment, developing a progressively more cubic structure in comparison to normal hexagonal portlandite crystals. Moreover, the most porous areas of the sample (located where carbonation of portlandite had taken place) showed typical long needles of ettringite (images87-88).

Finally, the SEM images provided detailed observations of the biochar's distribution within the cementitious matrix. Images 86-91 clearly show the porous structure of biochar, with visible hydration products of cement paste passing through the channels. In image 88, a closer look at these channels shows that while some elements from the cement matrix are penetrating the biochar, large parts of the space remain unfilled with cement particles, which indicates weak bonding between the biochar and the surrounding cementitious material. Image 90 further displays this problem; these sections didn't totally bind with the material, leaving voids. These findings indicate that the biochar has limited adhesion to the cement matrix, probably because of chemical incompatibility, and this may be detrimental to the mechanical performance and durability of the 3D-printed cementitious composite. These findings highlight the importance of improving biochar-cement compatibility to optimize the material's properties for enhanced performance.

SAMPLE 4. Sample with a water-to-cement (w/c) ratio of 0.36 and produced through traditional casting method.

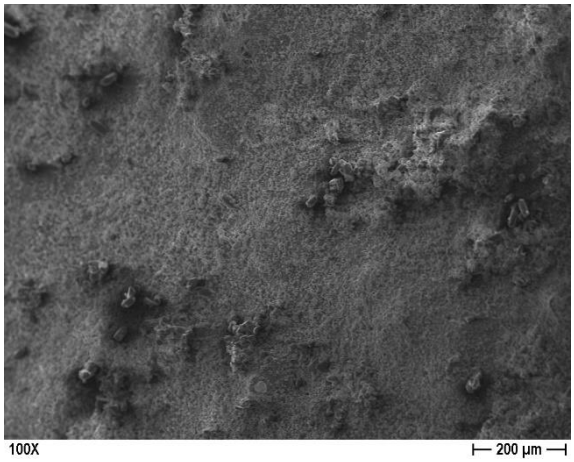

Image 92 SEM image of Sample 4 at 100x magnification, captured during analysis

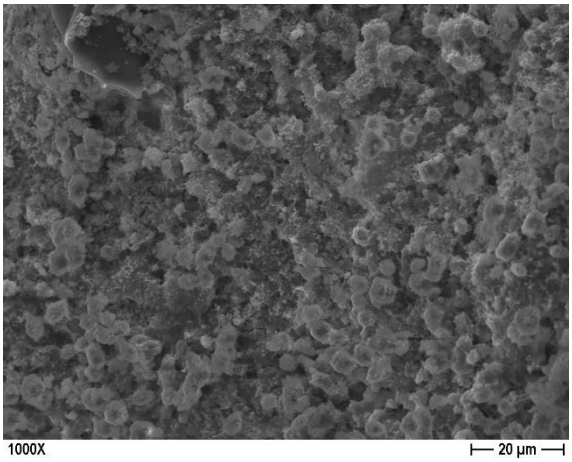

Image 93 SEM image of Sample 4 at 1000x magnification, captured during analysis

Image 94 SEM image of Sample 4 at 200x magnification, captured during analysis

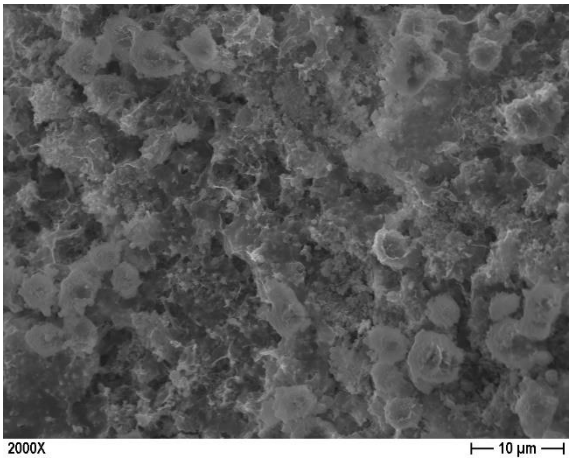

Image 95 SEM image of Sample 4 at 2000x magnification, captured during analysis

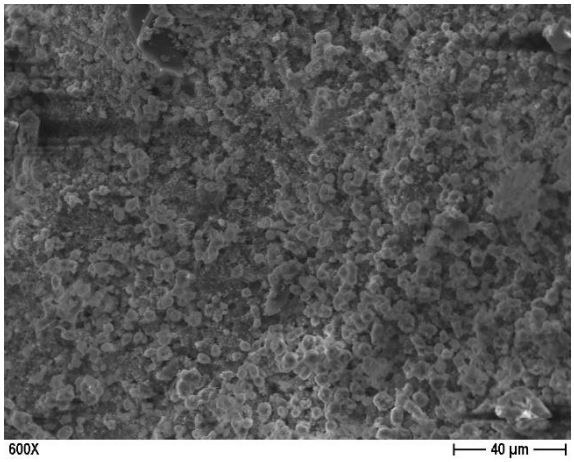

Image 96. SEM image of Sample 4 at 600x magnification, captured during analysis

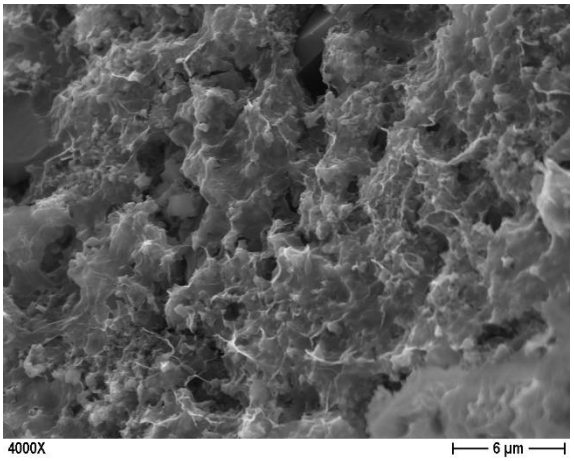

Image 97. SEM image of Sample 4 at 4000x magnification, captured during analysis

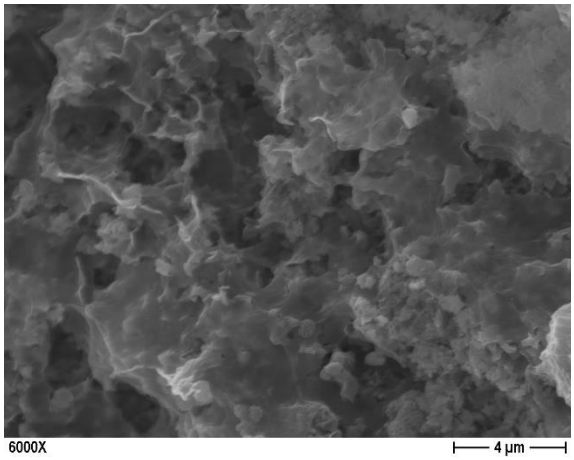

Image 98 SEM image of Sample 4 at 6000x magnification, captured during analysis

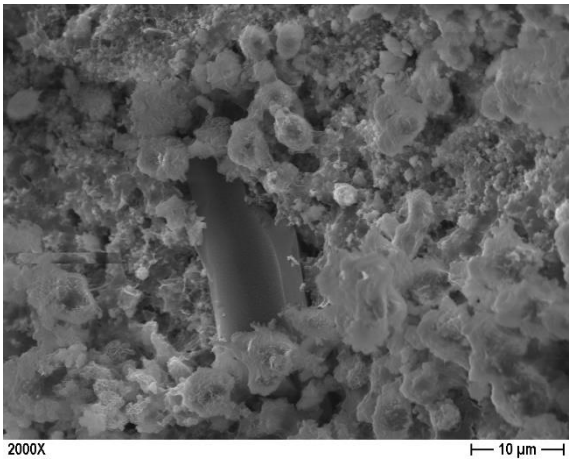

Image 99 SEM image of Sample 4 at 2000x magnification, captured during analysis

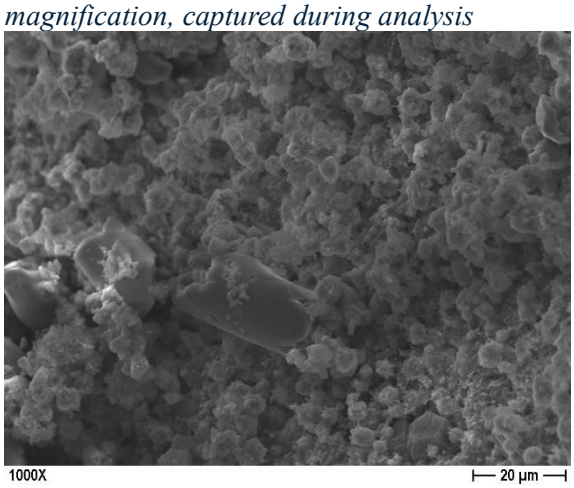

Image 100 SEM image of Sample 4 at 1000x magnification, captured during analysis

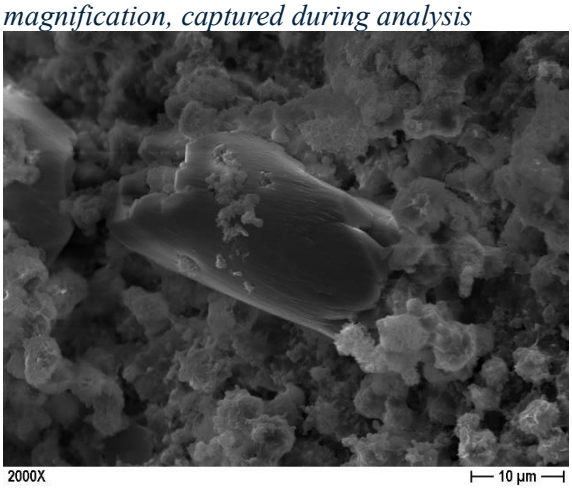

Image 101 SEM image of Sample 4 at 2000x magnification, captured during analysis

The sample with a water to cement (w/c) ratio of 0.36 prepared by the traditional casting method was analyzed with the help of SEM. The most outstanding findings evident from images 92-95 were the abundant presence of calcium carbonate crystals ($CaCO_3$). This indicates that portlandite ($Ca(OH)_2$) in the cement matrix has reacted chemically with atmospheric CO_2, a prevalent phenomenon in cementitious materials. Additionally, biochar particles were identified throughout the matrix; they displayed minimal attachment to the surrounding cementitious components, as already observed in the previous samples (images 99-101).

The observation was complicated to perform as the sample had insufficient metallization, which created challenges during SEM imaging. The inadequate conductive coating led to a reduction in the quality and clarity of the observations. Despite these difficulties, it was evident that the sample exhibited an elevated level of porosity throughout all analyzed areas. This pervasive porosity not only facilitates carbonation but also reduces the material's structural integrity, providing pathways for potentially harmful agents to penetrate and degrade the matrix.

SAMPLE 5. Sample with a water-to-cement (w/c) ratio of 0.38 and produced through 3D printing (nozzle 2 mm) method.

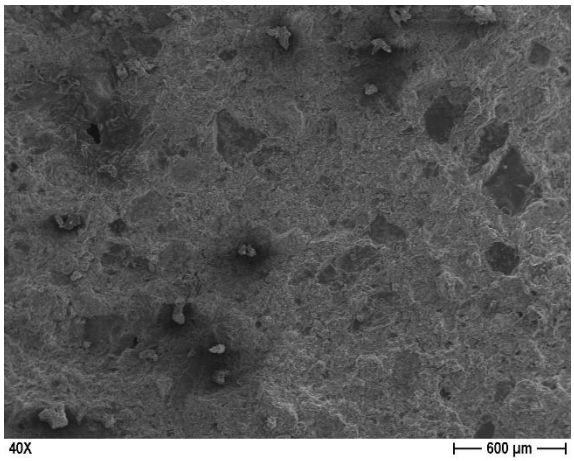

Image 102 SEM image of Sample 5 at 40x magnification, captured during analysis

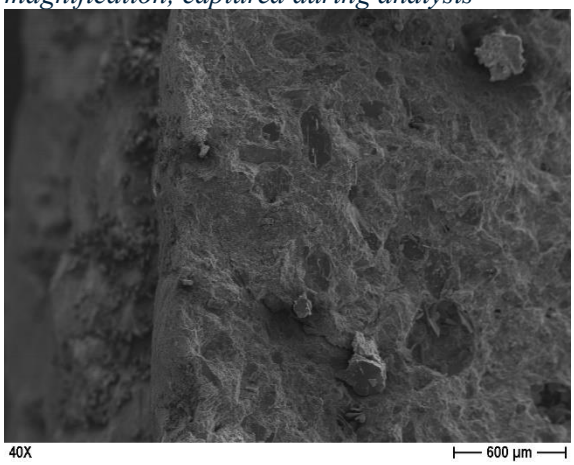

Image 103 SEM image of Sample 5 at 40x magnification, captured during analysis

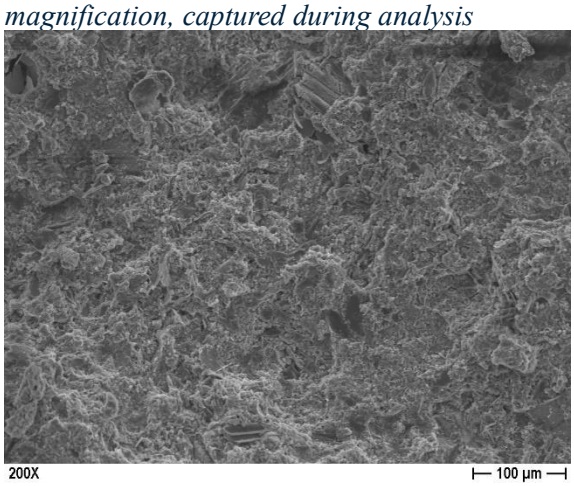

Image 104 SEM image of Sample 5 at 200x magnification, captured during analysis

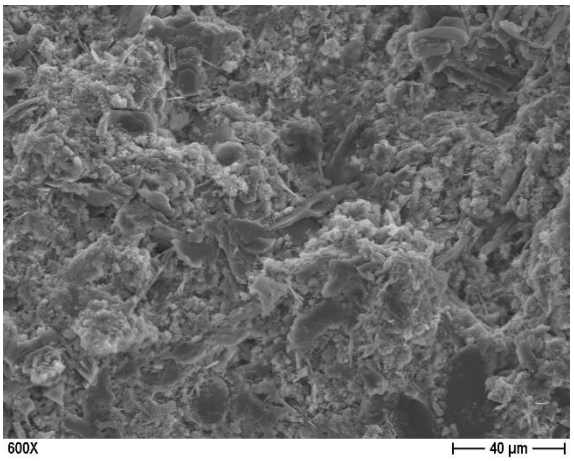

Image 105 SEM image of Sample 5 at 600x magnification, captured during analysis

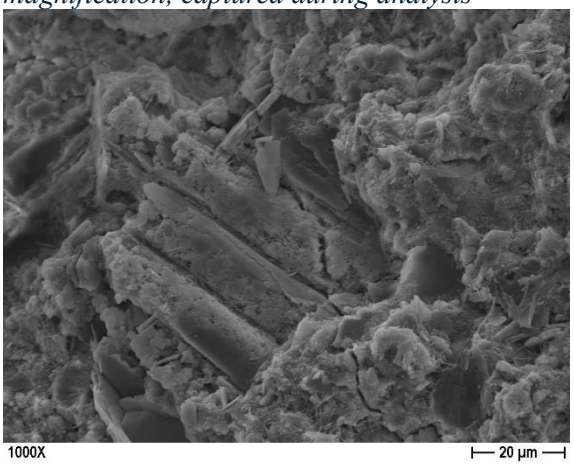

Image 106 SEM image of Sample 5 at 1000x magnification, captured during analysis

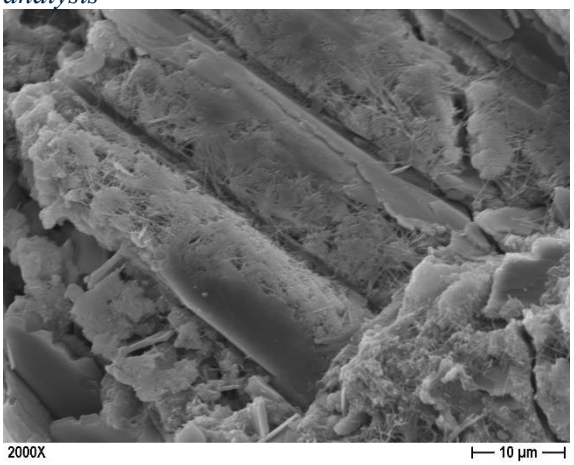

Image 107 SEM image of Sample 5 at 2000x magnification, captured during analysis

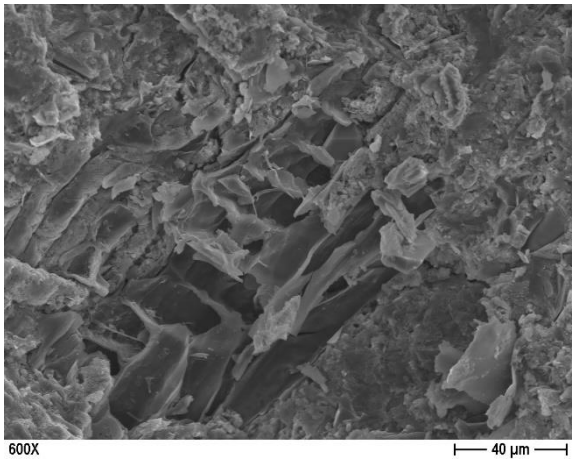

Image 108 SEM image of Sample 5 at 600x magnification, captured during analysis

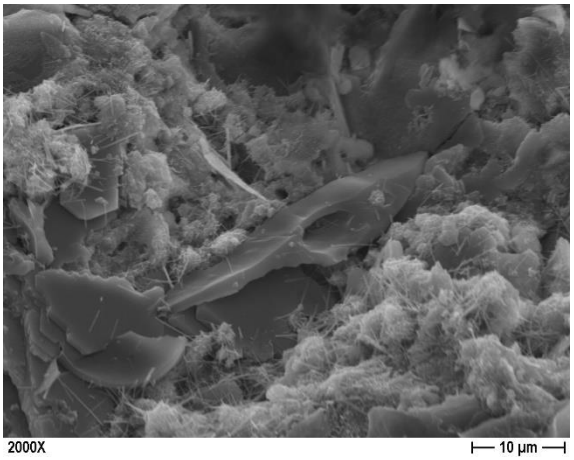

111 SEM image of Sample 5 at 2000x magnification, captured during analysis

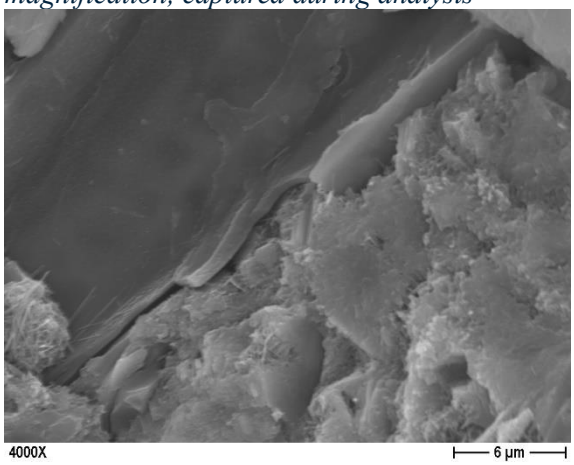

Image 109 SEM image of Sample 5 at 4000x magnification, captured during analysis

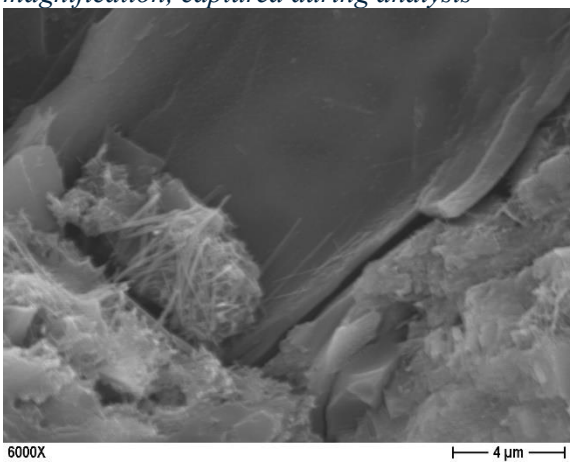

112 SEM image of Sample 5 at 6000x magnification, captured during analysis

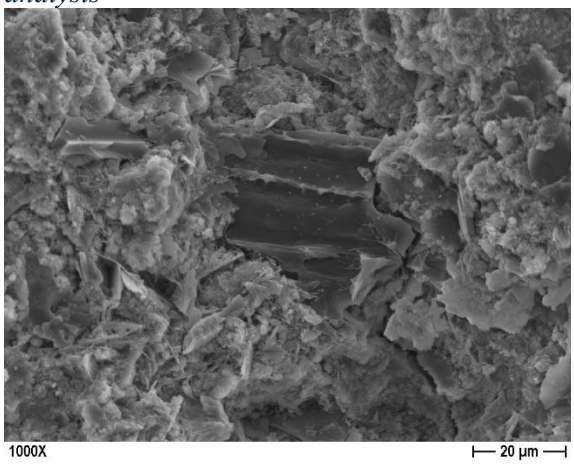

Image 110 SEM image of Sample 5 at 1000x magnification, captured during analysis

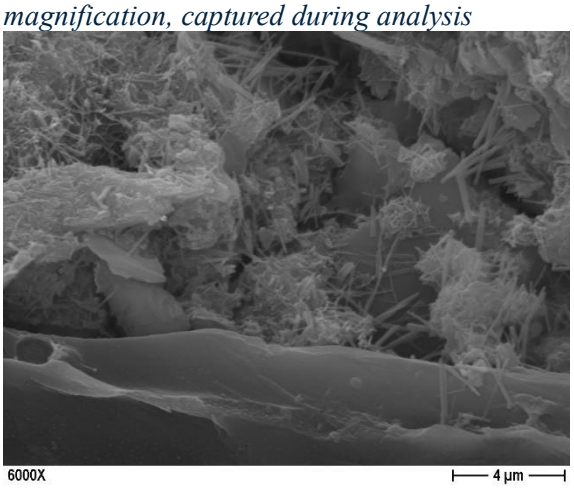

113 SEM image of Sample 5 at 6000x magnification, captured during analysis

In this analysis, a 3D-printed w/c ratio of 0.38 sample was evaluated, with a modified printing orientation compared to the previous sample. In this case, the layers were placed in a non-transversal section, resulting in a different perspective, as shown in Image 103. Unlike the previous transversal section, where gaps between layers were clearly visible, this new orientation annuls any perceptibility of gaps, and the sample appeared more integrated. As shown in Image 102, the layers were well-bonded, with fewer visible air voids. This improvement in layer attachment reflects a uniform distribution of material during the 3D printing process, facilitating better layer fusion. Additionally, as perceived in Images 106-113, the distribution of biochar appeared homogenous throughout the cement matrix. As previously observed, biochar particles are only partially covered by the hydrated cement paste products (Images 52-110)

Moreover, some fractures were observed in the sample, particularly in Images 109-110. However, it was difficult to determine whether these fractures resulted from the mechanical testing or occurred during the preparation of the sample for SEM analysis, where the sample was broken into smaller pieces. The fractures seem to follow an irregular path, sometimes contouring, sometimes fracturing biochar particles.

SAMPLE 6. Sample with a water-to-cement (w/c) ratio of 0.40 and produced through 3D printing (nozzle 2 mm) method.

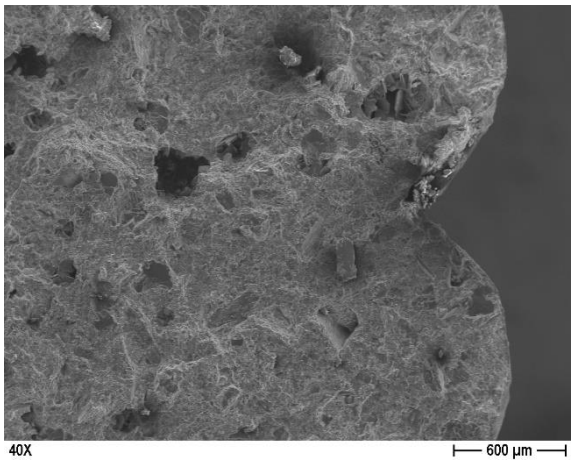

Image 114 SEM image of Sample 6 at 40x magnification, captured during analysis

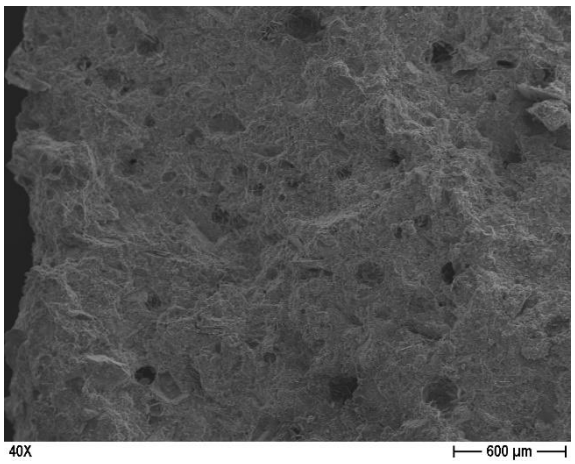

Image 115 SEM image of Sample 6 at 40x magnification, captured during analysis

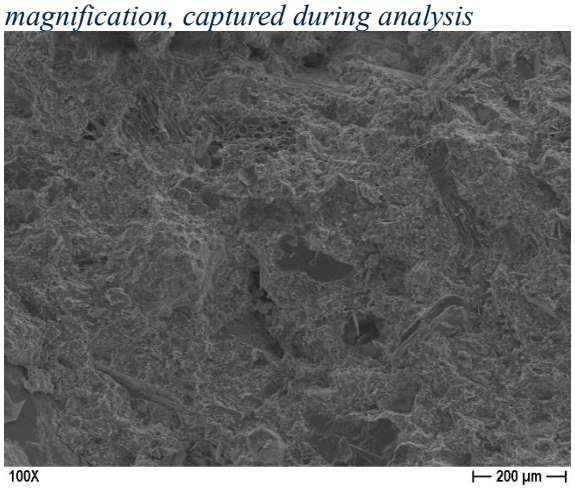

Image 116 SEM image of Sample 6 at 100x magnification, captured during analysis

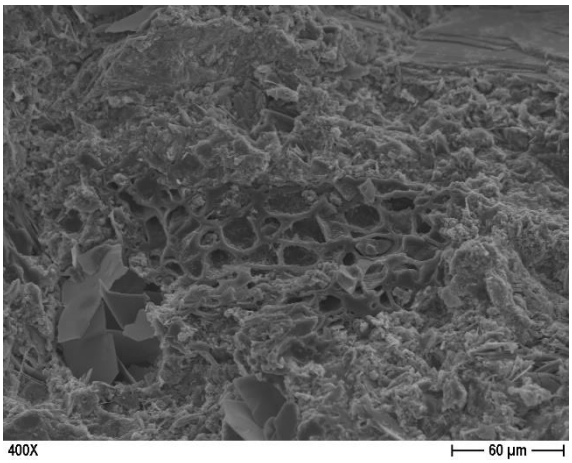

Image 117 SEM image of Sample 6 at 400x magnification, captured during analysis

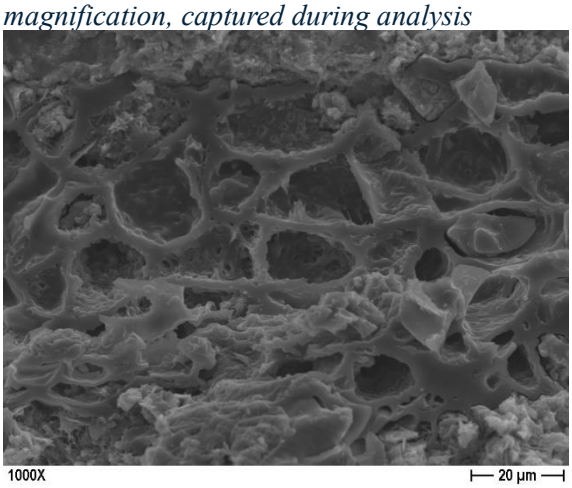

Image 118 SEM image of Sample 6 at 1000x magnification, captured during analysis

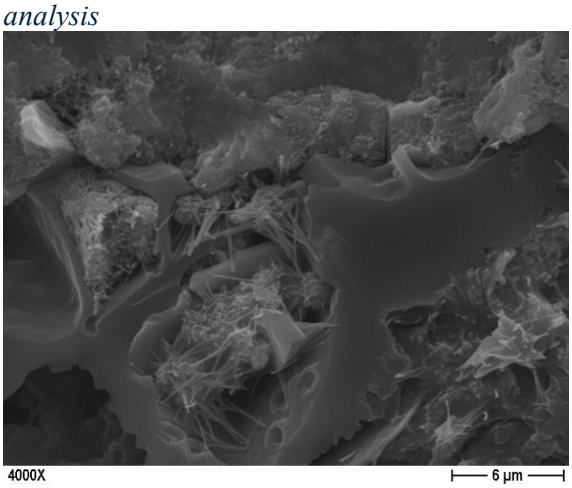

Image 119 SEM image of Sample 6 at 4000x magnification, captured during analysis

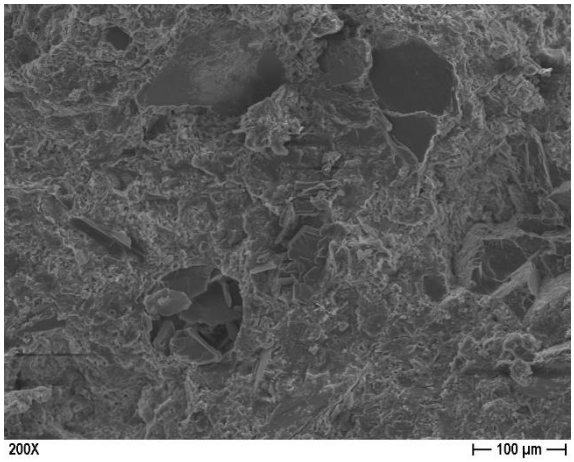

Image 120 SEM image of Sample 6 at 200x magnification, captured during analysis

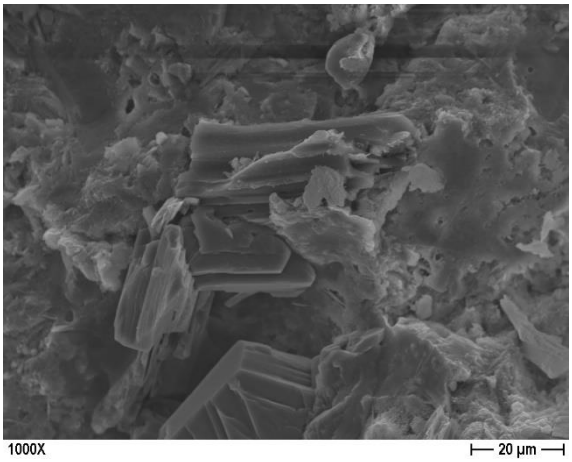

Image 122 SEM image of Sample 6 at 1000x magnification, captured during analysis

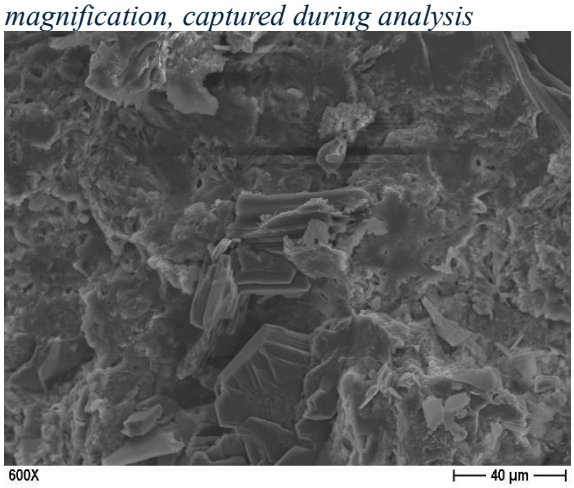

Image 121 SEM image of Sample 6 at 600x magnification, captured during analysis

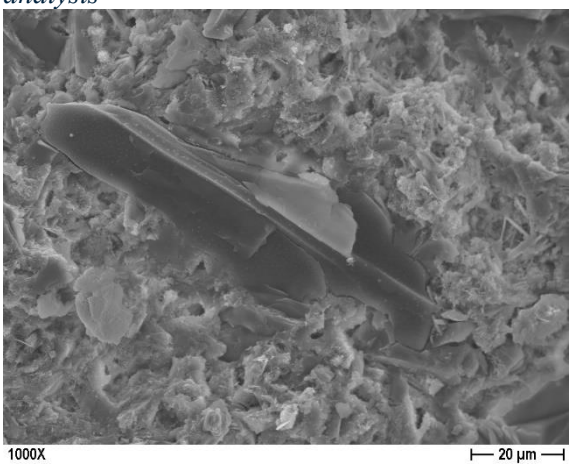

Image 123 SEM image of Sample 6 at 1000x magnification, captured during analysis

3D printed sample with a w/c ratio of 0.40 was examined, the positioning on the sample holder of the SEM was similar as sample 3 (image114). The SEM images shown in images 117, 121 and 123 illustrate a good dispersion of biochar within the cement matrix. Moreover, hydration products are surrounding biochar particles, such as portlandite (see Images 117 and 120), and C-S-H (image 119).

In Images 120-123, the biochar particles are distributed uniformly with sand particle surrounded by C-S-H and portlandite, providing structural support to the entire formed sample. Specifically, Image 119 shows a portion of biochar oriented longitudinally and completely enclosed by C-S-H and portlandite, all of which demonstrate that biochar particles are incorporated into the cementitious matrix, if not effectively bound to it.

AN OVERALL VIEW

The SEM observations of the six samples, three of them produced through the traditional casting and the other three performed via 3D printing, provided information on how biochar and varying water-to-cement (w/c) ratios can affect the microstructure of cement-based materials. This evaluation indicates significant differences in performance, structural integrity, and explains biochar integration within the cement matrix.

The traditional casting method, particularly for samples with w/c ratios of 0.38 (Sample 1) and 0.40 (Sample 2), demonstrated the typical hydration products of cement, such as calcium silicate hydrate (C-S-H) and portlandite, which are essential for the material's strength and durability. However, there were some struggles to incorporate biochar particles, as it was evident the poor bonding with cement matrix for both samples. The porous interface, along with problems such as porosity, air voids and carbonation, contribute long-term durability issues in these biochar-cement systems. The limited bonding provided by biochar contributed to minimal performance of these samples.

The 3D-printed samples (Samples 3, 5, and 6), however, demonstrated distinguishing characteristics. These samples showed a better integration of biochar within the cement matrix (especially in Sample 5 and 6) with a more homogeneous distribution of biochar particles. Regardless of whether it has been printed in layers, the material morphology is more homogeneous and with less void space at least perceptible. Hydration products like portlandite and C-S-H were more homogenously distributed around the biochar particles which may improve the overall mechanical properties of the material. Some minor defects, such as air voids and poor layer bonding in Sample 3 and Sample 6 were visible. Though these imperfections were significant, they did not majorly impact the overall material quality.

Though all samples show consistent signs of carbonation, this phenomenon appears to be greatest at areas of higher porosity. The positive effects of biochar in enhancing the performance of cement are clear, however mechanical properties are also dependent on biochar distribution within the matrix and its attachment to the cement matrix. The 3D printing process seems to have substantial advantages regarding the dispersion of biochar and the homogeneity of the material, which may result in improved mechanical performance.

Overall, results indicate that the 3D-printed samples had better biochar integration, hydration product distribution, and better material homogeneity than the cast samples, probably because of the extrusion process during printing. Sample 5 showed more uniform biochar distribution and better bonding between layers, thus reflecting the potential of 3D printing with biochar-cement composites. Nonetheless, both production methods still must be optimized to overcome problems with carbonation, and biochar–cement attachment that limit the durability of these materials.

SAMPLE	(w/c) Ratio	Production Method	Observations	Microstructural Characteristics	Hydration Products	Issues Identified	Challenges
SAMPLE 1	0.38	Traditional Casting	Poor biochar adhesion, carbonation of portlandite	Air voids disrupting consistency, carbonation in portlandite	C-S-H, portlandite $CaCO_3$	Poor biochar-cement bonding, surface carbonation, porosity	Weak adhesion between biochar and cement, reduced long-term durability due to carbonation
SAMPLE 2	0.40	Traditional Casting	Limited biochar integration	Biochar poorly bonded	C-S-H, portlandite $CaCO_3$	Poor bonding between biochar and cement	Increased porosity, low biochar-cement adhesion
SAMPLE 3	0.36	3D Printing (2 mm nozzle)	Layer bonding issues, porosity, biochar distribution	Weak bonding between biochar and cement, carbonation	Portlandite C-S-H $CaCO_3$	Layer bonding issues, weak biochar-cement bond	Inconsistent bonding between layers, potential weakness due to poor adhesion
SAMPLE 4	0.36	Traditional Casting	High carbonation, minimal biochar attachment	High porosity, carbonation, poor biochar integration	$CaCO_3$ C-S-H	Extreme carbonation, insufficient metallization	Porosity reducing structural integrity, poor adhesion between biochar and cement
SAMPLE 5	0.38	3D Printing (2 mm nozzle)	Improved layer bonding, good biochar distribution	Better adhesion of biochar, uniform distribution	C-S-H, portlandite	Minor fractures	Occasional fractures, but overall improvement in material structure
SAMPLE 6	0.40	3D Printing (2 mm nozzle)	Good biochar distribution, minimal defects	Uniform biochar distribution with C-S-H and portlandite	C-S-H, portlandite, $CaCO_3$	Minor irregularity	Biochar well integrated, but minor defects due to air voids during extrusion

Table 49 Summary chart of the SEM analysis highlighting the best-performing sample among all tested samples

Given this context, the research in this thesis explored the incorporation of biochar as a sustainable admixture to cementitious mixtures, the rationale for the selection lies in its potential to reduce cement content, thereby lowering CO_2 emissions, while enhancing the lifecycle performance of cement-based materials. Biochar's inclusion not only aligns with the principles of circular economy but also transforms what was traditionally considered waste into a valuable resource for construction. Biochar, a byproduct of the pyrolysis process used in biomass production, is derived from organic waste materials, such as wood, some of its benefits are its porous structure and electromagnetic properties allowing it to contribute to carbon sequestration while also offering environmental benefits, including the adsorption of heavy metals and organic pollutants, as well as electromagnetic shielding.

During the sample preparation process, several key factors were identified that significantly influenced the performance of the biochar-enhanced mixtures. Initial conclusions indicated the importance of handling biochar in a liquid state to ensure proper grinding and reduce particle size to approximately 250 μm, this particle size reduction and subsequent homogenization of materials were crucial in achieving better adhesion and cohesion within the mortar paste. This is done to ensure proper material management during this stage, ensuring a consistent and cohesive mixture, which was critical for successful mortar preparation.

Regarding admixtures, early trials revealed a significant incompatibility between superplasticizers and biochar as the chemical reaction between these components led to increased viscosity, which negatively impacted the workability and printability of the mortar paste. This issue caused the removal of superplasticizers from the formulation, instead, polyethylene glycol (PEG) proved to be a key component, providing the required flowability and workability to ensure the successful execution of the extrusion test and the production of printable samples. PEG's role was instrumental in achieving the correct mixture rheology for 3D printing while maintaining structural integrity.

From the mixture design phase, the optimal formulation emerged at the sample developed by a mixture with a 0.38 w/c ratio, a 0.95:1 s/c ratio, 5% biochar supplementation, and the inclusion of polyethylene glycol with a molecular weight of 10,000 g/mol, applied at a proportion of 2 grams per 10 grams of cement. This combination exhibited superior performance across key mechanical and rheological parameters, making it the most promising formulation for 3D printing applications.

The 0.38 w/c ratio was particularly effective in balancing workability and strength development, providing sufficient fluidity for extrusion while maintaining structural integrity. Meanwhile, the 0.95:1 s/c ratio ensured a cohesive and homogenous mixture, minimizing segregation and enhancing the mechanical stability of the printed layers. The 5% biochar addition not only reduced the cement content, thus lowering the environmental footprint, but also contributed to the material's durability and internal curing properties because of porous nature, which enhances water retention and hydration efficiency.

PEGs role was critical in this optimized design. By mitigating the viscosity issues observed in earlier trials with superplasticizers, PEG facilitated smoother extrusion and consistent layer adhesion during the printing process. Its molecular weight of 10,000 g/mol provided an ideal balance of lubrication and cohesion, ensuring the mortar's flowability without compromising its structural performance. This mixture allowed for successful 3D printing trials, demonstrating high cohesion between layers and minimal deformation during extrusion.

In relation to the mechanical properties results of both the three-point bending test and the compression test highlight that the mortar sample with a 0.38 water-to-cement w/c ratio

consistently achieved the highest mechanical performance, coming closest to meeting the EN normative thresholds for both flexural and compressive strength.

The analysis of the flexural strength results from the three-point bending test demonstrates that all samples, regardless of their production method, met the minimum strength requirements established by European standards. However, traditional cast samples consistently exhibited higher flexural strength values than their 3D-printed counterparts. For 3D printing, no clear correlation between the w/c ratio and tensile strength was observed, though the 0.38 w/c ratio sample printed with a 2 mm nozzle outperformed the others.

For the 3D printing tests, the results suggest that the reduction of nozzle size enhances the cohesion between printed layers, leading to better structural development and fewer weaknesses within the layers. Conversely, in traditional cast samples, variations in the w/c ratio did not significantly impact flexural strength, confirming that the tensile strength results remained relatively stable across different ratios. However, despite this stability, altering the w/c ratio can notably affect workability, which becomes critical in large-scale construction where precise handling and flowability are necessary.

In terms of compressive strength, the results showed that although none of the samples fully met the EN standard threshold of 30 MPa, traditional cast samples nearly achieved this benchmark. These samples exhibited double the compressive strength of 3D-printed samples, with the 0.38 w/c ratio again emerging as the most effective formulation.

As with flexural strength, no clear correlation was found between w/c ratio and compressive strength in 3D-printed samples. However, the 2 mm nozzle yielded better compressive results compared to the larger nozzle size, likely due to improved layer cohesion and reduced porosity in the printed structure. In traditional casting, the 0.38 w/c ratio sample also recorded the highest compressive strength, confirming its superior performance across both mechanical tests.

Overall analysis of mechanical testing indicates that the tested mixtures exhibit higher compressive strength than flexural strength, but the flexural strength were nearest to the standard threshold than the compression ones suggesting their potential use in horizontal structural elements such as beams, both 3D-printed and traditionally cast samples demonstrated sufficient flexural performance for such applications. Even though the use of biochar-modified mortars in vertical structural elements remains viable only for traditional casting, the compressive strength of 3D-printed samples falls below acceptable thresholds.

The granulometry and SEM (Scanning Electron Microscopy) analyses played an important role in validating the reliability of the experimental procedures and providing a deeper understanding of the mortar's microstructural behavior.

The granulometry analysis provided critical insights into the particle size distribution of the mortar mixture, essential for ensuring workability and flowability in 3D printing applications. Although a margin of error remains due to the challenges posed by the small particle size and the irregular shapes of particles, which can lead to discrepancies between the actual particle size and the measured values, the results were overall satisfactory. Most particles fell within or near the target size range, indicating that the grinding and sieving processes were conducted effectively, achieving a small and uniform particle size was crucial, as it directly enhanced the flowability of the mortar, ensuring smoother extrusion and consistent layer deposition during 3D printing. This success in particle size refinement supports the feasibility of using biochar as a fine aggregate while maintaining the necessary properties for 3D printing.

The SEM analysis provided valuable insights into the microstructural integrity of the mortar post-curing. Key aspects examined included the presence of bubbles, fractures, chemical reactions, and the cohesion and adhesion of the composite materials. Any fractures detected were attributed

to mechanical testing performed prior to the STEM analysis, indicating a successful curing process and a well-executed methodology. Biochar distribution from the SEM observations confirmed the uniform distribution of biochar throughout the mortar matrix. This event highlights the effectiveness of the mixing process, ensuring that the biochar is well integrated into the composite.

The analysis revealed the formation of essential hydration products such as Calcium Silicate Hydrate (C-S-H), portlandite ($Ca(OH)_2$), and ettringite, which are critical to the mechanical strength of cementitious materials. Furthermore, the interaction between the mortar's outer surfaces and the external environment led to the development of calcium carbonate. This is a common reaction in cementitious materials exposed to air, indicating natural carbonation.

Despite the biochar's uniform distribution, the analysis indicated a lack of chemical compatibility between the biochar and the cement matrix. Like traditional aggregates, biochar did not form significant chemical bonds with the surrounding materials, suggesting that its role in the mixture is primarily physical filling rather than chemical binding. This lack of cohesion could potentially impact on the long-term durability and strength of the material, requiring further research into how biochar can be chemically modified or combined with other admixtures to improve compatibility.

This research demonstrated that integrating biochar into cementitious mixtures can lead to promising advancements in the field of sustainable construction materials. By substituting a portion of cement with biochar, not only is the cement's carbon footprint reduced, but the resulting material also shows potential for enhanced durability and long-term environmental benefits. These findings reinforce the necessity of continuing to develop and implement innovative materials that address both environmental concerns and the mechanical performance demands of the construction industry.

This thesis contributes to the growing body of knowledge that supports the shift towards a sustainable construction paradigm, providing a pathway for future research and practical applications in reducing the environmental impact of cement while meeting the industry's performance expectations. By bridging the gap between sustainability goals and technological advancements, this study contributes to the ongoing transformation of the construction industry into a more resilient, responsible, and future-ready sector.

OBSERVATIONS AND FURTHER APPLICATION

This optimized mixture design offers a significant step forward in the development of sustainable 3D-printable cementitious materials. By demonstrating that a combination of biochar supplementation and PEG-based admixture optimization can achieve both environmental benefits and mechanical performance, this research opens the door for broader adoption of eco-friendly construction technologies. Future research could explore further refinements in biochar particle size, alternative admixture formulations, and scaling up for larger structural applications, additionally, long-term durability studies and environmental impact assessments will be crucial in validating the feasibility of this mixture in real-world construction scenarios.

While conventional casting outperformed 3D printing in mechanical tests, it is important to recognize that 3D concrete printing remains a relatively new and evolving technology. Improvements in printing accuracy, layer cohesion, and mixture design are necessary to close the performance gap. Future research should focus on optimizing mixture formulations, including adjustments to biochar content, admixtures, and printing parameters, to enhance the structural integrity and mechanical properties of 3D-printed mortars. With continued experimentation, it is likely that 3D printing will become a viable, sustainable alternative for a broader range of structural applications.

Based on the outcomes of this study, several key areas for future research and practical applications have been identified to improve the performance of biochar-enhanced 3D-printed mortars and explore their broader use in construction. To advance the structural capabilities of 3D-printed mortar, future research should focus on enhancing the mixture design efficiency to accommodate smaller nozzle diameters (1.5 mm or 1 mm). Successfully printing with smaller nozzles could improve layer cohesion and precision, resulting in more compact structures. And mechanical performance, as smaller nozzles typically lead to better layer bonding and increased density, potentially boosting both flexural and compressive strengths.

A critical next step is the examination of the long-term impact of biochar in mortar. Future studies should investigate durability over time, understanding how biochar-enhanced mortar performs over extended periods will behave. Impacts of weathering and environmental exposure, evaluating the mortar's resistance to environmental factors such as moisture, freeze-thaw cycles, and carbonation. And aging tests, performing mechanical tests at various curing stages (e.g., 7 days, 28 days, and 56 days) to track changes in mechanical strength development over time, helping to clarify the long-term hydration and microstructural stability of the biochar-mortar system.

For practical applications, integrating this biochar-enhanced mortar into reinforced concrete systems could be the key to reaching the required structural thresholds. Reinforced concrete could benefit from improved flexural and compressive strengths through enhanced mixture designs, potentially enabling the biochar mortar to serve as structural-grade material. And hybrid solutions combining 3D-printed elements and traditional reinforcements to leverage the strengths of both technologies for structural projects.

Innovative future applications could also involve using biochar-mortar for 3D-printed capsules designed for self-healing concrete. This approach could introduce biochar-based capsules into concrete mixtures that release self-healing agents when cracks form, improving concrete's durability and lifespan. This type of application also reduces maintenance costs by minimizing crack propagation and promoting automatic repair of micro-damages, aligning sustainable construction goals. As part of the further development of self-healing concrete, this work investigates the implementation of 3D-printed mortar capsules intended for encapsulation of self-healing agents. They were manufactured with the same composition as the previous concrete matrix (0.38 w/c ratio, 5% biochar) in the form of capsules with dimensions of 5 cm high, 1 cm

in diameter, and a nozzle of 2 mm thickness. The capsules were printed with a hollow cavity considered to be filled with self-healing agents (e.g., bacterial spores or chemical healing agents) and then integrated into a standard mortar sample.

Self-healing concrete is an innovation in construction materials, contributing to the ability to autonomously repair cracks that can threaten structural integrity. This feature in concrete was inspired by the natural self-healing ability found in concrete, such as autogenous healing (through the hydration of unreacted cement) or carbonation processes[302]. However, while it works with small fissures, it is less controllable for practical use than other healing systems, as it requires the presence of water. These limitations inspired the development of advanced self-healing concrete, using approaches like the introduction of bacteria, or other sealed healing substances[303].

An outstanding technique is microbial-induced calcite precipitation, where bacteria such as the *Bacillus* species are employed to produce calcium carbonate that successfully and sustainably fills cracks. Not only do these materials contribute to the durability of construction, but they also save on expenses and minimize the environmental footprint, integrating them into sustainable building. Such a method is beneficial to overcome problems like corrosion of reinforcement, usually caused by exposure to moisture and oxygen forced by cracks[304]. This feature would reduce repair needs, thus providing both economic and environmental benefits, which makes self-healing concrete an active research topic in the field of construction and materials science.

For this application the software documentation suggests software application and implementation. G-code files were developed in Simply 3D Slicing Software for the 3D printing to realize the capsule samples. These files were designed to control the 3D printer's movements and extrusion parameters, to obtain uniform samples. The use of G-code allows a precise layer-by-layer deposition, to reach the correct geometry and dimensions. As mentioned in the chapter of Samples Results, the software provided a digital simulation of the layer-by-layer printing process, which allows identify discrepancies that may need adjustment before transferring the file to the SD card for printing.

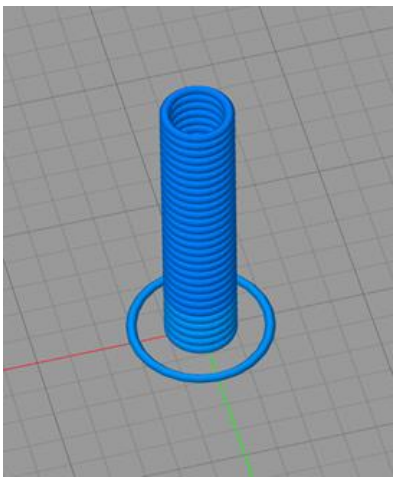

Figure 67 Simply 3D Slicing Software printing model of capsule
Source: (Author).

Below are going to be presented all the parameters that were established to obtain the 3D printing for 2 mm nozzle applied.

[302] **Specificata fonte non valida.**
[303] **Specificata fonte non valida.**
[304] **Specificata fonte non valida.**

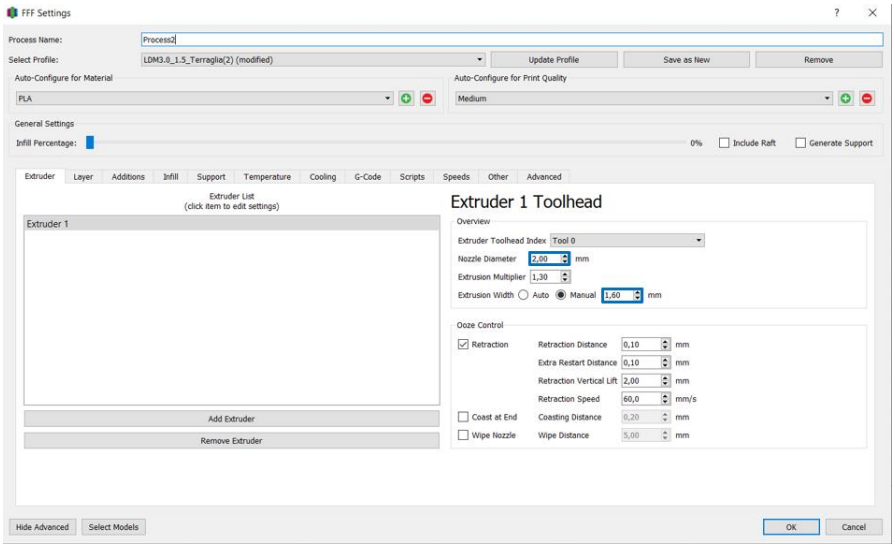

Figure 68 Simply 3D Slicing Software Speed tab parameters (2 mm nozzle).

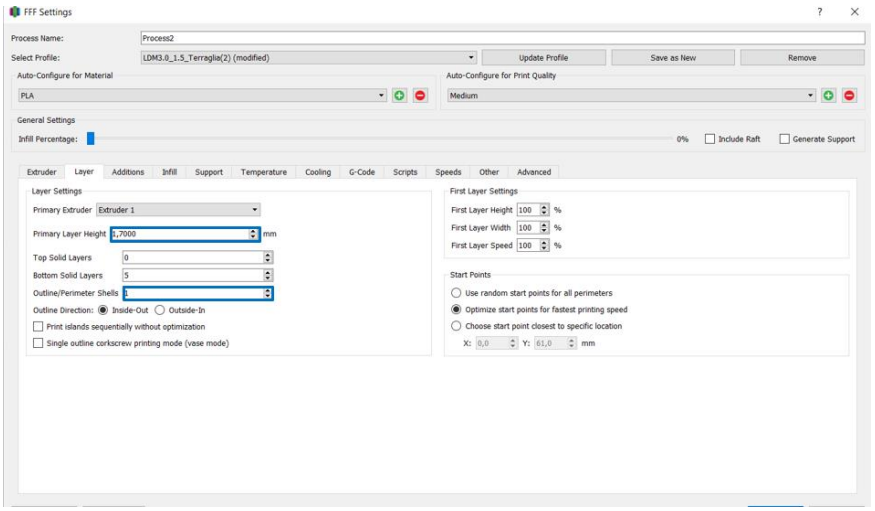

Figure 69 Simply 3D Slicing Software Speed tab parameters (2 mm nozzle).

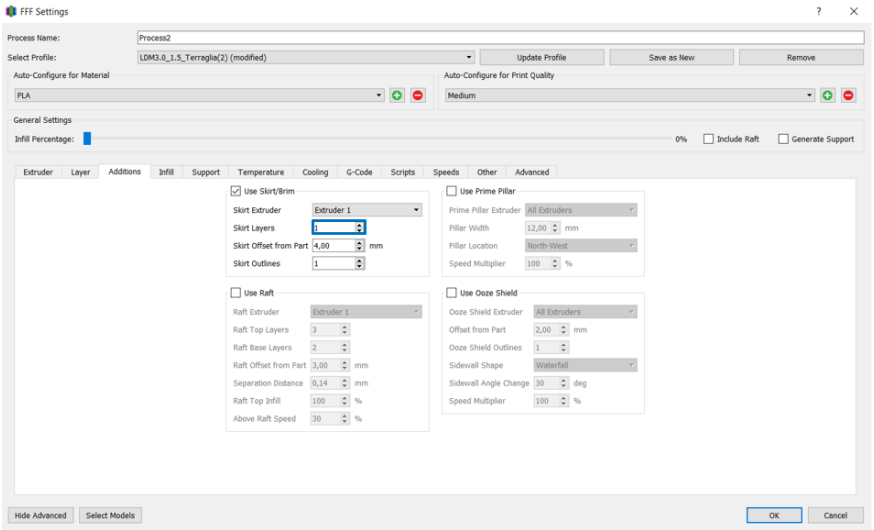

Figure 70 Simply 3D Slicing Software Speed tab parameters (2 mm nozzle).

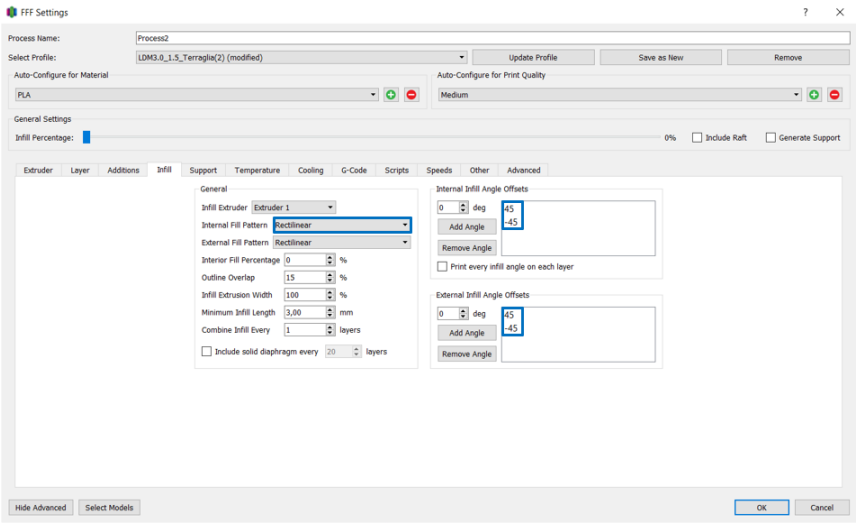

Figure 71 Simply 3D Slicing Software Speed tab parameters (2 mm nozzle).

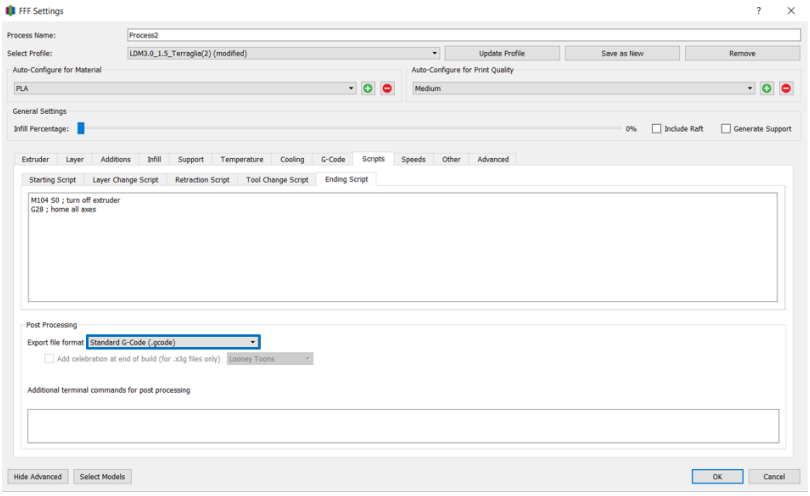

Figure 72 Simply 3D Slicing Software Speed tab parameters (2 mm nozzle).

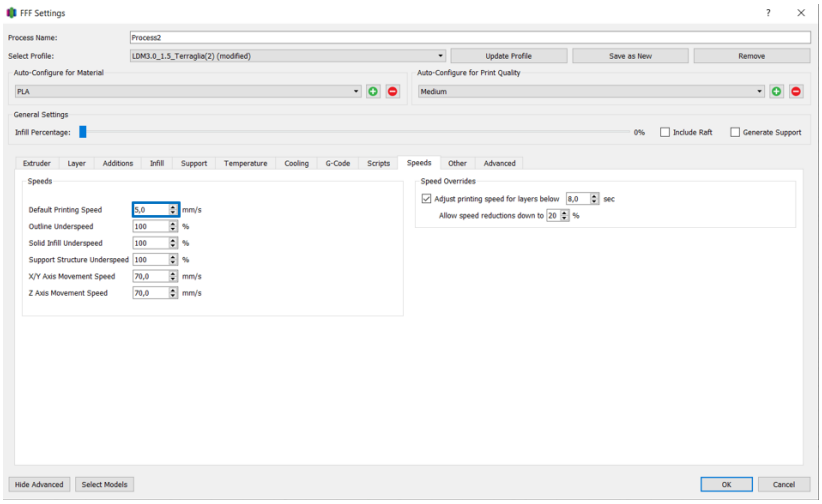

Figure 73 Simply 3D Slicing Software Speed tab parameters (2 mm nozzle)

The parameters highlighted with the blue frames were identified as having the greatest influence on the printing characteristics and overall effectiveness of the 3D printing process.

First trials of printing this capsule developed the following outputs from the 3D printing trials reflected the factors that affected the quality and functionality of the capsules. The first trial gave

the most potent capsules due to the freshness of the mix and a more consistent pressure during extrusion. Follow-up trials, using a more rigid consistency, required higher pressures, which compromised both homogeneity and stability. Moreover, the nozzle height during build-up of layers presented additional challenges, leading to irregular layers, and the structural narrowness of capsules caused handling issues and required proper drying time between the printing and removal of the capsules.

Image 125 First 3D-printed capsule recently developed
Source: (Author).

Image 126 All the capsules produced using 3D printing
Source: (Author).

Image 127 3D printed capsules after curing process
Source: (Author).

These early results give valuable information about the weak spots and opportunities for enhancement in the 3D printing procedure of self-healing concrete capsules. While benchmarks from the initial trials showed compromising, difficulty presented in the later experiments highlight the need to optimize the printing parameters to obtain uniform quality and stable characteristics.

As the capsules are composed of material that is compatible with the surrounding concrete matrix, it would integrate seamlessly and does not compromise the overall mechanical properties. When the cracks form in the matrix, capsules would break, releasing healing agents to effectively seal the cracks. The approach uses the precision of 3D printing to provide uniformity in capsule quality

and allows for controlled dispersion of the contents within the matrix. This aspect also underlines the need to optimize the 3D printing process to achieve the required functionality of the capsule in future developments.

This thesis serves as a guide for future studies looking to enhance self-healing concrete, which might be directed towards improving capsule composition for augmented rupture efficiency and healing outcomes. It should also be explored how biochar enhancement of the mortar interacts with the action of the self-healing agents, so that the mechanical reinforcement from biochar works together with the self-healing efficiency to benefit. Furthermore, searching for alternative healing agents and assessing their environmental impacts could enhance the sustainability of this technology. Thus, incorporating 3D-printed capsules into the mortar matrix is an advancement to develop an enhancement on self-healing concrete. Raising concrete durability and minimizing repairs clearly supports the development of more sustainable infrastructure. These recommendations provide a pathway for advancing biochar-enhanced 3D-printed mortar as a sustainable and innovative solution in modern construction. By deepening the understanding of its mechanical performance, long-term durability, and practical integration into reinforced concrete, biochar mortar could contribute significantly to reducing the environmental footprint of the construction industry while maintaining structural integrity and performance.

ANNEXES

ANNEX 1. Buzzi Unicem Cement Type I 52.2 R technical data sheet.

Buzzi Unicem

DICHIARAZIONE DI PRESTAZIONE
N° 1372-CPR-2769
Ai sensi del REGOLAMENTO DELEGATO (UE) n° 574/2014 del 21 febbraio 2014

1. Codice di identificazione unico del prodotto-tipo:

Cemento Portland EN 197-1 – CEM I 52,5 R

2. Usi previsti:

Preparazione di calcestruzzo, malta, malta per iniezione o altre miscele per costruzione e fabbricazione di prodotti da costruzione, etc.

3. Fabbricante:

BUZZI UNICEM S.r.l. – Via L. Buzzi 6 – 15033 Casale Monferrato (AL) – ITALIA

4. Mandatario:

Non applicabile

5. Sistema di VVCP: (Valutazione e Verifica della Costanza della Prestazione)

Sistema 1+

6.a Norma armonizzata:

UNI EN 197-1:2011

Organismi notificati:

TECNO PIEMONTE, notificato con il numero 1372, ha effettuato la determinazione di prodotto-tipo sulla base delle prove (compreso il campionamento), l'ispezione iniziale dello stabilimento e del controllo di produzione della fabbrica, la sorveglianza, la valutazione e la verifica continue del controllo di produzione di fabbrica, e le prove di verifica di tipo dei campioni prelevati prima della immissione sul mercato del prodotto sotto il sistema 1+ e ha rilasciato il relativo certificato.

7. Prestazioni dichiarate

Caratteristiche essenziali	Prestazione
Costituenti e composizione del cemento comune	CEM I
Resistenza a compressione (normalizzata e iniziale)	52,5 R
Tempo di presa	*Passa*
Residuo insolubile	*Passa*
Perdita al fuoco	*Passa*
Stabilità - Espansione - Contenuto di SO_3	 *Passa* *Passa*
Contenuto di cloruro	*Passa*

8. Documentazione tecnica appropriata e/o documentazione tecnica specifica:

Non applicabile

La prestazione del prodotto sopra identificato è conforme all'insieme delle prestazioni dichiarate. La presente dichiarazione di prestazione viene emessa, in conformità al regolamento (UE) n. 305/2011, sotto la sola responsabilità del fabbricante sopra identificato.

Firmato a nome e per conto del fabbricante da:

Paolo Zelano – Amministratore Delegato

Casale Monferrato, 02.01.2024

Rev. 1

ANNEX 2. Nero Biochar technical data sheet.

ANNEX 3. Mapei Dynamon SP1 technical data sheet.

DYNAMON SP1

Superplasticizer based on acrylic polymer for precast concrete

CE
EN 934-2
T 3.1-3.2-3.7

DESCRIPTION OF PRODUCT

Dynamon SP1 is an admixture based on modified acrylic polymer specially designed for the precast concrete industry, part of the MAPEI **Dynamon SP** system.

WHERE TO USE

Concrete with **Dynamon SP1** has a high level of workability (consistency class S4 or S5, according to EN 206-1), and is consequently easy to apply when fresh. At the same time it offers excellent mechanical performances when hardened. **Dynamon SP1** is especially suitable for precast concrete and wherever there is the need for a strong water reduction, along with a relatively high acceleration of mechanical strengths at an early age in different consistency classes and at curing temperatures above +15°C or with accelerated steam curing treatment.
Its performance makes it particularly suitable for manufacturing self-compacting concrete since **Dynamon SP1** can ensure high workability. At the same time it does not significantly slow down the development of mechanical strengths at early age.
The main applications of **Dynamon SP1** are the production of concrete for:

- manufacturing pre-stressed reinforced beams with a high level of workability and a minimum compressive strength, R_{ckj}, to cut the prestressed tendons, equal to 35 N/mm²;
- manufacturing pre-stressed reinforced concrete roofing slabs, with a high level of workability, and a minimum R_{ckj}, to cut the prestressed tendons, equal to 35 N/mm² and with an excellent appearance;
- manufacturing cladding panels with a high level of workability, a very refined surface and an excellent appearance;
- self-compacting concrete for precasting. Together with **Viscofluid SCC/10** or **Viscostar 3K**, viscosity modifying admixtures, **Dynamon SP1** is suitable for manufacturing self-compacting concrete which can be poured without vibration. Its characteristics of fluidity and resistance to segregation are also suitable for a fast casting procedure.

TECHNICAL CHARACTERISTICS

Dynamon SP1 consists of a water solution containing acrylic polymers (with no formaldehyde). The polymers can efficiently disperse the cement grains.

APPLICATION PROCEDURE

Dynamon SP1 develops maximum dispersing action when added after other mixture ingredients (cement, aggregates, mineral additions or filler and at least 80% of the mixing water) and before **Viscofluid SCC/10** or **Viscostar 3K**.

COMPATIBILITY WITH OTHER PRODUCTS

Dynamon SP1 admixture is compatible with other products for preparing special concretes, especially with:

- hardening accelerating chloride-free admixtures from the **Mapefast** range for reaching very high mechanical strengths at early ages;
- air entraining admixtures from the **Mapeair AE** range used in the production of concrete resistant to freeze/thaw cycles;
- **Viscofluid SCC/10** or **Viscostar 3K**, viscosity modifying admixtures for manufacturing self-compacting concretes;
- **Mapeplast SF**, silica fume based powder admixture for manufacturing "top-quality" concrete (strength, impermeability, durability);

MAPEI

- **Expancrete**, expansive agent for manufacturing shrinkage compensated concrete;
- fly ash for manufacturing standard and self-compacting concrete;
- different types of limestone fillers for manufacturing self-compacting concrete and any other type of concrete that require these fillers;
- **DMA** and **Mapeform Eco** form-release agents, for releasing concrete from formworks;
- curing compounds from **Mapecure** range to protect form-released concrete structures from rapid mixing water evaporation (floorings).

Our technical services department is available to evaluate which admixture is the most suitable to manufacture freeze/thaw cycles resistant concretes, depending on the type of cement used.

CONSUMPTION

Dosage by volume:
from 0.6 to 1.2 l per 100 kg of cement.
Different dosages from those suggested must be previously tested through concrete trials, in addition to consulting MAPEI Technical Services Department.

PACKAGING

Dynamon SP1 is available in bulk, 200 l drums, 1000 l tanks

STORAGE

Dynamon SP1 may by stored 12 months in sealed containers and protect from frost. Exposure to direct sunlight can provoke variations of the colour tone without altering in any way the performances of the product.

SAFETY INSTRUCTIONS FOR THE PREPARATION AND APPLICATION

Dynamon SP1 is not considered dangerous according to the European regulation regarding the classification of mixtures. It is recommended to wear gloves and goggles and to take the usual precautions taken for the handling of chemicals. For further and complete information about the safe use of our product please refer to the latest version of our Material Safety Data Sheet.
PRODUCT FOR PROFESSIONAL USE.

TECHNICAL DATA (typical values)	
PRODUCT IDENTITY	
Consistency:	liquid
Colour:	amber
Density according to ISO 758 (g/m³):	1.08 ± 0.02 at +20°C
Main action:	increased workability and/or reduction of mixing water and rapid development of mechanical strengths at early ages and at T > 15°C
Classification according to EN 934-2:	high range water reducing, hardening accelerating, superplasticizer, tables 3.1, 3.2 and 7
Classification according to ASTM C494:	type F and type C
Classification according to ASTM C1017:	type I
Chlorides soluble in water according to EN 480-10 (%):	< 0.1 (absent according to EN 934-2)
Alkali content (Na_2O equivalent) according to EN 480-12 (%):	< 3.0

pH content according to ISO 4316:	6.5 ± 1.0

WARNING

Although the technical details and recommendations contained in this product data sheet correspond to the best of our knowledge and experience, all the above information must, in every case, be taken as merely indicative and subject to confirmation after long-term practical application; for this reason, anyone who intends to use the product must ensure beforehand that it is suitable for the envisaged application. In every case, the user alone is fully responsible for any consequences deriving from the use of the product.
Please refer to the current version of the Technical Data Sheet, available from our website www.mapei.com

671-3-2014-gb

Any reproduction of texts, photos and illustrations published here is prohibited and subject to prosecution

MAPEI

ANNEX 4. Sigma-Aldrich Polyethylene Glycol 10 000 technical data sheet.

Scheda delle specifiche

Nome del prodotto	Poli(etilenglicole) 10,000
N° Catalogo	81280
Marchio del prodotto	SIAL
Numero CAS	25322-68-3
Peso molecolare	

TEST	SPECIFICHE
APPEARANCE (COLOR)	Colorless or White
APPEARANCE (FORM)	Powder or Crystals or Flakes
Molecular Number Mn (GPC-Analysis)	Report Result
Molecular Weight Mp (GPC-Analysis)	Report Result
Molecular Weight Mw (GPC-Analysis)	Report Result
Molecular Weight Mz (GPC-Analysis)	Report Result
Polydispersity Index (PDI) (GPC-Analysis)	Report Result
MELTING POINT	62 - 65 C
SOLUBILITY (COLOR)	Colorless
SOLUBILITY (TURBIDITY)	Clear
SOLUBILITY (METHOD)	1G IN 10ML WATER
WATER	≤ 1.0 %
SULFATED ASH	≤ 0.2 %
INFRARED SPECTRUM	CONFORMS TO STRUCTURE
VISCOSITY (ROTATION)	550 - 750 mPas
VISCOSITY (CONDITIONS)	50 % IN WATER, 20 C
HYDROXYL VALUE	9.8 - 13.2 mg KOH/g
Remark	MOLECULAR MASS (CALCULATED FROM HYDROXYL VALUE)

BIBLIOGRAPHY

3Ds Dassault Systemes. (n.d.). *Directed Energy Deposition*. Retrieved november 2024, from 3Ds Dassault Systemes: https://www.3ds.com/make/guide/process/directed-energy-deposition

Ahmad , S., Tulliani, J., Ferro, G., Khushnood, R., Restuccia, L., & Jagdale, P. (2015). Crack path and fracture surface modifications in cement composites. *Frattura ed Integrità Strutturale*, 524-533. Retrieved february/november 2024

Aitcin, P. (1998). *High Performance Concrete.* (1, Ed.) London: CRC Press. Retrieved November 2024

Akhtar, A., & Sarmah, A. (2018, March). Novel biochar-concrete composites: Manufacturing, characterization and evaluation of the mechanical properties. *Science of The Total Environment, 616-67*, 408-416. Retrieved November 2024

Allwood, J., Cullen, J., & Waught, R. (2010). *Options for Achieving a 50% Cut in Industrial Carbon Emissions by 2050.* Cambriedge: Department of Engineering, University of Cambridge. Retrieved November 2024

Amalina, F., Syukor Abd Razaka, A., Krishnan, S., Sulaiman, H., Zularisam, A., & Nasrullah, M. (2022). Biochar production techniques utilizing biomass waste-derived materials and environmental applications – A review. *Journal of Hazardous Materials Advances*. Retrieved november 2024

Americal Concrete Insttute (ACI). (2002). *ACI 211.1-91: Standard Practice for Selecting Proportions for Normal, Heavyweight, and Mass Concrete.* ACI. Retrieved November 2024

American Biogas Council. (n.d.). *What is Anaerobic Digestion?* Retrieved november 2024, from American Biogas Council: https://americanbiogascouncil.org/resources/what-is-anaerobic-digestion/

Apis Cor, a Manufacturer of Construction 3D Printing Robots, Announces Strategic Investment by D.R. Horton. (2024, march 11). Retrieved november 2024, from PR Newswire: https://www.prnewswire.com/news-releases/apis-cor-a-manufacturer-of-construction-3d-printing-robots-announces-strategic-investment-by-dr-horton-302084850.html

Arsalan Khushnood, R., Ahmad, S., Ferro, G., Restuccia , L., Tulliani, J., & Jagdale , P. (2015). Modified fracture properties of cement composites with nano/micro carbonized bagasse fibers. *Frattura ed Integrità Strutturale*, 534-542. Retrieved february/november 2024

ASTM. (1940). *Designation: C150/C150M − 21.* Washigton: American Society for Testing and Materialas. Retrieved November 2024

ASTM. (1940). *Designation: C150/C150M − 21.* Washigton: American Society for Testing and Materialas. Retrieved November 2024

ASTM. (2024). *American Society for Testing and Materials (ASTM)*. Retrieved November 2024, from Partner Engineering and Science, Inc.: https://www.partneresi.com/resources/glossary/american-society-testing-and-

materials-astm/#:~:text=Currently%20known%20as%20ASTM%20International,of%20international%20voluntary%20consensus%20standards.

Author, S. (n.d.). Retrieved november 2024, from Zwick Roell: https://www.zwickroell.com/it/prodotti/macchine-di-prova-materiali-statiche/macchine-di-prova-universali-per-applicazioni-statiche/proline/

Banfill, P. (1991). *Rheology of Fresh Cement and Concrete.* Edinburgh: School of the Built Environment, Heriot-Watt University. Retrieved November 2024

Barbhuiya, S., Bhusan Das, B., & Kanavaris, F. (2024). *Biochar-concrete: A comprehensive review of properties, production and sustainability.* London: Elsevier. Retrieved november 2024

Barnes, H., Hutton, J., & Walter, K. (1989). *An Introduction to Rheology* (Vol. 3). Amsterdam: ELSERVIER SCIENCE B.V. Retrieved November 2024

Beesley, L., Moreno Jimenez, E., & Gomez Eyles, J. (2010). *Effects of biochar and greenwaste compost amendments on mobility, bioavailability and toxicity of inorganic and organic contaminants in a multi-element polluted soil.* Liverpool: Elsevier. Retrieved November 2024

Bilek, V., Kalina, L., & Novotny, R. (208, March 30). Polyethylene glycol molecular weight as an important parameter affecting drying shrinkage and hydration of alkali-activated slag mortars and pastes. *Construction and Building Materials, 166*, 564-571. Retrieved November 2024

Blewitt, J. (2015). *International Encyclopedia of the Social & Behavioral Sciences.* Orlando: Elservier. Retrieved August 2024

Box, G. E., Hunter, J., & Hunter, W. (2005). *Statistics for Experimenters: Design, Innovation, and Discovery* (2 ed.). WILEY-INTERSCIENCE. Retrieved November 2024

British Standards Institution. (2013). *BS EN 206: Concrete – Specification, performance, production and conformity.* British Standards Institution. Retrieved November 2024

Buzzi Unicem. (n.d.). *Cement Products*. Retrieved November 2024, from Buzzi Unicem USA: https://www.buzziunicemusa.com/csa

Buzzi Unicem S.r.l. (n.d.). *Tipo I 52,5 R*. Retrieved November 2024, from Buzzi Unicem: https://www.buzziunicem.it/-/tipo-i-52-5-1

Caltrans. (2013). Chapter 3 Review of Concrete Mix Designs. In *CONCRETE TECHNOLOGY MANUAL* (pp. 3-52). Caltrans. Retrieved November 2024

CEMBUREAU. (2022). *CEMBUREAU The European Cement Association.* Retrieved October 2024, from Key Facts & Figures: https://cembureau.eu/about-our-industry/key-facts-figures/

CEMEX. (2002). *Cement History & Facts*. Retrieved November 2024, from CEMEX: https://www.cemexusa.com/products-and-services/cement/history-facts

CEN. (2011). *EN 197-1: Cement - Part 1: Composition, specifications and conformity criteria for common cements. European Committee for Standardization.* CEN. Retrieved November 2024

Center for climate and energy solutions. (2019, Aprile). *WHAT IS CLIMATE RESILIENCE AND WHY DOES IT MATTER?* Retrieved October 2024, from C2ES Climate Essentials: https://www.c2es.org/wp-content/uploads/2019/04/what-is-climate-resilience.pdf

Chasek, P. S., Downie, D. L., & Brown , J. (2017). *Global environmental politics.* (S. edition, Ed.) Boulder, CO : Westview Press. Retrieved November 2024

Choi, C. W., Yun, H. D., & Lee, J. Y. (2012, May). Mechanical Properties of Mortar Containing Bio-Char From Pyrolysis. *Journal of the Korea institute for structural maintenance inspection, 163*, 67-74. Retrieved November 2024

Civín, L. (2023). The concept of sustainability in history and the presnet. In L. Civín, *SUSTAINABILITY* (pp. 11-23). Poznan: Bogucki Wydawnictwo Naukowe. Retrieved October 2024

Clarke, L., Edmonds, J., Jacoby, H., Pitcher, H., Reilly , J., & Richels , R. (2007). *Scenarios of Greenhouse Gas Emissions and Atmospheric Concentrations.* U.S. Climate Change Science Program. Retrieved November 2024

Cobbinah, P., Nzeukou, R., Onawale, O., & Matizamhuka, W. (2021). *Laser Powder Bed Fusion of Potential Superalloys: A Review.* Vanderbijlpark: MDPI. Retrieved november 2024

CUEMATH. (n.d.). *Surface Area of Sphere*. Retrieved November 2024, from CUEMATH: https://www.cuemath.com/measurement/surface-area-of-sphere/

Datis Export Group. (2020, July 05). *What is EN 197-1 Standard?* Retrieved November 2024, from Datis Export Group: https://datis-inc.com/blog/what-is-en-197-1-standard/#:~:text=EN%20197%2D1%20Scope,-EN%20197%2D1&text=This%20European%20Standard%20defines%20and,furnace%20cements%20and%20their%20constituents.

Dhir , R., & Jones, M. (2014). *EURO-CEMENTS Impact of ENV 197 on Concrete Construction.* London: E & FN SPON. Retrieved November 2024

Djettene, R., Dubois, L., Duprez, M. E., Weireld, G., & Thomas, D. (2024, July). Integrated CO2 capture and conversion into methanol units: Assessing techno-economic and environmental aspects compared to CO2 into SNG alternative. *Journal of CO2 Utilization, 85*, 102879. Retrieved November 2024, from https://www.sciencedirect.com/science/article/pii/S2212982024002142?via%3Dihub

enel. (2024, August 9). *The 3 pillars of sustainability: environmental, social and economic.* Retrieved October 2024, from enel: https://www.enel.com/company/stories/articles/2023/06/three-pillars-sustainability

Engineering Product Design. (2019, November 24). *Sheet Lamination*. Retrieved November 2024, from Engineering Product Design: https://engineeringproductdesign.com/knowledge-base/sheet-lamination/

Escalante Rebolledo, A., Pérez López, G., Hidalgo Moreno, C., López Collado, J., Campo Alves, J., Valtierra Pacheco, E., & Etchevers Barra, J. (2016). *Biocarbón (biochar) I: Naturaleza, historia, fabricación y uso en el suelo.* Ciudad de Mexico: Terra Latinoamericana. Retrieved October 2024

European Parliament. (2023, May 24). *Circular economy: definition, importance and benefits.* Retrieved November 2024, from Topics European Parliament:

https://www.europarl.europa.eu/topics/en/article/20151201STO05603/circular-economy-definition-importance-and-benefits

Eurpean Committee fro Standardization. (2019). *EN 12390-3: Testing Hardened Concrete – Compressive Strength of Test Specimens.* Brussels: CEN. Retrieved November 2024

Flatt, R., & Schober, I. (2012). Superplasticizers and the rheology of concrete. In R. Flatt, I. Schober, & N. Roussel (Ed.), *Understanding the Rheology of Concrete* (pp. 144-208). Woodhead Publishing Series in Civil and Structural Engineering. Retrieved November 2024

Freeman Technology. (2019, july 17). *Developing an effective metal powder specification for binder jet 3D printing*. Retrieved november 2024, from Freeman Technology: https://www.freemantech.co.uk/news/developing-an-effective-metal-powder-specification-for-binder-jet-3d-printing

Fujino, J., Nair, R., Kaniuma, M., Masui, T., & Matsuoka, Y. (2006). Multi-gas Mitigation Analysis on Stabilization Scenarios Using Aim Global Model. *The Energy Journal, 27*, 343-353. Retrieved November 2024

Gartner, E., & Hirao, H. (2015, April). A review of alternative approaches to the reduction of CO2 emissions associated with the manufacture of the binder phase in concrete. *Cement and Concrete Research, 78*, 126-142.

Ge , S., Nai Yuh Yek, P., Wang Cheng, Y., Xia, C., Adibah , W., Keey Liew, R., . . . Shiung Lam , S. (2021). Progress in microwave pyrolysis conversion of agricultural waste to value-added biofuels: A batch to continuous approach. *Renewable and Sustainable Energy Reviews*. Retrieved November 2024

Geiger, O. (2011, September 18). *A Blueprint for a Climate Friendly Cement Industry.* Retrieved October 2024, from Geopolymer House Blog: https://geopolymerhouses.wordpress.com/2011/09/18/a-blueprint-for-a-climate-friendly-cement-industry/

Geissdoerfer, M., Savaget, P., bOCKEN, N. M., & Hultink, E. J. (2017). *The Circular Economy – A new sustainability paradigm?* Retrieved November 2024

Gibson, I., Rosen, D., & Stucker, B. (2015). *Additive Manufacturing Technologies.* London: Springer. Retrieved november 2024

Glass, L. M., & Newig, J. (2019). *Governance for achieving the Sustainable Development Goals: How important are participation, policy coherence, reflexivity, adaptation and democratic institutions?* Luneburg: Research Group Governance, Participation & Sustainability, Leuphana University Lüneburg, Germany. Retrieved November 2024

Golisano Institude for Sustainability. (2021, January 20). *What is biochar and how is it made?* Retrieved October 2024, from RIT Golisano Institude for Sustainability: https://www.rit.edu/sustainabilityinstitute/blog/what-biochar-and-how-it-made

González , A., Sendra, C., Herena, A., Rosquillas, M., & Vaz, D. (2021). *Methodology to assess the circularity in building construction and.* Barcelona: ScienceDirect. Retrieved September 2024, from : www.sciencedirect.com/journal/

Griffiths, S., Sovacool, B., Furszyfer Del Rio, D., Foley , A., Bazilian, M., Kim, J., & Uratani, J. (2023, July). Decarbonizing the cement and concrete industry: A systematic review of

socio-technical systems, technological innovations, and policy options. *Renewable and Sustainable Energy Reviews, 180*, 11329. Retrieved November 2024

Gupta, S., & Chaudhary, S. (2020). *Journal of Cleaner Production* (Vol. 261). ELSEVIER. Retrieved October 2024

Gupta, S., Kua, H., & Low, C. (2018, March). Use of biochar as carbon sequestering additive in cement mortar. *Cement and Concrete Composites, 87*, 110-129. Retrieved November 2024

Gupta, S., Tulliani, J.-M., & Wei Kua, H. (2022). *Carbonaceous admixtures in cementitious building materials: Effect of particle size blending on rheology, packing, early age properties and processing energy demand.* Turin: Elsevier. Retrieved february/november 2024

Habert, G. (2013). Environmental impact of Portland cement production. In F. Pcheco-Torgal, S. Jalali, J. Labrincha, & V. John, *Eco-Efficient Concrete* (pp. 265-278). Woodhead Publishing. Retrieved October 2024

Hertwich, E., Lifset, R., Pauliuk, S., & Heeren, N. (2020). *RESOURCE EFFICIENCY AND CLIMATE CHANGE Material Efficiency Sustainability for Low-Carbon Future.* United Nations Environment Programme. Retrieved November 2024

Hewlett, P. C. (1935). *Lea´s Chemestry of Cement and Concrete* (4 ed.). Woburn: BUTTERWORTH HEINEMANN. Retrieved November 2024

Hu, L., Wu , Z., Jiang, Y., Wang , X., He, A., Song, J., . . . Xu, J. (2020). *Recent advances in catalytic and autocatalytic production of biomass-derived 5-hydroxymethylfurfural.* Huaian: School of Chemistry and Chemical Engineering, Huaiyin Normal University. Retrieved October 2024

Huang , B., Gao, X., Xu, X., Song, J., Geng, Y., Sarkis, J., . . . Nakatani, J. (2020). *A Life Cycle Thinking Framework to Mitigate the Environmenta Impact of Building Materials.* ey Laboratory of the Three Gorges Reservoir Region's Eco-Environment, Ministry of Education, Chongqing University. Chongqing: One Earth. Retrieved September 2024, from One Earth: https://www.researchgate.net/publication/346372319_A_Life_Cycle_Thinking_Framework_to_Mitigate_the_Environmental_Impact_of_Building_Materials

Hulme , M. (2017). *Weathered: Cultures of Climate.* SAGE Publications Ltd. Retrieved October 2024

Ige, O. E., Olanrewaju, O., Duffy, K., & Obiora, C. (2001, Novmber 15). A review of the effectiveness of Life Cycle Assessment for gauging environmental impacts from cement production. *Journal of Cleaner Production, 324*, 129213. Retrieved November 2024

International Biochar Initiative (IBI). (2024). *Biochar Feedstocks*. Retrieved November 2024, from International Biochar Initiative: https://biochar-international.org/about-biochar/how-to-make-biochar/biochar-feedstocks/#:~:text=Feedstock%20Considerations&text=Biomass%20waste%20materials%20appropriate%20for,forestry%20wastes%2C%20and%20animal%20manures.

International, A. (2021). *ASTM C78: Standard Test Method for Flexural Strength of Concrete (Using Simple Beam with Third-Point Loading).* West Conshohocken: PA: ASTM International. Retrieved November 2024

IPCC. (2014). *Climate Change 2014: Synthesis Report. Contribution of Working Groups I, II and III to the Fifth Assessment Report of the Intergovernmental Panel on Climate Change.* Geneva: IPCC. Retrieved November 2024

IPCC. (2018). *Special Report: Global Warming of 1.5 ºC.* IPCC In Press. Retrieved November 2024

IPCC. (2021). *Climate Change 2021: The Physical Science Basis. Contribution of Working Group I to the Sixth Assessment Report of the Intergovernmental Panel on.* Cambridge, United Kingdom and New York, NY, USA: Cambridge University Press,. Retrieved November 2024

Jindo, K., Mizumoto, H., Sawada, Y., Sanchez-Monedero, M., & Sonoki, T. (2014). *Physical and chemical characterization of biochars derived from different agricultural residues.* Tokyo: Biogeosciences. Retrieved october 2024

Juneger, M., Snelling, R., & Bernal, S. (2019, August). Supplememtary cementitious materials: New sources,charcaterization, and performance insigth. *Cement and Concrete Research, 122*, 257-273.

Just, J., Wyrzykowski, M., Bajare, D., & Lura, P. (2015, October). Internal curing by superabsorbent polymers in ultra-high performance concrete. *Cement and Concrete Research, 76*, 82-90. Retrieved November 2024

Kates , R. W., Parris, T. M., & Leiserowitz, A. A. (2005). What is Sustainabile Development? Goals, Indicators, Values, and Practices. *Issue of Environment: Science and Policy for Sustainable Development, 47*, 8-21. Retrieved August 2024

Kee Lam, M., Chun Minh Loy, A., Yusup, S., & Teong Lee, K. (2019). Chapter 9 - Biohydrogen Production From Algae. *Biohydrogen (Second Edition)*, 219-245. Retrieved November 2024

Khaled, F., & Erriquez, P. (2019/20). *Biochar addition to a lime-hemp insulating plaster.* Master degree in Architecture for the Sustainability Design, Politecnico di Torino. Retrieved november 2024

Khan, I., & Young, G. (2024, June 14). Role of supplementary cementiteous materials in mitigating heat of hydration in mass concrete elements. *Construction and Building Materials, 431*, 126482. Retrieved November 2024

Khan, M., Sanchez, F., & Zhou, H. (2020). *3-D printing of concrete: Beyond horizons.* Tennessee: Elsevier. Retrieved november 2024

KHUSHNOOD, R., AHMAD, S., RESTUCCIA, L., SPOTO, C., JAGDALE, P., TULLIANI, J.-M., & FERRO, G. (2016). *Carbonized nano/microparticles for enhanced mechanical properties and electromagnetic interference shielding of cementitious materials.* Turin: Higher Education Press and Springer-Verlag Berlin Heidelberg. Retrieved february/november 2024

Kosmatka, S., Kerkhoff, B., & Panarese, W. (2002). *Design and Control of Concrete Mixtures.* (14, Ed.) Illinois: Portland Cement Association. Retrieved Novemeber 2024

Kubiszewski, I., Contanza , R., Franco, C., Laws, P., Talberth, J., Jackson, T., & Aylmer, C. (2013). *Beyond GDP: Measuring and achieving global genuine progress* (Vol. 93). Ecological Economics. Retrieved November 2024

Kwaku Armah, E., Chetty, M., Adebisi Adedeji, J., Estrice, D., Mutsvene, B., Singh, N., & Tshemese, Z. (2023). *Biochar: Production, Application and the Future.* IntechOpen. Retrieved November 2024

Lehman, J., Kern, D., Glaser, B., & Woods, W. (2004). *Amazonian Dark Earths.* Netherlands: Kluwer Academic Publishers. Retrieved october 2024

Lehmann, J., & Joseph, S. (2024). *Biochar for Environmental Management: Science, Technology and Implementation.* London: Routledge. Retrieved October 2024

Levin, K., & Tompkins, F. (2014, March 25). *Visualizing the Global Carbon Budget*. Retrieved November 2024, from World Resource Institution: https://www.wri.org/insights/visualizing-global-carbon-budget

Li , X., Dengler , J., & Hesse, C. (2023, Jue). Reducing clinker factor in limestone calcined clay-slag cement using C-S-H seeding – A way towards sustainable binder. *Cement and Concrete Research, 168*, 107151. Retrieved November 2024

Lin , X., Li, W., Guo, Y., Dong, W., Castel, A., & Wang, K. (2023, Semtember 20). Biochar-cement concrete toward decarbonisation and sustainability for construction: Characteristic, performance and perspective. *Journal of Cleaner Production*, 138219. Retrieved November 2024

Liu, D., Zhingan , Z., Zhang , X., & Chen, Z. (2023, November 17). 3D printing concrete structures: State of the art, challenges, and opportunities. *Construction and Building Materials*, 133364. Retrieved November 2024

Lopez-Cano, I., Cayuela, M., Mondini, C., Takaya, C., rOSS, A., & Sanchez-Monedero, M. (2018). *Suitability of Different Agricultural and Urban Organic Wastes as Feedstocks for the Production of Biochar—Part 1: Physicochemical Characterisation.* MDPI. Retrieved November 2024

Lorenzini, S., & Cassata, F. (2022). *THE STOCKHOLM CONFERENCE AT 50.* Annals of the Fondazione Luigi Einaudi. Retrieved October 2024, from Annals of the Fondazione Luigi Einaudi.

Malvern Panalytical. (2024). *MASTERSIZER 3000 Smarter particle sizing.* Retrieved november 2024, from Malvern Panalytical: https://www.malvernpanalytical.com/en/assets/mrk1872-07-en_ms3000_broch_brandupdate_lr_web_tcm50-17232.pdf

Mann, M. E. (2024, November 12). *Global Warming.* Retrieved November 2024, from Encyclopedia Britanica: https://www.britannica.com/science/global-warming

Manulak, M. W. (2023). *Change in Global Environmental Politics Temporal Focal Points and the Reform of International Institutions.* Ottawa: Carleton University. Retrieved November 2024

Mapei. (n.d.). *Dynamon SP1 application guidelines.* Mapei. Retrieved November 2024

Mapei. (n.d.). *DYNAMON SP1 Superplasticizer based on acrylic polymer for precast concrete.* Mapei. Retrieved November 2024

Mather, B. (2004, January). Concrete durability. *Cement and Concrete Composites*, 3-4. Retrieved November 2024

Meadowcroft, J. (2024, October 25). *Sustainability*. Retrieved October 2024, from Britannica: https://www.britannica.com/science/sustainability

Meadows D.H., M. D. (2004). *The Limits to Growth: The 30-Year Update.* Chelsea Green Publishing. Retrieved September 2024

Meadows. Donella H, M. D. (1972). *The Limits to Growth.* New York: Universe Books. Retrieved August 2024

Mehta, P. K., & Monteiro, P. J. (2014). *Concrete: Microstructure, Properties, and Materials* (4 ed.). New York: McGraw-Hill Education.

Merriam Webster. (n.d.). *concrete*. Retrieved November 2024, from Merriam Webster: https://www.merriam-webster.com/dictionary/concrete#:~:text=concrete%20%E2%80%A2%20%5Ckahn%2DKREET%5C,to%20or%20made%20of%20concrete

Meyer, D. (2009). *Biochar - A Survey.* Energy and Process Engineering. Tampere: Tampere University of Technology. Retrieved october 2024

Mindess, S., Young , J. F., & Darwin, D. (2003). *Concrete.* (2, Ed.) United States: Prentice Hall. Retrieved November 2024

Mishra, G., Danoglidis, P., Shah, S., & Gdoutos, M. (2024, November 7). Optimization of biochar and fly ash to improve mechanical properties and CO2 sequestration in cement mortar. *Construction and Building Material*. Retrieved November 2024

Montgomery, D. C. (2017). *Design and Analysis of Experiments* (9 ed.). New York: John Wiley & Sons. Retrieved November 2024

Mravcová, A. (2023). CLIMATE CHANGE. In *SUSTAINABILITY.* Poznan: Bogucki Wydawnictwo Naukowe. Retrieved November 2024

Muller, C. (2023). How standards support sustainability of cement and concrete in Europe. *Cement and Concrete Research, 173*, 107288. Retrieved November 2024

Myllyviita, T. (2013). *Sustainability assessment of forest resources – tools for a problem-orientated approach* (Vol. Thesis). Vantaa, Finland: University of Eastern Finland. Retrieved November 2024

National Academy. (1999). *Our Common Journey a transition towards sustainability.* Washington D.C.: National Academy Press. Retrieved November 2024

National Center for Biotechnology Information. (2024). *ompound Summary for, Polyethylene Glycol.* Retrieved November 2024, from PubChem: https://pubchem.ncbi.nlm.nih.gov/compound/Polyethylene-Glycol

National Geographic Society. (2023, October 19). *Encyclopedia Entry Anthropocene.* Retrieved November 2024, from National Geographic Education: https://education.nationalgeographic.org/resource/anthropocene/

NERO. (2022). *Produttori di Biochar - carbone vegetale*. Retrieved November 2024, from nero biochar: https://www.nerabiochar.com/prodotto/biochar-15-litri/

NERO. (n.d.). *Vuoi contribuire anche tu a salvare il pianeta sottraendo CO2 dall'atmosfera?* Retrieved November 2024, from neo biochar: https://www.nerabiochar.com/#44

Neville , A., & Brooks, J. (2010). *Concrete Technnology.* (2, Ed.) Edinbutgh: Pearsons. Retrieved November 2024

Neville, A. (2011). *Properties of Concrete.* (5, Ed.) Pearson Education Limited. Retrieved October 2024

Nobis, R. (n.d). *Illustrated History of Cement and Concrete.* Retrieved November 2024, from WCA World Cement Association.

Oliver, J. G. (2022). *TRENDS IN GLOBAL CO2 AND TOTAL GREENHOUSE GAS EMISSIONS 2021 Report.* PBL Netherlands Environmental Assessment Agency. Retrieved November 2024

Oliwia. (2024, April 11). *Exploring the Four Dimensions of Sustainability.* Retrieved October 2024, from One More Tree Foundation: https://one-more-tree.org/blog/2024/04/11/exploring-the-four-dimensions-of-sustainability/#:~:text=Economic%20sustainability%20entails%20promoting%20resource,environmental%20impact%20of%20economic%20activities.

Otton, J., Hussain, T., Birbara, N., & Greil, G. (2017). 3D printing from cardiovascular CT: A practical guide and review. *Cardiovascular Diagnosis and Therapy*, 507-526. Retrieved november 2024

Pachauri, R. K., Meyer, L., & Core Writing Team. (2014). *IPCC, 2014: Climate Change 2014: Synthesis Report. Contribution of Working Groups I, II and III to the Fifth Assessment Report of the.* Geneva, Switzerland: IPCC. Retrieved November 2024

Piketty, T., & Goldhammer, A. (2014). *Capital in the Twenty-First Century.* Harvard University Press. Retrieved November 2024, from https://www.jstor.org/stable/j.ctt6wpqbc

Pomponi, F., & Moncaster, A. (2017). *Circular economy for the built environment: A research framework.* Cambridge: University of Cambridge, Department of Engineering - Centre for Sustainable Development. Retrieved November 2024

Pourakbar, S., & Huat, B. (2016, August). A review of alternatives traditional cementitious binders for engineering improvement of soils. *International Journal of Geotechnical Engineering*(11:2), 206-216.

Rajamani, L. (2016). AMBITION AND DIFFERENTIATION IN THE 2015 PARIS AGREEMENT: INTERPRETATIVE POSSIBILITIES AND UNDERLYING POLITICS. *International & Comparative Law Quarterly*. Retrieved November 2024, from https://www.cambridge.org/core/journals/international-and-comparative-law-quarterly/article/ambition-and-differentiation-in-the-2015-paris-agreement-interpretative-possibilities-and-underlying-politics/CD4237FABBA8B88854F093BC02453960

Re-elaboration from the author, S. (n.d.).

Renner, C. (n.d.). *The World's First 3D Printed Canal House*. Retrieved november 2024, from IGNANT: https://www.ignant.com/2016/09/16/the-worlds-first-3d-printed-canal-house/

Riahi, K., Shilpa, R., Krey, V., & Cho, C. (2011, November). RCP 8.5—A scenario of comparatively high greenhouse gas emissions. *Climate Change, 109*, 33-57. Retrieved November 2024

Rockström J., S. W. (2009, January 01). *Planetary Boundaries: Exploring the Safe Operating Space for Humanity.* Retrieved from Ecology & Society: https://www.ecologyandsociety.org/vol14/iss2/art32/

Rockström J., S. W. (2015, January 15). *Planetary bound aries: Guiding human development on a changing planet.* Retrieved November 2024, from Science: https://www.science.org/doi/10.1126/science.1259855

Rockström Johan, W. S. (2009, September 23). *A safe operating space for humanity.* Retrieved October 2024, from Nature: https://www.nature.com/articles/461472a#citeas

Roussel, N. (2011). *Understanding the Rheology of Concrete.* Woodhead Publishing. Retrieved November 2024

Royal Meteorogical Society. (2024). *The Changing Carbon Cycle*. Retrieved november 2024, from MetLink Royal Meteorogical Society: https://www.metlink.org/resource/the-changing-carbon-cycle/

Sachini Supunsala , S., Souradeep , G., Harn Wei , K., Deyi , H., Sumin , K., C.W. Tsang, D., & Yong , S. (2023). *Cement and Concrete Composites: Application of Biochar in Concrete – a Review.* Korea University, APRU Sustainable Waste Management & Division of Environmental Science and Ecological Engineering. Sejong: Elsevier. Retrieved October 2024

Sachs, J. D. (2015). *The Age of Sustainable Development.* Columbia University Press. Retrieved October 2024

Schmidt , M., Py-Daniel, A., Moraes, C., Valle, R., Caromano, C., Texeira, W., & Barbosa, C. (2014). *Dark earths and the human built landscape in Amazonia: a widespread pattern of anthrosol formation.* Rio de Janerio: Elservier.

Schumacher, G., & Juniper, L. (2023). Coal utilization in the cement and concrete industries. In *The Coal Handbook* (Vol. Second edition, pp. 627-663). Woodhead Publishing Series in Energy. Retrieved October 2024

Sen, A. (1999). *Development as freedom.* New York: Anchor Books. Retrieved October 2024

Sheil, D., Imam , B., German, L., Kuyper, T. W., Limberg, G., Puri, R. K., . . . Wollenberg, E. (2012). Do Anthropogenic Dark Earths Occur in the Interior of Borneo? *Forests*, 207-229. Retrieved october 2024

SIAL. (n.d.). *Scheda delle specifiche.* Retrieved November 2024, from MERK: https://www.sigmaaldrich.com/IT/it/specification-sheet/SIAL/81280

Sirico, A., & Bernardi, P. (2021). *Biochar from wood waste as additive for structural concrete.* Parma: Elsevier. Retrieved october 2024

Sorlin, S., & Paglia , E. (2024). *Stockholm and the Rise of Global Environmental Governance.* Cambriedge: Cambiredge University Press. Retrieved November 2024

Spears, S. (2018, May 16). *What is Biochar?* Retrieved October 2024, from Regeneration International: https://regenerationinternational.org/2018/05/16/what-is-biochar/

Spina, R., & Morfini, L. (2024). *Material Extrusion Additive Manufacturing of Ceramics: A Review on Filament-Based Process.* Bari: MDPI. Retrieved november 2024

Standardization, E. C. (2019). *EN 12390-5: Testing Hardened Concrete – Flexural Strength of Test Specimens.* Brussels: CEN. Retrieved November 2024

Stockhol University. (2023). *Planetary boundaries*. Retrieved October 2024, from Stockholm Resilinece Center: https://www.stockholmresilience.org/research/planetary-boundaries.html

Suarez-Riera, D., Lavagna, L., Carvajal, J., Tulliani, J.-M., Falliano, D., & Restuccia , L. (2024). *Enhancing Cement Paste Properties with Biochar: Mechanical and Rheological Insights.* Politecnico di Torino. Torino: MDPI. Retrieved November 2024

Tagliaferro, A., Rosso, C., & Giorcelli, M. (2020). *Biochar Emerging Applications.* Turin: IOP Publishing. Retrieved october 2024

Tattersall, G., & Banfill, P. (1983). *THE RHEOLOGY OF FRESH CONCRETE.* London: Pitman Books Limited. Retrieved November 2024

Taylor , H. (1997). *Cement Chemestry.* (2, Ed.) London: Thomas Telford. Retrieved October 2024

The Universty of Nottingham. (2012, February 21). *The Open University University of Nottingham*. Retrieved September 2024, from Sustainability: The Buisness Perspective: https://rdmc.nottingham.ac.uk/bitstream/handle/internal/86/Business_edit/15_sustainability__a_brief_history.html

Thomas , M. (2013). *Supplementary Cementing Materials in Concrete.* (1, Ed.) Boca Raton: CRC Press. Retrieved November 2024

Thormark , C. (2002). *A low energy building in a life cycle—its embodied energy, energy need for operation and recycling potential.* Lund, Sweden: Department of Building Science, Lund Institute of Technology. Retrieved October 2024

Tu, H., Wei, Z., Bahrami, A., Kahla, N. B., Ahmad, A., & Ozkilic, Y. (2023, December). Recent advancements and future trends in 3D concrete printing using waste materials. *Developments in the Built Environment, 16*, 100187. Retrieved November 2024

Turner, G. (2008). *A comparison of The Limits to Growth with 30 years of reality. Global Environmental Change-human and Policy Dimensions,.* Retrieved November 2024

UN. (1972). *Report of The United Nations Conference on The Human Environment.* Stockholm: United Nations. Retrieved September 2024

UN. (2012, June 20-22). *Report of the World Commission on Environment and Development: Our Common Future.* Retrieved October 2024, from Sustainable Development: https://www.un.org/en/academic-impact/sustainability

UN. (n.d.). *The Paris Agreement*. Retrieved November 2024, from United Nations Climate Action: https://www.un.org/en/climatechange/paris-agreement

UN. (n.d.). *United Nations Conference on Environment and Development, Rio de Janeiro, Brazil, 3-14 June 1992*. Retrieved November 2024, from United Nations Conferences | Environment and sustainable development: https://www.un.org/en/conferences/environment/rio1992

UNESCO. (1998). *Intergovernmental Conference on Cultural Policies for Development.* Stockholm: UNESCO. Retrieved September 2024

UNFCC. (2011). *Fact sheet: The Kyoto Protocol.* United Nations Framework Convention on Climate Change. Retrieved November 2024

UNFCC. (2013). *Doha Amendment to the Kyoto Protocol.* United Nations Framework Convention on Climate Change. Retrieved November 2024

United Nations. (2015). *Transforming our world: the 2030 Agenda for.* United Nations General Assembly. Retrieved November 2024, from https://documents.un.org/doc/undoc/gen/n15/291/89/pdf/n1529189.pdf

University of Edinburgh. (n.d.). *UK Biochar Research Centre*. Retrieved October 2024, from What is Biochar?: https://www.biochar.ac.uk/what_is_biochar.php

University of Washington, state DOTs, FHWA. (2024). *Portland Cement.* Retrieved November 2024, from Pavement interactive: https://pavementinteractive.org/reference-desk/materials/portland-cement/

University of Washington, state DOTs, FHWA. (2024). *Portland Cement.* Retrieved November 2024, from Pavement interactive: https://pavementinteractive.org/reference-desk/materials/portland-cement/

Ural, N. (2021). The significance of scanning electron microscopy (SEM) analysis on the microstructure of improved clay: An overview. *Open Geosciences, 13*, 197-218. Retrieved november 2024

USGS. (n.d.). *What is the difference between global warming and climate change?* Retrieved November 2024, from USGS science fro a chnagng world: https://www.usgs.gov/faqs/what-difference-between-global-warming-and-climate-change#:~:text=%E2%80%9CGlobal%20warming%E2%80%9D%20refers%20to%20the,%2C%20temperature%2C%20and%20wind%20patterns.

Van Vuuren, D., Edmods, J., Kainuma, M., & Riahi, K. (2011, August). The representative concentration pathways: an overview. Climatic Change. This issue. *Climatic Change*. Retrieved November 2024

Vergara , L., Perez, J., & Colorado, H. (2023). *3D printing of ordinary Portland cement with waste wood derived biochar obtained from gasification.* Medellin: Elsevier. Retrieved february/november 2024

Wansbrough, H. (2017). *THE MANUFACTURE OF PORTLAND CEMENT.* Retrieved November 2024, from https://nzic.a2hosted.com/unsecure_files/book/9B.pdf

Woods, W., Teixeira, W., Lehmann, J., Steiner, C., WinklerPrins, A., & Rebellato, L. (2008). *Amazonian Dark Earths: Wim Sombroek's Vision.* Springer. Retrieved october 2024

Woolf, D., Amonette, J., Street-Perrott, F., Lehmann, J., & Joseph, S. (2010). *Sustainable biochar to mitigate global climate change.* Nature Communications. Retrieved November 2024

Worell , E., Price, L., Hendriks, C., & Meida , L. (2001). CARBON DIOXIDE EMISSIONS FROM THE GLOBAL CEMENT INDUSTRY. *Annual Review of Environment and Resources, 26*. Retrieved November 2024

World Commission on Environment and Development. (1987). *Our Common Future.* Oxfrod University Press. Retrieved November 2024

Xiaofei , T., Yunguo , L., Guangming , Z., Xin , W., Xinjiang , H., Yanling , G., & Zhongzhu , Y. (2015). *Application of biochar for the removal of pollutants from aqueous solutions.* Hunan Normal University. Changsha: Elsevier. Retrieved october 2024

Zhang , N., Zhang , D., Zuo, J., Miller, T. R., Duan, H., & Schiller, G. (2022). Potential for CO2 mitigation and economic benefits from accelerated carbonation of construction and demolition waste. *Renewable and Sustainable Energy Reviews, 169*, 112920. Retrieved November 2024, from https://www.sciencedirect.com/science/article/abs/pii/S1364032122008012?via%3Dihub